

STELLINGEN

behorende bij het proefschrift

Breach growth in sand-dikes

van

P.J. Visser

Delft, 8 december 1998

1. In het proces van bresgroei in zanddijken kunnen vijf stadia onderscheiden worden.

Dit proefschrift.

2. Er zijn ronde, vierkante en rechthoekige wielen.

Dit proefschrift.

3. Het proces van bresgroei in dijken met een forse kern van zand kan met het in dit proefschrift gepresenteerde model in redelijk betrouwbare mate voorspeld worden.

Dit proefschrift.

4. Een solide teenconstructie op het buitentalud van een dijk (bijvoorbeeld bestaande uit een kraagstuk met bestorting en een teenopsluiting met damwand) kan na het bezwijken van de dijk het inundatieproces van een relatief grote polder vertragen en derhalve tot een reductie van het aantal slachtoffers leiden. Het inundatieproces bij zanddijken kan verder aanzienlijk vertraagd worden door in de zandkern op zekere afstanden (bijvoorbeeld elke 100 m) moeilijk te eroderen constructies (bijvoorbeeld kleipropen of damwanden in het dwarsprofiel) aan te brengen.

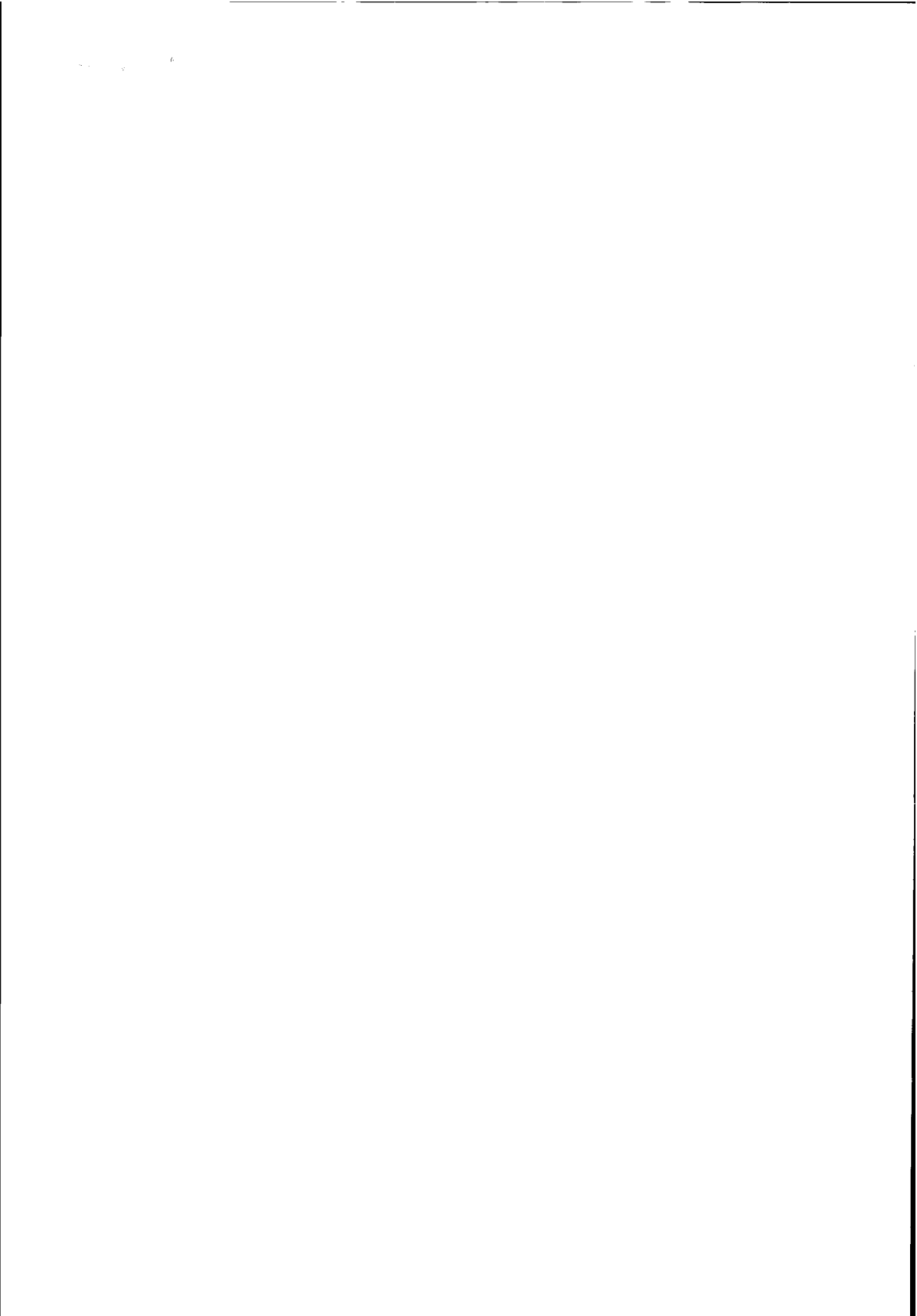
Dit proefschrift.

5. Teneinde bij toekomstige dijkdoorbraken gegevens van het bresgroeiproces te kunnen verkrijgen is het noodzakelijk een goed opgezet meetplan te ontwikkelen.

6. Het is van groot belang bij experimenten in golfbakken naar golfgedreven uniforme langsstromen grote zorg te besteden aan de recirculatie van het langsstroomdebiet.

Visser, P.J., 1991. Laboratory measurements of uniform longshore currents. Coastal Eng., 15, pp. 563-593.

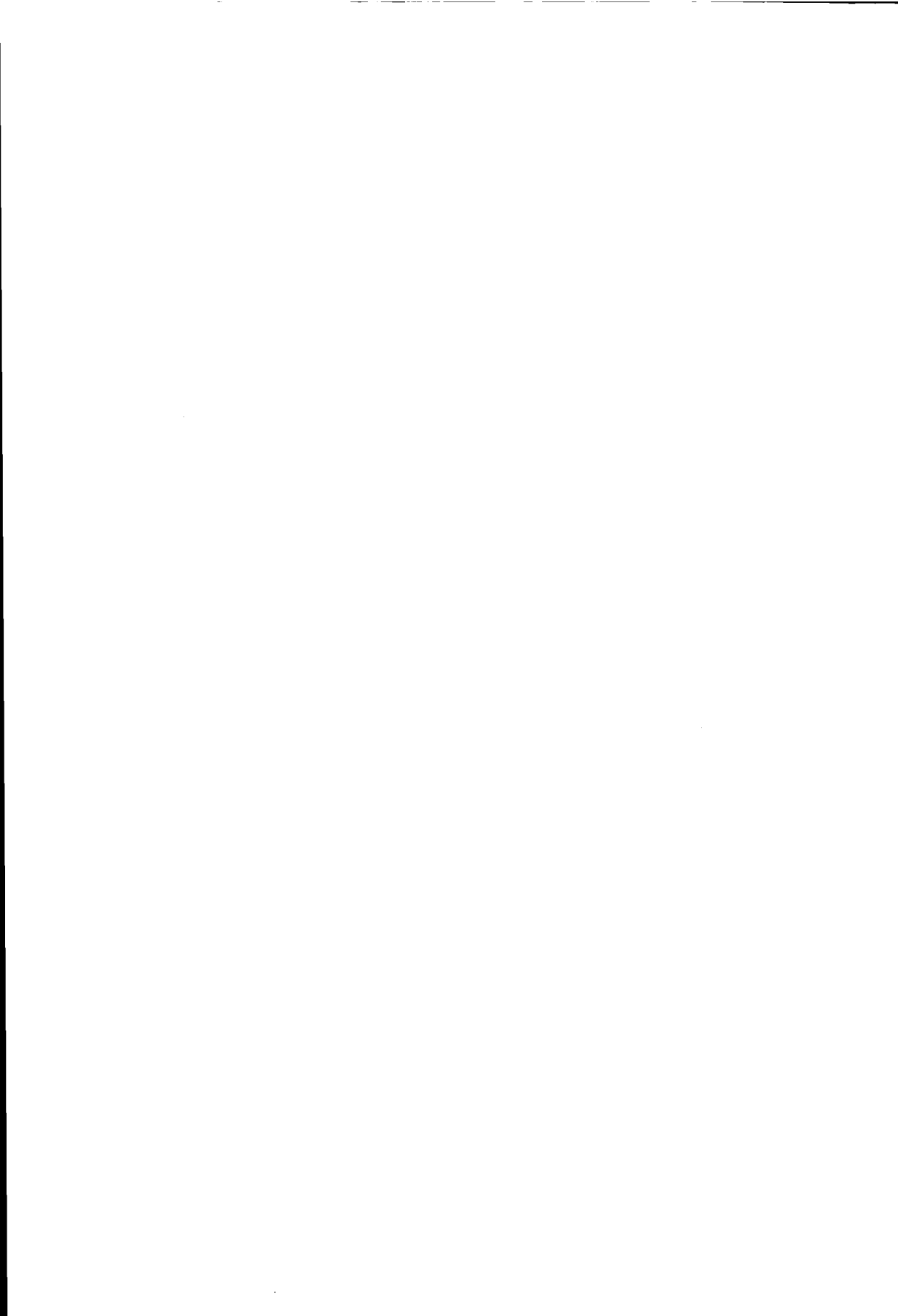
7. Het rond te pompen recirculatiegebied bij experimenten in golfbakken naar golfgedreven uniforme langsstromen kan bepaald worden door het interne circulatiegebied te minimaliseren.
Visser, P.J., 1991. Laboratory measurements of uniform longshore currents. Coastal Eng., 15, pp. 563-593.
8. De vele loftuitingen aan het adres van het Nederlandse poldermodel gaan voorbij aan het feit dat het op zich waardevolle streven naar consensus tot schadelijk uitstelgedrag kan leiden.
9. Het somtijds succes van de technische analyse van aandelenkoersen is hoofdzakelijk gebaseerd op 'self-fulfilling prophecy'.
10. Het plaatsen van een kind met het syndroom van Down op een gewone basisschool is veelal niet in het belang van het kind.
11. Goede rekenmodellen zijn een vereenvoudigde afbeelding van de werkelijkheid en onderscheiden zich daarin wezenlijk van fotomodellen.
12. Ludieke stellingen leiden de aandacht van het proefschrift af.



710219
TR 3250

**BREACH GROWTH IN
SAND-DIKES**

P.J. Visser



Breach growth in sand-dikes



PROEFSCHRIFT

ter verkrijging van de graad van doctor
aan de Technische Universiteit Delft,
op gezag van de Rector Magnificus prof. ir. K.F. Wakker,
in het openbaar te verdedigen ten overstaan van een commissie,
door het College voor Promoties aangewezen,
op dinsdag 8 december 1998 te 16.00 uur

door

Pleun Joris VISSER

civiel ingenieur

geboren te Sliedrecht

Dit proefschrift is goedgekeurd door de promotor:
Prof. dr. ir. J.A. Battjes

Samenstelling promotiecommissie:

Rector Magnificus, voorzitter

Prof. dr. ir. J.A. Battjes, Technische Universiteit Delft, promotor

Prof. ir. K. d'Angremond, Technische Universiteit Delft

Prof. dr. ir. L.C. van Rijn, Universiteit Utrecht

Prof. dr. ir. H.J. de Vriend, Universiteit Twente en Technische Universiteit Delft

Prof. drs. ir. J.K. Vrijling, Technische Universiteit Delft

Dr. ir. J.S. Ribberink, Universiteit Twente

Front cover: flow through breach in sand-dam in Zwin'94 experiment
flow through breach in Noord Dike in Papendrecht, 1 February 1953
(copyright: Foto Scheermeijer, Sliedrecht)

Back cover: flow downstream of breach in sand-dam in Zwin'94 experiment

ISBN 90-9012279-6

Copyright ©1998 by Paul Visser, Dordrecht, The Netherlands
All rights reserved.

Also published in the series 'Communications on Hydraulic and Geotechnical Engineering',
Faculty of Civil Engineering and Geosciences, Delft University of Technology, Report No.
98-1 (ISSN 01690-6548).

Printed by Beeld- en Grafisch Centrum, Delft University of Technology, The Netherlands.

Samenvatting

De laaggelegen gebieden in Nederland worden beschermd tegen hoogwater door een stelsel van duinen, dijken, dammen, kademuren, stuwen en stormvloedkeringen. Dit enorme stelsel van waterkeringen moet Nederland vrijwaren van overstromingen, waar het in het verleden honderden malen door is geteisterd. Deze overstromingen waren vrijwel altijd het gevolg van het doorbreken van dijken, een aantal hiervan met desastreuze gevolgen, duizenden doden en een enorme economische schade. Met name het doorbreken van een groot aantal dijken in de stormvloedramp van 1953 heeft geleid tot een radicale omslag in het denken over veiligheidsnormen voor waterkeringen.

De Technische Adviescommissie voor de Waterkeringen heeft in 1990 besloten de huidige ontwerpmethodiek op basis van een overschrijdingskans van de waterstand te vervangen door een inundatie-risico benadering. Hierbij bestaat het risico uit de kans op een overstroming, gecombineerd met de schade die erdoor ontstaat. Voor het berekenen van de bij een dijkdoorbraak te verwachten schade is het noodzakelijk het verloop van de inundatie van de polder te kennen. Dit inundatieverloop wordt mede bepaald door het debiet dat de polder instroomt, en daarmee door de afmetingen van de bres in de dijk. Het is dus van belang de ontwikkeling van het stroomgat te kunnen voorspellen. Een betrouwbaar model voor de groei van het stroomgat en het verloop van het instroomdebiet bij dijkdoorbraak is daarvoor noodzakelijk.

In dit proefschrift wordt een mathematisch model beschreven voor de groei van het stroomgat in een doorbrekende dijk en het verloop van het debiet door de bres. Er is uitgegaan van een dijk opgebouwd van zand waarbij de taludbekledingen verondersteld worden geen vertragend effect te hebben op het erosieproces.

Het model is gebaseerd op het mechanisme van bresgroei als waargenomen in verscheidene experimenten in het laboratorium en het veld. Uitgaande van een relatief kleine initiële bres aan de kruin van de dijk, kunnen hierbij vijf stadia onderscheiden worden. In de eerste twee stadia vreet de bres zich een weg door de dijk, waarbij het debiet nog nauwelijks toeneemt. In het derde stadium nemen de afmetingen van de bres versneld toe, en daarbij ook het debiet. In het vierde stadium is de dijk in de bres verdwenen en groeit de bres vooral in de breedte, bij een constante buitenwaterstand lineair in de tijd. In het vijfde stadium is de waterstand in de polder zo hoog geworden dat deze de stroomsnelheden door de bres vertragen, als gevolg waarvan ook de bresgroei afneemt. Als de stroomsnelheden in de bres zo klein zijn geworden dat de Shieldsparameter kleiner is dan de kritieke waarde hiervan stopt

de erosie van het stroomgat. Vervolgens stopt de stroming door de bres als de waterstand in de polder gelijk is geworden aan de buitenwaterstand.

Het bresgroeiproces in de laatste twee stadia is afhankelijk van de ondergrond van de dijk, van de buitentaludbekleding en van de hoogte van het voorland van de dijk. Het model berekent als functie van deze randvoorwaarden de groei van de bres en het debiet door het stroomgat.

Een essentieel onderdeel van een bresgroeimodel is de formulering van de opname en het transport van het sediment waarmee de dijk is opgebouwd. Als gevolg van de grote stroomsnelheden in de bres bestaat dit transport vooral uit transport in suspensie. In het model is een vereenvoudigde beschrijving voor het oppikken van sediment volgens Galappatti (1983) toegepast. De benadering van Galappatti (1983) vereist een formule voor de capaciteit van het sedimenttransport. De stroomsnelheden in de bres van een doorbrekende dijk kunnen echter dusdanig groot zijn dat er geen sedimenttransport-formules zijn, die voor deze omstandigheden zijn ontwikkeld. Voor toepassing in het huidige model, zijn een aantal bestaande sedimenttransport-formuleringen getoetst aan eerdere bresgroei-proeven. Slechts een gering aantal formules bleek geschikt te zijn voor toepassing in het model. Deze formules zijn ingebouwd in het model voor nadere confrontatie met experimentele resultaten.

Twee experimenten zijn uitgevoerd om gegevens te verkrijgen voor de calibratie en validatie van het bresgroeimodel, de Zwin'94 veldproef en een laboratoriumexperiment (Caan, 1997). In beide experimenten zijn gedetailleerde waarnemingen gedaan van de toename van de breedte en de diepte van de bres, waterstanden boven- en benedenstrooms van het stroomgat en stroomsnelheden in en buiten de bres.

De calibratie van het model aan het Zwin'94 experiment laat zien dat toepassing van de zandtransport-formules van zowel Bagnold-Visser (1989) als Wilson (1987) goede overeenstemming geeft voor de eerste drie stadia van het bresgroeiproces. Hetzelfde geldt voor de formuleringen van Van Rijn (1984a,b) en (in wat mindere mate) van Engelund-Hansen (1967) voor de laatste twee stadia. Op grond van de resultaten van de toetsing van de sedimenttransport-formuleringen aan eerdere bresgroei-proeven, is voor de eerste drie stadia de Bagnold-Visser (1989) formule geselecteerd. De overeenstemming van het aldus gecalibreerde model met de data van het laboratoriumexperiment is goed.

De confrontatie van het model met de gegevens van de doorbraak van de Noorddijk in Papendrecht in 1953 wijst op een bresbreedte van ongeveer 110 m, die al na ongeveer 2,5 uur bereikt zou zijn. Dit laatste is min of meer in overeenstemming met een ooggetuige-verslag. De Noorddijk brak door ter plaatse van een 'hulpgat', waar de dijk over een lengte van ongeveer 100 m een drempel van harde klei had en de dijkkern in plaats van klei uit zand bestond. Berekeningen met het model tonen aan dat de solide drempel en de beperkte lengte van de zandkern de uiteindelijke inundatiediepte in de polder aanzienlijk hebben beperkt.

Summary

About 60 % of The Netherlands are protected against high waters by a system of dunes, dikes, dams, quay walls, barrages and storm flood barriers. This enormous system of water defences has to protect The Netherlands against floods, which have occurred hundreds of times in the past. Almost all of these floodings resulted from failures of dikes, some with disastrous outcomes, thousands of deaths and enormous economical losses. Particularly the failure of numerous dikes in the 1953 flood disaster has induced a marked change in thinking about safety standards for flood defence structures.

The Technical Advisory Committee on Water Defences (TAW) in The Netherlands has decided in 1990 to replace the present design method for dikes based on a frequency of exceedance of the water level by an inundation risk approach. In this method safety levels will be expressed in terms of risks. Risk is here defined as the product of the probability of inundation and the expected damage caused by the inundation. It is necessary to predict the rate of inundation of the polder in order to be able to estimate this damage. This inundation rate depends heavily on the flow rate through the breach in the failing dike, which in its turn depends on the development of the breach in time. Hence, it is necessary to have a reliable dike breaching model.

In this thesis a mathematical model is described for the growth of the breach in a failing dike and for the inflow rate through the breach. It is assumed that the dike has been constructed with sand and that the clay-layers and the revetments on the slopes do not decelerate the erosion process.

The model is based on the mechanism of breach erosion as observed in various tests in the laboratory and the field. It is assumed that the process starts with a small initial breach at the top of the dike. Then, five stages are distinguished in the resulting dike breaching process. In the first two stages, the breach eats its way into the dike, with hardly any increase of the breach inflow rate. In the third stage the growth of breach depth and width accelerates, and consequently also the discharge through the breach. After the wash-out of the dike in the breach at the end of the third stage, the breach grows further in the fourth stage, mainly laterally. In the fifth stage backwater in de polder decelerates the flow in the breach, and so also the increase of the breach width. Rising tailwater ultimately stops the flow of water through the breach.

The breach erosion process in the last two stages depends on the erodibility of the base of the dike, and on the stability of the toe construction of the dike or the height of the

foreland in cases where the subsoil has low resistance against erosion. The model calculates the breach growth and the breach discharge as function of these boundary conditions.

An essential part of a breach erosion model is the description of the entrainment of the sediment and its transport through the breach. Due to the large flow velocities in the breach the sediment is transported mainly in suspension. In the mathematical model a simplified version of Galappatti's (1983) description for the entrainment of sediment is applied. This approach requires a formulation for the equilibrium value of the sediment transport. None of the existing sediment transport formulae has been derived and tested for the relatively steep initial longitudinal slopes and the large flow velocities which occur throughout most of the breach erosion process. For application in the model, the feasibility of a number of existing sediment transport formulae for breach erosion has been investigated, leaving only a few formulae with a reasonable performance. These transport formulations have been implemented in the model for the test with experimental results and prototype data.

Two experiments were performed to obtain data for the calibration and validation of the mathematical model, the Zwin'94 field experiment and a laboratory experiment (Caan, 1997). In both experiments increase of both width and depth of the breach, outside and inside water levels, flow velocities in and near the breach were observed in detail.

The calibration of the model with the data of the Zwin'94 experiment shows that application of both the Bagnold-Visser (1998) and Wilson (1987) sand transport formulae gives good agreement in Stages I, II and III. The same applies to the formulations of Van Rijn (1984a,b) and (in some less degree) Engelund-Hansen (1967) in Stages IV and V. The Bagnold-Visser (1989) formula is selected for Stages I, II and III, taking into account also the results of the feasibility study of sediment transport formulae for breach erosion. The agreement of the calibrated model with the data of the laboratory experiment is good.

The confrontation of the model with the data of the failure of the Noord Dike in Papendrecht in 1953 indicates a final breach width of about 110 m already present after about 2.5 hr, which is more or less in agreement with a crude eye-witness report. The Noord Dike failed at the location of an auxiliary spillway, where along a length of about 100 m the dike had a solid foundation of clay and the core of the dike was built of sand and not of clay. Computations with the model show that the solid clay-layer and the limited length of the sand-core have restricted the final inundation depth in the polder significantly.

Contents

Samenvatting (Summary in Dutch)

Summary

Chapter 1	Introduction	1
1.1	The Netherlands, a history of flooding	1
1.2	Present design standards for flood defences	2
1.3	Future probabilistic design approach	3
1.4	Development of evacuation plans	5
1.5	Objective of present study	5
1.6	Approach of problem	5
Chapter 2	Review of literature	9
2.1	Introduction	9
2.2	Developments in The Netherlands	9
2.3	Wash-out of erodible fuse plugs	11
2.4	Breaching of earth-dams	14
2.5	Breaching of flood levees on alluvial plains	18
2.6	Breaching of sand-barriers along coasts	19
2.7	Discussion	21
Chapter 3	Breach erosion process	23
3.1	Introduction	23
3.2	Causes of failure of dikes	23
3.2.1	Overflowing and wave overtopping	23
3.2.2	Sliding of inner or outer slope	24
3.2.3	Erosion of outer slope	25
3.2.4	Seepage and piping	25
3.2.5	Initial breach	26
3.3	Process of breach erosion	27
3.3.1	Introduction	27
3.3.2	Development of initial breach in Stages I, II and III	29
3.3.3	Breach development in Stages IV and V	35
3.3.4	Discussion	42

Chapter 4	Mathematical model	45
4.1	Introduction	45
4.2	Development of initial breach in Stages I and II	47
4.2.1	Flow along inner slope	47
4.2.2	Sediment transport along inner slope	50
4.2.3	Rate of erosion along inner slope	53
4.2.4	Steepening of inner slope in initial breach in Stage I	56
4.2.5	Decrease of width of dike crest in breach in Stage II	57
4.3	Acceleration of breach growth in Stage III	59
4.3.1	Decrease of crest height	59
4.3.2	Increase of breach width	60
4.4	Continuation of breach growth in Stage IV	62
4.5	Deceleration of breach growth in Stage V	70
4.6	Computational scheme	71
4.7	Discussion	73
Chapter 5	Sediment transport formulae	75
5.1	Introduction	75
5.2	Tested sediment transport formulae	76
5.3	Experimental conditions	77
5.3.1	Introduction	77
5.3.2	Schelde Flume experiment T3	79
5.3.3	Schelde Flume experiment T5A	81
5.3.4	Zwin'89 field experiment	84
5.4	Determination of sand transport rates in experiments	85
5.4.1	Schelde Flume experiment T3	85
5.4.2	Schelde Flume experiment T5A	86
5.4.3	Zwin'89 field experiment	87
5.5	Results of sediment transport calculations	87
5.6	Discussion	91
Chapter 6	Experiments for verification	95
6.1	Introduction	95
6.2	Zwin'94 field experiment	95
6.2.1	Introduction	95
6.2.2	Location Het Zwin	95
6.2.3	Sand-dam built in Zwin Channel	96

6.2.4	Experimental procedure	98
6.2.5	Experimental results	101
6.2.6	Discussion	109
6.3	Laboratory experiment	110
6.3.1	Introduction	110
6.3.2	Experimental procedure	110
6.3.3	Experimental results	113
6.3.4	Discussion	115
 Chapter 7 Calibration and validation of the model		 119
7.1	Introduction	119
7.2	Calibration with data of Zwin'94 field experiment	119
7.3	Validation against data of laboratory experiment	123
7.4	Confrontation with 1953 failure of Noord Dike	125
7.5	Discussion	129
 Chapter 8 Conclusions and recommendations		 131
8.1	Introduction	131
8.2	Conclusions	131
8.3	Recommendations	133
 Appendix A Tested sediment transport formulae		 135
A.1	Introduction	135
A.2	Formulae for sand-water mixture flows	136
A.2.1	Wilson (1966, 1987)	136
A.2.2	Mastbergen and Winterwerp (1987)	138
A.3	Formulae for sediment transport on steep slopes	140
A.3.1	Smart and Jaeggi (1983)	140
A.3.2	Bathurst, Graf and Cao (1987)	141
A.3.3	Rickenmann (1991)	142
A.4	Formulae for total sand transport in river regimes	143
A.4.1	Engelund and Hansen (1967)	143
A.4.2	Van Rijn (1984a,b)	144
A.5	Energetics-based formulae	147
A.5.1	Bagnold-Bailard (1981)	147
A.5.2	Bagnold-Visser (1989)	149

Appendix B Computer program 151

B.1 Introduction 151

B.2 Computation of sediment fall velocity 151

B.3 Definition of functions 152

B.4 Module Stage I 155

B.5 Module Stage II 156

B.6 Module Stage III 156

B.7 Module Stage IV 157

B.8 Module Stage V 157

Acknowledgements 159

List of main symbols 161

List of Dutch words 165

References 167

Chapter 1

Introduction

1.1 The Netherlands, a history of flooding

Archaeological research has shown that in The Netherlands the basins of the rivers Rhine and Meuse and their numerous distributaries were inhabited as far back as 1800 BC. These rivers flooded the surrounding land again and again, so settlement was mainly confined to the naturally higher grounds of the river banks and the 'donken', isolated sand dunes dating from the last ice-age. Archaeological research has also shown that people living near the coast in the northern part of The Netherlands started to build 'terpen' (artificial dwelling mounds, several meters high) around 500 BC to protect their lives and properties against flooding.

The first more or less organized efforts to protect the land against flooding date from around 1000 AD. In this period the inhabitants began to encircle their settlements with embankments. The first dikes along the rivers and in the delta area were constructed around 1200. However, the construction of these dikes did not end the battle against the floods. At least 150 cases of flooding are known to have happened in the next six centuries, both along the rivers and in the coastal areas, some of these with many deaths (e.g. the St. Aagten Flood of 1287 with tens of thousands people drowned, the St. Elisabeth Flood of 1421 and the All Saints Flood of 1570, both with thousands of deaths).

During the French period (1795–1815), the central government decided to improve the discharge capacity of the rivers by straightening the river bends, and to provide in this way a better protection against flooding. These measures were succeeded by raising of the dikes. For the first time these works were performed with some coherence by using available data of maximum river flows and related water levels. Together these measures resulted in a decreasing number of dike failures in the nineteenth century.

A disastrous storm in 1916, causing extensive flooding in the areas around the Zuiderzee, gave the last impulse to close the Zuiderzee with the IJsselmeer Dam ('Afsluitdijk'). It took two other disasters (along the Rhine and its distributaries in 1926 and in the coastal provinces Zeeland and South Holland in 1953) to induce a marked change in thinking about safety standards for flood defence structures. Before 1953 dikes were built based on a water level of 1.0 m above the highest known flood level increased by a surcharge for wave run-up. The dangers of this experience-based approach emerged in 1953. The damage of this flooding

was enormous: 1835 people dead, tens of thousands livestock drowned, about 4500 buildings destroyed or seriously damaged and a direct economical loss of about 14 % of the Dutch GDP, see Rijkswaterstaat (1961). Immediately after the 1953 flood disaster the government installed the so-called Delta Committee.

1.2 Present design standards for flood defences

The Delta Committee recommended in 1960 to apply design water levels with a frequency of exceedance ranging between 1/2000 and 1/10000 per year, depending on the economical value of the areas to be protected (1/2000 for the Wadden Sea areas, 1/10000 for Central Holland and 1/4000 for other areas). Under design conditions each dike section should be absolutely safe.

The flood protection standard of 1/3000 per year for river dikes, formulated in 1956, was reduced in 1977 to 1/1250 per year as recommended by the Commission on River Dikes (1977). This commission justified lower safety standards for river dikes than for water defences in the delta by arguing that 1) the warning-time for extreme high water levels in rivers is much longer than for storm surges at sea, 2) fresh water floodings are less destructive for the inundated land than salt water floodings, and 3) tidal variations of the water level complicate the repair of breached water defences in the delta area compared to that of river dikes.

The safety standards based on a water level with a certain exceedance frequency are still applied. Throughout the years, however, several adaptations have been introduced such as new criteria for wave run-up and geotechnical failure. The main features of the present approach are (see Kraak et al., 1995):

- safety levels are based partly on economical (1953 situation) and LNC¹⁾ values of the area and partly on the location of the polder (in the delta zone, the upper river zone or the transition zone);
- probabilistic description of the hydraulic conditions (exceedance frequency of water level);
- merely deterministic approaches for other failure mechanisms as geotechnical failure;
- dike section approach (correlations between adjacent sections are not considered).

It may be clear that the present design method for flood defences is rather inconsistent.

¹⁾ L = of the landscape, N = natural, C = cultural

1.3 Future probabilistic design approach

The Technical Advisory Committee on Water Defences (TAW) in The Netherlands has decided (in 1990) to aim at an overall consistent design method for dikes. This new method is referred to as the inundation risk approach (see Kraak et al., 1995). In this method safety levels will be expressed in terms of risks. Risk (R) is here defined as the product of the probability of failure (i.e. of inundation, P_f) and the expected damage caused by the inundation (D):

$$R = P_f D \quad (1.1)$$

Risk can be expressed in loss of human lives and/or in monetary units. Loads as well as strengths will be incorporated probabilistically. Correlations between dike sections will be taken into account. Polders with high risk values should have a lower inundation probability than areas with lower risk values. In this approach both the acceptable risk level and the risk itself have to be assessed. The assessment of an acceptable risk level is a political choice. For the assessment of the risk the following steps are necessary:

- estimation of the failure probability of the flood defence system²⁾,
- description of the inundation process in case of failure,
- determination of the expected damage (material and immaterial) in case of inundation.

For the estimation of the failure probability all known failure possibilities have to be gathered and arranged in a so-called fault tree, see TAW/CUR (1990). The top event of the tree is inundation, the branches are the possible failure mechanisms such as (for dikes) overtopping, sliding, erosion of the outer slope, piping, etc.

For the estimation of the expected flood damage, past floodings have been analyzed. These analyses have resulted in mathematical relations between damage parameters (such as percentage of casualties, damage factor for buildings) and inundation parameters (ultimate inundation depth, inundation speed, inundation duration and quality of inundation water), see TAW/CUR (1990). Figure 1.1 shows an example, i.e. the percentage of people drowned as function of the inundation depth³⁾. It is clear that the application of this type of relations requires good estimates of the inundation parameters. These parameters depend heavily on

²⁾ In general a flood defence system (along a sea, a river, a lake or a canal) may comprise a combination of dikes, dunes, dams, quay walls and may incorporate structures as storm surge barriers and locks. The present study applies only to dikes, dunes and dams (see also Section 1.6).

³⁾ It can be expected that the percentage of people drowned depends even stronger on the inundation speed and the flood velocities than on the (ultimate) inundation depth.

Breach growth in sand-dikes

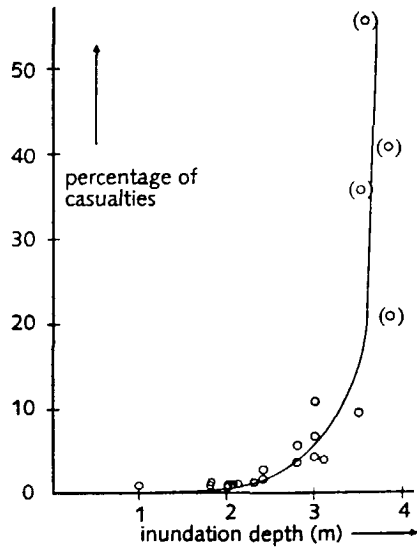


Figure 1.1 Percentage of people drowned in inundated polders as function of the inundation depth (TAW/CUR, 1990, see also Kraak et al., 1995).

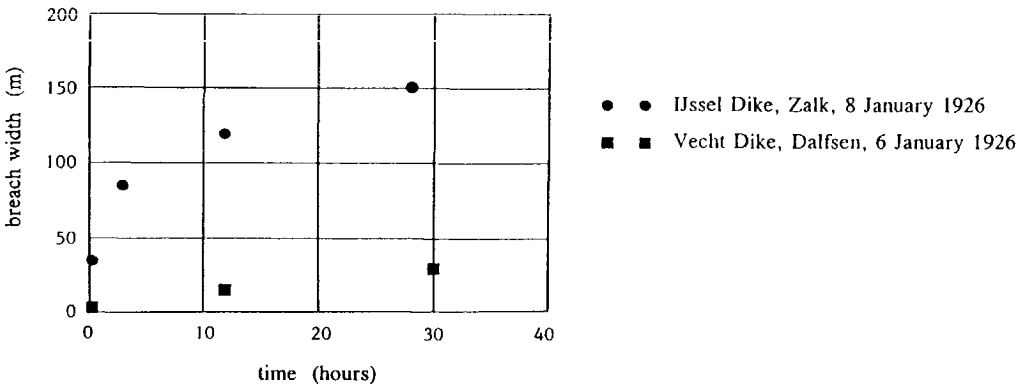


Figure 1.2 Development of breach width in time from eye-witness reports (TAW/TNO, 1984, see also TAW/CUR, 1990); Zalk and Dalfsen are in The Netherlands.

the flow rate through the breach in the failing flood defence structure, which in its turn depends on the development of the breach in time.

1.4 Development of evacuation plans

Early in 1995, the water levels in the Dutch rivers rose to almost 1926 levels and by way of precaution about 250000 people (and millions of livestock) were evacuated from the polders along the river Rhine and its distributaries Waal, Lek and Boven Merwede. Fortunately no main flood defence failed and the people could return to their homes in about a week. This event has revealed, however, that also for the development of disaster management strategies, in which evacuation of people is essential, it is important to be able to predict the process of flooding in a polder.

1.5 Objective of present study

Until recently, the knowledge of the process of breach growth in dikes was very poor, at least in The Netherlands (see also Chapter 2). Also prototype data of dike breaching are scarce and far from complete. Most information has been based on eye-witness reports of past dike-bursts. An example is given in Figure 1.2. This kind of information is also not very usable for lack of knowledge about the hydraulic conditions and the geotechnical parameters of the dike.

From the foregoing it is clear that it is of importance to develop a mathematical model for breach erosion with which it is possible to predict the breach growth and the discharge rate through the breach as function of the parameters involved. These parameters are:

- geometry of the cross-section of the dike or dune (height, width, angles of the slopes),
- structure of the dike or dune (material, revetments, foundation),
- area of the polder,
- hydraulic conditions (water level against the flood defence structure, wave conditions).

It is the aim of the present work to develop and verify such a model.

1.6 Approach of problem

Figure 1.3 shows a representative cross-section of a modern dike in The Netherlands: a body of sand with a watertight part on the water-retaining side of the dike. The TAW recommends

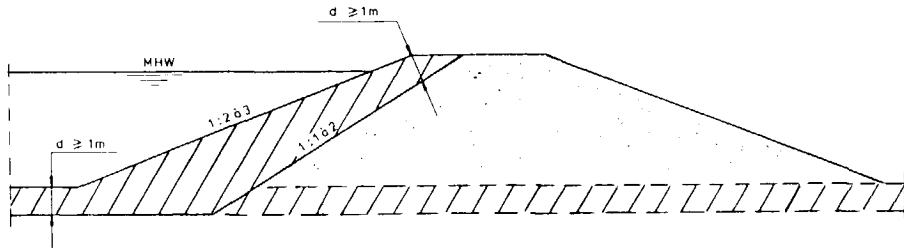


Figure 1.3 Representative cross-section of a dike (after TAW/CUR, 1991).

for the watertight part 'a clay layer with a minimum thickness of 1 m and a clay percentage ranging from 20 % to 35 %', see TAW/CUR, 1991. This clay layer has frequently a wedge-shape. The core of sand gives the dike stability; the porosity of the sand provides sufficient discharge of seepage water to prevent high pore-water pressures which endanger this stability. A revetment of stone, concrete blocks or asphalt on the outer slope, a toe construction down below this slope and a clay covering with a grass blanket on the crest and the inner slope protect the dike against erosion by current and wave attack, rain and wind.

The present study is limited to the breach erosion process of sand-dikes, sand-dams and dunes. The limitation to the breaching process means that it is assumed that there is an initial breach in the upper part of the dike body and that this initial damage to the flood defence structure is so severe that the flow through it starts the breaching process. How this initial breach was formed through one of the possible failure mechanisms (see Chapter 3) is not the subject of the present thesis. Also the effect of waves on the breach erosion process has been left out of the study.

The limitation to sand-dikes and dunes is (for the moment) necessary because of the complexity of the process and the very poor knowledge of the erodibility of clay. This approach might seem rather unrealistic, but in fact this is not the case. As described above, it is assumed that the initial damage to the flood defence system is so large that it breaches. This means for the dike of Figure 1.3 that the damage is so large that it has uncovered the sand core of the dike. Then it may be expected that the remaining clay-layers and revetments can hardly resist the strong flow through the initial breach. This means that the dike of Figure 1.3 breaches more or less like a sand-dike. So the limitation of the present model to sand-dikes and dunes does not mean that it is only applicable to flood defences constructed purely with sand but that it can also be applied to dikes with a core of sand. It also means that the application to clay-dikes or earthen dams is inaccurate and that this application will, most likely, yield an overestimation of the flooding process (which of course can be used as

being the most unfavourable situation).

Chapter 2 contains a review of literature on dike-breaching and related subjects as breaching in earth-dams and sand-barriers and wash-out of erodible fuse plugs. A phenomenological description of the process of breach erosion of sand-dikes is given in Chapter 3. In this process five different stages can be distinguished. The mathematical description of each of these five stages is outlined in Chapter 4. An important parameter in the model is the sediment transport capacity of the flow through the breach. The best qualified sediment transport formulae are summarized in chapter 5, including the validity ranges (if known) and some background information. Chapter 5 holds also a comparison of the predictions of experimental data by these sediment transport formulations. Two experiments were done to calibrate and test the mathematical model, one in the field and one in the laboratory. The procedures and results of these breach growth experiments are described in Chapter 6. The calibration of the model against the data of the field experiment, its test with the data of the laboratory experiment and the confrontation with a prototype dike failure are described in Chapter 7. The conclusions and recommendations from this study are given in Chapter 8.

Breach growth in sand-dikes

Chapter 2

Review of literature

2.1 Introduction

This chapter presents a review of literature on breaching in embankments, i.e. on the breach erosion process of dikes, levees, earth-dams, fuse plugs and sand-barriers. The developments in The Netherlands till now are summarized in Paragraph 2.2. This description includes also the author's earlier work on dike breaching. The subjects covered in the remaining paragraphs are:

- wash-out of erodible fuse plugs (Paragraph 2.3),
- breaching of earth-dams (Paragraph 2.4),
- breach growth in flood levees on alluvial plains (Paragraph 2.5),
- breaching of sand-barriers along coasts (Paragraph 2.6).

The breaching process in these cases have all some features in common.

2.2 Developments in The Netherlands

The investigations triggered by the 1953 flood were at first focused on the failure mechanism of dikes and on design standards for safer dikes, and not on the breaching mechanism. Edelman (1960), for instance, analyzed many dike-bursts of the 1953 flood and concluded that severe damages of the inner slopes were always wrought by overtopping water.

Only rather recently, the first serious attempts were made to describe mathematically the breaching process in dikes. For the feasibility study of a pumped storage plant in The Netherlands (a 25 m high water reservoir in Lake IJsselmeer), Voogt (1985) proposed the following simple equation for the breach width B as function of time t :

$$B = B_{\max} (t/t_{\max})^{0.5} \quad (2.1)$$

where B_{\max} is the final breach width and t_{\max} is the time interval in which the breach width attains its final width. Equation (2.1) was based on the few available observations of $B(t)$, shown in Figure 1.2. The problem with equation (2.1) is obvious: B_{\max} and t_{\max} have to be

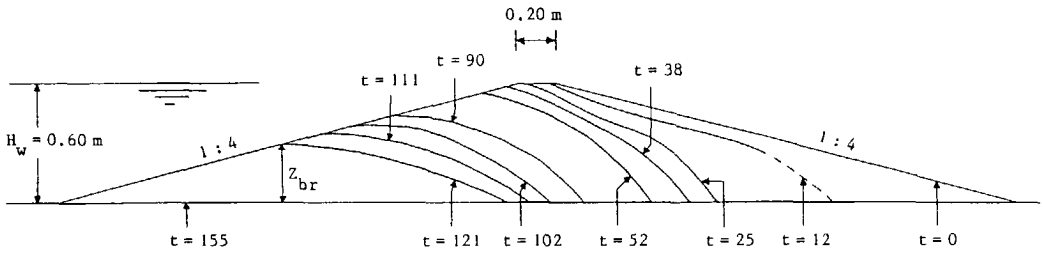


Figure 2.1 Development in time t (in seconds) of a breach in a sand-dike in a laboratory flume in Experiment 3 of Visser et al. (1986), see also Visser (1989).

known, instead of being predicted by the breach growth model.

To avoid this problem, the author developed a breach growth model which can predict the maximum discharge Q_{max} through the breach and its time of occurrence, see Visser et al. (1986) and Visser (1989). In essence, this model is a first version of the present breach growth model. It was developed for the feasibility study for a 75 m high pumped storage plant off the Dutch coast. The comparison of the model predictions with the results of three laboratory tests has shown good agreement (see Visser et al., 1986 and Visser, 1989). Figure 2.1 shows the development in time of a breach in a sand-dike in one of these tests.

On 13 December 1989 a field experiment was performed in the Zwin Channel in order to observe the process of breach growth in a prototype sand-dike, see De Loeff (1990) and Visser et al. (1991). The Zwin Channel is a tidal inlet in the nature reserve Het Zwin, at the border of The Netherlands and Belgium (see Chapters 5 and 6). The process of breach erosion as observed in the 2.2 m high sand-dam of the Zwin'89 experiment was similar to that in the 0.6 m high laboratory dikes of Visser et al. (1986) and Visser (1989).

In 1990 the Technical Advisory Committee on Water Defences (TAW) in The Netherlands decided to develop a breach growth model in order to be able to apply probabilistic methods to sea defences. So far, the following investigations have been carried out within this program:

- Schelde Flume experiments in 1991: measurements of the breach growth in vertical direction in the first three stages of the breach erosion process, see Steetzel and Visser (1992, 1993) and Chapter 5.
- Schelde Basin experiments in 1992: measurements of the growth of the breach width in the final three stages of the breach erosion process, see Steetzel (1996a).

- Study of the applicability of sediment transport formulae to sand-dike breach erosion, see Visser (1995) and Chapter 5.
- Zwin'94 field experiment: a large-scale experiment to test mathematical breach growth models, see Visser et al. (1996a, 1996b) and Chapter 6.

The TAW also decided to develop a breach growth model, see Steetzel (1996b) for the preliminary results.

2.3 Wash-out of erodible fuse plugs

A fuse plug is an erodible spillway in an earth-fill or concrete dam of a water reservoir. A fuse plug is designed to wash away in a predictable and controlled way when the water elevation in the reservoir exceeds a critical level. Figure 2.2 shows an example of a fuse plug (this one is designed to be mounted on a concrete spillway). After breaching and wash-out by the flood waters, the fuse plug can be constructed again at relatively low costs. A fuse plug may reduce the size of the concrete permanent spillway of the dam without diminishing its spilling capacity. Concrete spillways are expensive structures and substantial savings may be realized by reducing their sizes (Chee, 1978). Fuse plug sections have also been built in embankments along rivers in several countries for reducing extraordinary floods (Tinney and Hsu, 1961).

Tinney and Hsu (1961) performed laboratory experiments (with 1 : 20 and 1 : 40 models) and a field experiment (with a 1 : 2 scale model at the project site) to investigate the feasibility of a fuse plug in the spillway of the Oxbow Dam in the Snake River between Oregon and Idaho in the USA. The experiments have shown that the wash-out process consists of two phases: 1) breaching of the pilot channel (see Figure 2.3), and 2) erosion of the embankment face. Tinney and Hsu (1961) also observed that the wash-out rates of fuse plugs built with well-graded material with apparent cohesion was about 25 % of the wash-out rates of fuse-plugs built with uniform, cohesionless material. Tinney and Hsu (1961) have used a theoretical scale ratio (with the 1/3 power of the length scale) for the rate of lateral erosion of the embankment face of the prototype fuse plug.

Chee (1978) investigated the mechanics and time rates of the vertical erosion of many types of erodible control embankments with hydraulic scale models in a laboratory flume. Chee (1978) has derived an empirical relation for the wash-out time of erodible embankments, and from this equation the time scale ratio for the erosion process. With this time scale ratio, Chee (1978) could calculate wash-out times of prototype fuse plugs from the model tests.

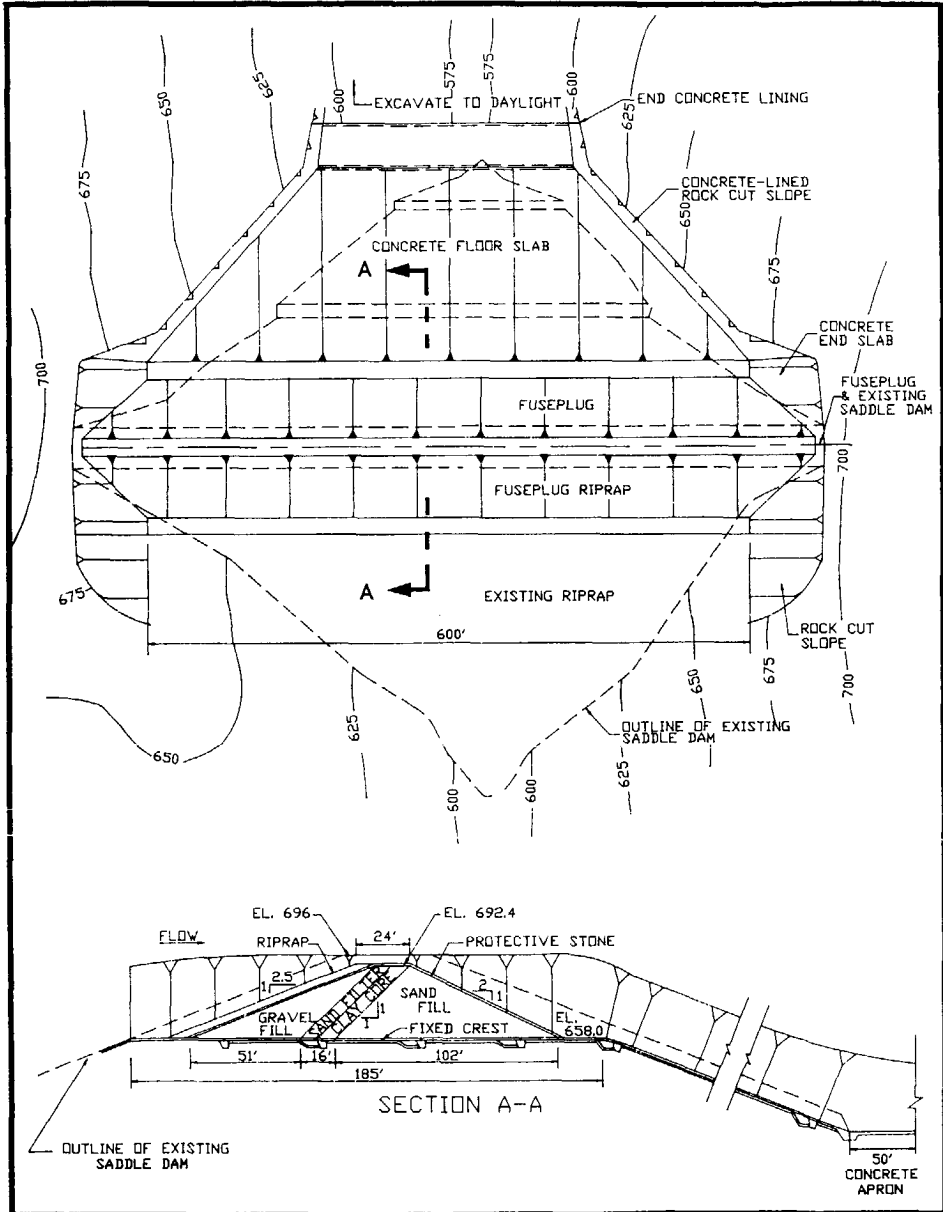


Figure 2.2 Example of a fuse plug design (after Fletcher and Gilbert, 1992).

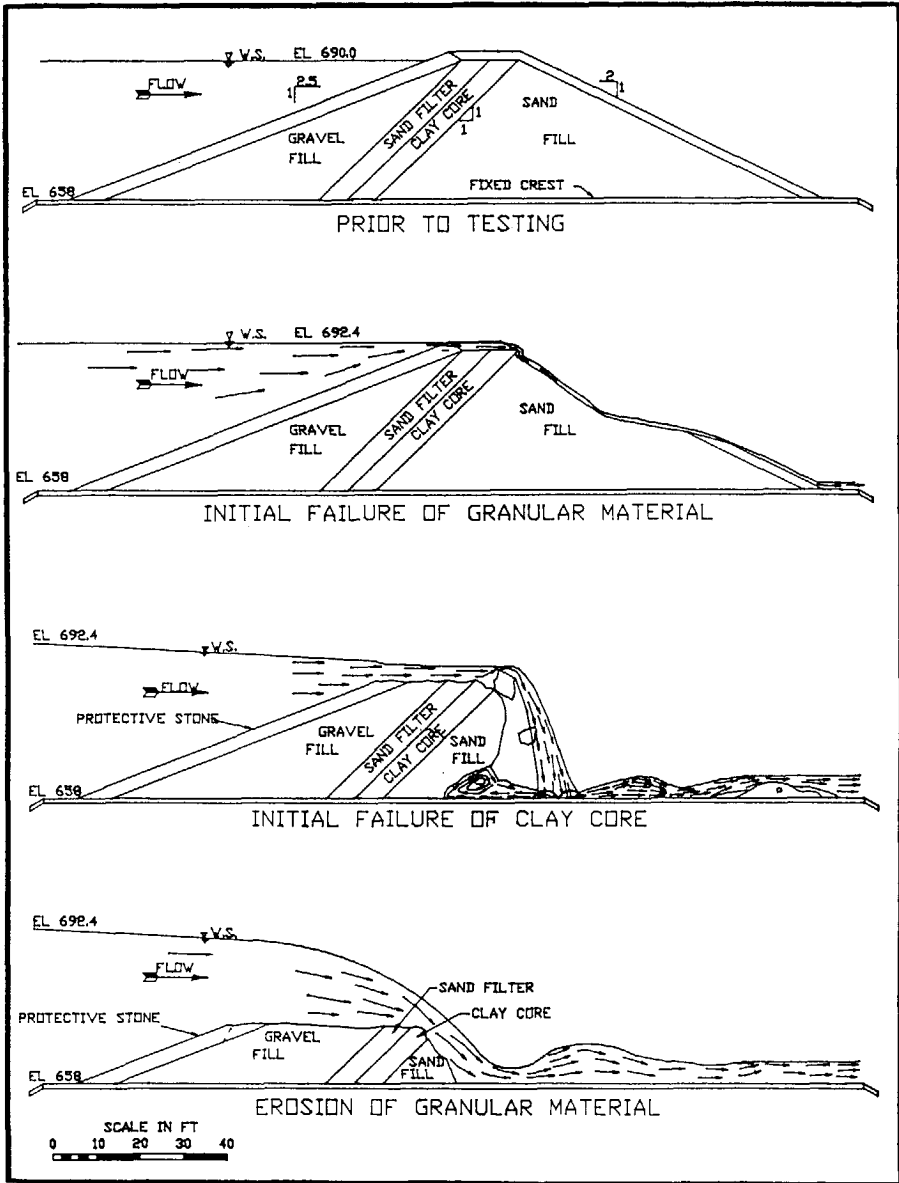


Figure 2.3 Typical failure sequence in Phase 1 of fuse plug of Figure 2.2 (after Fletcher and Gilbert, 1992).

Pugh (1985) conducted hydraulic model studies for the development of guidelines for fuse plugs. Eight tests with model embankments at scales 1 : 10 and 1 : 25 were conducted for a variety of prototype fuse plugs from 3 m to 9 m high. Sediment particle diameters were converted to model particle diameters with Froude scaling of the sediment fall velocities. Pugh (1985) has derived from these tests (applying Froude scaling) the following expression for the lateral erosion rate of prototype fuse plugs:

$$\frac{dB}{dt} = 4H_D + 46 \quad [\text{m/hr}] \quad (2.2)$$

where B is the fuse plug width in meters, t is the time in hours, H_D is the fuse plug height above its base in meters (in terms of this thesis: the height of the dike above polder level).

Fletcher and Gilbert (1992) performed similar model experiments as Pugh (1985) at scales 1 : 20 and 1 : 40 for the 10 m high and 180 m wide fuse plug of the Center Hill Dam in the Caney Fork River, Tennessee, USA to develop a satisfactory design that would fail in about 30 minutes. Both Pugh's (1985) and Fletcher and Gilbert's (1992) experiments have confirmed Tinney and Hsu's (1961) observation that in the washout process of fuse plugs two phases can be distinguished (see above).

The above studies on erodible fuse plugs have in common that they are all semi-empirical and all directed towards the washout time of fuse plugs. Their importance for the process of breach erosion of sand-dikes is that the processes are partly similar (see Section 3.3.4).

2.4 Breaching of earth-dams

Dam-break flood wave propagation is a classical problem of unsteady open channel flow which has been investigated by many scientists and hydraulic engineers for over a century. Significant advances in dam-breach flood wave modeling have been achieved during the last 20 years, see Wurbs (1987) and Singh (1996).

Since the reservoir outflow is governed largely by the development with time of the breach, simulation of the breaching process is an important aspect of dam-breach flood wave modeling. The process of earth-dam breaching has been investigated by numerous researchers during the last few decades, resulting in a number of mathematical models, see Singh (1996) for a review of most of them and Mojib (1990), Havnø et al. (1989) and Bechteler and Broich (1991). Table 2.1 contains the main features of these models. In models 1 and 8 the initial breach is assumed to be caused by overtopping, in models 2 through 7 and 9 the failure may be caused by overtopping or piping. The models 3 through 7 incorporate tail-

Model and year	Hydrodynamics	Sediment transport	Breach shape	Input parameters
1. Cristofano (1965)	broad-crested weir flow	empirical formula	trapezoidal, with constant bottom width	angle of repose, others
2. Brown and Rogers (1981)	broad-crested weir flow	Schoklitsch (1930) bed-load formula	parabolic	breach dimensions, sediments
3. Ponce and Tsivoglou (1981)	full hydrodynamic system	Meyer-Peter and Müller (1948) bed-load formula	regime type breach morphology	critical shear stress, sediment
4. Fread (1984a)	broad-crested weir flow	linear predetermined erosion	rectangular, triangular, trapezoidal	breach dimensions, sediments
5. Fread (1984b)	broad-crested weir flow	Meyer-Peter and Müller (1948) bed-load formula, Smart (1984) bed-load formula	rectangular, triangular, trapezoidal	critical shear stress, sediment
6. Singh and Scarlatos (1987)	broad-crested weir flow	Einstein-Brown (1950) bed-load formula	rectangular, trapezoidal	sediments, others
7. Havnø et al. (1989)	broad-crested weir flow	linear predetermined erosion, or Meyer-Peter and Müller (1948) formula, Engelund and Hansen (1967) total load formula	trapezoidal	sediments, others
8. Mojib (1990)	broad-crested weir flow	Du Boys (1879) bed-load formula, Smart (1984) bed load formula	rectangular, triangular, trapezoidal	sediments, others
9. Bechteler and Broich (1991)	broad-crested weir flow	Meyer-Peter and Müller (1948) formula, Cristofano (1965) formula, Smart (1984) formula	varies in time	sediments, others

Table 2.1 Mathematical models for breach growth in earth-dams (see Singh, 1996, for summaries of papers describing models 1 through 6).

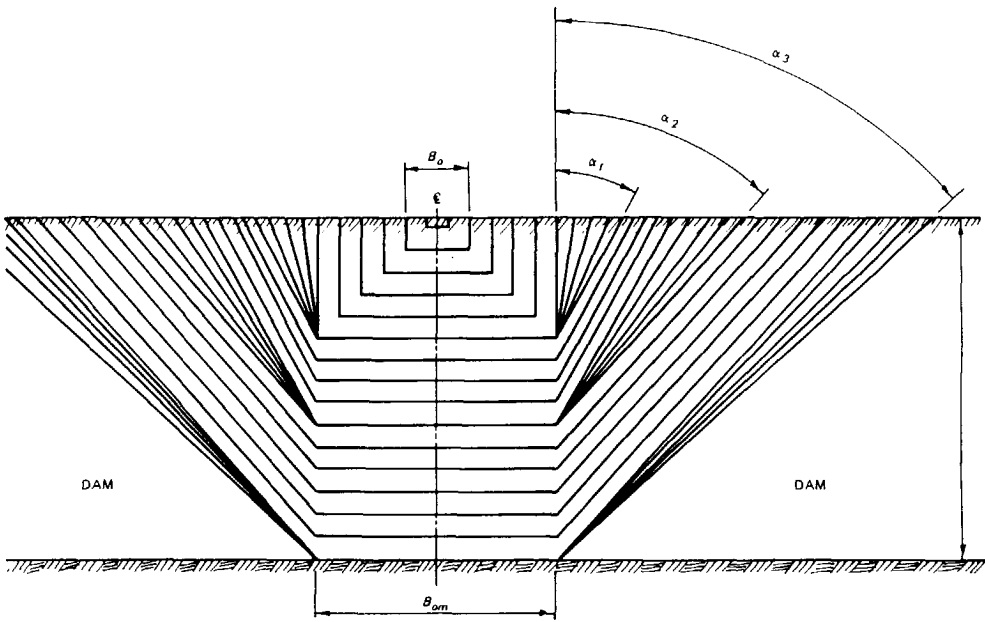


Figure 2.4 Front view of dam with sequence of breach formation as predicted by the BREACH model (after Fread, 1984b; see also Singh, 1996).

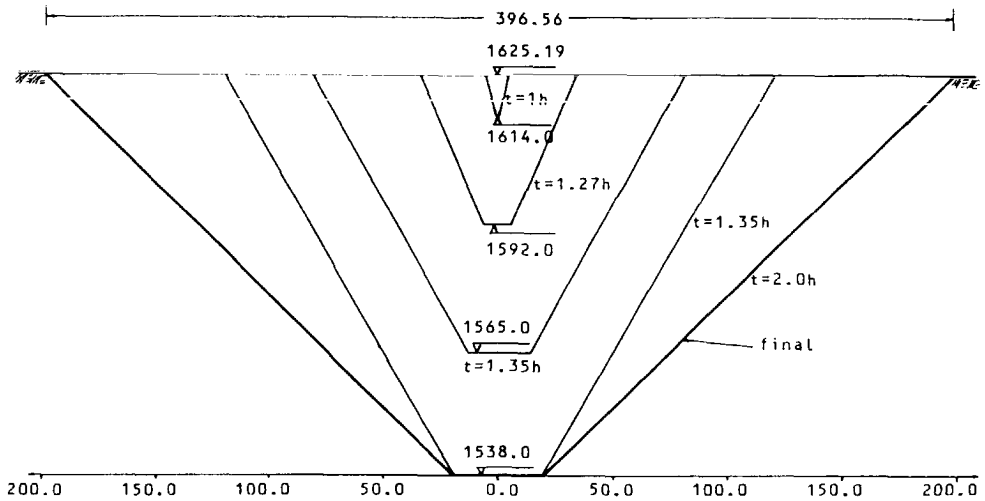


Figure 2.5 Breach evolution for the Teton Dam as calculated with the BEED model (all dimensions are expressed in m, after Singh, 1996).

		Historical dam failure					
		South Fork Dam		Buffalo Creek Dam		Teton Dam	
Output variable		Computed	Observed	Computed	Observed	Computed	Observed
Q_p	[m ³ /s]	6090	7050	1510	1400	68580	65000
T_f	[h]	3.4	3.5	0.56	0.5	1.35	1.5
B_t at T_f	[m]	82	-	48	-	239	-
B_t final	[m]	108	-	48	-	397	-
$S_p * 10^6$	[kg/s]	11.6	-	9.7	-	70.5	-
$V_w * 10^6$	[m ³]	18.0	18.9	0.52	0.48	358	310
$W_s * 10^6$	[kg]	1239	-	241	-	5085	6120

Q_p = water peak discharge S_p = sediment peak discharge
 T_f = breach formation time V_w = sediment peak discharge
 B_t = breach top width W_s = released weight of sediment

Table 2.2 Breach erosion simulation of historical dam failures by the BEED model (after Singh, 1996).

water effects, and the models 5 and 6 also breach slope instability.

Brown and Rogers (1977) tested their BRDAM model to the failure of the Teton Dam, Idaho, USA in 1976 (see Anonymous, 1977, and Singh, 1996) and found good agreement between computed and recorded peak flow. The dam-breach model of Ponce and Tsvoglou (1981) was applied to the failure of the Huaccoto Dam (a natural dam formed by a massive landslide) in Peru in 1974. The good reproduction of the basic characteristics of the flood wave is not so remarkable since the same data were used for model calibration. The DAMBRK model of Fread (1984a) was tested on five historical dam failures. The test on the Teton Dam failure showed good agreement between computed and observed hydrographs, see Singh (1996).

In the BREACH model of Fread (1984b) the breach is assumed to have a rectangular shape initially. When the depth of the breach reaches a critical value h_c , the sides of the breach channel collapse and the rectangular-shaped channel is transformed into a trapezoidal channel, see Figure 2.4. The critical depth h_c depends upon the dam's material properties of

internal friction, cohesion and bulk density (see Singh, 1996). The BREACH model was applied to three historical dam failures, among these the failures of the Huaccoto Dam and the Teton Dam. The computed values for outflow rates and final breach widths were in good agreement with the observed values.

In the BEED model of Singh and Scarlatos (1987) the breach is divided into two reaches, a horizontal breach section (at the crest of the dam) and a sloping breach channel (in the downstream slope of the dam). Erosion rates along both stretches are calculated applying the Einstein-Brown (1950) bed-load formula. Side-slope instability is incorporated for saturated soils. Singh and Scarlatos (1987) tested the BEED model to four earth-dam failures: South Fork Dam, Pennsylvania, USA in 1889, Buffalo Creek Dam, West Virginia, USA in 1972, Teton Dam, Idaho, USA, in 1976 (see Table 2.2) and Huaccoto Dam, Peru, in 1974. Figure 2.5 shows the computed breach evolution for the Teton Dam. The calculated value of about 40 m for the width of the final breach at the bottom is in reasonable agreement with the observed value of 46 m, see Singh (1996). According to Brown and Rogers (1977) the observed estimate for the width of the final breach at the dam crest was 198 m; the reviews of historical dam failures of MacDonald and Langridge-Monopolis (1984) and Singh (1996, see Table 2.2) suggest that the top width of the final breach of the Teton Dam failure was not measured.

Havnø et al. (1989) and Bechteler and Broich (1991) applied their models also to the Teton Dam failure. Havnø et al.'s (1989) model predictions for the dimensions of the final breach (width at the bottom of 49 m, width at the dam crest of 186 m) are in close agreement with the observed values. Bechteler and Broich's (1991) results obtained with their program DEICH for the peak flow and the shape of the hydrograph are in good agreement with the corresponding measured data.

Mojib (1990) tested his model to the failure of the Laurel Run Dam, Pennsylvania, USA in 1977. This test has shown good agreement between computed and observed hydrographs.

Singh (1996) has concluded that "the state-of-the-art of dam failure simulation is still in embryonic stage. The complexities involved and the diversity of the knowledge required for thorough and comprehensive simulation are too great at this time. Nevertheless, there has been a significant progress in the modeling technology over the past thirty years."

2.5 Breaching of flood levees on alluvial plains

A series of dike failures along large rivers in Japan between 1953 and 1983 stimulated the Disaster Prevention Research Institute of Kyoto University in Japan to start studies on safety

evaluations of levees (river dikes) and flood-fighting technology' (see Fujita et al., 1984, and Fujita and Tamura, 1987). Fujita and Tamura (1987) performed model experiments in which the dike height H_D was varied from 8 cm to 30 cm. The D_{50} of the sand in their tests was 0.21 mm (H_D : 10 cm and 15 cm), 0.64 mm (H_D : 8 cm, 10 cm and 15 cm) and 1.42 mm (H_D : 10 cm, 20 cm and 30 cm). Fujita and Tamura (1987) observed in their experiments that four phases can be distinguished in the breach erosion process:

- (1) deepening and some widening of initial breach (a pilot channel with a triangular cross-section); the flow rate through the breach is relatively small in this phase; this phase ends when incision of the breach reaches the outside slope;
- (2) enlargement of depth and width of the breach over its entire length resulting in a rapid increase of the discharge rate through the breach;
- (3) widening of the breach at a practically constant discharge rate per unit breach width;
- (4) decrease of the water head over the breach resulting in a minor further widening of the breach; the total discharge rate through the breach is approximately constant.

Unfortunately Fujita and Tamura (1987) have not defined their Phases (2), (3) and (4) in terms of measurable morphological and hydraulic transitions (as in the present model, see Section 3.3.4).

Fujita and Tamura (1987) quite rightly consider the breach erosion process as very difficult to model in detail, and therefore have developed a model based on their observations that a control section appears in the breach opening and that the sediment load from that section can be estimated from ordinary equations for sediment transport. Fujita and Tamura (1987) have applied a bed-load formula in their model similar to Ashida et al.'s (1978) formulation for $\beta = 0$. Fujita and Tamura (1987) have concluded from their study that the calculated values for discharge rate and breach width agree fairly well with the experimental ones.

2.6 Breaching of sand-barriers along coasts

In various coastal areas in the world there are lagoons with entrances to the sea which can be temporarily blocked by a sand barrier. Heavy rainfall may cause a significant rise of the water level in a closed lagoon, leading to overtopping and breaching across the sand barrier. After such a breakout the lagoon becomes tidal until, after some time, the entrance is re-sealed with sand transported into the mouth by wave activity (Gordon, 1991), see Figure 2.6. With the entrance closed, heavy rainfall may induce again a water level rise in the lagoon and a subsequent breaching of the barrier. Some lagoons are subjected to several breakouts and closures in one year.

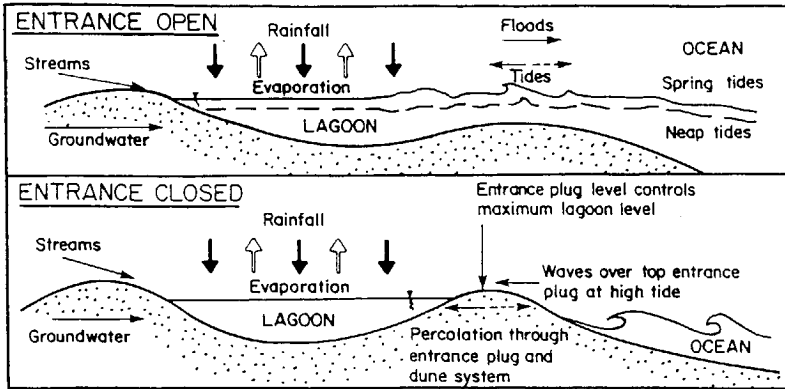


Figure 2.6 Lagoon water balance (after Gordon, 1991).

Increasing urbanization around lagoons has stimulated studies to develop strategies for the control of both level and quality of the water in the lagoon. Gordon (1991) has described field observations of both the lagoon water balance and the entrance behaviour, and model studies of the breaching process. These observations have shown that the breakout process of closed lagoons has three distinct stages:

- (1) slow cutback across the barrier in the initiation channel stage;
- (2) formation of a curved weir upstream in the sand plug behind the beach berm and then rapid widening of the breach (Froude number $Fr > 1$);
- (3) the river flow stage ($Fr < 1$).

Odd et al. (1995) have described a breakout from the $5 \cdot 10^5 \text{ m}^2$ Wamberal Lagoon (New South Wales, Australia) on 13 September 1993. The breakout process of this lagoon followed the three stages described above. In Stage (1), which lasted about two hours, the channel widened from 3 m to 9 m. The flow was subcritical except on the 1 : 10 beach slope, where the flow was supercritical and created a step in the bottom of the breach which moved upstream due to erosion (Odd et al., 1995). In Stage (2) a crescent shaped weir was formed in the sand plug which controlled the rate of flow into the channel. The flow in the channel was supercritical throughout its length. In Stage (2) the flow depth was about 1 m and the breach widened from 9 m to 50 m in about 1.5 hours. In Stage (3) the flow was subcritical and the rate of widening and deepening was almost negligible during the 30 minutes that this stage lasted.

Odd et al. (1995) have applied and calibrated a modified version of TELEMAC (a 2D

finite element system developed by Laboratoire National d'Hydraulique, Chatou, France) to the breakout of the Wamberal Lagoon. Sand transport rates were calculated with Van Rijn's (1984a,b) formulations. Van Rijn's (1984b) suspended sand transport rates, however, had to be multiplied by a factor 4 in order to achieve good agreements with the observations.

2.7 Discussion

Singh (1986) has concluded that "the technology of earth-dam breaching is far from advanced and is still in the early stages". This conclusion applies also to breaching of dikes. In view of the many kilometres of dikes built in The Netherlands, and the numerous failures of these structures (see Chapter 1), it is in fact astonishing that the state-of-the-art of simulation of dike breaching is so poor and that only rather recently the first serious attempts were undertaken to describe mathematically the process of breach growth in dikes.

To the author's knowledge, only very limited data are available of the numerous historical failures of earth-dams and dikes all over the world (as may be concluded from the poor data described in this and previous chapter). Of course, when an earth-dam or dike fails, life of people and animals may be in danger and collecting data will not have priority. However, this explains only partly the lack of accurate and detailed data. The main cause is that the importance of collecting and preserving data was not emphasized until recently.

As described in Chapter 1 it is the aim of the present study to fill in some of the voids in the knowledge of the breach erosion process of sand-dikes.

Chapter 3

Breach erosion process

3.1 Introduction

The purpose of this chapter is to describe qualitatively the process of breaching in sand-dikes. It is assumed that there is a relatively small initial breach in the top of the dike which is so large that water flows through it starting the breach erosion process. Several causes for the formation of an initial breach can be distinguished, depending on the hydraulic conditions and the strength and structure of the dike. The main causes of failure for dikes in The Netherlands are (also called failure mechanisms, see TAW/CUR, 1990 and 1991):

1. overflowing and wave overtopping,
2. sliding of inner slope or outer slope,
3. erosion of outer slope,
4. piping and seepage.

These causes of failure are described in Paragraph 3.2.

The flow velocities in the initial breach are critical and supercritical, i.e. already relatively high shortly after the formation of the initial breach. The entrainment of sand from the dike body by this flow starts the breach erosion process. In this process five successive stages can be distinguished. These stages are described in Paragraph 3.3.

3.2 Causes of failure of dikes

3.2.1 Overflowing and wave overtopping

It is obvious that if the water level at a dike exceeds the level of the crest, water will flow over it. This is called overflowing or overtopping by water level (TAW/CUR, 1990). Overtopping waves can also cause ingress of water into the polder or, in case of overflowing water, increase the impact of the overflowing water on the crest and the inner slope of the dike.

If the dike remains completely intact, the total flow rate by overtopping will generally be limited and need not lead to catastrophic flooding of the polder, unless the polder area is very small. Anyhow, breaching will not occur, and for the simulation of the inundation of

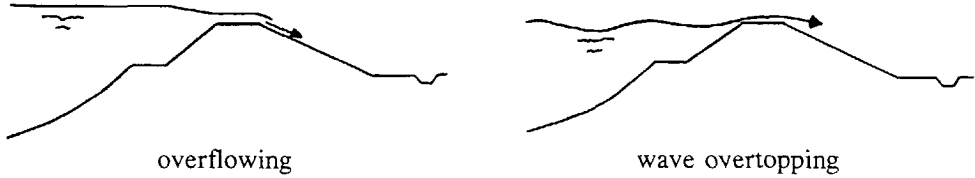


Figure 3.1 Overflowing and wave overtopping.

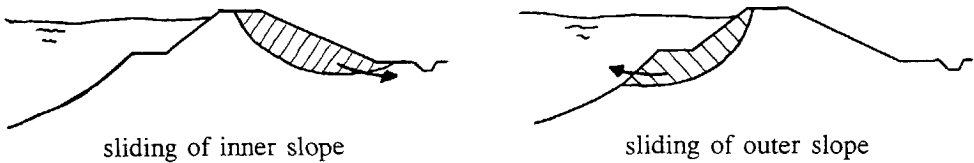


Figure 3.2 Sliding of inner slope or outer slope.

the polder it is not necessary to have a breach erosion model.

The overtopping water will partly infiltrate into the inner slope, leading to a decrease of the stability of the slope due to saturation or air inclusion; both effects may induce slip of the inner slope. Allersma et al. (1994) observed in their tests in a small geotechnical centrifuge that the failure of sand-dikes during water infiltration at the top is initiated by local instability induced by seepage (see Section 3.2.4). Overtopping water flowing down the inner slope may also erode this slope. Both slip and erosion of the inner slope, and the mechanisms possibly induced by them (as sliding of larger parts of one of the slopes, see Section 3.2.2), can initiate the development of a breach in the dike.

3.2.2 Sliding of inner or outer slope

A high water level at a dike causes water to penetrate into the dike body, initiating an increase of both ground water pressures and weight of the ground. Long lasting high water at a dike can cause sliding of a slope along a failure surface (in Figure 3.2 a circle with a certain radius). Such a macro-instability occurs when the overturning moment (increased by the weight increase of the ground) becomes larger than the resisting moment (decreased by



Figure 3.3 Erosion of outer slope.

the increase of the water pressures and the resulting decrease of the intergranular pressures and the internal shearing resistance). Both inner and outer slope can slide; especially a rapid fall of the water level after a long lasting high water may endanger the stability of the outer slope.

3.2.3 Erosion of outer slope

Waves and large flow velocities may induce erosion of the revetment and the clay-layer of the outer slope (see Figure 3.3). The rate of erosion depends on the hydraulic conditions and on the type of revetment (stone, asphalt or grass) and its condition. The clay layers of river dikes are mainly covered with grass and locally, where some wave attack can be expected, with stone revetments. The outer slope of a sea dike is generally covered by a robust revetment of concrete blocks or asphalt to protect the clay-layer against the more intense (compared with river dikes) wave attack.

The resistance of a dike against further erosion by waves and flow velocities dramatically decreases when the erosion of the outer slope has uncovered the sand-core of the dike.

3.2.4 Seepage and piping

A long lasting high water level may cause a ground-water flow through the dike, seeping out at the lower section of the inner slope (see Figure 3.4). This seepage may erode soil particles from the surface of the inner slope (see TAW/CUR, 1990). In practice, this erosion occurs in non-cohesive materials as sand.

Seepage of water through a sand layer under a dike may result in the entrainment of sand particles by this flow, resulting in the formation of boils discharging water with sand. In The Netherlands such boils have frequently been observed, not only along river dikes but also along sea dikes (TAW/CUR, 1990). When large amounts of sand are transported, this process is called piping (see Figure 3.5). Piping undermines the dike and can induce a local collapse of the dike body resulting in a start of the breaching process.



Figure 3.4 Seepage.

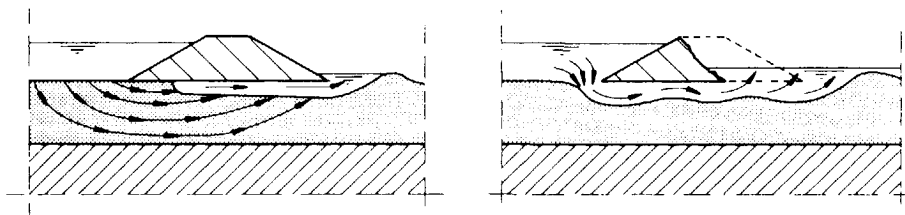


Figure 3.5 Piping.

3.2.5 Initial breach

The above enumeration of possible causes of failure of dikes is slightly schematized. Combinations of failure mechanisms are also possible and can result in the formation of an initial breach through which water starts to flow. Most of the failure mechanisms will induce a breach at the top of the dike. Also in case of 'piping', the 'pipe' through the dike will collapse after some time, resulting in a breach at the dike crest.

Hence it can be assumed that the initial breach is located at the top of the dike. As stated in Chapter 1, it is also assumed that the initial damage is so large that it has uncovered the sand core of the dike. Then it may be expected that the remaining revetments and clay-layers can hardly resist the strong flow through the (initial) breach and that the dike breaches more or less like a sand-dike.

From historical descriptions of dike-bursts less is known about the shape of initial breaches. Therefore, and to avoid needless complexities in the mathematical model, it is assumed that the initial breach has a trapezoidal cross-section with side-slope angles γ about equal to the angle of repose ϕ (see Paragraph 3.3 and Chapters 4 and 7).

3.3 Process of breach erosion

3.3.1 Introduction

As stated above the breach erosion is assumed to start (at $t = t_0$) with the flow of water through a small initial breach at the top of the sand-dike. It will be outlined in this paragraph that in general five stages can be distinguished in the process of breach erosion (see Figure 3.6). These five stages are:

- I. Steepening of the slope angle β of the channel in the inner slope from an initial value β_0 at $t = t_0$ up to a critical value β_1 at $t = t_1$.
- II. Retrograde erosion of the inner slope at constant angle β_1 for $t_1 < t \leq t_2$, yielding a decrease of the width of the crest of the dike in the breach; this stage ends at t_2 when the crest vanishes and the breach inflow starts to increase.
- III. Lowering of the top of the dike in the breach, with constant angle of the breach side-slopes and equal to the critical value γ_1 , resulting in an increase of the width of the breach for $t_2 < t \leq t_3$. At $t = t_3$ the dike in the breach is completely washed out down to the base of the dike at polder level.
- IV. Critical flow stage, in which the breach flow is virtually critical throughout the breach for $t_3 < t \leq t_4$, and the breach continues to grow mainly laterally. The side-slope angles remain at the critical value γ_1 . The breach growth in vertical direction depends in this stage on the erodibility of the base of the dike. At t_4 the flow through the breach changes from critical ($Fr = 1$ for $t_3 < t \leq t_4$ to subcritical ($Fr < 1$ for $t > t_4$).
- V. Subcritical flow stage, in which the breach continues to grow, mainly laterally due to the subcritical flow in the breach for $t_4 < t \leq t_5$. At t_5 the flow velocities in the breach become so small (incipient motion) that the breach erosion stops. The side-slope angles remain at the critical value γ_1 . The flow through the breach continues and stops when at t_6 the water level in the polder has equalled the outside water level.

In Stages I, II and III the initial breach cuts itself into the dike. Most of the discharge through the breach takes place in the Stages IV and V. At the end of Stage IV backwater starts to effect the flow through the breach. In case of a relatively tiny polder with a very small storage capacity, the downstream submergence may start earlier. In theory this may occur in each of the Stages I, II and III. In practice, however, it will take place in Stage III, since the total flow through the breach is too small in Stages I and II to allow downstream submergence. Hence, in case of a relatively tiny polder, Stage IV may be passed over.

The breach growth processes in Stages I, II and III are described qualitatively in Section 3.3.2, those in Stages IV and V in Section 3.3.3. The mathematical descriptions of the five stages are given in Chapter 4.

Breach growth in sand-dikes

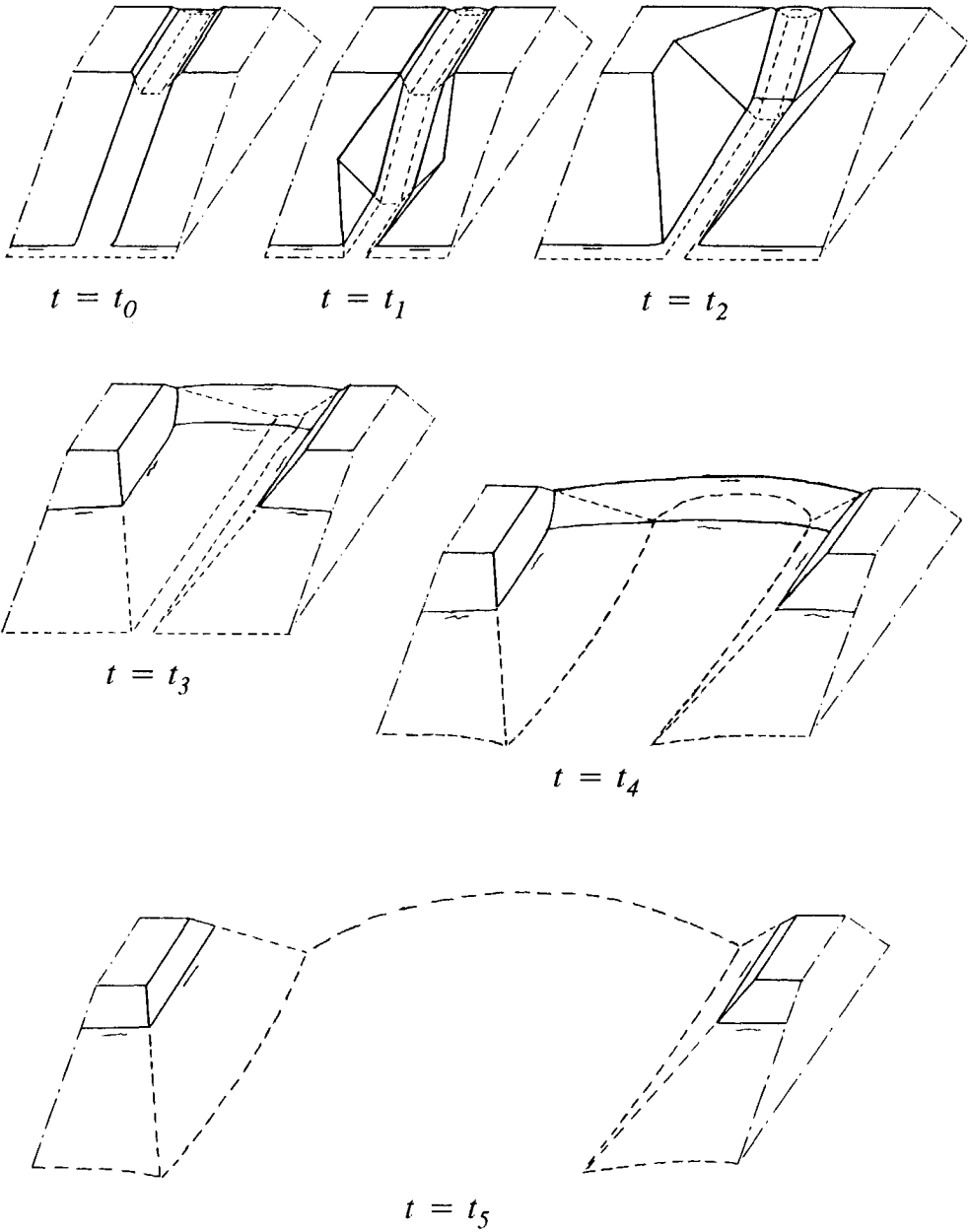


Figure 3.6 Schematic illustration of breach growth in a sand-dike.

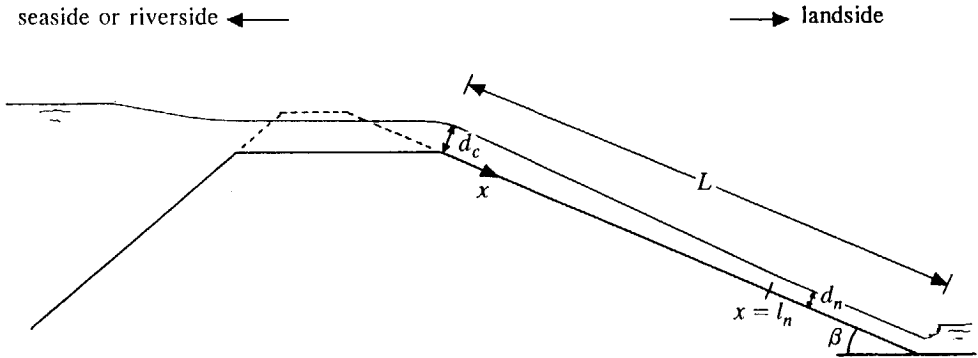


Figure 3.7 Cross-section over initial breach in Stage I shortly after the start of the breaching process.

3.3.2 Development of initial breach in Stages I, II and III

Figure 3.7 shows a cross-section of the dike over the initial breach at $t = t_0^+$ shortly after the start of the breaching process at $t = t_0$. From a hydraulic point of view the slopes of dikes are very steep, i.e. $\sin\beta \gg C_f$ (the slope angle β is defined here as the inclination of the inner slope or scour hole in the flow direction with respect to a horizontal line, C_f is the bottom friction coefficient, see Chapter 4). This means that the water depth at the top of the inner slope at $x = 0$ (x is the coordinate along the inner slope) is equal to the critical depth d_c . The flow on the inner slope accelerates between $x = 0$ and $x = l_n$, and is virtually uniform for $x \geq l_n$. Consequently the capacity to transport sand also increases along the stretch $0 < x < l_n$ and is nearly constant for $x \geq l_n$. This means (in Chapter 4 it is shown mathematically) that the rate of erosion increases between $x = 0$ and $x = l_n$ and is virtually constant for $l_n \leq x \leq l_a$ (where l_a is the adaptation length of the suspended sediment transport, similarly to l_n being the adaptation length of the flow). As a result of this the inner slope becomes steeper and steeper along the slope and in time for $0 < x < l_n$, and for $l_n \leq x \leq l_a$ the inclination of the inner slope remains constant, see Figure 3.8. The slope angle along the stretch $0 < x < l_n$ will, however, not exceed a limit β_1 (say $\beta_1 \approx \phi$, where ϕ is the angle of internal friction). If this limit has been reached along the entire stretch $0 < x < l_n$ (at $t = t_1$), the rate of erosion becomes constant for $0 \leq x < l_n$ as indicated by the lines for $t \geq t_1$ in Figure 3.8, and Stage II starts.

In Stage II retrograde of the inner slope of the dike in the breach occurs at constant angle β_1 , resulting in a decrease of the width of the crest of the dike in the breach. Stage II ends when the width of the crest has become zero (at $t = t_2$).

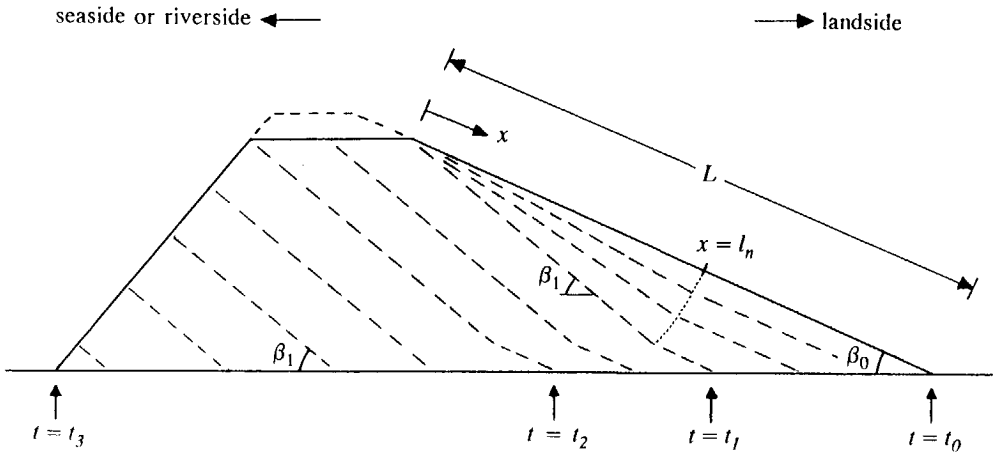


Figure 3.8 Erosion inner slope in Stages I, II and III if $l_n < L < l_a$.

It can be concluded that for $t_0 < t \leq t_2$ the rate of erosion of the inner slope in the breach is controlled by the erosion at $x = l_n$ (or also by the erosion along $l_n \leq x \leq l_a$). This means that only the rate of erosion at $x = l_n$ has to be known.

In Stage I the width of the channel (initial breach) in the crown of the dike remains at its initial value. The increase of the depth of the channel in the inner slope causes also an increase of the width of this channel in the slope (see Figure 3.6). At $t = t_1$ the width of the breach starts to grow at the downstream side of the dike-crown.

If the length L of the inner slope is larger than the adaptation length l_a of the suspended load transport, the increase in sediment transport rate stops at $x = l_a$ and consequently the erosion along $x > l_a$ also stops. After some time a bar will be formed at $x \approx l_a$ (see Figure 3.9), causing a significant deceleration of the supercritical flow, so also an increase of the turbulence intensity for $x \approx l_a$. More turbulence increases the sediment transport capacity, which means that, with some delay, also the sediment downstream of $x = l_a$ will be removed (as observed in the Schelde Flume experiments, see Figures 5.1 and 5.2, see also Steetzel and Visser, 1992, 1993).

The removal of the sediment near $x \approx l_a$ is likely not complete if the length L of the inner slope is much longer than the adaptation length l_a (see Figure 3.10). Then the erosion of the inner slope takes place in two steps: in the first step the crown of the dike will be

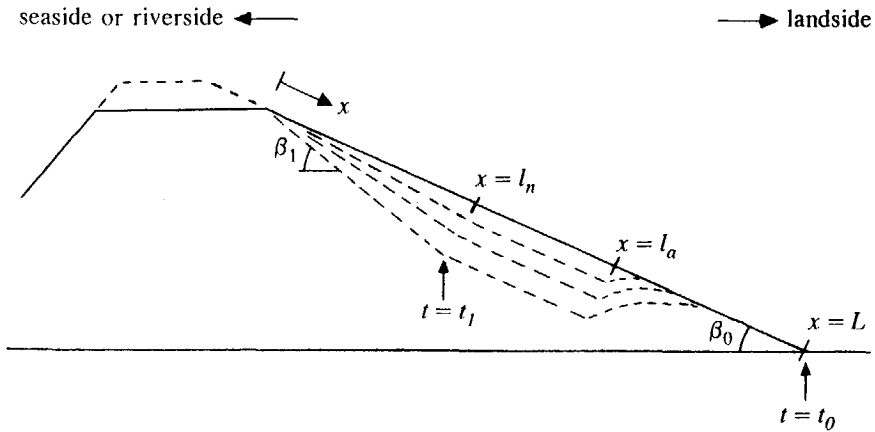


Figure 3.9 Erosion inner slope if $L > l_a$.

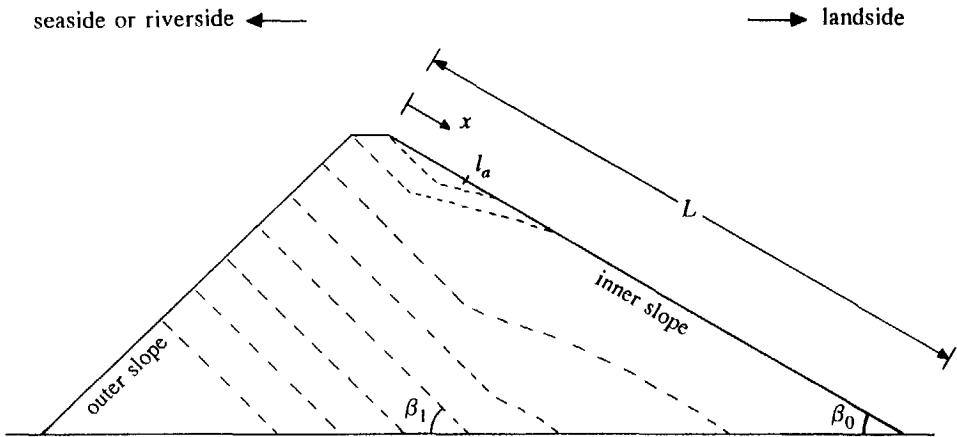


Figure 3.10 Erosion inner slope if $L \gg l_a$.

lowered (see Figure 3.10), and in the second step the resulting larger flow rate removes the remaining sediment further down on the inner slope (after which the erosion process proceeds as shown in Figure 3.8).

As long as the flow accelerates, its capacity to transport sediment increases. This means that the adaptation length for the sediment transport is always larger than the adaptation length

Breach growth in sand-dikes

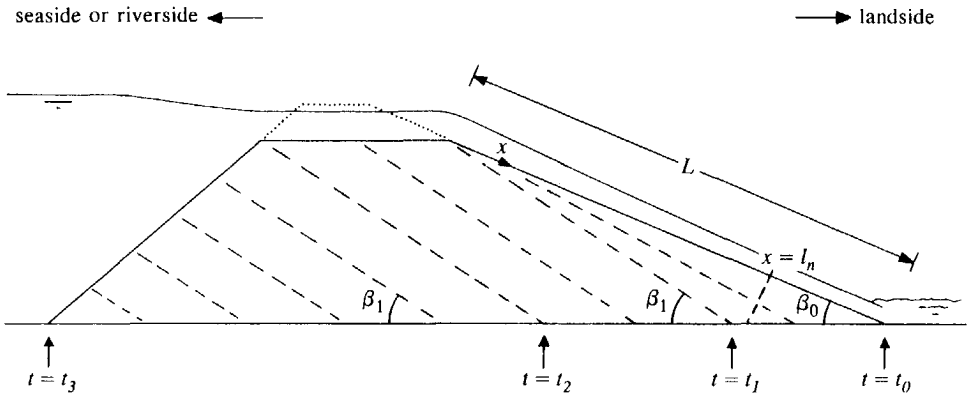


Figure 3.11 Flow on inner slope of dike in breach in Stage I (solid line) and development of this slope in Stages I, II and III (dashed lines) for a typical dike in The Netherlands (i.e. $l_n \approx L \leq l_a$).

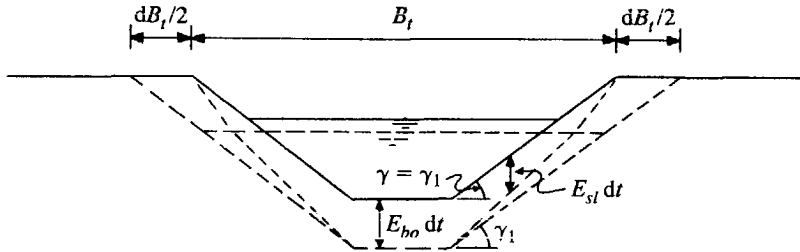


Figure 3.12 Increase dB_t in time dt of breach width B_t near the inflow in Stage III.

for the flow, i.e. $l_a > l_n$. In Section 4.2.1 the following practical approximation for l_n is derived:

$$\frac{l_n}{L} \approx 10 \frac{h}{H_D} \tag{3.1}$$

where h is the depth of the breach in the crest of the dike, H_D is the height of the dike above the polder level Z_p and L is the length of the inner slope.

A relatively high dike in The Netherlands has a height $H_D \approx 10$ m. If it is assumed that $h \approx 1$ m (i.e. the 1 m thick clay-layer at the crest of the dike has been washed out by the high

water), then the ratio $l_n/L \approx 1$. Hence, the development of the inner slope in Stages I and II of the breach erosion process of such a typical dike will be as shown in Figure 3.11, which is easier to describe mathematically than the developments shown in Figures 3.9 and 3.10 (if $l_a < L$).

Figure 3.11 shows also the triangular cross-section of the dike through the axis of the breach at $t = t_2$. Due to the proceeding erosion process, the top of the dike in the breach starts to drop. As a result, both the discharge per unit width q_{br} and the breach width (see Section 4.3.2) increase for $t_2 < t \leq t_3$. The increase of q_{br} involves an increase of l_n , see equation (4.20). So if $l_n < L$ at $t = t_2$, this generally will change into $l_n > L$ in the course of Stage III. It is assumed that also in this stage the angle of the inner slope remains at the critical value β_1 . So again the rate of erosion is constant along the entire stretch $0 \leq x \leq l_n$, and also in the interval $t_2 < t < t_3$ it is entirely determined by the erosion at the toe of the slope.

At $t = t_2$ the width of the breach at the upstream side of the crown also starts to grow (see Figure 3.6). The rate of erosion at the breach bottom (E_{bo}) is larger than the erosion rate at the side-slopes (E_{sl}) due to the larger flow velocities (as a result of the larger water depths). For the same reason the erosion rate at the toe of the side-slopes is larger than higher on the slopes. This means that in Stage III the width B_t of the breach at the dike crest increases as shown in Figure 3.12 and that the side-slope erosion is entirely controlled by the erosion at the bottom (i.e. the increase of the breach depth). Hence, the rate of increase of breach width is controlled by the rate of erosion at the breach bottom:

$$\frac{dB_t}{dt} = \frac{2}{\tan\gamma_1} E_{bo} \quad (3.2)$$

In Stage III the breach growth accelerates drastically when deepening of the breach opening magnifies the inflow rate and the latter accelerates the erosion process. Consequently the flow and the sediment transport through the breach change drastically in this stage: from a supercritical flow with a Froude number $Fr \gg 1$ at $t = t_2$ to a supercritical flow with Fr slightly above 1 at $t = t_3$, from sheet flow transport with a Shields' mobility parameter θ of orders 10 and 100 at $t = t_2$ to sediment transport with θ of order 1 at $t = t_3$ (see Chapter 5).

It is clear that the duration of the breach erosion process in Stages I, II and III depends largely on the dimensions of the initial breach. The larger these are, the shorter the total duration of these stages is, and consequently an accurate description of the breach erosion process in Stages I, II and III is then less important for the evaluation of the rate of flooding of the protected low-lying land.

Breach growth in sand-dikes

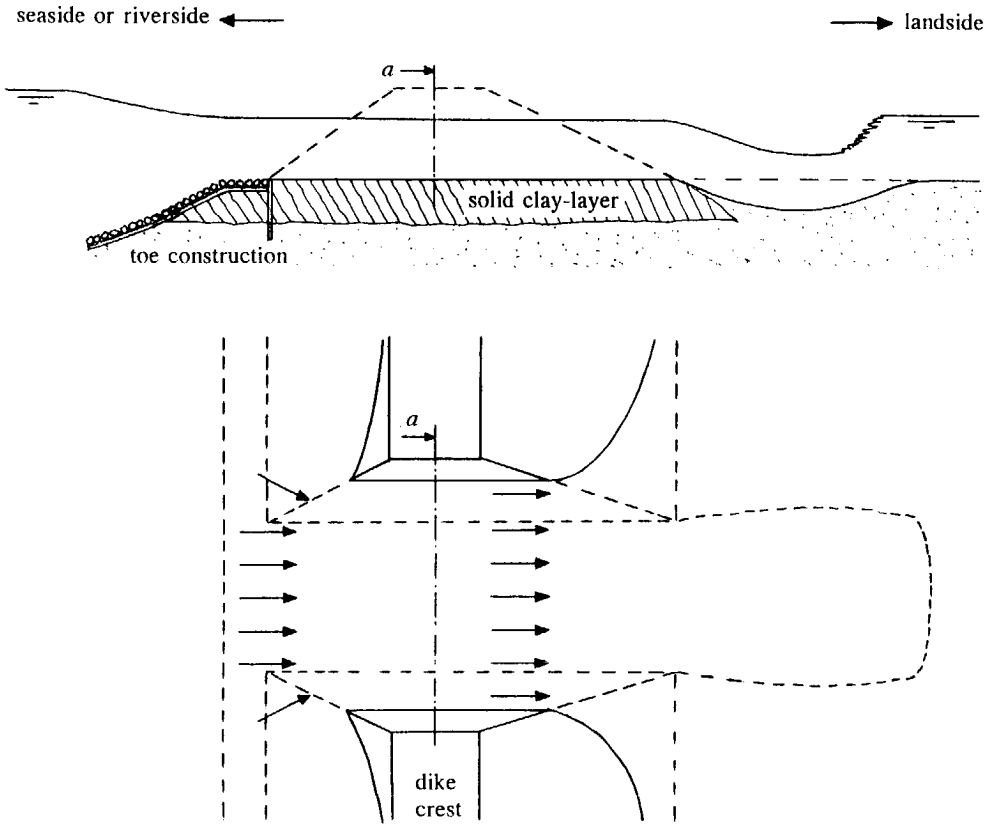


Figure 3.13 Cross-section and top view of flow in Stage IV through a breach in a dike constructed on a solid clay-layer (Type A breach).

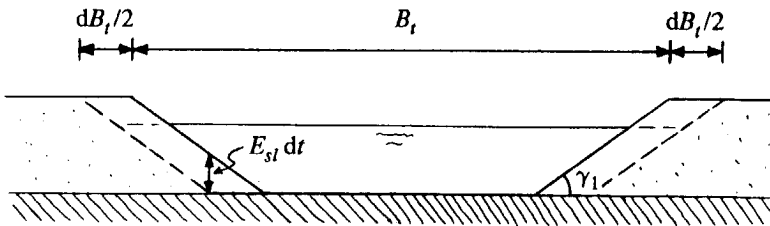


Figure 3.14 Cross-section of breach (cross-section a, see Figure 3.13) showing increase of the breach width in a Type A breach in Stages IV and V (B_t is breach width at the dike crest).

3.3.3 Breach development in Stages IV and V

The continuation of the breach erosion process after the complete wash-out of the dike in the breach at t_3 depends on the following geometrical and material conditions of the dike:

- the resistance against further erosion of the base of the dike;
- the presence or absence of a toe construction at the toe of the outer slope and its ability to protect the outer slope against further erosion;
- the presence or absence of a relatively high foreland and its resistance against erosion.

Three types of breaches can be distinguished, dependent of these conditions. In a Type A breach the vertical erosion at the breach inflow is prevented by a solid clay foundation of the dike, or by a solid toe construction on the outer slope or by a solid, relatively high foreland (solid means here: with relatively high resistance against erosion). Dikes breach as Types B or C in the absence of a solid clay foundation, or a solid toe construction or a solid high foreland. If a relatively high (erodible) foreland is present then the dike breaches as Type B, otherwise as Type C. The Types A, B and C breaches are described further in next.

Type A breach

If the base of the dike consists of a solid clay-layer, then this layer will considerably slow down or prevent further vertical erosion, see Figure 3.13. This means that the breach continues to grow laterally in Stages IV and V, as shown in Figure 3.14. Since the erosion at the toe of the side-slopes is larger than higher on the slopes, the angle γ remains at its critical value γ_1 . Hence, the erosion at the toe of each of the side-slopes (E_{sl} in Figure 3.14) determines the erosion of the overall side-slope, and consequently also the growth of the breach width. The discharge through the breach can be described simply by the formula for the flow over a broad-crested weir (see Chapter 4).

The lower parts of the outer slopes of sea dikes and river dikes in The Netherlands are protected against waves and currents by a toe construction (for instance a mattress of brushwood with rip-rap and a row of wooden piles), see Figures 3.13 and 3.15. Less is known about the behaviour of toe constructions in breaching dikes. It is, however, likely that these constructions may hinder or slow down further growth of the scour hole in upstream direction in cases where the foundation of the dike does not consist of solid clay. Downstream of this toe construction the breach continues to grow in vertical direction resulting in the formation of a scour hole, see Figure 3.15. The toe construction acts as a spillway (broad-crested or sharp-crested, which has only a secondary influence on the discharge coefficient of the spillway) controlling the breach inflow rate. It is outlined in Chapter 4 that also the growth of the breach width is determined at this upstream control section, resulting in an increase of the breach width as in the above situation of an erosion resistant base of the dike.

Breach growth in sand-dikes

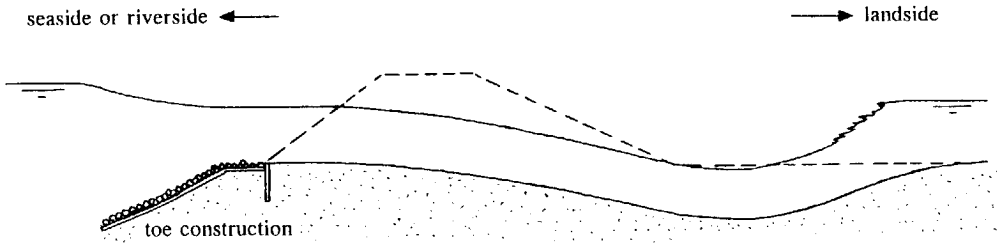


Figure 3.15 Flow in Stage IV through a breach when a toe construction protects the lower part of the outer slope against further erosion.

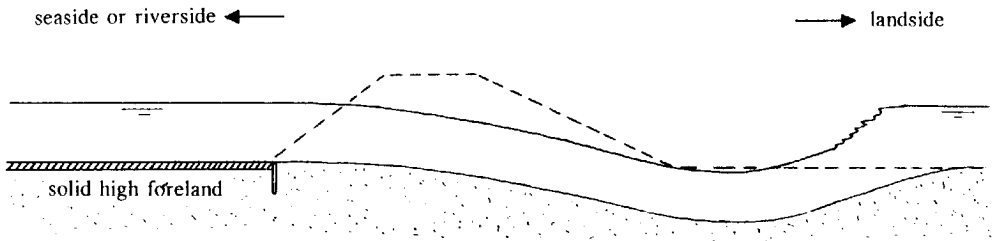


Figure 3.16 Flow in Stage IV through a breach in a dike with a relatively high foreland which has a large resistance against erosion.

In cases where the dike has a relatively high foreland with a relatively large resistance against erosion, the development of the breach inflow and the breach growth is similar to that of a dike with a solid toe construction on the outer slope, see Figure 3.16.

An example of a dike-burst where a solid clay-layer and a toe construction slowed down the vertical erosion is the failure of the Noord Dike (in Dutch 'Noorddijk') in Papendrecht on 1 February 1953, see Figure 3.17. This dike failed just at the site of an auxiliary spillway (in Dutch 'hulpgat'). At the location of an auxiliary spillway the dike has a core of sand that can be dug off quickly, and a foundation of solid clay that can act as a spillway in order to drain water into the river after inundation of the polder.

The breach in the Noord Dike was closed on 5 February 1953, only four days after its failure. This timely closure has limited the maximum depth of the scour hole downstream of the breach to about NAP - 7.2 m⁴.

⁴) NAP is 'Normaal Amsterdams Peil' (Normal Amsterdam Level), being the reference level in The Netherlands at about mean sea level.

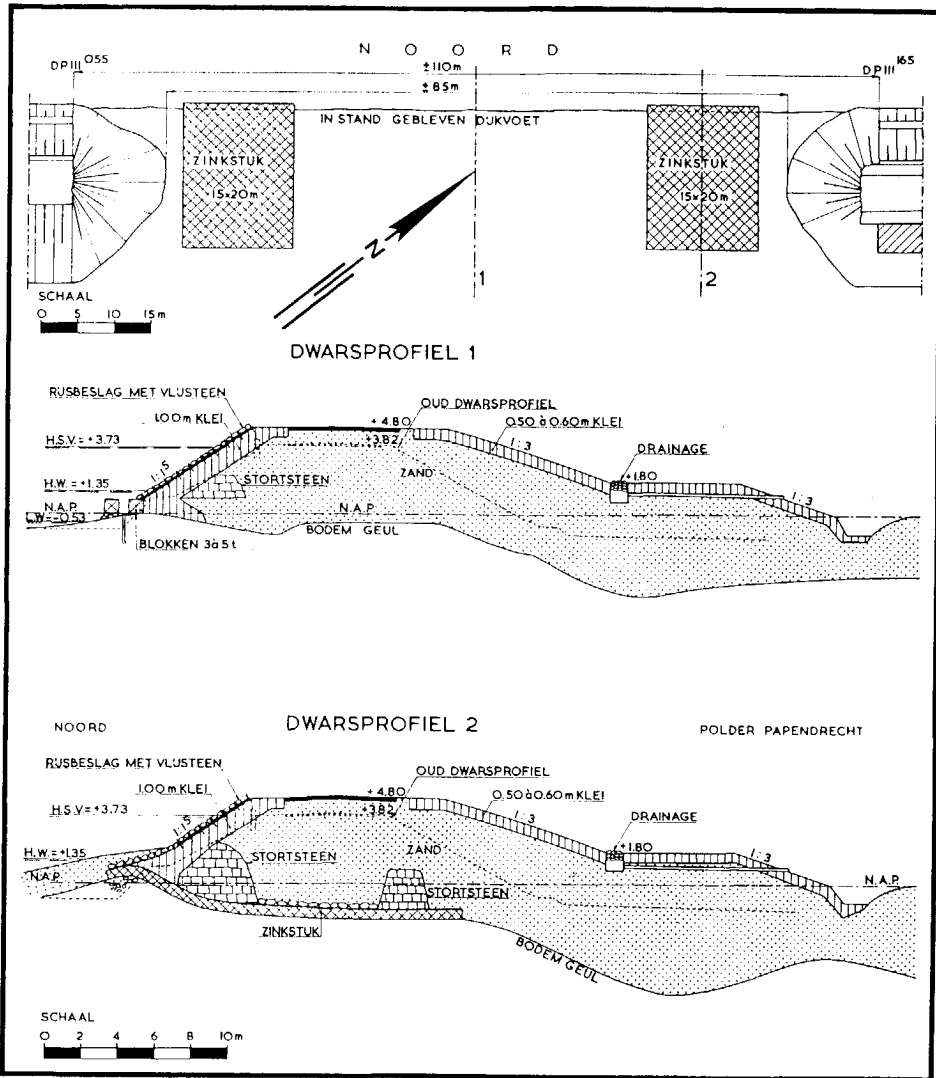


Figure 3.17 Top view and cross-sections over final breach in Noord Dike in Papendrecht (The Netherlands, 1953 flood, after Rijkswaterstaat, 1961); the figure also shows cross-sections over the reconstructed Noord Dike (see List of Dutch words for English translations).

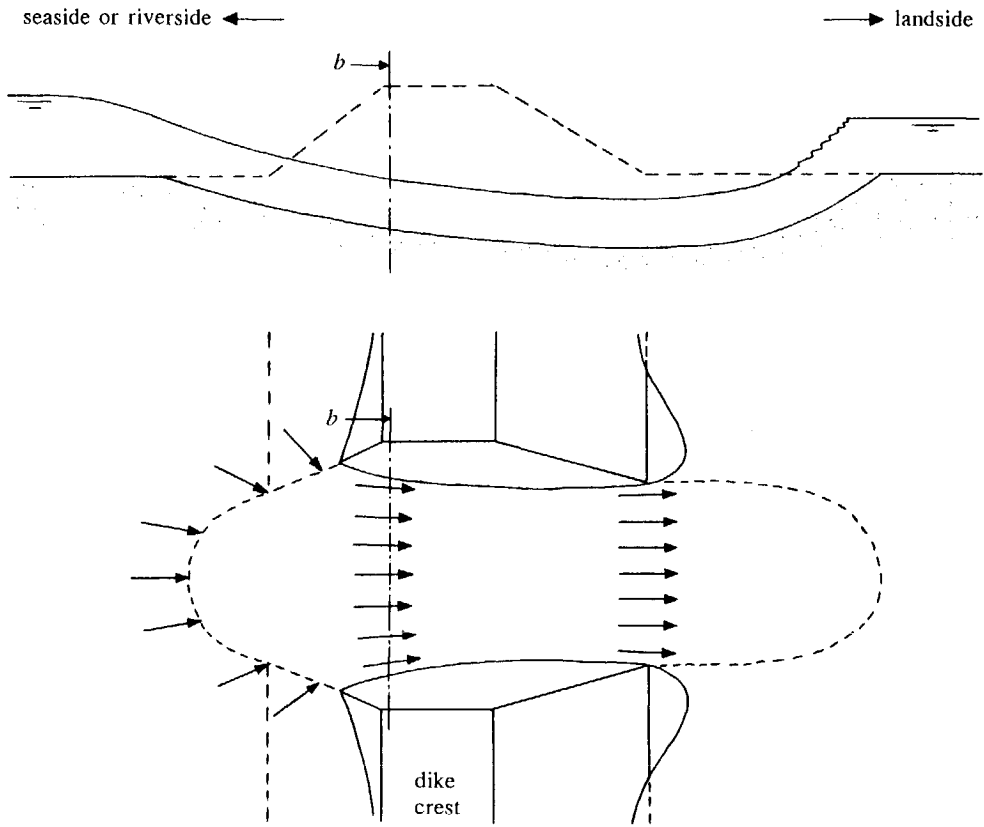


Figure 3.18 Cross-section of breaching dike in Stage IV in a Type B breach.

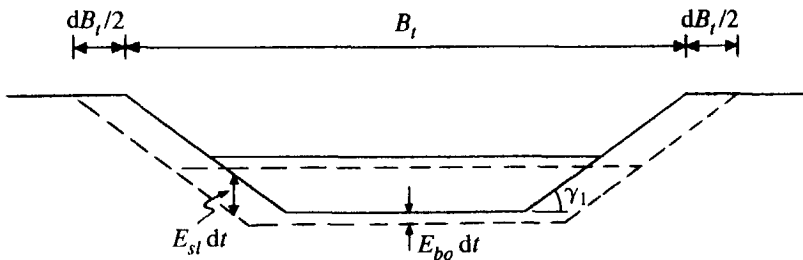


Figure 3.19 Cross-section of breach (cross-section b , see Figure 3.18) showing growth of breach width B_t in Stages IV and V in a Type B breach.

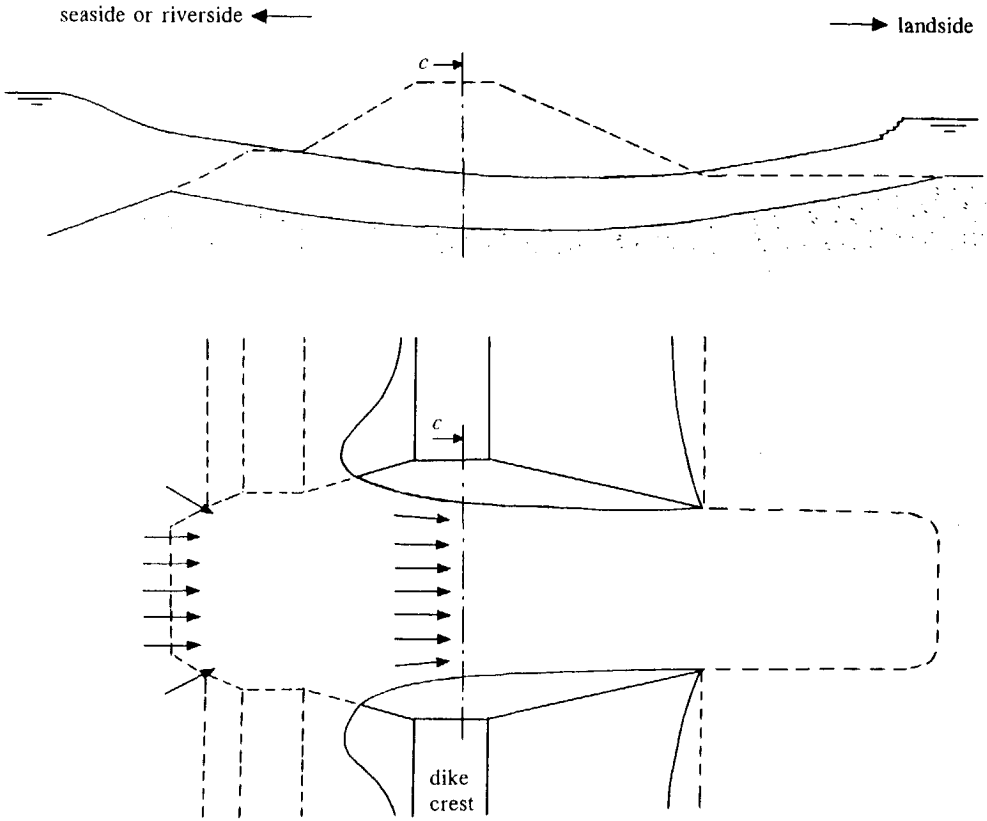


Figure 3.20 Cross-section of breaching dike in Stage IV in a Type C breach.

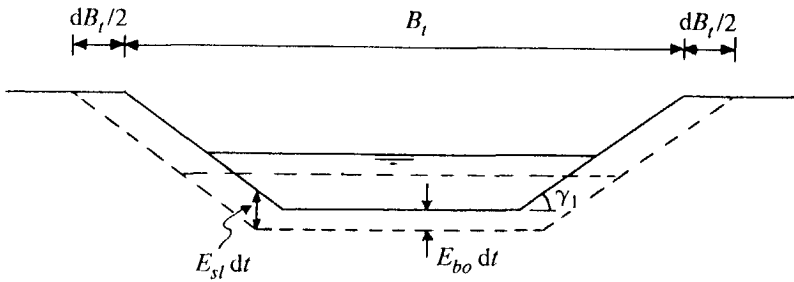


Figure 3.21 Cross-section of breach (cross-section c, see Figure 3.20) showing growth of breach width B_t in Stages IV and V in a Type C breach.

Types B and C breaches

If the base of the dike does not have much resistant against erosion and the dike does not have a solid toe construction, the breach continues to grow vertically (scour hole grows both with and against the flow, see Figures 3.18 and 3.20) and laterally (widening of the breach, see Figures 3.19 and 3.21). Upstream of the breach a spillway is formed which controls the breach inflow. The alignment of this spillway depends on the height of the foreland in front of the dike. The alignment of the overfall will be curved (elliptic or circular) in a Type B breach in a dike with a relatively high foreland (see Figure 3.18). In a situation where the outer slope abuts on the water the shape of the spillway will be straight in the middle and curved near the side-slopes; this is called a Type C breach (see Figure 3.20).

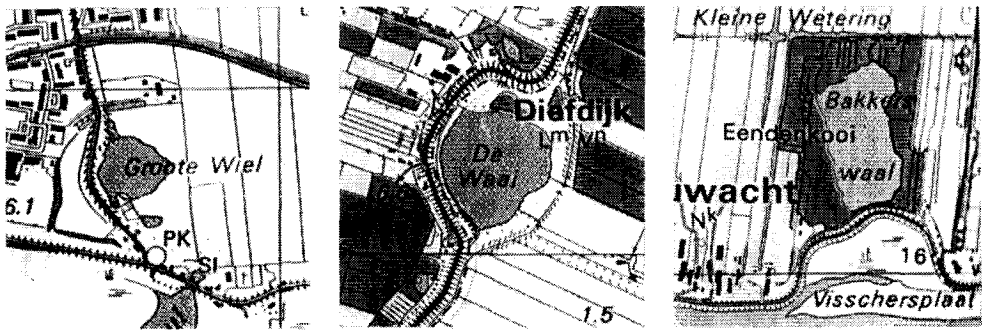


Figure 3.22 Top views of scour pools scoured in a Type A breach (Groote Wiel in Gorinchem), in a Type B breach (De Waai along the Diefdike⁵⁾ in Culemborg) and in a Type C breach (Bakkerswaal in Nederlek), all in The Netherlands.

Figure 3.22 shows outlines of scour pools⁶⁾ scoured in Types A, B and C of breaching. The Groote Wiel in Gorinchem is an example of the result of the scouring process in a Type A breach, i.e. no scouring upstream of the breach, consequently the dike could be reconstructed almost along its old alignment. The pool scoured in a Type A breach extends only towards

⁵⁾ In Dutch 'Diefdijk'.

⁶⁾ A scour pool is in Dutch a 'wiel', also called 'waal', 'weel' and 'waai'. The many scour pools still existing along the rivers and in the delta area in The Netherlands reflect the many dike failures in the past. Some of these scour pools have relatively large depths (up to 20 m).

the downstream end of the dike.

The Diefdike is part of the old Dutch water defence line. It is a dike without a water course (as a secondary dike), with slopes covered with only grass and not with revetments, and with toes of the slopes not protected against erosion by toe constructions. De Waai along the Diefdike (see Figure 3.22) is a clear example of a scour pool scoured in a Type B breach, i.e. with scouring both upstream and downstream of the dike. Reconstruction of the dike along its original alignment would have required large amounts of soil, hence the dike was rebuilt round about the relatively deep scour hole instead of right across it. Hence, a Type B breach brings on a more or less circular scour pool with its centre approximately at the original dike alignment.

The Bakkerswaal in Nederlek may possibly⁷⁾ be considered as an example of a scour pool scoured in a Type C breach. It is entirely situated at one side of the original dike trace, and it has a more or less rectangular shape with a width comparable to that of a Type A scour pool and a length that is considerably larger.

As described in Section 3.3.2, the growth of the breach width in Stage III is controlled by the rate of erosion at the breach bottom (E_{bo}), and not by the erosion rate at the side-slopes (E_{sl}). In Stages IV and V, however, it is the erosion rate at the side-slopes (E_{sl}) which determines the increase of the breach width (see Figures 3.14, 3.19 and 3.21):

$$\frac{dB_t}{dt} = \frac{2}{\tan\gamma_1} E_{sl} \quad (3.3)$$

The argument behind this conclusion is simple. The order of magnitude of the widths of final-breaches is 100 m (see Table 3.1), while the order of magnitude of their depths is 10 m. Hence, the widths of final breaches have always been much larger than their depths, so that

$$E_{bo} \ll \frac{2}{\tan\gamma_1} E_{sl} \quad (3.4)$$

In scour pools developed in Type A breaches these maximal depths are located downstream of the dike and not in the breach itself at the original location of the dike, see Figure 3.17.

In Stage V ($t_4 < t \leq t_5$) the breach continues to grow laterally. The continuous flow through the breach causes the water level in the polder to increase and the flow velocity in the breach

⁷⁾ Both historical research and soil exploration at the site are necessary for a more accurate characterisation of this scour pool. To some lesser amount this applies also to the other scour pools of Figure 3.22.

Breach growth in sand-dikes

Place, river or dike, name of scour pool	Type ⁸⁾	Width [m]	Length [m]
Alblasserdam, Noord, Rijkenwaal	C	100	150
Alblasserdam, Noord, Lammetjeswaal	A or C	100	250
Ameide, Zouwendijk, De Zouwe	B	130	230
Boven-Hardinxveld, Merwede	A	80	80
Culemborg, Diefdijk, De Waai	B	230	200
Dalem, Waal	A	120	70
Gorinchem, Waal, Groote Wiel	A	120	150
Nederlek, Lek, Bakkerswaal	A or C	130	300
Papendrecht, Noord, Noordhoekse Wiel	A	100	150
Papendrecht, Merwede, Groote Wiel	A	100	100

Table 3.1 Typical examples of scour pools along the rivers Lek, Merwede, Noord and Waal in The Netherlands and their widths (measured along the dike) and lengths; the Zouwendijk and the Diefdijk are secondary dikes in the polders Alblasserwaard and Culemborgerwaard respectively.

to decrease, resulting in a deceleration of the breach growth.

At t_5 the flow velocities in the breach become so small (incipient motion) that the breach erosion stops. As far as the rate of flooding of the polder is concerned, Stages IV and V are the most important stages, since in these stages most of the water is discharged through the breach and the ultimate dimensions of the breach are determined.

3.3.4 Discussion

It may be concluded from this and previous chapters that the breach erosion processes in embankments as fuse plugs, earth-dams, sand-barriers and dikes have some similarities.

Phase 1 of the washout process in fuse plugs (see Paragraph 2.3) is comparable to the present Stages I through III, in which the vertical erosion governs the increase of the breach

⁸⁾ Both historical research and soil exploration at the different sites are necessary for a more accurate characterisation of these scour pools.

width (see Section 3.3.2). A closer observation of the washout process of a fuse plug might indicate that in Phase 1 the Stages I, II and III of the erosion process in dike breaches can be identified. At the end of Phase 1 the breach in a fuse plug has reached the fixed crest of the spillway preventing further vertical erosion. The lateral erosion of both faces of a fuse plug embankment in Phase 2 is more or less comparable to the erosion process in a Type A dike breach in Stage IV. After the complete washout of the fuse plug at the end of Phase 2 the erosion process stops, while in a dike the process of breach erosion continues in a final Stage V, and only ends when the flow velocities have become sufficiently small.

The authors of the dam breach models summarized in Paragraph 2.4 have not identified different stages in the earth-dam breach erosion process nor in their models. The breach evolutions shown in Figures 2.4 and 2.5 calculated with the BREACH and BEED models, respectively, can be compared with the present breach growth process in Stage III and Stage IV of the Type A breach. Singh and Scarlatos (1987) describe in their BEED model also the flow and sediment transport on the downstream slope of the dam shortly after the start of the dam failure. This is similar to Stages I and II of the present model, except for the modeling of the sediment entrainment (see Chapter 4).

As already described in Paragraph 2.5, Fujita and Tamura (1987) have not defined their Phases (2), (3) and (4) in terms of measurable morphological and hydraulic transitions (as in the present model). Therefore their four phases cannot be compared uniquely with the five stages of the present breach erosion model. Only their Phase (1) is similar to a phase of the present model, i.e. to Stages I and II. Fujita and Tamura (1987) have not presented the time frames of their four phases in their experiments either.

The upstream movement of the step in the bottom of a sand-barrier breach in Stage (1), see Paragraph 2.6, can be compared with the retrograde erosion of the inner slope in a breaching dike in Stage II. Stage (2) of the sand-barrier breach erosion process is partly comparable with Stages III and IV of the present breach growth model. Gordon's (1991) Stage (3) can be compared with Stage V of the present model, except for the time frame (depending on the polder area and the outside water level, Stage V may last for many hours).

Chapter 4

Mathematical model

4.1 Introduction

This chapter contains a mathematical description of the five-step breach erosion process as outlined in the previous chapter. The modeling of the development of the initial breach in Stages I and II is described in Paragraph 4.2. The mathematical descriptions of the further growth of the breach in Stages III, IV and V are described in Paragraphs 4.3, 4.4 and 4.5, respectively. The resulting mathematical model has been implemented into the numerical model BRES (**B**reach **E**rosion in **S**and-dikes), of which the computational scheme is outlined in Paragraph 4.6.

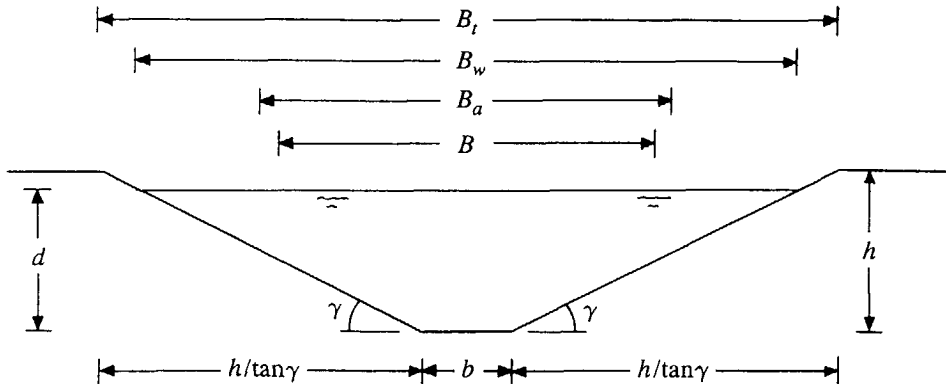


Figure 4.1 Trapezoidal cross-section of the breach.

It is assumed that the breach has a trapezoidal cross-section (see Figure 4.1), with a depth h at the bottom, side-slope angles γ , a width b at the bottom, a depth-averaged (over water depth d) width B , an averaged (over breach depth h) width B_a , a width B_w at the water line, a width B_t at the dike top, a cross-sectional flow area A and a hydraulic radius R . The equations for B , B_w , R , B_a , B_t and A as function of b , d , h and γ read, respectively

Breach growth in sand-dikes

$$B = b + \frac{d}{\tan\gamma} \quad B_w = b + \frac{2d}{\tan\gamma} \quad R = \frac{A}{b + \frac{2d}{\sin\gamma}} \quad (4.1, 4.2, 4.3)$$

$$B_a = b + \frac{h}{\tan\gamma} \quad B_t = b + \frac{2h}{\tan\gamma} \quad A = Bd \quad (4.4, 4.5, 4.6)$$

It is assumed that the bed shear stress τ_b is described by

$$\tau_b = C_f \rho U^2 \quad (4.7)$$

where C_f is a dimensionless bed friction coefficient, ρ is the water density and U is the depth-averaged flow velocity. Breach erosion is attended with large bed shear stresses causing entrainment of large amounts of sediment resulting in high sediment concentrations (in particular near the bottom, see Chapter 5 and Fig. A.1 in Appendix A) and high sediment transport rates. These high sediment concentrations cause the viscosity of the flowing sand-water mixture to be much higher than that of water without sediment. This results in relatively large values for the roughness height k in the equation for the bed friction coefficient:

$$C_f = \frac{\kappa^2}{[\ln(12R/k)]^2} \quad (4.8)$$

Based on the experiments of Einstein and Chien (1955, see Van Rijn, 1993) and Winterwerp et al. (1990), Van Rijn (1993) proposed the following formulae for k :

$$k = 3D_{90} \quad \text{voor } \theta < 1 \quad (\text{lower regime, plane bed}) \quad (4.9)$$

$$k = 3\theta D_{90} \quad \text{voor } \theta \geq 1 \quad (\text{upper regime}) \quad (4.10)$$

The parameter θ in (4.9) and (4.10) is Shields' particle mobility parameter, which reads

$$\theta = \frac{\tau_b}{\rho \Delta g D} = \frac{u_*^2}{\Delta g D} = \frac{C_f U^2}{\Delta g D} \quad (4.11)$$

where $\Delta = (\rho_s - \rho)/\rho$ is the specific density, ρ_s is the sediment density and D is the averaged sediment particle diameter. The parameter θ is an important parameter in the sediment transport formulae described in Appendix A (as the similar parameter u_*'/w_s , see (4.32)), and somewhat less also its critical value (θ_{cr}), which is a parameter for incipient motion. Equation (4.10) is similar to the relation

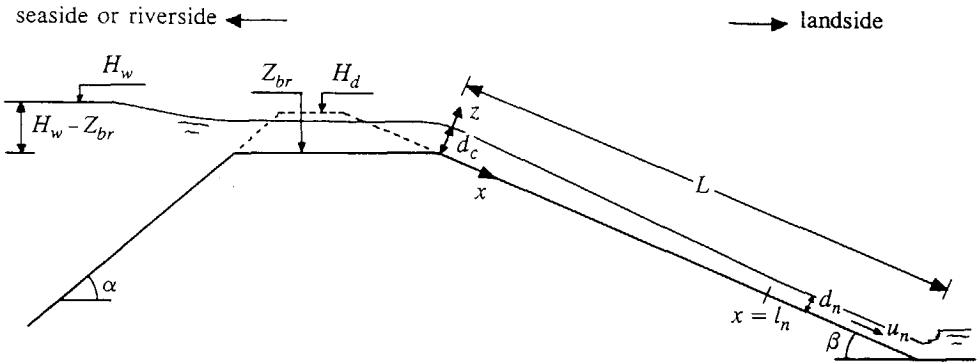


Figure 4.2 Flow on a relatively steep sloping bed.

$$k = 5\theta D_{50} \quad \text{voor } \theta \geq 1 \quad (4.12)$$

proposed by Wilson (1989) and Wilson and Nnadi (1993). It can be concluded from (4.8), (4.10), (4.11) and (4.12) that for $\theta > 1$ the roughness height k is (almost) independent of the particle diameter D .

4.2 Development of initial breach in Stages I and II

4.2.1 Flow along inner slope

Figure 4.2 shows schematically the situation of flow on the relatively steep inner slope of a sand-dike (with angle of inclination β); x is the coordinate along the inner slope, z is the coordinate perpendicular to the inner slope in Stages I, II and III ($z = 0$ at the initial level of the inner slope at the start of each stage, H_w is the outside water level and Z_{br} is the height of the bottom of the breach (in Stages I, II and III the channel in the dike crest), both measured above the reference level $Z = 0$ (NAP in The Netherlands). Since the flow on the inner slope is supercritical, the equation for the discharge Q_{br} through the breach is

$$Q_{br} = m \left(\frac{2}{3}\right)^{3/2} \sqrt{g} B (H_w - Z_{br})^{3/2} \quad \text{for } t_0 < t \leq t_3 \quad (4.13)$$

where g is the acceleration of gravity and m is the discharge coefficient ($m \approx 1.0$, see also Paragraph 4.4), so it is assumed that the friction along the crest of the dike in the breach is negligibly small. Equation (4.13) holds not only in Stages I and II but also in Stages III and

Breach growth in sand-dikes

IV. As described below, the erosion of the most upstream point of the dike crest is negligible in Stages I and II, consequently $Z_{br} \approx \text{constant}$ for $t_0 < t \leq t_2$. Since the duration $t_2 - t_0$ is relatively short, also $H_w \approx \text{constant}$ in Stages I and II. This means:

$$Q_{br} \approx \text{constant} \quad \text{for} \quad t_0 < t \leq t_2 \quad (4.14)$$

The flow on the inner slope accelerates up to $x = l_n$, beyond which the flow is uniform with depth-averaged flow velocity U_n and water depth d_n (the subscript n refers to the word normal):

$$U_n = \frac{(g R_n \sin \beta)^{1/2}}{C_f^{1/2}} \quad \text{for} \quad x \geq l_n \quad (4.15)$$

$$d_n = \frac{Q_{br}}{U_n B_n} \quad \text{for} \quad x \geq l_n \quad (4.16)$$

For $0 < x < l_n$ the general differential equation for gradually varied flow (equation of Bélanger) can be applied. This equation reads

$$\frac{dd}{dx} = \frac{\sin \beta - C_f Q_{br}^2 / g R A^2}{\cos \beta - Q_{br}^2 B_w / g A^3} \quad (4.17)$$

The water depth $d(0)$ for $x = 0$ is equal to the critical depth d_c . The equation for d_c follows from (4.17):

$$d_c^3 = \frac{Q_{br}^2 (B_w)_c}{g B_c^3 \cos \beta} \quad (4.18)$$

Substitution of (4.15) and (4.16) into (4.17) yields

$$\frac{dd}{dx} = \frac{d^2 - R_n A_n^2 / R B^2}{d^2 (1 - Fr^2)} \tan \beta \quad (4.19)$$

where

$$Fr^2 = \frac{U^2}{g d_a \cos \beta} = \frac{U^2}{g d \frac{B \cos \beta}{B_w}} \quad (4.20)$$

in which d_a is the width-averaged water depth.

If the deviation between d and d_n is relatively small, then the following approximations hold:

$$d^2 - R_n A_n^2 / R B^2 \approx d^2 - A_n^2 / B_n^2 = (d + d_n)(d - d_n) \approx 2d_n(d - d_n) \quad (4.21)$$

$$1 - Fr^2 \approx 1 - Fr_n^2 \quad (4.22)$$

Substitution of (4.21) and (4.22) into (4.19) gives

$$\frac{dd}{dx} \approx \frac{2(d_n - d)}{\lambda} \quad (4.23)$$

where

$$\lambda = \frac{(Fr_n^2 - 1)d_n}{\tan\beta} \quad (4.24)$$

Assuming λ to be constant, integration of (4.23) gives with the boundary condition $d = d(0) = d_c$ for $x = 0$

$$d - d_n \approx [d_c - d_n]e^{-2x/\lambda} \quad (4.25)$$

The parameter λ is a typical adaptation length for this type of gradually varied flow: for $x = \lambda$ the difference $d - d_n$ is about 14% of the deviation $d(0) - d_n$ at $x = 0$, for $x = 2\lambda$ it is 1.8% and for $x = 2.5\lambda$ it is only 0.7%. Hence it can be assumed that $l_n \approx 2.5\lambda$, giving

$$l_n = \frac{2.5(Fr_n^2 - 1)d_n}{\tan\beta} \quad (4.26)$$

So the approximation for the water depth d along the stretch $0 < x < l_n$ reads

$$d \approx d_n + [d_c - d_n]e^{-5x/l_n} \quad \text{for } 0 < x < l_n \quad (4.27)$$

Equation (4.27) predicts a smooth decrease of the water depth d for $x \uparrow 0$, physically more realistic than the steep decrease given by (4.17). Hence, although (4.26) predicts a larger value for l_n than (4.17), this approximation is not necessarily also less realistic.

Similarly an approximation for the depth-averaged flow velocity U along $0 < x < l_n$ can be derived (U_c is critical flow velocity):

$$U \approx U_n + [U_c - U_n]e^{-5x/l_n} \quad \text{for } 0 < x < l_n \quad (4.28)$$

As described in Chapter 3, the adaptation length l_n is an important parameter in the first three stages of the breach erosion process. A practical approximation for l_n/L can be derived from

(4.26), since in these stages the following approximations apply (see Visser, 1995b):

- $d_n \approx 0.4 d_c \approx 0.3 (H_w - Z_{br})$,
- $Fr_n^2 - 1 \approx 15$,
- $\tan\beta \approx \sin\beta \approx (H_d - Z_p)/L$, where H_d is the height of the dike and Z_p is the polder level, both measured above the reference level $Z = 0$. These approximations are valid for sandy slopes varying from 18° to 32° (see Visser, 1995b). Substitution of these values into (4.26) gives

$$\frac{l_n}{L} \approx 10 \frac{H_w - Z_{br}}{H_d - Z_p} \approx 10 \frac{H_d - Z_{br}}{H_d - Z_p} = 10 \frac{h}{H_D} \quad (4.29)$$

where h is the depth of the channel in the crest of the dike and H_D is the height of the dike above the polder level Z_p ; in practice $H_d \approx H_w$ in situations where a dike starts to breach.

A similar approximation for l_n can be derived from (4.26) for the flow on the upstream slope of the scour hole in Stage IV (see Paragraph 4.4):

$$l_n \approx \frac{H_w - Z_{br}}{C_f} \approx \frac{h}{C_f} \quad (4.30)$$

since then

- $d_n \approx 0.4 d_c \approx 0.3 (H_w - Z_{br})$,
- $Fr_n^2 - 1 \approx Fr_n^2 \approx \sin\beta / C_f$,
- $\tan\beta \approx \sin\beta$.

4.2.2 Sediment transport along inner slope

The sediment transport rate $S(x)$ through the trapezoidal breach consists of a part $S_{bl}(x)$ that is transported as bed-load in a relatively thin layer (some particle diameters thick) just above the bed and a part $S_{sl}(x)$ that is transported as suspended load:

$$S(x) = S_{bl}(x) + S_{sl}(x) \quad (4.31)$$

The sediment transport rate $S(x)$ is here defined such that $S(x)$ contains only sediment and no voids; it is expressed in units of volume of sediment per unit of time (SI: m^3/s). Whether the transport is in the suspended load mode or in the bed-load mode can be estimated with the parameter

$$\frac{u_\star}{w_s} = \sqrt{C_f} \frac{U}{w_s} \quad (4.32)$$

where u_\star is the bed shear velocity and w_s is the sediment fall velocity. For $u_\star/w_s \ll 1$

(roughly $u_{\star}/w_s < 1$) bed-load transport dominates suspended load transport. Conversely for $u_{\star}/w_s > 1$ (roughly $u_{\star}/w_s > 2$) most of the transport takes place as suspended load. In practice, $u_{\star}/w_s \gg 1$ in the first four stages of the breach erosion process (see Table 5.1 in Chapter 5), and almost in the entire Stage V u_{\star}/w_s is larger than one, so bed-load transport is small compared with suspended load transport.

It is assumed that the pick up of sediment and the resulting sediment transport $S(x)$ starts at $x = 0$ at the top of the inner slope: $S(0) = 0$. This assumption is based on the laboratory observations of Visser et al. (1986, see also Visser, 1989). The data of the Schelde Flume experiments (see Steetzel and Visser, 1992, 1993) support this assumption (see Figures 5.1 and 5.2). At a distance l_a (is adaptation length of the suspended load transport) from $x=0$ the suspended load transport S_{sl} reaches its equilibrium value S_s , which is written in parameterised form as

$$S_s = B_w s_s = M B_w U^n \quad \text{for} \quad x \geq l_a \quad (4.33)$$

where M is a dimensional coefficient and n is a dimensionless exponent ($n \geq 3$).

There are various descriptions of the process of sediment entrainment. Among these is Galappatti's (1983) model, see also Galappatti and Vreugdenhil (1985). Galappatti's (1983) description for the increase of the suspended load transport in a uniform two dimensional flow from $s_{sl}(x) = 0$ at $x=0$ to $s_{sl}(x) = s_s$ at $x = l_a$ can be approximated as

$$s_{sl}(x) = \left(\frac{x}{l_a}\right)^{n_1} s_s \quad \text{for} \quad 0 \leq x \leq l_a \quad (4.34)$$

where n_1 is a dimensionless exponent ($0.5 < n_1 < 1$). For large values of u_{\star}/w_s , $n_1 \rightarrow 1$ (see Galappatti, 1983) and $s(x) \approx s_{sl}(x)$. So, for the present application (4.34) can be written as

$$s(x) = \frac{x}{l_a} s_s \quad \text{for} \quad 0 \leq x \leq l_a \quad (4.35)$$

The adaptation length l_a can be approximated by (see Galappatti, 1983)

$$l_a = \xi \frac{U d}{w_s \cos \beta} \quad (4.36)$$

in which ξ is a coefficient being about equal to 0.4 in case of a (nearly) uniform flow. Visser (1995b) found that for the accelerating flow on a relatively steep sloping bed that ξ is of order 1 (in that case l_a includes also l_n , see Paragraph 5.6). This means for the present model that $\xi \approx 1$ in Stages I, II and III and $\xi \approx 0.4$ in Stages IV and V (see Paragraph 4.4).

Breach growth in sand-dikes

D_{50} [mm]	0.20	0.30	0.40	0.60	0.80	1.0
l_a/L ($T = 4^\circ\text{C}$)	2.0	1.0	1.0 (0.7)	1.0 (0.5)	1.0 (0.4)	1.0 (0.3)
l_a/L ($T = 20^\circ\text{C}$)	1.4	1.0 (0.8)	1.0 (0.6)	1.0 (0.4)	1.0 (0.4)	1.0 (0.3)

Table 4.1 Ratio l_a/L as $h/H_D \approx 1/10$, $\tan\beta = 1/3$ (i.e. $\xi \approx 1$) and $B_w/B_t \approx 0.7$ for various D_{50} (as $T = 4^\circ\text{C}$ and $T = 20^\circ\text{C}$).

D_{50} [mm]	0.20	0.30	0.40	0.60	0.80	1.0
l_a/L ($T = 4^\circ\text{C}$)	3.7	2.0	1.4	1.0 (0.9)	1.0 (0.7)	1.0 (0.6)
l_a/L ($T = 20^\circ\text{C}$)	2.7	1.6	1.2	1.0 (0.8)	1.0 (0.7)	1.0 (0.6)

Table 4.2 Ratio l_a/L as $h/H_D = 1/10$, $\beta = \beta_1 = 32^\circ$ ($\xi \approx 1$) and $B_w/B_t = 0.7$ for various D_{50} (as $T = 4^\circ\text{C}$ and $T = 20^\circ\text{C}$).

Equation (4.36) applies to two dimensional flows. For the present trapezoidal breaches (see Figure 4.1) it is assumed that the pick up of sediment takes place over the entire width B_w of the breach at the water line. The dike material above the water line will slide down and fall into the breach reducing the adaptation length of the sediment transport:

$$l_a = \xi \frac{B_w}{B_t} \frac{U d}{w_s \cos\beta} \quad (4.37)$$

A practical approximation for l_a/L (L is the length of the inner slope of the dike) in Stages I, II and III can be derived from (4.37), since the following approximations hold in these stages (see Visser, 1995b):

- $U d \approx U_c d_c \approx 2(g h)^{1/2} h/3$ (again it is assumed that $H_w \approx H_d$),
- $\cos\beta = \sin\beta/\tan\beta \approx [(H_d - Z_p)/L]/\tan\beta = (H_D/L)/\tan\beta$.

Substitution of these values and $\xi \approx 1$ into (4.37) yields

$$\frac{l_a}{L} \approx \frac{1}{2} \frac{B_w}{B_t} \frac{\sqrt{g h}}{w_s} \frac{h}{H_D} \tan\beta \quad (4.38)$$

where w_s is the fall velocity of the sand in the dike.

A typical value for the height of a relatively high dike in The Netherlands is $H_D \approx 10\text{m}$ and for the inner slope $\tan\beta_0 = 1/3$. If it is assumed that $h = 1\text{m}$ (the 1 m thick clay-layer

at the crest of the dike has been washed out by the high water) and $B_w/B_t \approx 0.7$, then from (4.29) $l_n/L \approx 1$, and the ratio l_a/L varies for practical values of D_{50} (as $T = 4^\circ\text{C}$ and $T = 20^\circ\text{C}$) as shown in Table 4.1 (for $\tan\beta = 1/3$) and Table 4.2 (for $\beta = \beta_1 = 32^\circ$). The values between brackets in Table 4.1 have been obtained with (4.38) and have been corrected with equation (4.29) to 1.0 since l_a is by definition not smaller than l_n .

To determine the development of the inner slope, it is assumed that equations (4.33) and (4.35) hold also for $0 < x < l_n$:

$$s(x) = \frac{M}{l_a} x U^n \quad \text{for } 0 < x < l_n \quad (4.39)$$

In principle it is possible to select for U both the local flow velocity $U(x)$ and the normal flow velocity U_n (in the test of sediment transport formulae in Chapter 5 called approach 1 and approach 2, respectively). Substitution of the local flow velocity $U(x)$ into (4.39) gives an acceleration of $s(x)$ for $0 < x < l_n$ and a linear increase of $s(x)$ along $l_n \leq x < l_a$. Substitution of U_n into (4.39) gives a linear increase of $s(x)$ along $0 < x < l_a$.

The entrainment of sediment causes the specific flow rate $q(x)$ of the sand-water mixture to increase along the inner slope:

$$q(x) = q_{br} + s(x) \quad (4.40)$$

where q_{br} is the specific flow rate of the discharge over the dike (it is assumed that the voids are filled with air and not with water). Under normal hydraulic conditions $s(x) \ll q(x)$ and the increase of the flow rate due to sediment entrainment can be neglected. In Stages I and II of the breaching process, however, the sediment transport can become relatively large (see Chapter 5), and it may be important to account for this. However, Stages I and II contribute relatively little to the total flow through the breach compared with Stages IV and V, where most of the breach erosion takes place. Therefore, the effect of an increase of $q(x)$ on u , d , l_a , etc. will be ignored.

4.2.3 Rate of erosion along inner slope

The conservation equation for sediment volume along the inner slope is

$$(1 - p) \frac{\partial(B_a h)}{\partial t} - \frac{\partial S}{\partial x} = 0 \quad (4.41)$$

where p is the bed porosity and

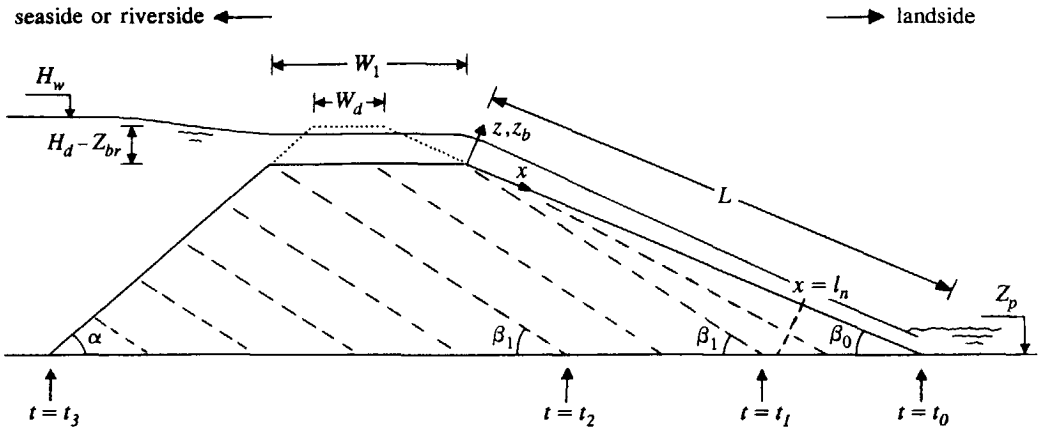


Figure 4.3 Flow on inner slope in breach in Stage I (solid line) and development of inner slope in Stages I, II and III (dashed lines) for a typical dike in The Netherlands (i.e. when $l_n \approx L \leq l_a$).

$$S = B_w s \tag{4.42}$$

Substitution of (4.4), (4.5) and (4.42) into (4.41) gives

$$(1 - p) \left[h \frac{\partial b}{\partial t} + B_t \frac{\partial h}{\partial t} \right] - \frac{\partial (B_w s)}{\partial x} = 0 \tag{4.43}$$

As will be shown in Section 4.3.2, in Stages I through III is $\partial b / \partial t \approx 0$, which means that if $\partial b / \partial x \approx 0$ at $t = t_0$ that also $\partial B_w / \partial x \approx 0$ throughout these stages. Then (4.43) reduces to

$$(1 - p) B_t \frac{\partial z_b}{\partial t} + B_w \frac{\partial s}{\partial x} = 0 \tag{4.44}$$

where z_b is the position of the inner slope in z -direction (see Figure 4.3, $z_b = 0$ at the initial level of the inner slope at the start of each stage). Substitution of (4.39) into (4.44) yields

$$E = - \frac{\partial z_b}{\partial t} = \frac{B_w}{B_t} \frac{M}{(1 - p) l_a} U^n \left(1 + n \frac{x}{U} \frac{\partial U}{\partial x} \right) \quad \text{for } 0 < x < l_n \tag{4.45}$$

in which it has been assumed that the coefficient M is constant (so also the friction coefficient C_f and $\cos \beta$).

For breaches where (4.37) computes a larger l_a than l_n given by (4.26), it follows from

substitution of (4.37) into (4.45) that the effect of the dike being higher than the water level in the breach (so $B_t > B_w$, see Figure 4.1) does not influence the rate of erosion E in vertical direction compared to the two-dimensional situation (occurring in a laboratory flume for instance, see Sections 5.3.2 and 5.3.3). For breaches where l_a given by (4.37) is smaller than l_n given by (4.26), the adaptation length l_a is set equal to l_n . Then the factor B_w/B_t in (4.45) will slow down the erosion rate E .

It follows from (4.45) that

$$\frac{\partial}{\partial x} \left| \frac{\partial z_b}{\partial t} \right| > 0 \quad \text{for} \quad 0 < x < l_n \quad (4.46)$$

since both x/U and $\partial U/\partial x$ increase in positive x -direction for $0 < x < l_n$. So the rate of erosion of the inner slope increases along the slope and the inner slope becomes steeper in x -direction and in time (see Figure 4.3).

When $L \geq l_n$ the flow velocity U approaches for $x = l_n$ the normal value for uniform flows given by (4.15). Substitution of (4.33) and (4.35) into (4.44) gives

$$E = -\frac{dz_b}{dt} = \frac{B_w}{B_t} \frac{M}{(1-p)l_a} (U_n)^n \quad \text{for} \quad l_n \leq x \leq l_a \quad (4.47)$$

This means that

$$\frac{\partial}{\partial x} \left| \frac{dz_b}{dt} \right| = 0 \quad \text{for} \quad l_n \leq x \leq l_a \quad (4.48)$$

i.e. the rate of erosion of the inner slope is constant for these values of x , see Figure 4.3.

It follows from above that the inner slope becomes steeper and steeper with x and in time for $0 \leq x < l_n$. It is assumed that the slope angle will not exceed a limit β_1 , say $\beta_1 \approx \phi$ (ϕ is angle of repose). If this limit has been reached on the entire stretch $0 \leq x < l_n$ (at $t = t_1$), then the erosion rate becomes constant for $0 \leq x < l_n$, as indicated by the lines for $t \geq t_1$ in Figure 4.3, and Stage II starts.

In Stage II the erosion of the inner slope of the dike in the breach continues, resulting in a decrease of the width of the dike crest in the breach for $t_1 < t \leq t_2$; the inner slope angle remains (in this line of thought) at its critical value β_1 . Stage II ends when the width of the dike crest has become zero.

It can be concluded that for $t_0 < t \leq t_2$ the rate of erosion of the inner slope in the breach is controlled by the erosion at $x = L$ if $L < l_n$ (as for a typical dike in The Netherlands, see Section 4.2.2) and by the erosion at $x = l_n$ (or by the erosion along $l_n \leq x \leq l_a$) if $L \geq l_n$. This means that only the erosion rate at $x = L$ if $L < l_n$ or at $x = l_n$ if $L \geq l_n$ has

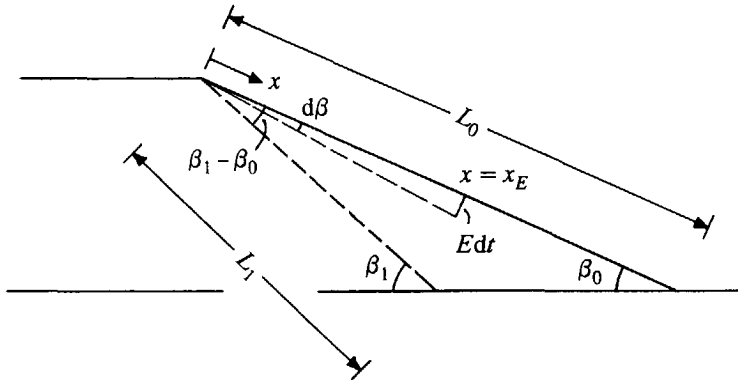


Figure 4.4 Increase of inner slope angle β from an initial value β_0 at $t = t_0$ to a critical value β_1 at $t = t_1$ in Stage I.

to be known. These erosion rates can be calculated with equations (4.45) and (4.47), respectively.

In Stages I and II the width of the breach (pilot channel in the crown of the dike) remains at its initial value near the breach inflow. The increase of the depth of the channel in the inner slope causes also an increase of the width of this channel (see Section 4.3.2). At $t = t_1$ the width of the breach starts to grow at the downstream side of the dike-crown.

4.2.4 Steepening of inner slope in initial breach in Stage I

The rate of erosion is maximal at $x = x_E = l_n$, for $l_n \leq x \leq l_a$ it is constant according to (4.47), see Figure 4.3. As described in Chapter 3, in practice the length L of the inner slope is not larger than l_n . This means that the rate of erosion is maximal at $x = x_E = L$. Due to this erosion process the angle β of the inner slope increases from an initial value β_0 at $t = t_0$ to a critical value β_1 at $t = t_1$ in Stage I, see Figure 4.4.

The equation for the increase $d\beta$ of β is

$$d\beta = \frac{-\frac{\partial z_b}{\partial t} dt}{x_E} = \frac{E}{x_E} dt \quad (4.49)$$

Integration of (4.49) between t_0 and t_1 gives

$$\beta_1 - \beta_0 = \int_{t_0}^{t_1} \frac{E}{x_E} dt \quad (4.50)$$

After substitution of (4.45), equation (4.50) can be integrated numerically. Since the duration of Stage I is relatively short, its importance is small compared to the subsequent stages. Hence, the following approximation is used in the model:

$$\beta_1 - \beta_0 = \int_{t_0}^{t_1} \frac{E}{x_E} dt \approx \frac{E(\beta_0^+)}{x_E} (t_1 - t_0) \quad (4.51)$$

where

$$\beta_0^+ = \frac{\beta_1 + \beta_0}{2} \quad (4.52)$$

From (4.51) the equation for t_1 becomes

$$t_1 = t_0 + \frac{(\beta_1 - \beta_0)x_E}{E(\beta_0^+)} \quad (4.53)$$

in which $x_E = L_0^+$ and $E(\beta_0^+)$ is given by (4.45) for $L_0^+ < l_n$, and $x_E = l_n$ and $E(\beta_0^+)$ is given by (4.47) for $L_0^+ > l_n$ (L_0^+ is the length of the inner slope for $\beta = \beta_0^+$).

4.2.5 Decrease of width of dike crest in breach in Stage II

At $t = t_1$ the angle of the inner slope is at its critical value β_1 . It stays at this value in Stage II. This means that the rate of erosion is constant along the entire stretch $0 \leq x \leq l_a$, see Figure 4.5. So the erosion of the inner slope for $t_1 < t < t_2$ is entirely determined by the erosion at the toe of the slope ($x = L_1$) since for a typical dike in The Netherlands $L_1 \leq l_a$ (see Table 4.2):

$$-L_1 B_t (1-p) \frac{dz_b}{dt} = B_w s(L_1) = B_w \frac{L_1}{l_a} s_s(L_1) \quad (4.54)$$

Consequently

$$\frac{dz_b}{dt} = -\frac{B_w}{B_t} \frac{s_s(L_1)}{(1-p)l_a} \quad (4.55)$$

Figure 4.5 shows that in the breach the length of the top of the dike (W , initial value W_1 at $t = t_1$) decreases for $t_1 < t < t_2$ due to the erosion of the inner slope. The relation between the decrease of the length of the dike-top (dW) and the erosion of the inner slope (dz_b) is

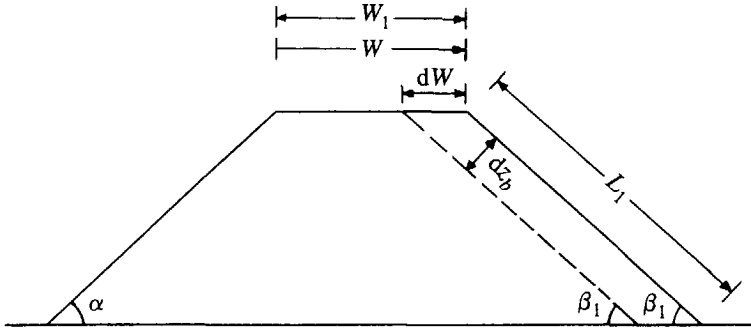


Figure 4.5 Decrease of width W of the top of the dike in the breach from an initial value W_1 at $t = t_1$ to $W = 0$ at $t = t_2$ in Stage II.

$$dW = \frac{1}{\sin\beta_1} dz_b \quad (4.56)$$

Substitution of (4.56) into (4.55) gives

$$\frac{dW}{dt} = -\frac{B_w}{B_t} \frac{s_s(L_1)}{(1-p)l_a \sin\beta_1} \quad (4.57)$$

Since the duration $t_2 - t_0$ is relatively short, $H_w \approx \text{constant}$ in Stage II. So the right hand side of (4.57) is also about constant for $t_1 < t \leq t_2$. Integration of (4.57) between $t = t_1$ and $t = t_2$ yields simply

$$\int_{t_1}^{t_2} \frac{dW}{dt} dt = -W_1 = -\frac{B_w}{B_t} \frac{s_s(L_1)}{(1-p)l_a \sin\beta_1} (t_2 - t_1) \quad (4.58)$$

in which

$$W_1 = W_d + (H_d - Z_{br}) \left(\frac{1}{\tan\alpha} + \frac{1}{\tan\beta_0} \right) \quad (4.59)$$

see Figure 4.3. So, the equation for t_2 becomes

$$t_2 = t_1 + \frac{B_t}{B_w} \frac{W_1 (1-p) l_a \sin\beta_1}{s_s(L_1)} \quad (4.60)$$

4.3 Acceleration of breach growth in Stage III

4.3.1 Decrease of crest height

Figure 4.6 shows a cross-section of the dike through the axis of the breach at $t = t_2$. Also in Stage III the discharge through the breach is described by (4.13). Due to the proceeding erosion process, the top of the dike in the breach starts to drop at $t = t_2$. As a result, the length of the inner slope of the dike in the breach (L_2) decreases and the breach width (see Section 4.3.2) increases for $t_2 < t \leq t_3$.

It is assumed that (as in Stage II) also for $t_2 < t \leq t_3$ the angle of the inner slope remains at the critical value β_1 . Then the rate of erosion is constant along the stretch $0 \leq x \leq l_a$. So for a typical dike in The Netherlands (where $L_2 \leq l_a$), also in Stage III the rate of erosion of the inner slope is entirely determined by the erosion at the toe of the slope ($x = L_2$):

$$-L_2 B_t (1-p) \frac{dz_b}{dt} = B_w s(L_2) = B_w \frac{L_2}{l_a} s_s(L_2) \quad (4.61)$$

Hence

$$\frac{dz_b}{dt} = -\frac{B_w}{B_t} \frac{s_s(L_2)}{(1-p)l_a} \quad (4.62)$$

The relation between the fall of the top of the dike in the breach (dZ_{br}) and the erosion rate of the inner slope (dz_b) follows from a simple geometrical consideration (see Figure 4.7):

$$dZ_{br} = \frac{\sin \alpha}{\sin(\alpha + \beta_1)} dz_b \quad (4.63)$$

Substitution of (4.62) into (4.63) yields

$$\frac{dZ_{br}}{dt} = -\frac{B_w}{B_t} \frac{\sin \alpha}{\sin(\alpha + \beta_1)} \frac{s_s(L_2)}{(1-p)l_a} \quad (4.64)$$

The fall dZ_{br} of the height of the crest of the dike in the breach causes an increase of the flow through the breach, see equation (4.13). Consequently, both the suspended load transport capacity s_s and the adaptation length l_a increase. This means that the right hand side of (4.64) is in general not constant and (4.64) must be integrated numerically:

$$\Delta Z_{br} = -\frac{B_w}{B_t} \frac{\sin \alpha}{\sin(\alpha + \beta_1)} \frac{s_s(L_2)}{(1-p)l_a} \Delta t \quad (4.65)$$

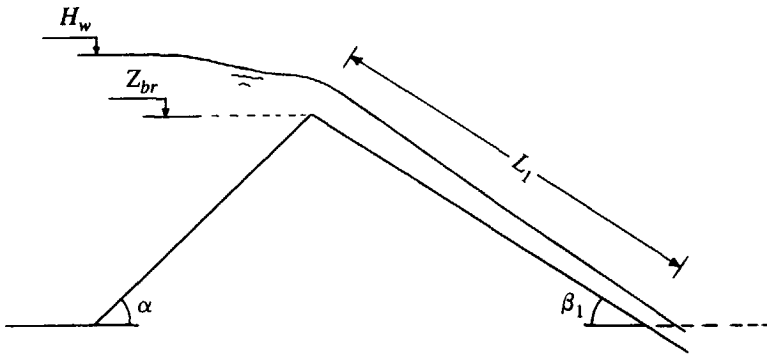


Figure 4.6 Cross-section through axis of breach at $t = t_2$.

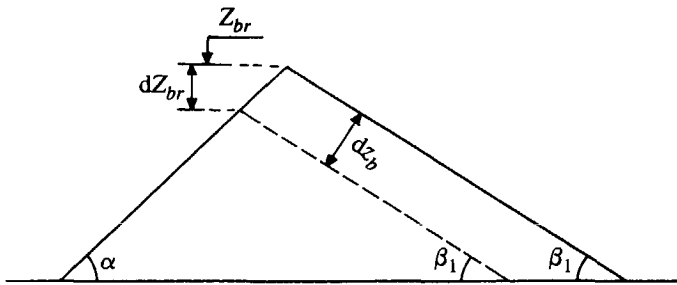


Figure 4.7 Relation between dZ_{br} and dz_b in Stage III.

In Stage III the flow and the sediment transport through the breach change drastically: from a strongly supercritical flow with a Froude number $Fr >> 1$ at $t = t_2$ to a moderately supercritical flow with Fr slightly above 1 at $t = t_3$, from sheet flow transport with a Shields' mobility parameter θ of orders 10 and 100 at $t = t_2$ to sediment transport with θ of order 1 at $t = t_3$ (see Chapter 5 or Visser, 1995b).

4.3.2 Increase of breach width

At $t = t_2$ the width of the breach at the upstream side of the crown also starts to grow. Consider a relatively small initial breach $A_0B_0C_0D_0$ (see Figure 4.8) with a depth-averaged width B_0 , a width b_0 at the bottom and a maximal depth h_0 . It is assumed that the process of initial breach formation has created side slopes with angles equal to the angle of repose ϕ . The direction of the flow through the breach is normal to the plane of the drawing.

The rate of erosion at the toes of the side-slopes is larger (due to the larger flow velocities, resulting from the larger water depths) than higher on the side-slopes. This means

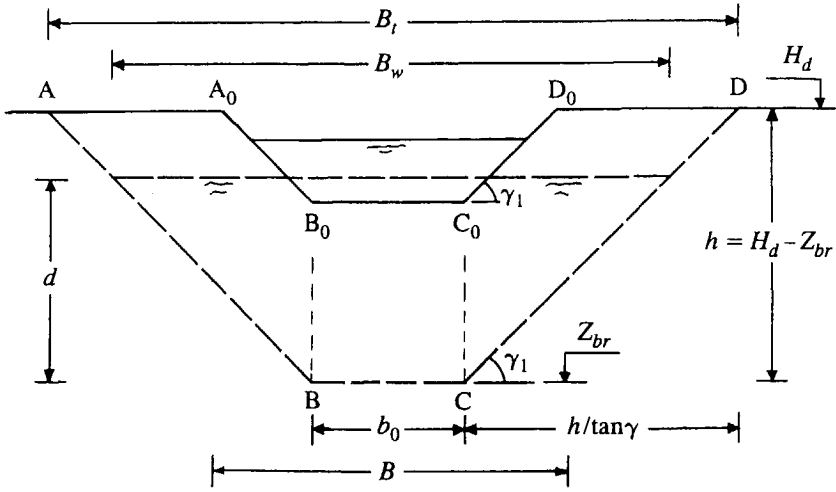


Figure 4.8 Development of breach ABCD from initial breach $A_0B_0C_0D_0$ in Stage III.

that the side-slopes become steeper. The side-slope angle (γ) will, however, not exceed a limit γ_1 . If this limit is attained, then the situation gets unstable and (amounts of) sand from the side-slopes will slide into the breach channel. This is in accordance with what was observed in the Zwin'94 field experiment (see Chapter 6). So, it can be assumed that the angle of the side-slopes is constant and equal to its critical angle γ_1 .

It is assumed that the sand-dike is homogeneous. Then the erosion rate just left from point C_0 equals that just right from this point (because of equal flow velocities). This means that the initial breach $A_0B_0C_0D_0$ will grow to a breach ABCD (see Figure 4.8) with a depth-averaged width B , a width B_w at the water line and a width B_t at the crest of the dike given by, respectively

$$B = b_0 + \frac{d}{\tan \gamma_1} \tag{4.66}$$

$$B_w = b_0 + \frac{2d}{\tan \gamma_1} \tag{4.67}$$

$$B_t = b_0 + \frac{2h}{\tan \gamma_1} \tag{4.68}$$

where h is the breach depth ($h = H_d - Z_{br}$).

Figure 4.8 shows that in Stage III $\partial b / \partial t \approx 0$, see Section 4.2.3.

4.4 Continuation of breach growth in Stage IV

After the complete wash-out of the dike in the breach at $t = t_3$, the breach continues to grow laterally in Stage IV ($t_3 < t \leq t_4$), and depending on the subsoil of the dike, also in vertical direction (scour hole). As described in Chapter 3, the continuation of the breach erosion in Stages IV and V depends on the erodibility of the foundation of the dike, the presence of a solid toe construction on the outer slope and the presence of a relatively high foreland. The following situations may be distinguished:

A.1 A solid clay-layer prevents further vertical erosion

Figure 4.9 shows the flow through the breach in Stage IV when a solid base of the dike prevents (or significantly slows down) further vertical erosion. The flow is virtually uniform along the breach, so the water depth d in the breach is also nearly constant and equal to the critical water depth d_c . This critical depth is given by

$$d_c^3 = \frac{Q_{br}^2 (B_w)_c}{g B_c^3} \quad (4.69)$$

see equation (4.18). The breach acts as a broad-crested spillway. As in the previous stages, the friction on the outer slope and inside the breach may be neglected. Then, application of Bernoulli's equation gives

$$H_w - Z_{br} = \frac{1}{2g} \frac{Q_{br}^2}{(B_c d_c)^2} + d_c \quad (4.70)$$

see Figure 4.9. Substitution of (4.70) into (4.69) gives

$$d_c = \frac{2}{2 + B/B_w} (H_w - Z_{br}) \quad (4.71)$$

$$Q_{br} = m \left(\frac{2}{3}\right)^{3/2} \sqrt{g} B (H_w - Z_{br})^{3/2} \quad \text{for } t_3 \leq t \leq t_4 \quad (4.72)$$

in which

$$m = \frac{3}{2 + B/B_w} \left[\frac{3}{1 + 2B_w/B} \right]^{1/2} \approx 1 \quad (4.73)$$

(it follows from (4.1) and (4.2) that $0.93 \leq m \leq 1$), and $Z_{br} \approx$ constant in this situation.

The flow velocity U in the breach is also virtually uniform along the breach and equal to its critical value U_c :

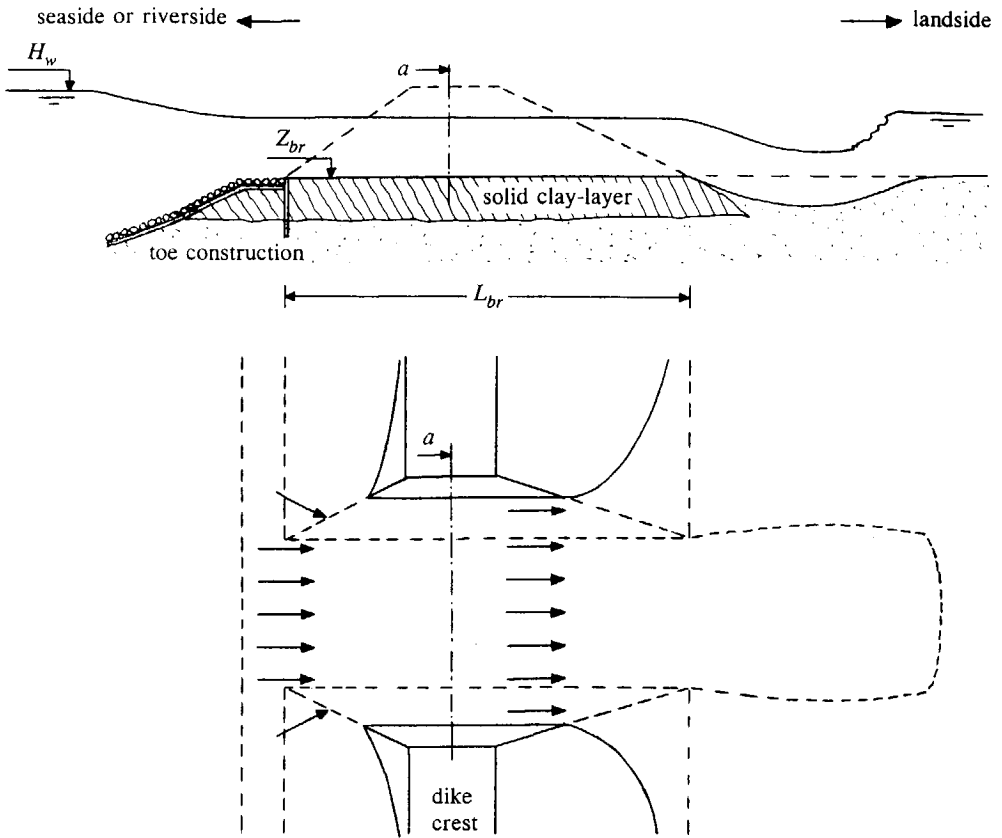


Figure 4.9 Cross-section and top view of flow in Stage IV through a breach in a dike built on a solid clay-layer (Type A breach).

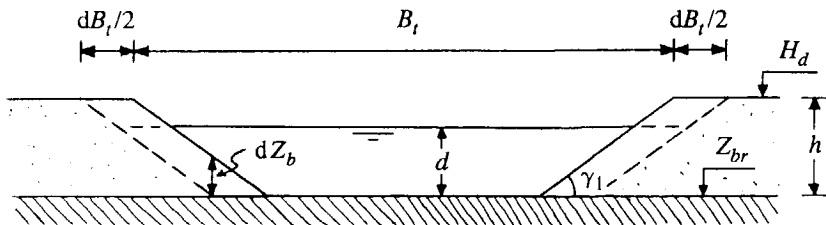


Figure 4.10 Cross-section over breach (cross-section a, see Figure 4.9) showing growth of breach width in a Type A breach in Stages IV and V.

$$U = U_c = (g d_a)^{1/2} = \left[g d_c \frac{B}{B_w} \right]^{1/2} \quad (4.74)$$

It is clear that equations (4.71) and (4.74) apply also to the flow along the crown of the dike in the breach in Stages I, II and III.

Due to the erosion process in Stage III, the angle of the side-slopes $\gamma = \gamma_1$. Since the erosion lower on the side-slopes is larger than higher on the slopes, the angle γ remains at its critical value γ_1 and the breach width increases as shown in Figure 4.10. The relation between the vertical erosion of the side-slopes (with vertical position of the bed Z_b) and the increase of the breach width B (and also B_t) is in this case simply

$$\frac{dB}{dt} = \frac{dB_t}{dt} = - \frac{2}{\tan \gamma_1} \frac{dZ_b}{dt} \quad (4.75)$$

The conservation equation for volume of sediment along both side-slopes of the breach is

$$(1 - p)(B_t - b) \frac{\partial Z_b}{\partial t} + (B_w - b) \frac{\partial s}{\partial x} = 0 \quad (4.76)$$

Substitution of (4.2) and (4.5) into (4.76) yields

$$(1 - p)h \frac{\partial Z_b}{\partial t} + d \frac{\partial s}{\partial x} = 0 \quad (4.77)$$

As in Stages I, II and III for the sediment transport on the inner slope (see Section 4.2.2), also the adaptation length for the sediment transport on the side-slopes is reduced by the fall of the surplus of sediment above the water line into the breach:

$$l_a = \xi \frac{d}{h} \frac{U d}{w_s} \quad (4.78)$$

in which $\xi \approx 0.4$ (see Section 4.2.2). Substitution of $d = d_c$ with (4.71) and (4.74) into (4.78) gives with $H_w - Z_{br} \approx H_d - Z_{br} = h$

$$l_a \approx \frac{0.15 \sqrt{g} h^{3/2}}{w_s} \quad (4.79)$$

consequently

$$\frac{l_a}{L_{br}} \approx \frac{0.02 \sqrt{g h}}{w_s} \quad (4.80)$$

D_{50} [mm]	0.20	0.30	0.40	0.60	0.80	1.0	2.0
l_a/L_{br} ($h = 0.5$ m)	2.4	1.3	0.9	0.6	0.5	0.4	0.2
l_a/L_{br} ($h = 10$ m)	11	5.6	3.9	2.6	2.1	1.8	1.0

Table 4.3 Ratio l_a/L_{br} for $h \approx H_D = 0.5$ m and $h \approx H_D = 10$ m and various D_{50} (sediment fall velocity w_s calculated for $T = 4^\circ\text{C}$, $\xi \approx 0.4$).

in which it is assumed that the width of the dike at its base is about 7 times as large as its height h above the breach bottom, so that the length L_{br} of the breach in Stages IV and V is about 7 times larger than its depth h . Table 4.3 shows some values of l_a/L_{br} for a typical laboratory dike ($h \approx H_D \approx 0.5$ m) and a relatively high prototype dike ($h \approx H_D \approx 10$ m) and D_{50} ranging from 0.20 mm to 2.0 mm. Clearly $l_a > L_{br}$ for prototype sand-dikes (i.e. with sediment diameter $D_{50} < 2.0$ mm), so the equation for the sand transport on the outer slopes in the breach is (see Section 4.2.2)

$$s(x) = \frac{x}{l_a} s_s \quad \text{for } 0 \leq x \leq L_{br} \tag{4.81}$$

Substitution of (4.81) into (4.77) gives

$$\frac{dZ_b}{dt} = - \frac{d}{h} \frac{s_s}{(1-p)l_a} \tag{4.82}$$

and substitution of (4.82) into (4.75) yields

$$\frac{dB}{dt} = \frac{dB_t}{dt} = 2 \frac{d}{h} \frac{s_s}{(1-p)l_a \tan \gamma_1} \tag{4.83}$$

It follows from substitution of (4.78) into (4.83) that the effect of the dike being higher than the water level in the breach (so $B_t > B_w$, see Figure 4.1), as in Stages I, II and III, does not influence the rate of erosion E in vertical direction compared to the two-dimensional situation. Only for relatively long breaches, the factor d/h in (4.78) may cause l_a to be smaller than the breach length L_{br} , slowing down the erosion rate in the breach.

A.2 A toe construction protects the outer slope against further vertical erosion

Figure 4.11 shows the flow through the breach in Stage IV when a solid toe construction on the outer dike slope (see Section 3.3.3) protects the lower part of this slope against further

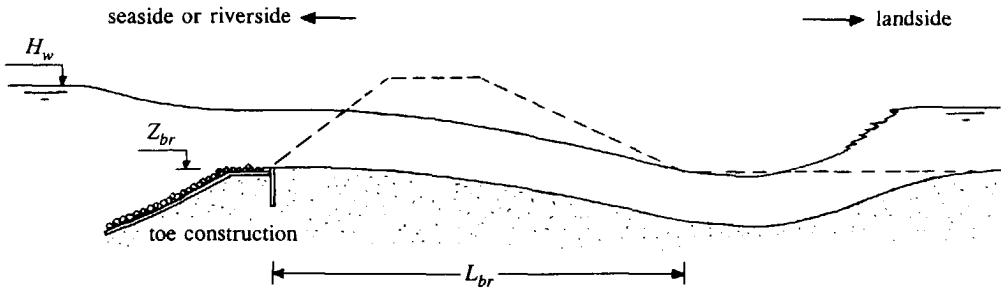


Figure 4.11 Flow in Stage IV through a breach when a solid toe protection protects the lower part of the outer slope against further erosion.

vertical erosion. It is assumed that the erodibility of the base is not negligible (otherwise the A.1 situation outlined above occurs). The toe construction acts as a spillway (broad-crested or sharp-crested, which has only a secondary influence on the discharge coefficient of the spillway). Downstream of the toe construction, the flow first accelerates (say in the breach, where the flow is supercritical) and then decelerates (say downstream of the breach) resulting in the formation of a hydraulic jump. In Section 4.2.1 the following practical approximation has been derived for the adaptation length l_n of the flow in Stage IV on the upstream slope of the scour hole:

$$l_n \approx \frac{H_w - Z_{br}}{C_f} \approx \frac{h}{C_f} \quad (4.30)$$

The order of magnitude of C_f in Stage IV is $C_f \approx 0.004$, yielding $l_n \approx 250h$ (breach depth h measured above the toe construction), i.e. about a factor 35 larger than the length L_{br} of the breach. Consequently also in case A.2 the flow in the breach in Stage IV is nearly uniform and about equal to the critical flow velocity. This means that the equations (4.13) and (4.69) through (4.83) of case A.1 can also be applied in this situation.

B A high foreland reduces the increase of the breach inflow

Figure 4.12 shows the flow through the breach in Stage IV when the dike has a relatively high foreland. The erodibility of this foreland and of the base of the dike is not small (otherwise the A.1 situation outlined above may occur). The retrograde erosion in Stage IV results in the formation of a curved spillway in the foreland where the flow into the breach takes place. It is assumed that the spillway has a semi-circular shape with a length $(\pi/2)b$. This spillway controls the flow discharge through the breach:

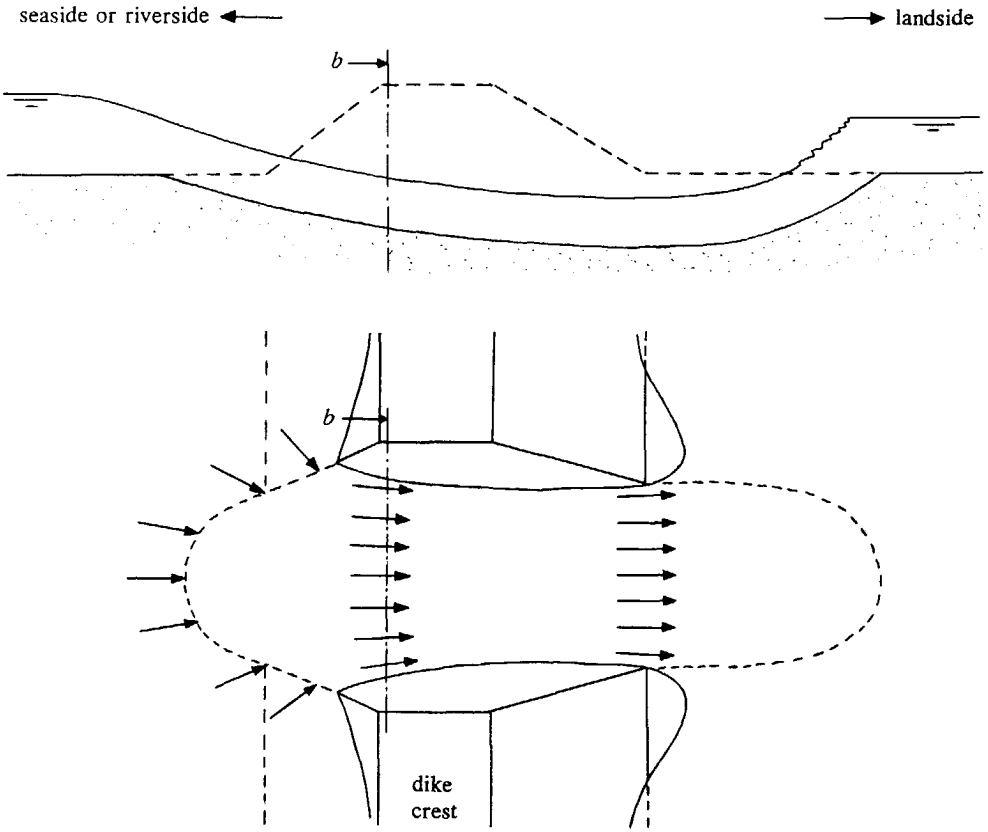


Figure 4.12 Flow in Stage IV through a breach in a dike with a relatively high foreland.

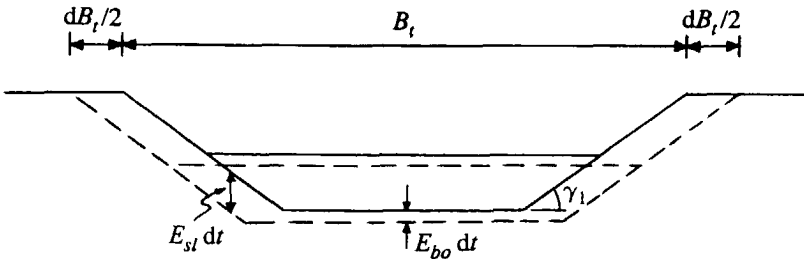


Figure 4.13 Cross-section over breach (cross-section b, see Figure 4.12) showing growth of breach width B_w in a Type B breach in Stages IV and V.

$$Q_{br} = m \left(\frac{2}{3}\right)^{3/2} \sqrt{g} B (H_w - Z_{br})^{3/2} \quad \text{for } t_3 \leq t \leq t_4 \quad (4.84)$$

in which Z_{br} is the constant level of the foreland and

$$m \approx \frac{\pi}{2} \quad (4.85)$$

i.e. compared to the A.1 situation the breach discharge is about a factor $\pi/2$ larger.

Figure 4.12 demonstrates that the flow through the breach is 2-dimensional, so the flow is not uniform along the breach length. Compared to the nearly 1-dimensional A.1 situation, the flow accelerates significantly to get the larger discharge across the same (depth-averaged) breach width B .

The breach grows both vertically and laterally, laterally faster than vertically ($E_{sl} > E_{bo}$, see Figure 4.13) as outlined in Section 3.3.3. So, the increase of the breach width B is determined by the erosion of both faces of the dike, so by the water depth and the flow velocity on the slope of these faces. The water depth can roughly be approximated by the critical depth on the spillway, the flow velocity is then simply given by:

$$U \approx \frac{Q_{br}}{Bd} \quad (4.86)$$

Further, equation (4.83) describes also the increase of the breach width in this situation.

Compared with the A.1 situation the breach is deeper (see Figure 4.13), which means that larger amounts of sediment will fall into the flow from the upper parts of the breach side-slopes above the water. This will not reduce the breach erosion process since l_a/L_{br} is also relatively large in this situation, so that there will be enough transport capacity to remove this sediment.

C Unobstructed breach growth

When the dike has not a toe construction to protect the lower part of the outer slope against erosion and not a relatively high foreland, and the base of the dike is not resistant against erosion, then the breach continues to grow also vertically in Stage IV. Figures 4.14 and 4.15 show the development of the breach in this situation. The spillway near the breach inflow which is formed in the outer slope of the dike, is more or less straight, so that the discharge through the breach is given by equation (4.72), in which the level Z_{br} of the breach bottom is not constant but decreases in time due to the entrainment of sediment. The decrease of the breach bottom level Z_{br} follows from equation (4.82):

$$\frac{dZ_{br}}{dt} = - \frac{d}{h} \frac{s_s}{(1-p)l_a} \quad (4.87)$$

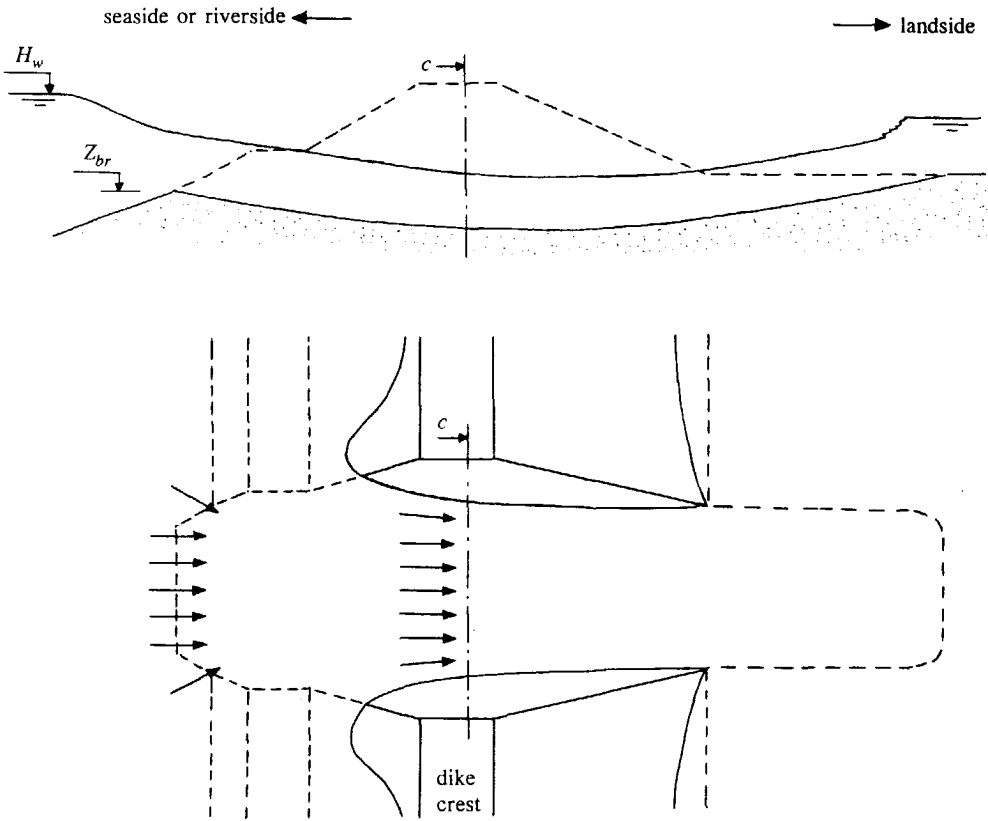


Figure 4.14 Cross-section and top view of flow in Stage IV through a Type C breach.

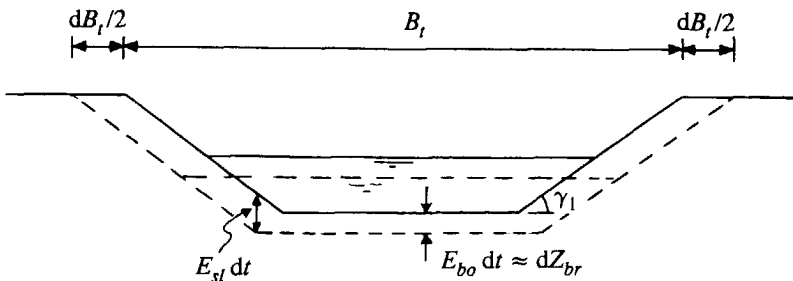


Figure 4.15 Cross-section of breach (cross-section c, see Figure 4.14) showing growth of breach width B_t in a Type C breach in Stages IV and V.

The present 1-dimensional approach cannot predict at which levels the erosion at the breach bottom decelerates and ultimately stops. It is to the user of the model to determine the final level of the breach bottom. This can be the bottom of the river or a deeper laying solid clay-layer. It should be remarked here, however, that non of the breaches levelled shortly after the 1953 flood in The Netherlands (see Rijkswaterstaat, 1961) had large depths at the inflow side.

The decrease of the breach bottom level at the inflow side results also in a larger water depth $d = d_c$ given by (4.71) and consequently also a larger flow velocity $U = U_c$ given by (4.74). As in breach Types A and B, $E_{sl} > E_{bo}$ (see Figure 4.15), consequently equation (4.83) describes the increase of the breach width also in this situation.

It has been outlined in this paragraph that the side-slope erosion in Stage IV (and also in Stage V) is not controlled by the growth of the breach depth as in Stage III (in which the linear relation (4.68) between breach width B_b and breach depth h is valid). Instead, it is the erosion below on the side-slopes that controls the erosion of the entire side-slope. This side-slope erosion is governed by the flow at the upstream spillway. Hence, the upstream spillway controls not only the breach discharge but also the breach growth.

The continuous flow of water through the breach in Stage IV causes the water level in the polder to increase. At the end of Stage IV at $t = t_4$, the inside water level H_p has risen to a level that

$$H_p - Z_{br} = d_c \quad (4.88)$$

so that backwater starts to reduce the flow velocities in the breach and Stage V begins.

In BRES the increase of the inside water level H_p in time Δt is simply calculated as

$$H_p(t + \Delta t) = H_p(t) + (Q_{br} \Delta t) / A_p \quad (4.89)$$

where A_p is the area of the polder. A model for the inundation of the polder can provide a more accurate prediction of H_p .

4.5 Deceleration of breach growth in Stage V

At $t = t_4$ the flow becomes subcritical ($Fr < 1$) and the flow velocity in the breach decreases, resulting in a deceleration of the breach growth for $t_4 < t < t_5$. The equations for the water depth and the flow velocity on the spillway are described by, respectively

$$d = H_p - Z_{br} \quad \text{for} \quad t_4 \leq t \leq t_5 \quad (4.90)$$

$$U = [2g(H_w - H_p)]^{1/2} \quad \text{for} \quad t_4 \leq t \leq t_5 \quad (4.91)$$

where H_p is the water level in the polder (above the reference level $Z = 0$) just downstream of the breach. The flow rate through the breach is given by

$$Q_{br} = mB(2g)^{1/2}(H_w - H_p)^{1/2}(H_p - Z_{br}) \quad \text{for} \quad t_4 \leq t \leq t_5 \quad (4.92)$$

with $m \approx 1$ in Types A and C breaches and $m \approx \pi/2$ in a Type B breach.

The flow velocities on the side-slopes follow from substitution of (4.90) and (4.92) into (4.86). Further, as in Stage IV, equation (4.83) describes the increase of the breach width in this stage, in all Types of breaches (A, B and C). So, also in Stage V the spillway regulates the breach inflow rate and the growth of the leading breach section.

At $t = t_5$ the flow velocities in the breach become so small that the pick up of sediment from the breach stops. In the model $t = t_5$ is determined when the Shields parameter θ has become equal to its critical value θ_{cr} (incipient motion). The flow through the breach continues until at $t = t_6$ the water level in the polder H_p has become equal to the outside water level H_w .

4.6 Computational scheme

In order to test the present breach erosion model to experimental results and to be able to make predictions for failures of prototype dikes, the numerical model BRES (**B**reach **E**rosion in **S**and-dikes; bres is also the Dutch word for breach) has been developed of which the computational scheme is outlined in this paragraph. Details are presented in Appendix B. BRES has been written in Borland C++ (Windows 95/98 version) for use on a PC.

The 'input data' for the BRES model consist of 1) data related to the water course, 2) data describing the geometry of the dike and the initial breach at $t = 0$ and characteristics of the sand in the dike body and 3) data representing the polder. For the present BRES version, it is to the user to determine whether the breaching process in Stages IV and V is of Type A, B or C (see Paragraph 4.4).

The input data for the water course are:

- outside water level $H_w(t)$ above a reference level $Z = 0$ for $t \geq 0$ (for Dutch dikes the reference level $Z = 0$ is NAP);

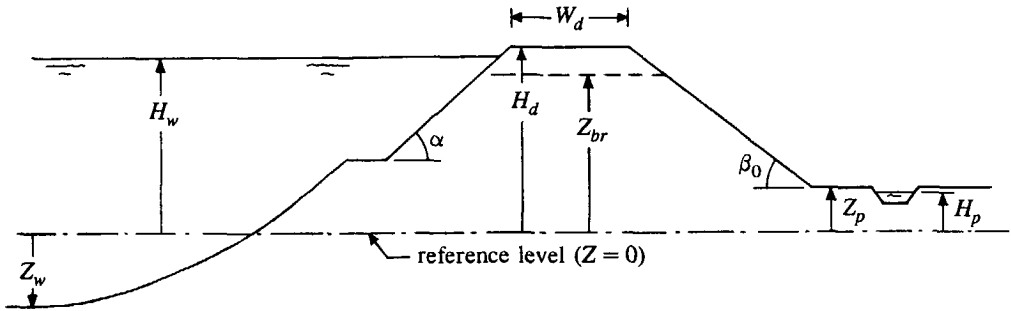


Figure 4.16 Cross-section of dike, water course and polder.

- bottom level Z_w of the water course above or below $Z = 0$;
- water temperature T in $^{\circ}\text{C}$ ($0^{\circ}\text{C} \leq T \leq 40^{\circ}\text{C}$, with a default value $T = 6^{\circ}\text{C}$);
- water density ρ at the temperature T (default value $\rho = 1000 \text{ kg/m}^3$);
- constant of Von Karman κ (default value $\kappa = 0.4$).

The input data describing the geometry of dike and initial breach at $t = 0$ (see Figure 4.16) and characteristics of the sand in the dike body are:

- dike height H_d above $Z = 0$;
- width of the dike top W_d ;
- level Z_{br} of the initial breach above $Z = 0$;
- width b of the initial breach at its bottom;
- inclination angles α of the outer dike slope and β_0 of the inner dike slope;
- D_{50} and D_{90} of the sand in the dike;
- porosity p of sand in the dike;
- angle of repose ϕ of the sand in the dike.

The input data for the polder are:

- polder level Z_p above or below the reference level $Z = 0$;
- water level H_p in polder at $t = 0$ with respect to the reference level $Z = 0$;
- polder area A_p as function of H_p .

In the module 'computation of sediment fall velocity' first the kinematic viscosity ν of the water is calculated as function of the water density ρ and the water temperature T . Then the sediment fall velocity w_s is calculated as function of D_{50} , Δ , ν and g , see Appendix B.2.

The module 'select sediment transport formulae' allows the user of BRES to select one of the following sediment transport formulations:

- Bagnold-Visser (1989);

- Englund-Hansen (1967);
- Van Rijn (1984a,b);
- Wilson (1987).

The selection of these formulae has been based on a test of a large number of sediment transport formulae to experimental data of breach erosion experiments, see Chapter 5. For each of the five stages a specific formula may be selected. The default formulae are Bagnold-Visser (1989) for Stages I, II and III and Van Rijn (1984a,b) for Stages IV and V.

In the module 'definition of functions' the following frequently returning computational functions have been defined (see Appendix B.3):

- function discharge: calculates the breach inflow rate in Stages I through IV;
- function normalflow: calculates the relevant quantities for the flow on the inner slope in Stages I, II and III;
- function flowslope: calculates the quantities determining the erosion of the inner slope in Stages I through III;
- function frictioncoeff: calculates the bed friction coefficient in Stages IV and V;
- function transportcapacity: this function calculates the sand transport capacity with the sediment transport formulae of Bagnold-Visser (1989), Englund-Hansen (1967), Van Rijn (1984a,b) or Wilson (1987).

The main modules of BRES are the five modules describing the breach erosion process in each of the Stages I through V.

For the present calculations less attention has been given to the handling of the output data. In the present version of BRES the output data contain the breach discharge $Q_{br}(t)$, the outside water level $H_w(t)$ above $Z = 0$, the inside water level $H_p(t)$ above $Z = 0$, the breach width $B_l(t)$ and the transition times t_1, t_2, t_3, t_4, t_5 and t_6 with respect to $t_0 = 0$.

Appendix B contains a description of the computer program.

4.7 Discussion

The mathematical model described above is surprisingly simple, in spite of its many equations. Especially the conclusion that the development of a scour hole hardly influences the erosion of the leading breach section, and thus also hardly the discharge through the breach, yields a great simplification of the mathematical description of the breach erosion process. This is important, because scouring is a complicated physical process and its mathematical simulation is still in an immature phase.

An important component of the model is the description of the sand transport capacity, see for instance equation (4.83). There exist an enormous number of sediment transport

Breach growth in sand-dikes

formulae. In the following chapter the applicability of a number of these formulations for sand-dike breach erosion is investigated.

Chapter 5

Sediment transport formulae

5.1 Introduction

An essential part of the mathematical breach growth model developed in Chapters 3 and 4 is the description of the equilibrium value of the sediment transport, especially that of the suspended load transport (s_s). The flow velocities in breaches can become very large, for instance if the outside water level measures about 4 m above the level of the breach bottom ($H_w - Z_{br} \approx 4$ m), the flow velocity in the breach in Stage IV is about 5 m/s. Also the slope angle β can become very large in the first three stages of the breach erosion process, with angles exceeding the angle of internal friction ϕ (see Figures 2.1, 5.1 and 5.2). To the author's knowledge, there is no sediment transport formula that has been derived and tested for such large flow velocities (data of experiments on sand transport in flow velocities larger than about 3 m/s are not available, see Voogt et al., 1991, and Sieben, 1993) and such steep slopes.

In order to avoid an enormous overestimation of the sediment entrainment due to the large flow velocities, a modified Bagnold's (1963, 1966) energetics-based sediment transport formulation (here termed the Bagnold-Visser formula, see Visser, 1989) was implemented in an earlier version of the present model. This model version described Stages I through III of the breach erosion process. The comparisons with both laboratory tests and the Zwin'89 field experiment in the Zwin Channel has shown good agreement, see Visser (1995a).

However, in spite of the good results obtained with the Bagnold-Visser formula, the question has arisen whether this formula is the best of all available formulae. To answer this question an investigation into the applicability of available sediment transport formulae for sand-dike breach erosion was made (see Visser, 1995b) which is summarized in this chapter.

Sand transport rates predicted by a selection of sediment transport formulae (see Paragraph 5.2) are compared with experimental sand transport rates. The experiments are described in Paragraph 5.3. The determination of the sand transport rates in these experiments is described in Paragraph 5.4. The sediment transport rates predicted by the formulae and the comparisons with the experimental rates are described in Paragraph 5.5.

5.2 Tested sediment transport formulae

In view of the steep slopes and the large flow velocities, the following sediment transport conceptions have been included in the study:

1. Formulae for sand-water mixture flows: Wilson (1966, 1987), Mastbergen and Winterwerp (1987), see also Winterwerp et al. (1992).
2. Formulae for sediment transport in flows on relatively steep slopes: Smart and Jaeggi (1983), Bathurst et al. (1987), Rickenmann (1991).
3. Formulae for river regimes which have been tested for (relatively) large flow velocities (large shear stress velocities): Engelund and Hansen (1967), Van Rijn (1984a,b), see Voogt et al. (1991).
4. Energetics-based sediment transport conceptions: Bagnold-Bailard, see Bailard (1981), Bagnold-Visser, see Visser (1989); both formulae are modifications of the original conception of Bagnold (1963, 1966).

The original study of Visser (1995b) has included also the formulations of Mizuyama (1977) and Takahashi (1987) for flows on relatively steep slopes (both limited to slope angles $\beta < 14^\circ$), the energetics-based sediment transport conceptions of Bagnold (1963, 1966) and Yang (1979) and the formulae of Takahashi (1978, 1980, 1987, 1991) for debris flows. These formulae give unrealistic (negative, infinitely large, or extremely large) values for the sediment transport rates in the present application (see Visser, 1995b) and have been passed over in the present thesis.

Descriptions of the above nine formulations are given in Appendix A. These formulae apply to the equilibrium value of the sediment transport (or the sediment transport capacity), either bed-load transport (s_b), total load transport (s_t), or total load transport consisting of bed-load transport and suspended load transport (s_s).

The sensitivity of the transport rates predicted by the formulae of Wilson (1966, 1987), Smart and Jaeggi (1983), Bathurst, et al. (1987), Rickenmann (1991) to a variation in particle diameter D is very small or not present, while the erosion rate given by the formula of Mastbergen and Winterwerp (1987) is only slightly dependent of a variation in particle diameter D . The sediment transport rate predicted by Engelund and Hansen (1967) is proportional to D^{-1} (apart from roughness effects). Van Rijn's (1984a,b) bed-load transport increases relatively strongly with D since the thickness of the bed-load transport layer increases both with D and the parameter T (see Appendix A). Van Rijn's suspended load transport decreases with D , as also the total load transport (see Visser, 1995b). The Bagnold-Bailard (1981) formula is very sensitive to a variation in D : the transport rate strongly decreases with an increasing D . To a somewhat lesser extent, this holds also for Bagnold-Visser (1989).

The relation between sediment transport capacity and friction coefficient C_f varies rather strongly in the various transport formulae:

$$s_b \sim C_f^{1/2} \quad : \text{Wilson (1966, 1987)}$$

$$s_t \sim C_f^{1/6} \quad : \text{Mastbergen and Winterwerp (1987)}$$

$$s_b \sim 1 \quad : \text{Smart and Jaeggi (1983), Bathurst et al. (1987), Rickenmann (1991), Bagnold-Bailard's (1981) bed-load transport}$$

$$s_t \sim C_f^{-1/6} \quad : \text{Engelund and Hansen (1967)}$$

$$s_s \sim C_f^{-1/3} \quad : \text{Bagnold-Bailard's (1981) suspended load transport (for } w_s/U \text{ being much larger than } 0.01 \tan\beta), \text{ Bagnold-Visser's (1989) suspended load transport}$$

$$s_t, s_s \sim C_f^{-1/2} \quad : \text{Van Rijn's (1984a,b) total and suspended load transport}$$

$$s_b \sim C_f^{-1} \quad : \text{Van Rijn's (1984a,b) bed-load transport}$$

The above relations between s_b , s_s or s_t on the one side and C_f on the other side follow from the substitution of (4.15) with $R_n = d_n$ into the various sediment transport formulations, giving expressions for the equilibrium values of the sand transport rates as function of the parameters q , β , D (or w_s) and C_f . Especially s_b in the formulae of Wilson (1966, 1987) and s_b and s_s in the formulae of Van Rijn (1984a,b) are sensitive to variations of C_f . To a lesser extent this also applies to the formulae for the suspended load transport of Bagnold-Bailard (1981) and Bagnold-Visser (1989).

Predictions of the nine sediment transport formulations are compared with the data of three experiments: the laboratory experiments T3 and T5A of the TAW experiments in the so-called Schelde flume (see Steetzel and Visser, 1992, 1993) and the Zwin'89 field experiment in the Zwin Channel (see De Looff, 1990, and Visser et al., 1991).

The experimental data involve the first three stages of the breach erosion process (see Chapters 3 and 4). So also the investigation summarized in this chapter has been restricted to these first stages of the breach erosion process. Further the effect of an increase of the specific flow rate $q(x)$ due to sediment entrainment on U , d , l_a , etc. is ignored, and is only taken into account in the calculation of the maximum sand transport rate from the maximum depth-averaged sediment concentration c (see Paragraph 5.5).

5.3 Experimental conditions

5.3.1 Introduction

In this paragraph the experimental conditions are described of the Schelde Flume experiments T3 and T5A and of the Zwin'89 field experiment (see Table 5.1).

Breach growth in sand-dikes

	Schelde Flume experiments						Zwin'89 exp.	
	T3		T5A					
D_{50} [mm]	0.10		0.22				0.22	
t [s]	10	30	10	30	100	240	45	240
q_{br} [$m^3/s/m$]	0.015	0.015	0.015	0.015	0.010	0.18	0.10	0.25
d_c [m]	0.028	0.028	0.028	0.028	0.022	0.15	0.10	0.18
U_c [m/s]	0.53	0.53	0.53	0.53	0.46	1.2	1.0	1.4
$C_f(0)$ [-]	0.0036	0.0036	0.0045	0.0045	0.0049	0.0028	0.0031	0.0029
$\theta(0)$ [-]	0.62	0.62	0.35	0.35	0.29	1.2	0.85	1.45
β [°]	20	23	20	28	32	32	25	32
$C_f(l_n)$ [-]	0.025	0.027	0.022	0.028	0.032	0.032	0.026	0.032
d_n [m]	0.012	0.012	0.011	0.011	0.0085	0.058	0.040	0.072
U_n [m/s]	1.3	1.3	1.3	1.3	1.2	3.1	2.5	3.4
$\theta(l_n)$ [-]	24	28	11	14	12	85	46	106
Fr_n [-]	3.8	3.9	4.0	4.3	4.4	4.4	4.2	4.4
l_n [m]	1.1	1.0	0.96	0.74	0.51	4.3	3.6	5.4
l_a [m]	1.8	1.8	0.96 (0.57)	0.74 (0.61)	0.51 (0.42)	7.6	3.6 (2.8)	7.4
L [m]	2.0	1.9	2.2	2.2	1.3	1.0	4.4	3.5
$d(L)$ [m]	d_n					0.087	0.040	0.076
$U(L)$ [m/s]	U_n					2.1	2.5	3.3
$C_f(L)$ [-]	$C_f(l_n)$					0.0063	0.026	0.019
$u_*(L)/w_s$ [-]	22	24	7.0	8.1	7.5	6.0	17	19
$Fr(L)$ [-]	$Fr(l_n)$					2.5	4.2	4.1
$\theta(L)$ [-]	$\theta(l_n)$					7.8	46	57

Table 5.1 Data of the eight cases of the Schelde Flume experiments and the Zwin'89 experiment that have been applied to the test of the various sediment transport formulae (measured quantities: q_{br} , D_{50} , β and L ; calculated parameters: q_{br} , d_c , U_c , $C_f(0)$, $\theta(0)$, $C_f(l_n)$, d_n , U_n , $\theta(l_n)$, Fr_n , l_n , l_a , $d(L)$, $U(L)$, $C_f(L)$, $Fr(L)$ and $\theta(L)$, calculated as described in Paragraph 5.3).

The Schelde Flume is 50 m long; its width is 1.00 m, and its depth is 1.20 m. The flume is located in Delft Hydraulics' De Voorst Branch. A total number of nine tests were done to measure the 2DV-development of a breach in a 0.70 m high sand-dike along the breach axis. The length of the sand-dike was 0.40 m, equal to the effective width of the flume at the dike. Significant variations in the erosion process along the flume width did not occur, so the breach had a rectangular cross-section with $b = B = B_w = B_t = 0.40$ m. Observations of the specific breach discharge q_{br} were done by measuring flow velocity profiles and water depths in various sections upstream of the breach. The observations of profile development were done by means of video. The role of the sediment particle diameter was included by using sand with a $D_{50} = 0.10$ mm (as in test T3) and sand with a $D_{50} = 0.22$ mm (as in test T5A).

The Zwin'89 experiment was performed in the Zwin Channel, a tidal inlet located at the Netherlands-Belgium border, that connects the nature reserve Het Zwin with the North Sea (see Chapter 6 for a more detailed description of the area). At high water the width of the inlet is about 150 m. A sand-dam was built, exclusively for the field experiment, at low water with local sand. The 2.2 m high dam temporarily closed the Zwin Channel.

The Zwin'89 experiment was aimed at an observation of the process of breach erosion rather than at an accurate measurement of the relevant quantities. The short time available for the preparation of the experiment did not allow such measurements. In 1994 a second field test (the Zwin'94 experiment) was done at the same location in which these quantities could be observed in detail, see Chapter 6.

5.3.2 Schelde Flume experiment T3

The model dike in this experiment was constructed with relatively fine sand ($D_{50} = 0.10$ mm, $D_{10} = 0.069$ mm, $D_{90} = 0.15$ mm). The mean fall velocity of this sediment at a water temperature $T \approx 18^\circ\text{C}$ is $w_s = 0.0090$ m/s. At the start of the experiment (at $t = t_0 = 0$ s), the cross-section of the sand-dike had the following dimensions: level of breach bottom Z_{br} above level of flume bottom Z_w is 0.70 m, crest width is 1.3 m, inclination angle of inner slope $\beta_0 = 18^\circ$ (slope 1 in 3), length inner slope $L_0 = 2.2$ m and inclination angle of outer slope is 1 : 30 (schematized dune erosion profile).

The outside water level H_w (measured above Z_w) was maintained as long as possible at $H_w - Z_w = 0.75$ m by recirculating the breach discharge to the upstream end of the flume. According to the weir formula (4.13), a water head $H_w - Z_{br} = 0.05$ m over the breach gives a discharge $Q_{br} = 0.0076$ m³/s, i.e. a specific flow rate $q_{br} = 0.019$ (m³/s)/m. Bed friction along the mild outer slope and the horizontal crest caused the discharge q_{br} to be somewhat smaller for $0 < t < 100$ s: $q_{br} \approx 0.015$ (m³/s)/m (see Steetzel and Visser, 1992).

Figure 5.1 shows the development of the cross-section in this experiment (observed from the video-images). The sediment transport rates at times $t = 10$ s and $t = 30$ s ($\approx t_1$) have

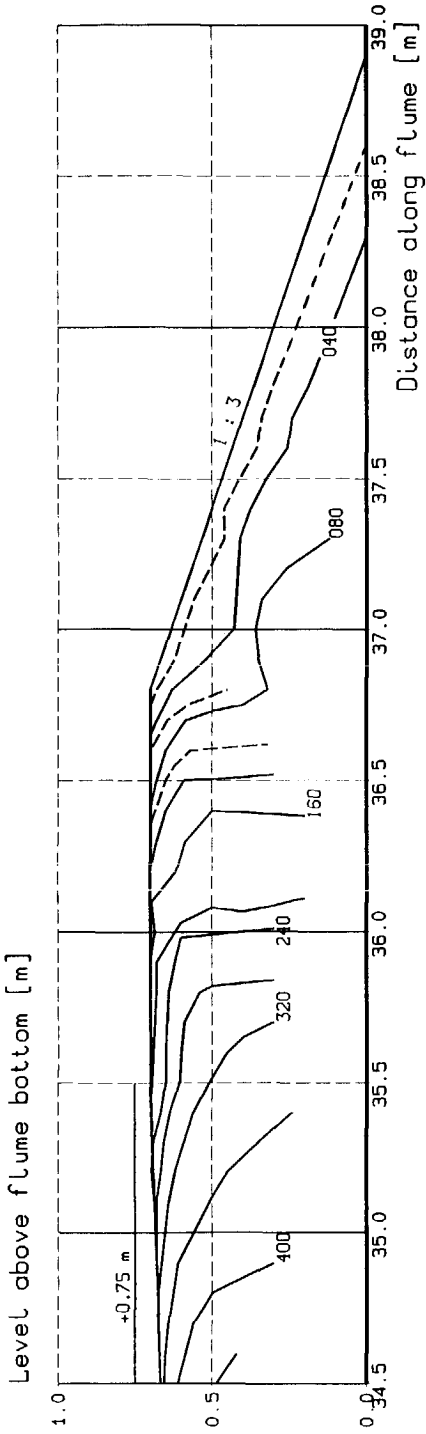


Figure 5.1 Development profile of sand-dam in Experiment T3; time in seconds, $t = 0$ at start of overflow.

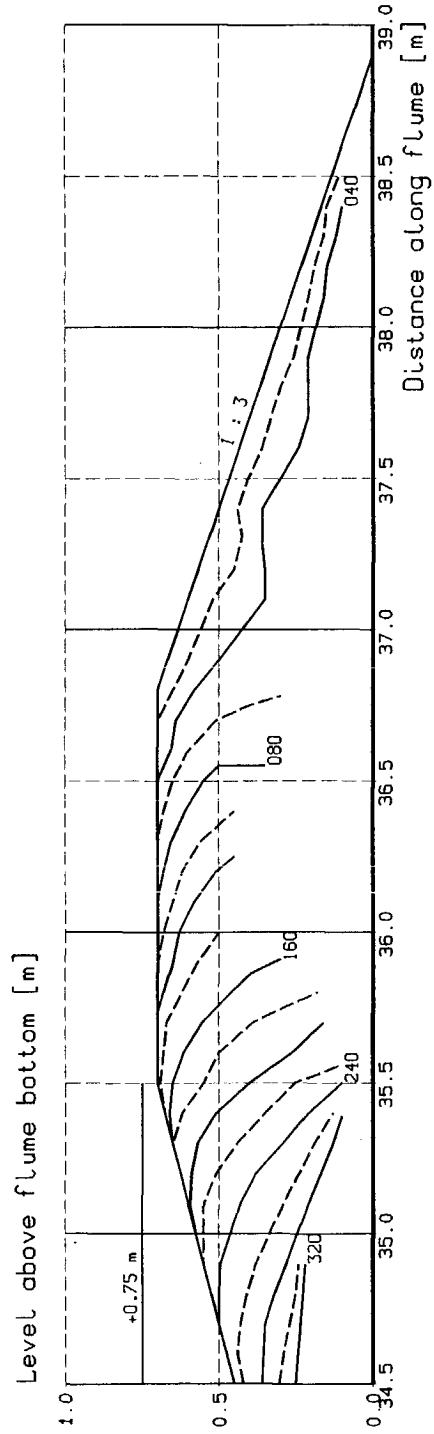


Figure 5.2 Development profile of sand-dam in Experiment T5A; time in seconds, $t = 0$ at start of overflow.

been determined from these profiles by assessing amounts of eroded sediment between $t = 0$ s and $t = 20$ s and between $t = 20$ s and $t = 40$ s, respectively, and dividing these amounts by $\Delta t = 20$ s (see Paragraph 5.4).

The water depth $d(0)$ and flow velocity $U(0)$ at the top of the inner slope ($x = 0$) can be calculated with (4.18): $d(0) = d_c = 0.028$ m, $U(0) = U_c = 0.53$ m/s as $q_{br} = 0.015$ (m³/s)/m. Equations (4.8), (4.9) and (4.11) give for $x = 0$ a friction coefficient $C_f(0) = 0.0036$ and a mobility parameter $\theta(0) = 0.62$.

The flow on the inner slope accelerated between $x = 0$ and $x = l_n$. For $\beta \approx 20^\circ$ (see Figure 5.1) and $q_{br} = 0.015$ (m³/s)/m, equations (4.8), (4.10), (4.11), (4.15), (4.16), (4.20) and (4.26) yield: $C_f(l_n) = 0.025$, $\theta(l_n) = 24$, $d_n = 0.012$ m, $U_n = 1.3$ m/s, $Fr_n = 3.8$ and $l_n = 1.1$ m at $t = 10$ s (as $L \approx 2.0$ m, see Figure 5.1). Identically for $t = 30$ s (as $\beta \approx 23^\circ$ and $L \approx 1.9$ m, see Figure 5.1): $C_f(l_n) = 0.027$, $\theta(l_n) = 28$, $d_n = 0.012$ m, $U_n = 1.3$ m/s, $Fr_n = 3.9$ and $l_n = 1.0$ m.

Above values for l_n have been calculated with (4.26) assuming that $C_f = C_f(l_n)$ along the entire inner slope, which yields an underestimation of l_n since in reality C_f will increase from $C_f(0)$ to $C_f(l_n)$. At the other hand, (4.26) gives an overestimation of l_n (see Chapter 4). So, the calculated values for l_n are estimated values. Substitution of the values for q_{br} and β into equation (4.36) for the adaptation length l_a of the suspended load transport gives with $\xi = 1$: $l_a = 1.8$ m both at $t = 10$ s and $t = 30$ s.

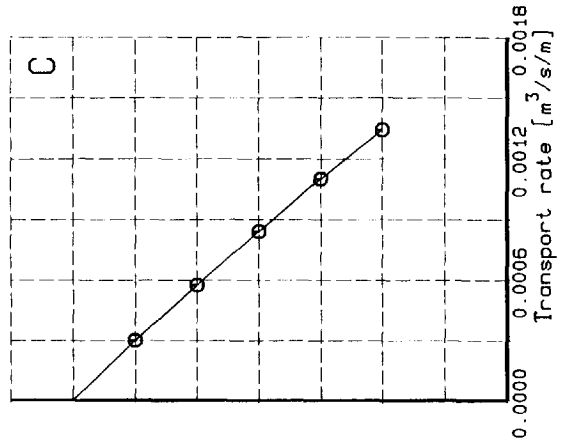
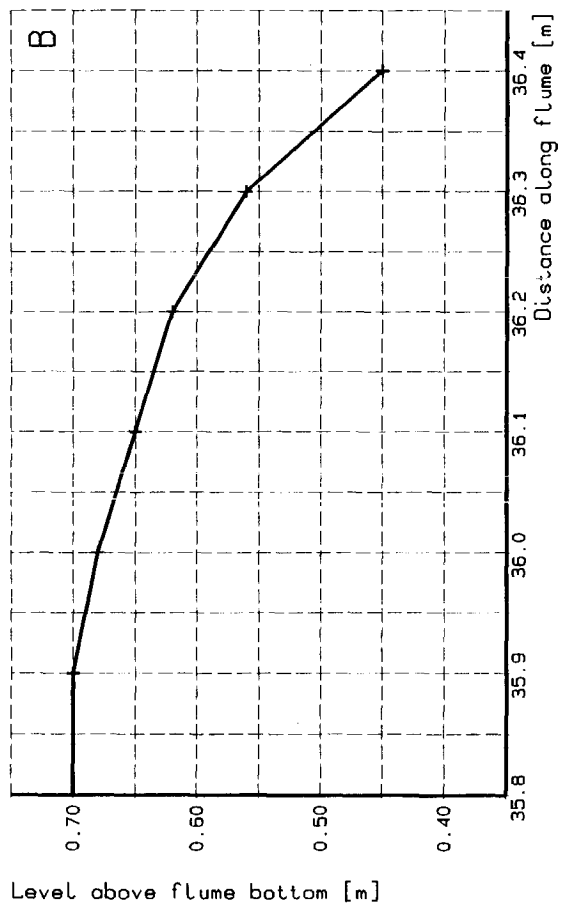
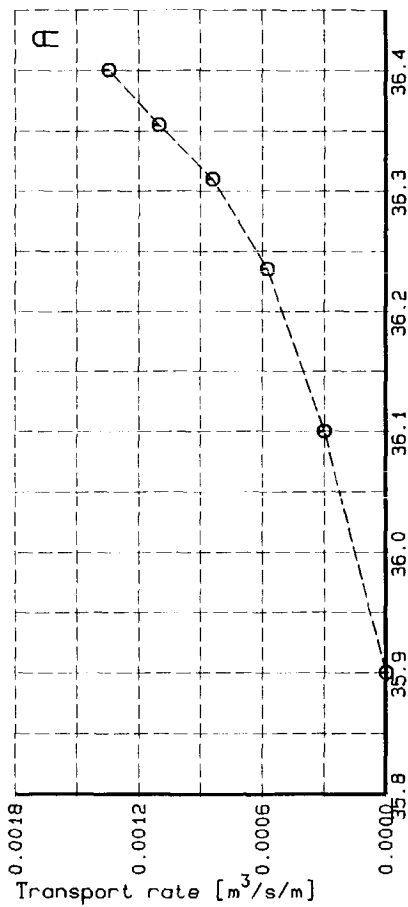
A friction coefficient $C_f \approx 0.025$ means a relatively extreme large bed shear (roughness height k equals magnitude of water depth). This is in agreement with what was measured in the laboratory experiments of Visser et al. (1986).

Table 5.1 summarizes the main values for the various quantities and parameters.

5.3.3 Schelde Flume experiment T5A

The sand-dike in this experiment was constructed with dune-sand ($D_{10} = 0.15$ mm, $D_{50} = 0.22$ mm, $D_{90} = 0.29$ mm, mean sediment fall velocity for $T \approx 18^\circ\text{C}$ is $w_s = 0.028$ m/s). The cross-sectional dimensions have been identical to those of T3, with the exception of the inclination of the outer slope (1 : 4 at $t = t_0 = 0$ s in T5A, i.e. a dike profile, see Figure 5.2). The upstream water depth was maintained again as long as possible at $H_w - Z_w = 0.75$ m by recirculating the breach flow. The measured q_{br} is for $0 < t < 100$ s almost equal to that of T3: $q_{br} \approx 0.015$ (m³/s)/m, see Steetzel and Visser (1992, 1993).

Also for this experiment, sediment transport computations have been done for $t = 10$ s and $t = 30$ s ($\approx t_1$). Figure 5.2 shows that at $t = 10$ s: $\beta \approx 20^\circ$ and $L \approx 2.2$ m, and at $t = 30$ s: $\beta \approx 28^\circ$ (along the adaptation length l_a) and $L \approx 2.2$ m. Sand transport calculations have also been done for $t = 100$ s, that is between $t = t_1$ en $t = t_2$, for a slope angle equal to the angle of repose ($\beta_1 = 32^\circ$). Due to some water level decrease inside the flume at $t = 100$ s, caused



SAND TRANSPORT RATE ALONG INNER SLOPE AT $t = 100$ s IN EXP. T5A

Test T5A

Figure 5.3

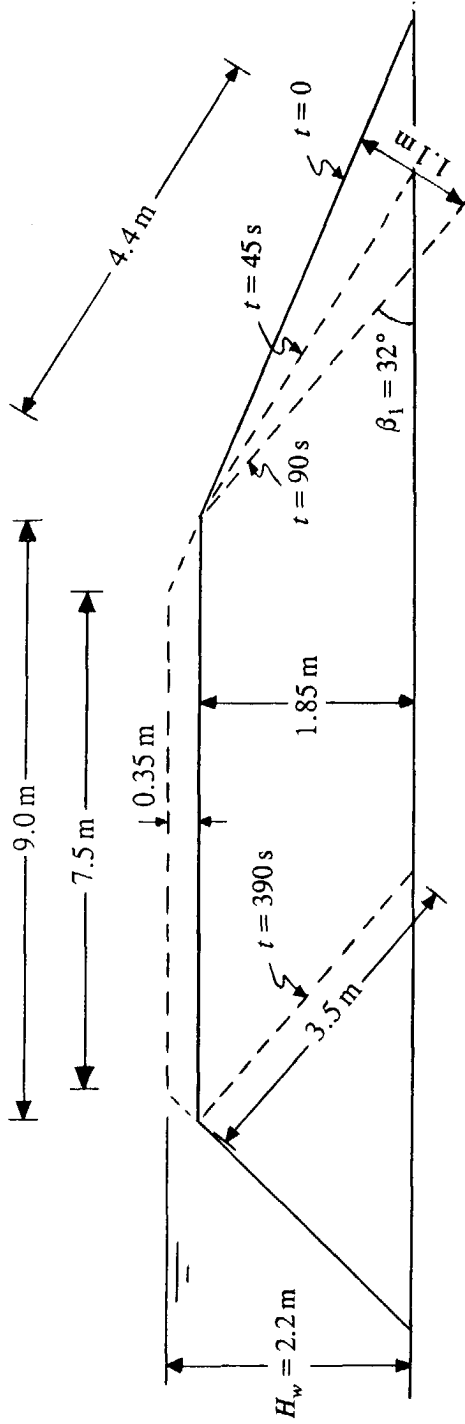


Figure 5.4 Observed development of cross-section of sand-dam in Zwin'89 experiment.

by the discharge of water over 100 s of about $0.015 \cdot 100 \text{ m}^3/\text{m} = 1.5 \text{ m}^3/\text{m}$ (the pumps started to recirculate water only after the water in the downstream section of the flume had risen to a certain level), the flow discharge at $t = 100 \text{ s}$ was somewhat lower than in the initial phase of the experiment, that is about $q_{br} \approx 0.010 \text{ (m}^3/\text{s)/m}$, see Steetzel and Visser (1992).

The above values for the various quantities and parameters for the flow over the inner slope at $t = 10 \text{ s}$, 30 s and 100 s , and the calculated values for d_c , U_c , $C_f(0)$, $\theta(0)$, $C_f(l_n)$, d_n , U_n , $\theta(l_n)$, Fr_n , l_n and l_a are shown in Table 5.1. Equation (4.36) predicts for $t = 10 \text{ s}$ an adaptation length of the sand transport ($l_a = 0.57 \text{ m}$) smaller than the magnitude of the adaptation length of the flow profile ($l_n = 1.2 \text{ m}$) as given by (4.26). Also if l_n is reduced by a factor 0.8 (the increase of the flow velocity between $x = 0.8l_n$ and $x = l_n$ is very small, see Section 4.2.1), giving $l_n = 0.96 \text{ m}$, this reduced l_n is larger than l_a . It is clear that the sand transport increases as the flow accelerates, at least as long as the sand concentration has not reached its maximum value. Consequently $l_a \geq l_n$, giving $l_a = 0.96 \text{ m}$ for $t = 10 \text{ s}$. The values for l_a at $t = 30 \text{ s}$ and $t = 100 \text{ s}$ have been adapted in the same way for the same reason.

In experiment T5A the dike crest started to drop at $t_2 \approx 140 \text{ s}$ (see Figure 5.2), causing the flow rate over the top to increase (see Steetzel and Visser, 1992, 1993). At $t_2^+ = 240 \text{ s}$ ($t_2 < t_2^+ < t_3$, Stage III): $H_w - Z_w \approx 0.72 \text{ m}$ and $Z_{br} - Z_w \approx 0.50 \text{ m}$. Substitution of these values into (4.13) gives: $q_{br} = 0.18 \text{ (m}^3/\text{s)/m}$, that is equal to the observed specific discharge (see Steetzel and Visser, 1992).

The slope angle β strongly varied at $t = t_2^+$. Assuming β to be equal to $\beta_1 = 32^\circ$ gives for t_2^+ : $d_c = 0.15 \text{ m}$, $C_f(l_n) = 0.032$, $d_n = 0.058 \text{ m}$, $l_n = 4.3 \text{ m}$ and $l_a = 7.6 \text{ m}$. At t_2^+ the length of the inner slope $L(t_2^+) \approx 1.0 \text{ m}$, so $L(t_2^+) < l_n$ and $L(t_2^+) \ll l_a$. This means that at t_2^+ the water depth $d(L)$ at the toe of the slope was larger than the normal water depth d_n . An estimation of $d(L)$ follows from (4.27): $d(L) \approx 0.087 \text{ m}$, so $U(L) \approx 2.1 \text{ m/s}$ and $\theta(L) \approx 7.8$ (see Table 5.1). The fact that $L(t_2^+) \ll l_a$ means that the sand transport $s(L)$ at the toe of the slope was much smaller than its equilibrium value at $t = t_2^+$.

5.3.4 Zwin'89 field experiment

This field experiment was performed with local sand from the Zwin area, with an estimated D_{50} about equal to that of the dune-sand of experiment T5A: $D_{50} \approx 0.22 \text{ mm}$. The values for D_{10} and D_{90} of the dune-sand are also adopted for the sand used in the Zwin'89 experiment ($D_{10} \approx 0.15 \text{ mm}$, $D_{90} \approx 0.29 \text{ mm}$). The mean fall velocity of this sand at a water temperature $T \approx 8^\circ \text{C}$ is $w_s = 0.024 \text{ m/s}$.

The angle of inclination β of the inner slope at the start of the experiment at $t = t_0 = 0 \text{ min}$ ($\approx 12 \text{ h } 49 \text{ min } 30 \text{ s}$ on 13 December 1989) was: $\beta_0 = 18^\circ$. The relevant dimensions of the sand-dam at $t = t_0$ have been: dam height $H_d \approx 2.2 \text{ m}$ above level Z_w of the bottom

of the Zwin Channel (which was about at mean sea level, $H_d - Z_w \approx 2.2$ m), length of crown ≈ 7.5 m and inclination outer slope 1 : 1.25 (see Figure 5.4). The depth of the small pilot (initial) channel in the top of the dam was at $t = t_0$: $H_d - Z_{br} \approx 0.35$ m. It is assumed that the breach had a rectangular cross-section throughout the breaching process.

The experiment was video-taped and photographed. The following values for t_1 , t_2 and t_3 have been estimated from this visual material: $t_1 \approx 1.5$ min, $t_2 \approx 6.5$ min and $t_3 \approx 7.7$ min, see De Looff (1990). At $t = t_4 \approx 20$ min the flow turned from virtually critical into sub-critical, see Visser et al. (1991).

Sand transport computations have been done for $t = 45$ s (just between $t = t_0$ and $t = t_1$ in Stage I, when $\beta \approx 25^\circ$ and $L \approx 4.4$ m) and for $t = 240$ s (just between $t = t_1$ and $t = t_2$ in Stage II, when $\beta \approx \beta_1 = 32^\circ$ and $L \approx 3.5$ m), see Table 5.1. The water depth downstream in the pilot channel between $t = t_0$ and $t = t_1$ was about 0.10 m (when $H_w - Z_w \approx 2.0$ m, where Z_w is the level of the bottom of the Zwin Channel just outside the breach and measured above the reference level $Z = 0$). Substitution of $d_c \approx 0.10$ m into (4.18) gives: $q_{br} \approx 0.10$ (m³/s)/m. Between $t = t_1$ and $t = t_2$, the outside water level H_w rose from about 2.0 m to about 2.1 m above the bottom level Z_w , yielding an increase of the water depth downstream in the pilot channel from about 0.15 m to about 0.20 m. Consequently the specific discharge through the breach at $t = 240$ s is estimated at $q_{br} \approx 0.25$ (m³/s)/m.

Table 5.1 summarizes the main values for the various quantities and parameters. The friction coefficients calculated with (4.8) and (4.10) are relatively large, as in the Schelde Flume experiments. This is roughly in agreement with what was observed in the field measurements in the Slaak estuary (in which $C_f \approx 0.016$), see Section A.2.2 of Appendix A. The adaptation lengths l_a have been calculated with (4.37) assuming that $B_w/B_l \approx 0.6$.

5.4 Determination of sand transport rates in experiments

5.4.1 Schelde Flume experiment T3

Figure 5.1 shows that experiment T3 supports the assumption of Section 4.2.2 that the entrainment of sediment starts at $x = 0$ at the top of the inner slope. Since $u_*'/w_s > 1$ (see Visser, 1995b), the sediment transport along the slope can be written for $l_n \leq x \leq l_a$ as

$$s(x, t) \approx s_b(t) + \frac{x}{l_a} s_s(t) \quad \text{for } l_n \leq x \leq l_a \quad (5.1)$$

(the time variable t has been added to stress the dynamic behaviour of the breach erosion process). At a distance l_n from the top of the inner slope ($x = 0$), the bed-load transport is equal to its equilibrium value and at $x = l_a$ the suspended load transport reaches its

equilibrium value or transport capacity ($l_n = 1.1$ m and $l_a = 1.8$ m at $t = 10$ s, $l_n = 1.0$ m and $l_a = 1.8$ m at $t = 30$ s). Theoretically for $x \geq l_a$ the sediment transport stays at its equilibrium value, i.e. it is constant.

Sand transport rates (volumes of sand particles without voids), for instance at $t = 10$ s, have been determined from the profiles shown in Figure 5.1 by estimating amounts of sand eroded between $t = 0$ s and $t = 20$ s along a length of $l_n = 1.1$ m (for the test of bed-load transport formulae) and along a length of $l_a = 1.8$ m (for the test of total load transport formulae), both measured from $x = 0$, and dividing the results by $\Delta t = 20$ s and multiplying them by the factor $1 - p = 0.6$ (the porosity p was measured in both Schelde Flume tests T3 and T5A as $p \approx 0.4$). The results are:

- at $x = l_n$: $s(1.1 \text{ m}, 10 \text{ s}) \approx 0.0016 \text{ (m}^3\text{/s)/m}$, $s(1.0 \text{ m}, 30 \text{ s}) \approx 0.0028 \text{ (m}^3\text{/s)/m}$,
- at $x = l_a$: $s(1.8 \text{ m}, 10 \text{ s}) \approx 0.0040 \text{ (m}^3\text{/s)/m}$, $s(1.8 \text{ m}, 30 \text{ s}) \approx 0.0060 \text{ (m}^3\text{/s)/m}$.

5.4.2 Schelde Flume experiment T5A

Figure 5.2 shows the observed development of the cross-section of the sand-dike in experiment T5A. The adaptation lengths of suspended load transport are $l_a \approx 0.96$ m at $t = 10$ s and $l_a \approx 0.74$ m at $t = 30$ s, both being much shorter than the length of the inner slope. The rates of sediment transport determined from Figure 5.2 are:

- at $x = l_n$: $s(0.96 \text{ m}, 10 \text{ s}) \approx 0.0023 \text{ (m}^3\text{/s)/m}$, $s(0.74 \text{ m}, 30 \text{ s}) \approx 0.0024 \text{ (m}^3\text{/s)/m}$,
- at $x = l_a$: $s(0.96 \text{ m}, 10 \text{ s}) \approx 0.0023 \text{ (m}^3\text{/s)/m}$, $s(0.74 \text{ m}, 30 \text{ s}) \approx 0.0024 \text{ (m}^3\text{/s)/m}$.

In the first instance, there is no erosion for $x > l_a$ (see Chapter 3), after some time resulting in the appearance of a bar downstream of $x = l_a$, along which eventually a hydraulic jump is formed. Due to the turbulence generated in the hydraulic jump, the transport capacity firmly increases, resulting in the pick up and discharge of large amounts of sand downstream of $x = l_a$. Hydraulic jumps were observed in Schelde Flume experiment T3 for $t > 40$ s (see profile inner slope at $t = 80$ s in Figure 5.1). Due to the flow of water over the dike crest, the water level decreased in the flume, leading to a decrease of q_{br} (see Steetzel and Visser, 1992). According to equation (4.36), a smaller discharge rate $q_{br} = Ud$ gives an adaptation length l_a smaller than the length of the inner slope, and thus as described above, a hydraulic jump.

The sand transport rates at time $t = 100$ s at $x = l_n = l_a = 0.51$ m have been estimated from Figure 5.3 as:

- at $x = l_n$: $s(0.51 \text{ m}, 100 \text{ s}) \approx 0.0012 \text{ (m}^3\text{/s)/m}$,
- at $x = l_a$: $s(0.51 \text{ m}, 100 \text{ s}) \approx 0.0012 \text{ (m}^3\text{/s)/m}$.

The sediment transport rate at $t = 240$ s at $x = L \approx 1.0$ m (at the toe of the slope) has been estimated from Figure 5.2 as:

- at $x = L$: $s(1.0 \text{ m}, 240 \text{ s}) \approx 0.0027 \text{ (m}^3\text{/s)/m}$.

5.4.3 Zwin'89 field experiment

Figure 5.4 shows the observed development of the cross-section of the sand-dam in the Zwin'89 experiment (from photo- and video-recordings). Estimating sediment transport rates from volumes eroded sand at $x = l_n = 3.6$ m and $x = L = 4.4$ m at time $t = 45$ s and at $x = L = 3.50$ m at time $t = 240$ s yields:

- at $x = l_n$: $s(3.6 \text{ m}, 45 \text{ s}) \approx (3.6/4.4)^2 * s(4.4 \text{ m}, 45 \text{ s}) \approx 0.018 \text{ (m}^3/\text{s)/m}$,
- at $x = l_a$: $s(3.6 \text{ m}, 45 \text{ s}) \approx (3.6/4.4)^2 * s(4.4 \text{ m}, 45 \text{ s}) \approx 0.018 \text{ (m}^3/\text{s)/m}$,
- at $x = L$: $s(4.4 \text{ m}, 45 \text{ s}) \approx [4.4 \text{ m} * (0.5 * 1.1 \text{ m}) * 0.6/0.6]/(90 \text{ s}) \approx 0.027 \text{ (m}^3/\text{s)/m}$,
- at $x = L$: $s(3.5 \text{ m}, 240 \text{ s}) \approx [9.0 \text{ m} * 1.85 \text{ m} * 0.6/0.6]/(300 \text{ s}) \approx 0.056 \text{ (m}^3/\text{s)/m}$.

The factor 0.6 represents the factor $1 - p$ (with a porosity $p = 0.4$ as in the Schelde Flume experiments). The factor $1/0.6$ represents an increase of sediment transport due to the factor B_w/B_t (see Paragraph 4.2) which is roughly estimated at 0.6.

5.5 Results of sediment transport calculations

Sediment transport calculations have been done with the formulations of Paragraph 5.2 for the test conditions described in Paragraph 5.3. The formulations of Wilson (1966, 1987), Smart and Jaeggi (1983), Bathurst et al. (1987) and Rickenmann (1991) apply to bed-load transport. In the first instance, the equilibrium values for the sand transport rates (s_b) predicted by these formulae have been compared with the experimental rates at $x = l_n$.

The formulations of Engelund and Hansen (1967) and Mastbergen and Winterwerp (1987) apply to total sediment transport, conceived here as suspended load transport with adaptation length l_a . The formulae of Van Rijn (1984a,b), Bagnold-Bailard (1981) and Bagnold-Visser (1989) apply to total sediment transport consisting of bed-load transport and suspended load transport. The equilibrium values for the sediment transport rates (s_t) given by these formulae have been compared with the experimental rates at $x = l_a$. The bed-load transport module of the Bagnold-Bailard (1981) formulation gives unrealistic large values and has been neglected ($s_b \ll s_s$, since $u_* / w_s \gg 1$). Identically the Bagnold-Visser (1989) bed-load transport has been limited very roughly as $s_b \leq 2(1 - p)D_{50}U$.

Equilibrium values for the sand transport and local rates of sand transport have been computed as volume transported sediment (sediment without voids). In cases where the transport formulae predict extremely large or even infinitely large transport rates, it has been assumed that

$$s(x) \leq 1.5 q_{br} \quad (5.2)$$

Equation (5.2) follows from the substitution of $c(x) \leq 0.6$ into the equation for the depth-averaged sediment concentration c :

$$c(x) = \frac{s(x)}{q(x)} = \frac{s(x)}{q_{br} + s(x)} \quad (5.3)$$

Table 5.1 shows that in six of the eight cases $L \geq l_a$ (so also $L \geq l_n$). For these cases the equilibrium values $s_b = s(l_n)$ for bed-load transport and $s_t = s(l_a)$ for total load transport have been computed. In Schelde Flume experiment T5A at $t = 240$ s and Zwin'89 experiment at $t = 240$ s the length of the inner slope L was smaller than l_n and l_a ($L \leq l_n \leq l_a$). It is described in Section 4.2.2 that two approaches exist for the calculation of the sediment transport $s(L)$ at the toe of the inner slope. In approach 1 the sediment transport $s(L)$ at the toe of the inner slope is calculated using the local flow conditions at $x = L$:

$$s(L,t) = s_b(L,t) + \frac{L}{l_a} s_s(L,t) \quad \text{if} \quad L \leq l_n \leq l_a \quad (5.4)$$

in which it is assumed that the adaptation length of the bed-load transport is negligible small, i.e. the bed-load transport is determined by the local flow velocity U . Table 5.2 summarizes the computational results obtained with (5.4), presented as the values of the ratio ϵ of calculated to experimental sand transport rates. Table 5.2 clearly indicates that most of the sediment transport formulae overestimate the experimental sand transport rates considerably.

A parameter r is defined such that $r = \epsilon$ if $\epsilon \geq 1$ and $r = 1/\epsilon$ if $\epsilon < 1$. Averaging r over the eight cases yields a mean value \bar{r} that is a measure for the discrepancy between formula and experiment. From Table 5.2 the following list of the five formulae with the lowest values for \bar{r} results:

1. Bagnold-Visser (1989): $\bar{r} = 1.5$; 2. Van Rijn (1984a,b): $\bar{r} = 1.6$; 3. Bagnold-Bailard (1981): $\bar{r} = 2.3$ (bed-load transport s_b neglected since $u_* / w_s \gg 1$); 4. Wilson (1966, 1987): $\bar{r} = 2.8$ and 5. Smart and Jaeggi (1983): $\bar{r} = 4.6$.

As described before, the relatively large values of the mobility parameter θ in the present experiments indicate that the sediment transport is not restricted to a layer immediately above the bed with a thickness of a few particle diameters. Instead, in the first stages of the breach erosion process the sediment particles are transported in a dense layer above the bed, supported by grain-grain interaction, with a thickness of about half the water depth (see Figure A.1 in Appendix A). This sheet flow has an adaptation length much larger than that of bed-load transport. Applying the above bed-load transport formulae, in approach 2 it is therefore further assumed that all sand transport has an adaptation length l_a .

For above five formulae with lowest values of \bar{r} , Table 5.2 indicates a significant

	Schelde Flume experiments										Zwin'89 exp.	
	0.10			0.22				0.22			0.22	
D_{50}	[mm]	10	30	10	30	100	240	45	240	45	240	
t	[s]	0.025	0.027	0.022	0.028	0.032	0.0089	0.026	0.032	0.018	0.019	
C_f	[-]	0.0016	0.0028	0.0023	0.0024	0.0012						
measured $s(l_n)$	[(m ³ /s)/m]	0.0040	0.0060	0.0023	0.0024	0.0012						
measured $s(l_a)$	[(m ³ /s)/m]						0.0027				0.056	
Wilson (1966, 1987)		3.6	2.5	2.4	3.5	5.6	1.3	2.7	1.2			
Mastbergen and Winterwerp (1987)		2.2	2.2	1.4	5.8	12	100	4.7	6.6			
Smart and Jaeggi (1983)		4.8	3.4	3.3	5.4	9.2	4.4	3.9	2.4			
Bathurst, Graf and Cao (1987)		1.9	1.4	1.3	2.3	3.9	31	1.7	2.1			
Rickenmann (1991)		8.1	6.1	5.2	9.2	12	100	7.8	6.6			
Engelund and Hansen (1967)		5.5	3.7	4.8	7.9	9.2	0.85	8.3	7.2			
Van Rijn (1984a,b)		0.88	0.62	0.96	1.0	1.2	0.36	0.87	0.32			
Bagnold-Bailard (1981)		2.2	2.3	0.78	1.1	1.5	0.25	2.9	3.5			
Bagnold-Visser (1989)		1.3	1.0	0.87	1.2	1.8	0.40	1.8	0.70			

Table 5.2 Values of ratio ϵ of computed to experimental sand transport rates resulting from approach 1; transport rates computed assuming that bed-load transport has an adaptation length l_n and suspended load transport an adaptation length l_a .

	Schelde Flume experiments												Zwin '89 exp.	
	0.10						0.22						0.22	
	10	30	10	30	100	240	30	100	240	45	240	0.026	0.032	
D_{50}	[mm]													
t	[s]	10	0.025	0.027	0.022	0.028	0.032	0.0089	0.026	0.032				
C_f	[-]													
measured $s(l_a)$	[(m ³ /s)/m]	0.0040	0.0060	0.0023	0.0024	0.0012								
measured $s(L)$	[(m ³ /s)/m]							0.0027					0.056	
Wilson (1966, 1987)		1.4	1.2	2.4	3.5	5.6	5.2	2.7	1.4					
Mastbergen and Winterwerp (1987)		2.2	2.2	1.4	5.8	12	100	4.7	6.6					
Smart and Jaeggi (1983)		1.9	1.6	3.3	5.4	9.2	8.0	3.9	2.2					
Bathurst, Graf en Cao (1987)		0.78	0.65	1.3	2.3	3.9	3.5	1.7	1.0					
Rickenmann (1991)		3.2	2.8	5.2	9.2	12	18	7.8	5.1					
Engelund and Hansen (1967)		5.5	3.7	4.8	7.9	9.2	57	8.3	20					
Van Rijn (1984a,b)		0.88	0.62	0.96	1.0	1.2	1.4	0.87	0.41					
Bagnold-Bailard (1981)		2.2	2.3	0.78	1.1	1.5	8.9	2.9	7.8					
Bagnold-Visser (1989)		1.3	1.0	0.87	1.2	1.8	4.4	1.8	1.3					

Table 5.3 Values of ratio ϵ of computed to experimental sand transport rates resulting from approach 2; transport rates computed assuming that both bed-load transport and suspended load transport have an adaptation length l_a .

decrease of the ratio ϵ between computed and experimental sand transport rates in Stage III (Schelde Flume experiment, $t = 240$ s) as the discharge q_{br} decreases. The BRES-model does confirm this indication by showing a dramatic deceleration of the erosion process as Stage III progresses leading to unrealistic long time intervals $t_3 - t_2$. Therefore, in approach 2 the sediment transport $s(L)$ at the toe of the slope is calculated if $L \leq l_n \leq l_a$ using the normal flow conditions at $x = l_n$:

$$s(L,t) = \frac{L}{l_n} s_b(l_n,t) + \frac{L}{l_a} s_s(l_n,t) \approx \frac{L}{l_a} [s_b(l_n,t) + s_s(l_n,t)] \quad \text{if } L \leq l_n \leq l_a \quad (5.5)$$

Table 5.3 summarizes the computational results obtained with (5.5). The list of best performing formulae becomes now: 1. Van Rijn ($\bar{r} = 1.4$), 2. Bagnold-Visser ($\bar{r} = 1.7$), 3. Bathurst et al. ($\bar{r} = 2.1$), 4. Wilson ($\bar{r} = 2.9$) and 5. Bagnold-Bailard ($\bar{r} = 3.5$).

The formulations of Van Rijn (1984a,b) and Bagnold-Visser (1989) give the best (in fact the less inaccurate) predictions for the experimental results, both in approach 1 and approach 2.

5.6 Discussion

The process of entrainment of sand from a relatively steep slope, and the resulting sediment transport occurring in the first three stages of the development of a breach in a sand-dike, is very exceptional from a hydraulic point of view:

- The mobility parameter θ varies between about 0.3 at the top of the inner slope and about 10 to 100 (or more) at $x \geq l_n$ along the slope (see Table 5.1).
- The Froude number Fr increases along this slope from $Fr = 1$ at the top to substantially larger values at $x \geq l_n$ or at $x = L$ (here: $1 \leq Fr \leq 4.4$, see Table 5.1).
- The angle of inclination attains values of $\beta \approx 32^\circ$ and larger.
- The nominal roughness height k given by the equations (4.9) and (4.10) increases from $3D_{90}$ at the top of the slope to values having the order of magnitude of the water depth at $x \geq l_n$.
- The depth-averaged sand concentration gets values at $x \geq l_n$ up to $c \approx 0.25$, see Visser (1995b).

None of the present sediment transport formulae have been set-up for and tested to such extreme conditions. The validity ranges of the formulae (if known) are well exceeded in the present tests, especially those of the mobility parameter θ , the slope angle β and (to a lesser extent for some formulae) the depth-averaged concentration c .

Most of the tested sediment transport formulae predict transport rates deviating substantially from the experimental rates. The formulations of Van Rijn (1984a,b) and Bagnold-Visser (1989) give the best (in fact the less inaccurate) predictions of the experimental results. This conclusion applies to the sand transport in Stages I through III of the five-step breach erosion process as described in Chapters 3 and 4, when the flow is supercritical (in the tests varied Fr from 1.0 at the top of the slope to about 4.4 at $x = l_n$, see Table 5.1) and when transport of sand in suspension dominates bed-load transport. Further it has been assumed that:

- Sediment transport has an adaptation length l_a that is described by (4.37) with $\xi = 1$ (sand transport on a relatively steep slope, see Section 4.2.2). Application of $\xi = 0.5$ and $\xi = 2$ gives worse predictions of the experimental results, see Visser (1995b). The value $\xi = 1$ for the Galappatti's (1983) parameter ξ applies only to the sand transport in Stages I through III.
- The friction coefficient is given by (4.8) with (4.9) and (4.10). Visser (1995b) has, however, shown that also with $C_f = 0.058$ (i.e. a Chézy coefficient $C = g/C_f^2 = 13 \text{ m}^{1/2}/\text{s}$, as measured by Visser (1989) in experiments comparable to the present Schelde Flume experiments) and for larger depths $C_f = 0.016$ (i.e. a Chézy coefficient $C = 25 \text{ m}^{1/2}/\text{s}$, as measured in the Slaak Estuary, see Section 5.3.4) the Bagnold-Visser and the Van Rijn formulae give the best predictions for the experimental data. Obviously this choice is not very sensitive to an accurate description of the bed friction coefficient C_f .

Due to the large sediment entrainment, the flow rate of the sand-water mixture increases substantially along the inner slope and the sand concentration becomes very large (so that the effect of hindered entrainment is possibly not negligible). Further study is necessary to investigate the effects of the large rate of sediment entrainment on the breach erosion process.

The investigation summarized in this chapter has not recommended a formulation for the important Stages IV (when $Fr = 1$ and slightly above 1) and V (when $Fr < 1$), in which most of the breach inflow and the breach erosion take place, and in which also the dimensions of the final breach are determined. Consequently the above conclusions do not apply to these stages. Detailed observations of the entrainment of sediment as done in the Schelde Flume experiments for Stages I and II are, to the author's knowledge, not available for these stages.

Voogt et al. (1991) tested the sand transport formulae of Engelund and Hansen (1967) and Van Rijn (1984a,b) for relatively large flow velocities in subcritical flow. They concluded that also in these circumstances both formulations give fair agreement with experimental data. So it might be that these formulae can be applied in the later stages of the breach erosion process.

The following sand transport formulae have been included in the BRES model as options: Bagnold-Visser (1989), Engelund and Hansen (1967), Van Rijn (1984a,b) and Wilson (1987). The tests of the present breach growth model has been done with these formulae. The default formulae resulting from these tests are Bagnold-Visser (1989) for Stages I through III and Van Rijn (1984a,b) for Stages IV and V. Application of the formula of Engelund and Hansen (1967) in Stages IV and V yields, however, also fair agreement between model predictions and experimental data. Reference is made to Chapter 7 for details of these tests.

Chapter 6

Experiments for verification

6.1 Introduction

The mathematical model developed in Chapter 4 needs empirical verification. For this purpose two experiments were performed which are described in this chapter. In both experiments the total breaching process was observed, i.e. both the development of the width and the depth of the breach in Stages I through V were measured. Paragraph 6.2 contains a description of the procedure and the results of the Zwin'94 experiment, a field experiment performed in 1994 in the Zwin Channel. Since the Zwin'94 experiment left some questions about the growth of the scour hole in Stages IV and V, an additional test in the laboratory was done, which is described in Paragraph 6.3.

6.2 Zwin'94 field experiment

6.2.1 Introduction

The Zwin'94 experiment was performed on 6 and 7 October 1994 in a joint project of the Department of Civil Engineering of the Delft University of Technology, Rijkswaterstaat and Delft Hydraulics within the framework of the breach erosion study of the Technical Committee on Water Defences (TAW). The experiment was prepared for the most part by M.J. Smit and D.W. Snip during their graduation study at the Delft University of Technology. The Zwin'94 experiment includes two tests; the successful test of 7 October was preceded by a less successful test on 6 October. For extensive descriptions of the procedures and the results of both tests reference is made to Louws and Van der Weijde (1995) and Visser et al. (1996a, 1996b). In this thesis only the test of 7 October is described.

6.2.2 Location Het Zwin

The Zwin'94 experiment was performed in the Zwin Channel, a tidal inlet at the Dutch-Belgian border connecting the nature-reserve 'Het Zwin' with the North Sea (see Figure 6.1). Het Zwin measures about 1.5 km² and consists largely of marshes and gullies. The tidal



Figure 6.1 Sand-dam in Zwin Channel (date: 6 October 1994).

range varies between about 2.85 m at neap tide and about 4.35 m at spring tide, being the largest tidal ranges along the Dutch coast. At high water, the width of the mouth of the Zwin Channel is about 150 m. The mean tidal prism is about 350000 m^3 . Smit and Snip (1995) derived the following relation for the polder area A_p as function of the polder water level H_p :

- $A_p = (170000 \text{ m})H_p - 100000 \text{ m}^2$ for $\text{NAP} + 0.60 \text{ m} \leq H_p \leq \text{NAP} + 2.3 \text{ m}$,
- $A_p = (2100000 \text{ m})H_p - 4540000 \text{ m}^2$ for $H_p > \text{NAP} + 2.3 \text{ m}$.

The bottom in the mouth of the Zwin Channel was levelled about one week prior to the experiment; it was found that the bottom elevation of the Zwin Channel near its axis and outside the sand-dam varied between $\text{NAP} + 0.5 \text{ m}$ and $\text{NAP} + 0.9 \text{ m}$, and was averaged at about $\text{NAP} + 0.7 \text{ m}$ (NAP is at about mean sea level). The experiment was done in quiet autumn weather (air-temperature of about 17°C , wind-speed of about 2 m/s from the south, negligible wave heights against the sand-dam).

6.2.3 Sand-dam built in Zwin Channel

The sand-dam was built with local sand from the Zwin Channel and the beach. It closed off the Zwin Channel completely. Table 6.1 shows the D_{10} , D_{50} and D_{90} values of the sand in six samples taken from the sand-dam. The table shows that the sediment in the Zwin Channel

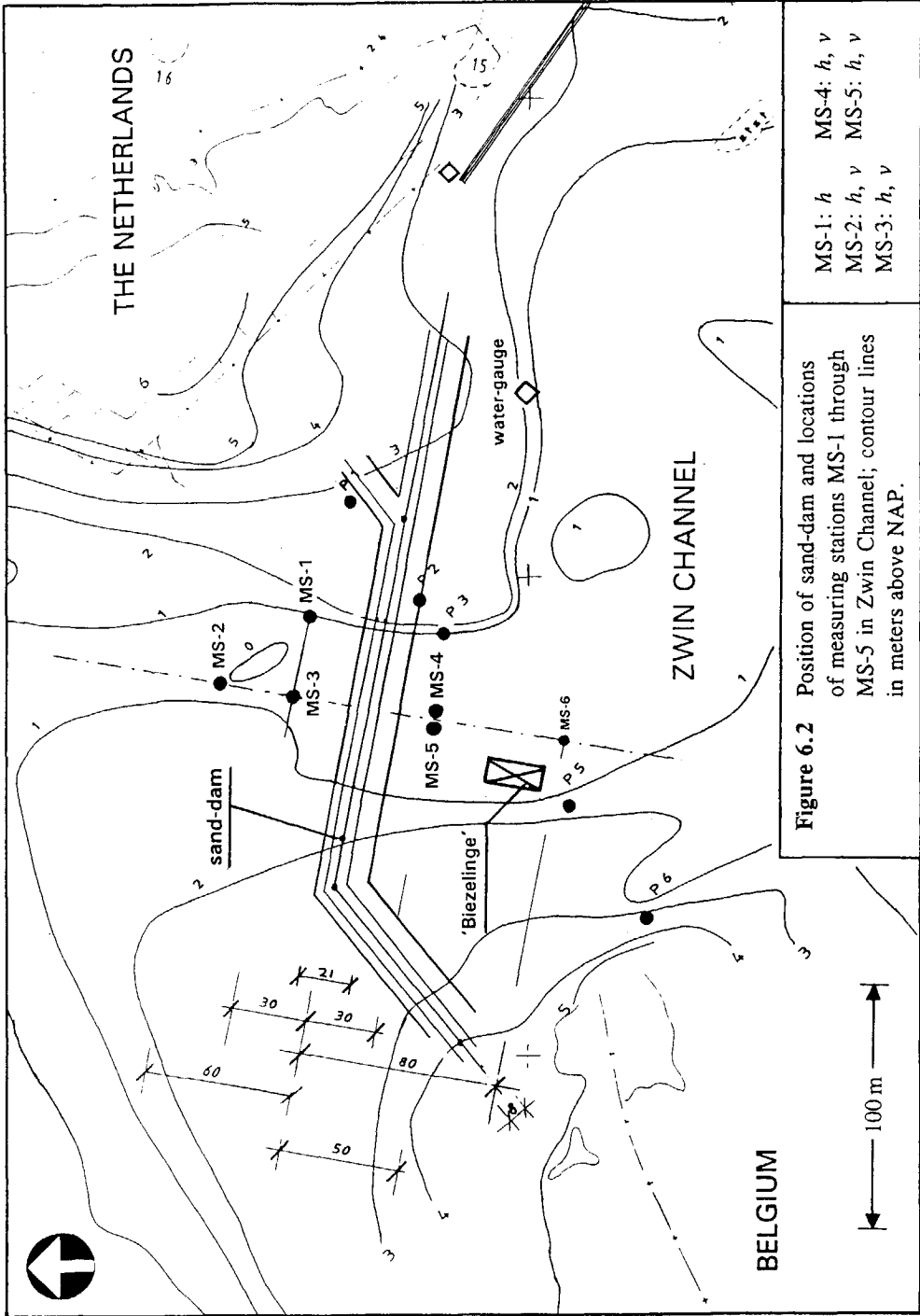


Figure 6.2 Position of sand-dam and locations of measuring stations MS-1 through MS-5 in Zwin Channel; contour lines in meters above NAP.

MS-1: h	MS-4: h, v
MS-2: h, v	MS-5: h, v
MS-3: h, v	

Sand	Sample	D_{10} [mm]	D_{50} [mm]	D_{90} [mm]
'Original' Zwin sand	II, III and VI	0.155	0.185	0.285
Suppletion sand	I, IV and V	0.215	0.315	0.600

Table 6.1 Values of D_{10} , D_{50} and D_{90} of the sand in the Zwin Channel.

consisted of 'original' Zwin sand with a D_{50} of 0.185 mm and of suppletion sand with a D_{50} of 0.315 mm. This suppletion sand has been transported from the Belgium coast by a net alongshore sand transport in northern direction of about 200000 m³/year. The relatively large D_{90} of the suppletion sand is partly due to some small shell particles which were found in the samples I, IV and V. Everywhere in the mouth of the Zwin Channel, both types of sand were found in the bottom, except in samples from a level of about 2.5 m beneath the bottom.

Figures 6.1 and 6.2 show the location of the sand-dam in the mouth of the Zwin Channel; the contour lines in Figure 6.2 give the elevations in meters above NAP. The sand-dam had a total length of about 250 m.

Figure 6.3 shows the cross-section of the sand-dam; the level of the crest was at NAP + 3.3 m, about 2.6 m above the bottom of the Zwin Channel at about NAP + 0.7 m. The width of the crest was about 8.0 m, while the inclination of the outer slope was 1 : 1.6 and that of the inner slope 1 : 3. A small pilot channel was made in the crest of the sand-dam to ensure breaching near the middle of the Zwin Channel (see Figures 6.4 and 6.6). This initial breach had a width of about 1.0 m near its bottom and about 3.6 m near the crest of the dam, and a depth of 0.8 m (so the bottom of the pilot channel was at NAP + 2.50 m, 0.27 m below the expected high water level).

6.2.4 Experimental procedure

Six piles (with a length of 8 m or 10 m) were injected into the bottom of the Zwin Channel in measuring stations MS-1 through MS-6 for the installation of the water level meters (pressure probes) and the flow velocity meters (Ott propeller type). Figure 6.2 shows the locations of the measuring stations MS-1 through MS-6.

The following observations were done in measuring stations MS-1 through MS-5 (see Louws and Van der Weijde, 1995):

- MS-1: pressure at NAP + 0.72 m (for measurement of water level);

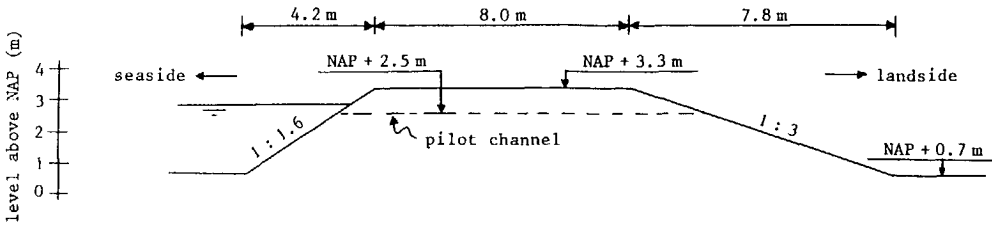


Figure 6.3 Cross-section of sand-dam in Zwin'94 experiment.

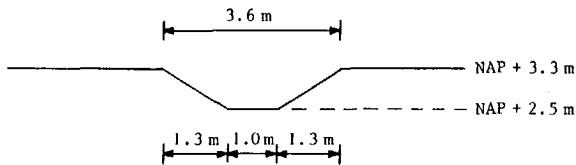


Figure 6.4 Section along sand-dam over pilot channel.

- MS-2: pressure at NAP + 1.27 m, flow velocity at NAP + 1.48 m and NAP + 2.36 m;
 - MS-3: pressure at NAP + 1.61 m, flow velocity at NAP + 1.62 m and NAP + 2.42 m;
 - MS-4: pressure at NAP + 1.65 m (water level was observed also visually with a telescope from the sand-dam), flow velocity at NAP + 1.70 m and NAP + 2.20 m;
 - MS-5: pressure at NAP + 1.37 m, flow velocity at NAP + 1.44 m and NAP + 2.14 m.
- (The observations of flow velocity, flow direction, sand concentration and salt concentration in MS-6 at a distance of 50 m downstream of MS-4 and MS-5 failed due to the fact that the instruments got choked up with sand.) The data were recorded on data-loggers placed at the top of each measuring station. Measurements of flow velocity in the breach were done by video-taping the horizontal displacement of floats along a 5 m long measuring-bar.

The increase of the breach width was both video-taped and photographed from the measuring vessel 'Biezellinge' (see Figures 6.1 and 6.2 for its position). Square 30 cm * 30 cm plates (marked with letters A through X, see Figure 6.6 for plate with letter M) were put in the crest of the dam at mutual distances of 2 m to allow the reading of the increase of the breach width in time from the video-images, slides and photos. The internal clock of one photo-camera and two clocks placed at the sand-dam provided the actual time on the photos taken from the 'Biezellinge' and on many slides and photos taken from other positions.

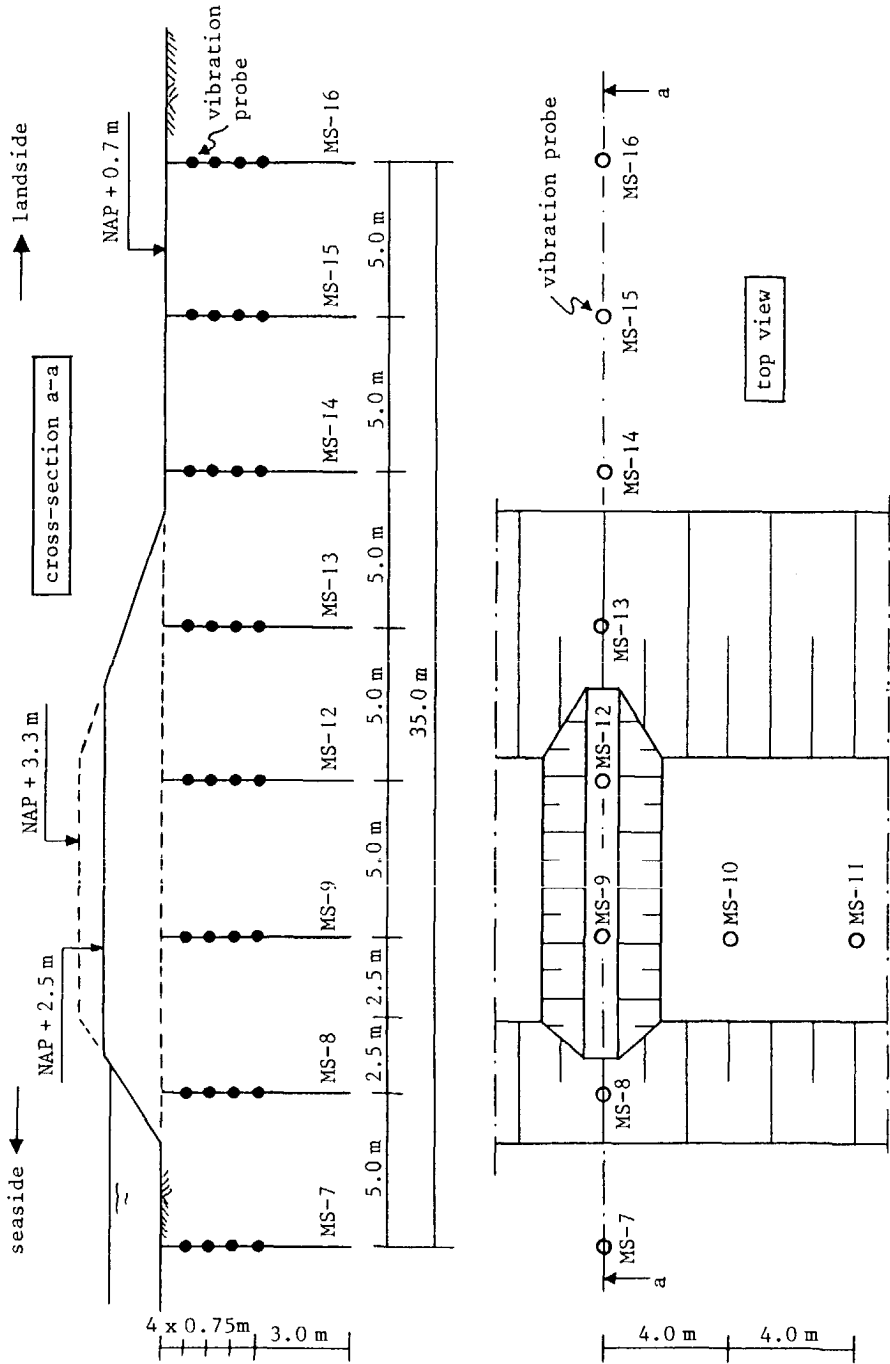


Figure 6.5 Cross-section and plan view of sand-dam with positions of vibration probes.



Figure 6.6 The pilot channel at $t = t_0 = 0$.

Vibration probes were entrenched in the sandy bottom of the Zwin Channel (in measuring stations MS-7 through MS-16, in each station four probes, see Figure 6.5) to detect the development of the breach under water in Stages IV and V. Each probe (length 19 cm, diameter 6 cm) acted as a burglar-alarm: by measuring its own rate of vibration it could detect when the erosion process had exposed it to the flowing water. The vibration probe system was tested and calibrated in a laboratory flume. The signals of all forty vibration probes were recorded on the hard disks of several personal computers on board of the 'Biezeling'. Unfortunately the cables of the twenty vibration probes in MS-7 through MS-11 did not survive the less successful test on 6 October. Inspection of the probes in measuring stations MS-12 through MS-16 and their signals after the experiment has shown that these probes have worked satisfactorily.

6.2.5 Experimental results

The experiment of 7 October 1994 started at 14:25 hour (is $t = t_0 = 0$), about 15 minutes before expected high water, by digging away the small dam in the pilot channel (see Figure 6.6) which started the discharge of water through the initial breach. At $t = 0$ the water level



Figure 6.7 The transition from Stage I into Stage II at $t = t_1 \approx 1.5$ min.



Figure 6.8 Flow through the breach in Stage II at $t \approx 4.0$ min.

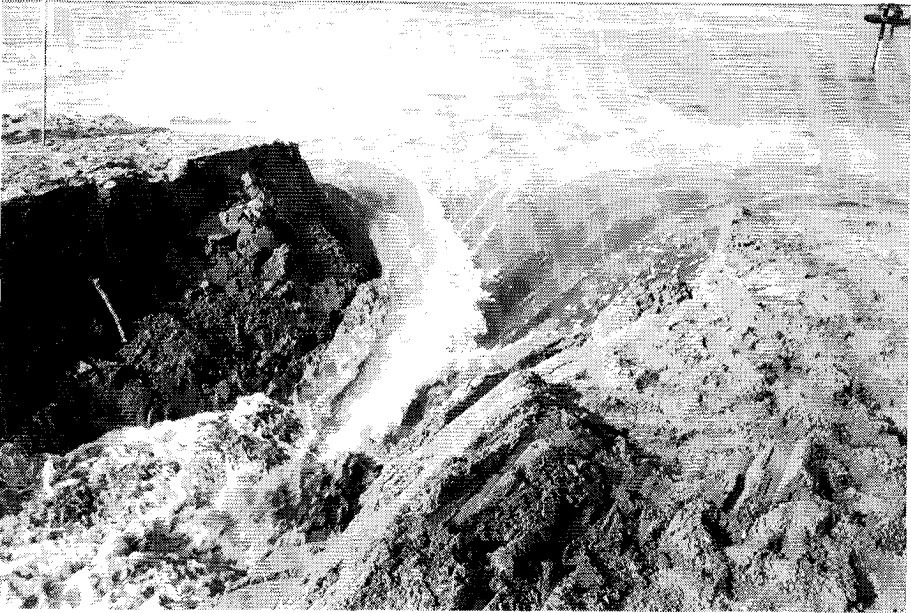


Figure 6.9 The transition from Stage II into Stage III at $t = t_2 \approx 6.5$ min.



Figure 6.10 The transition from Stage III into Stage IV at $t = t_3 \approx 8.5$ min.

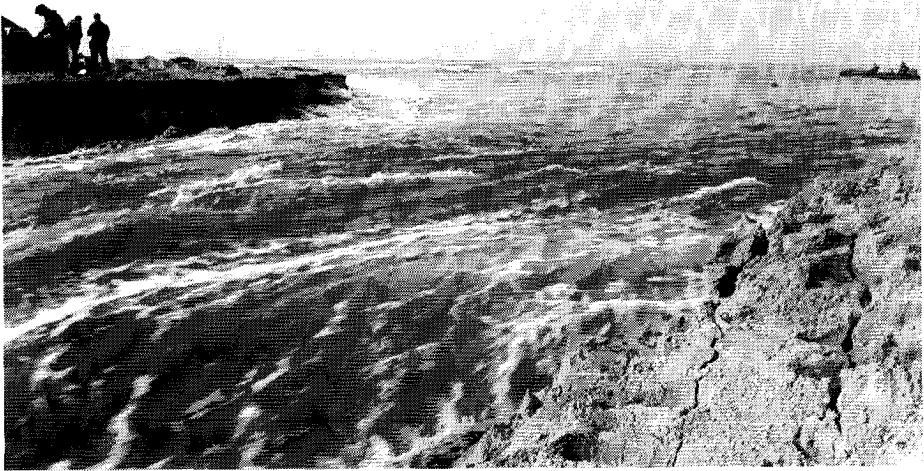


Figure 6.11 Flow through the breach in Stage IV at $t \approx 15$ min (about 8 minutes before the transition from Stage IV into Stage V at $t = t_4 \approx 23$ min).



Figure 6.12 End of the breach erosion process at $t = t_5 \approx 60$ min.

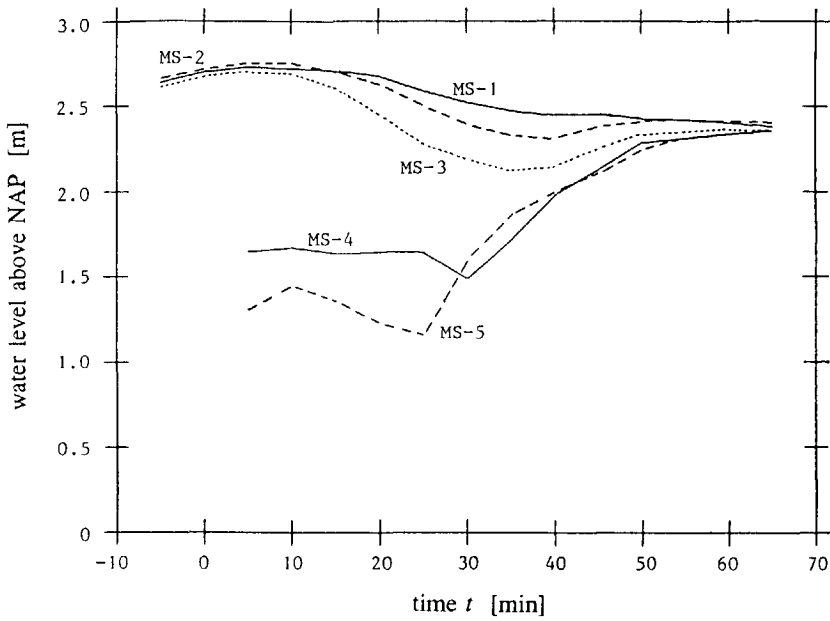


Figure 6.13 Results of water level measurements in MS-1 through MS-5.

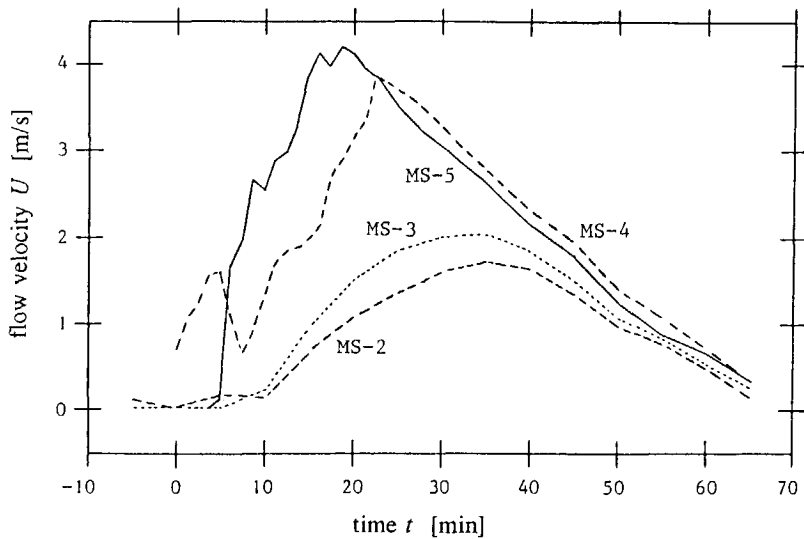


Figure 6.14 Results of velocity measurements in MS-2 through MS-5 (Ott propellers in MS-4 for $t < 35$ min and MS-5 for $t < 30$ min not continuously under water).

Breach growth in sand-dikes

t (min)	1.9	3.1	13.3	13.5	14.0	18.2	25.2
u_w (m/s)	1.4	1.3	4.2	4.3	4.2	4.4	3.8

Table 6.2 Observed flow velocities u_w in breach at water line.

t (min)	0	5	10	12.5	15	17.5	20	22.5	25
B_t (m)	4.0	4.0	8.5	11.4	15.2	18.4	21.2	25.0	28.6
t (min)	27.5	30	32.5	35	40	45	50	55	60
B_t (m)	31.5	33.1	35.4	37.1	38.6	39.7	40.3	40.7	41.0

Table 6.3 Observed breach width B_t at the crest of the dam at NAP + 3.3 m.

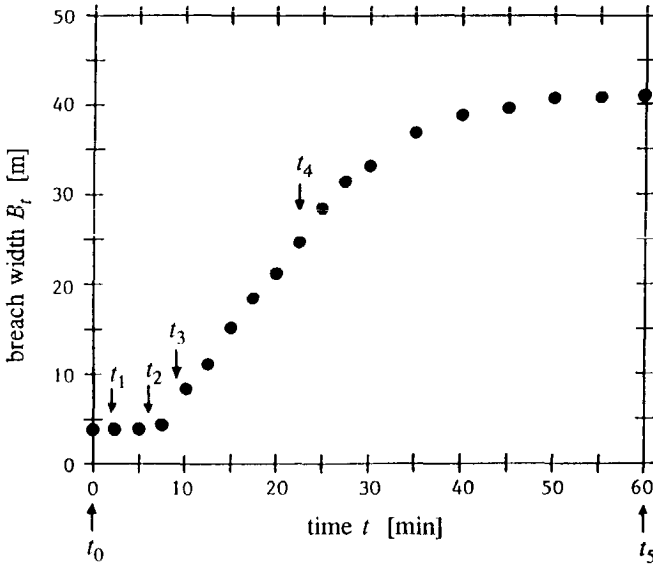


Figure 6.15 Increase of breach width B_t (observed at crest of dam at NAP + 3.3 m).

in MS-2 was measured at NAP + 2.72 m (NAP + 2.69 m averaged over MS-1, MS-2 and MS-3). For $5 \text{ min} \leq t \leq 10 \text{ min}$ (minutes) a highest high water level of $H_w = \text{NAP} + 2.75 \text{ m}$ was observed in MS-2 (NAP + 2.72 m averaged over MS-1, MS-2 and MS-3). The breaching process got well under way. After about 1.5 minute ($t_1 \approx 1.5 \text{ min}$) Stage I of the breach erosion process was completed (see Figure 6.7). Figure 6.8 shows the flow through the breach in Stage II at $t \approx 4.0 \text{ min}$. In a time interval of about five minutes the width of the crest of the dam became zero ($t_2 \approx 6.5 \text{ min}$, see Figure 6.9), and about two minutes later Stage III was passed through (at $t_3 \approx 8.5 \text{ min}$, see Figure 6.10). Figure 6.11 shows the flow through the breach in Stage IV at $t \approx 15 \text{ min}$. The transition from critical flow into subcritical flow took place at $t = t_4 \approx 23 \text{ min}$. At $t = t_5 \approx 60 \text{ min}$ the flow velocities in the breach had become so small that the process of sediment entrainment stopped. The turn of the tide was at $t \approx 75 \text{ min}$.

Figure 6.13 shows the results of the water level measurements in MS-1 through MS-5, Figure 6.14 those of the depth-averaged results of the flow velocity measurements in MS-2 through MS-5. The measured water levels in MS-4 and MS-5 indicate that the propellers of the flow velocity meters were not permanently under water for $0 \leq t < 35 \text{ min}$ in MS-4 and for $0 \leq t < 30 \text{ min}$ in MS-5. The results shown in Figure 6.14, however, look rather realistic and do not represent (only) the wind velocities of about 2 m/s at that time.

The results of the flow velocity observations in the breach with floats and video are given in Table 6.2. The inaccuracy of these data is estimated at about $\pm 5\%$. The number of results is limited due to the limited number of floats which were video-taped during their complete travel along the 5 m long measuring-bar.

Table 6.3 and Figure 6.15 show the results of the observations (from the video-images; results in agreement with observations from slides and photographs) of the growth of breach width B_t in time (observed at the crest of the dam): B_t increased from $B_t \approx 4 \text{ m}$ at $t = t_0 = 0$ up to $B_t \approx 41 \text{ m}$ at $t = t_5 \approx 60 \text{ min}$. The process of breach erosion was attended by large angles (about 60° or more) of those parts of the side-slopes above the water level.

Figure 6.16 shows some examples of the results of the analysis of the signals of the vibration probes, i.e. the development of the scour hole in the breach-axis for $16 \text{ min} \leq t \leq 24 \text{ min}$. It should be emphasized, however, that in spite of the calibration of the system in a laboratory flume the interpretation of the signals of the vibration probes has not been easy. The deepest point of the scour hole (at $t \approx 24 \text{ min}$) was about 2.3 m beneath the Zwin Channel bottom.

Breach growth in sand-dikes

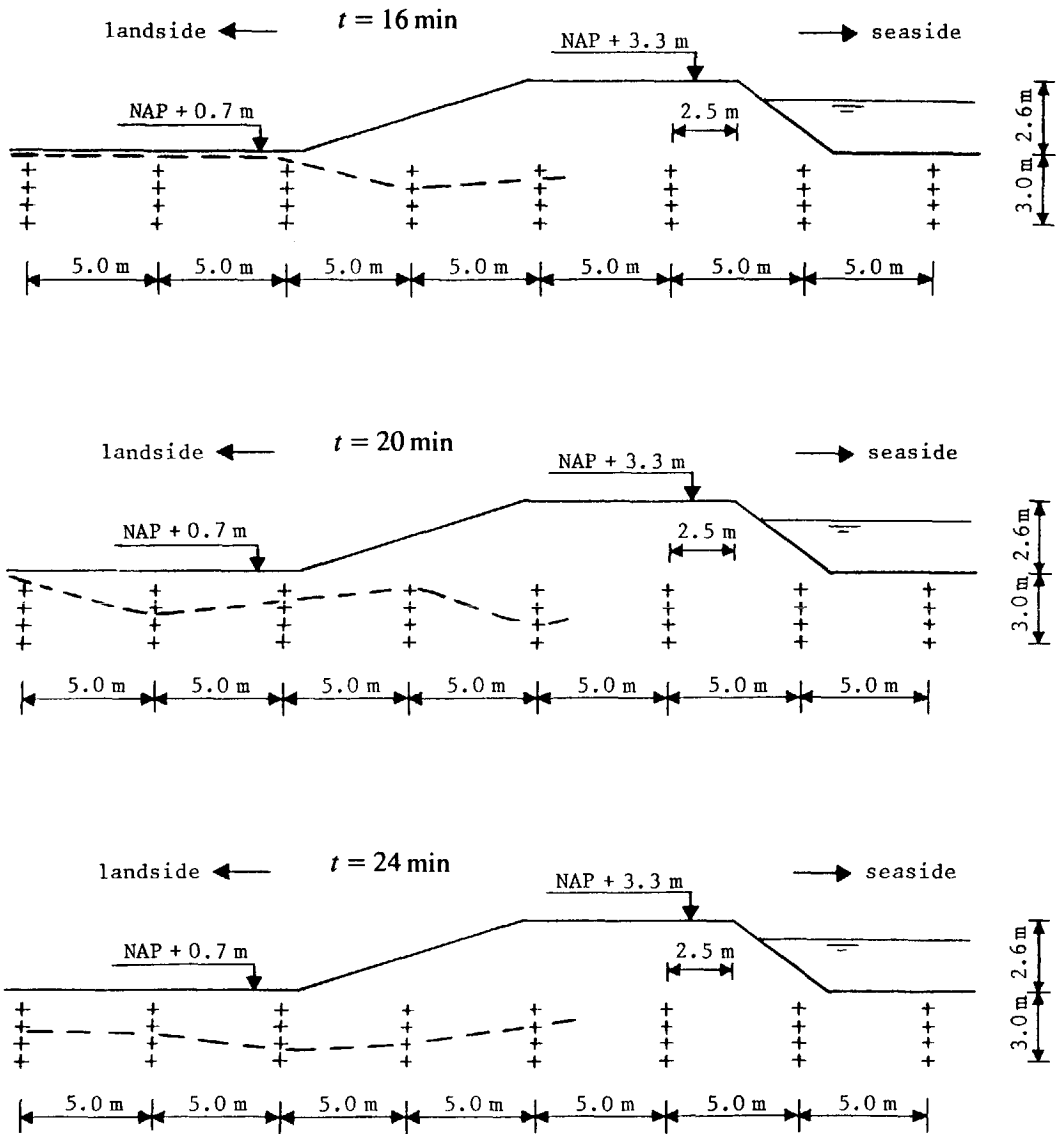


Figure 6.16 Development of scour hole in breach-axis for $16 \text{ min} \leq t \leq 24 \text{ min}$ (+ is a vibration probe).

6.2.6 Discussion

The Zwin'94 experiment clearly confirms the five-step breach erosion mechanism as described in Chapters 3 and 4 and as shown in Figure 3.6, see Figures 6.6 through 6.12. The field experiment has fulfilled most of its expectations: the total set of experimental results is very useful for the calibration and validation of mathematical breach growth models. The calibration of the present model using the data of the Zwin'94 experiment is described in the next chapter.

6.3 Laboratory experiment

6.3.1 Introduction

The laboratory experiment was performed on 3 June 1996 in the 34.0 m long, 16.6 m wide and 0.7 m deep (wave) basin of the Department of Civil Engineering of the Delft University of Technology. The experiment was prepared by C.P. Caan as part of his final year project at the Delft University of Technology. This paragraph holds a condensed description of the procedures and results of the experiment. Reference is made to Caan (1996) for a more extensive description of the experiment and two preparatory tests.

In the Zwin'94 experiment the scour hole depths could only be measured in a limited number of points. Moreover, as described in Section 6.2.5, the analysis of the vibration probe data left some questions about the accuracy of this method. Hence, the present laboratory experiment was especially aimed at an accurate observation of the development of the scour hole and its upstream spillway in Stages IV and V of the breach erosion process.

6.3.2 Experimental procedure

The development of a breach in a dike with a uniform cross-section along its alignment (both the geometry and the construction material) will be symmetrical with respect to the vertical plane standing perpendicular to the dike in the middle of the breach. So by placing a vertical wall in this symmetric plane, in scale models only half a dike has to be tested. This simple principle was applied in the laboratory experiment by constructing a small sand-dike perpendicular to a glass-wall, which allowed the observation of the vertical development of the breach (including the scour hole) in its symmetric plane. It also saved relatively large amounts of sand for the construction of the dike in the basin.

Figure 6.17 shows the position of the tested sand-dike in the basin; the dike was built normal to a 9.0 m long and 0.75 m high glass-wall on a 0.50 m thick sand-bed. The D_{10} , D_{50} and D_{90} of the sand of both the dike and the bed are $D_{10} = 0.070$ mm, $D_{50} = 0.088$ mm and $D_{90} = 0.120$ mm, respectively. Figure 6.18 shows the cross-section of the sand-dike in this experiment. The laboratory dike had a height of 15 cm and a width at the crest of 20 cm. The inclination of the outer slope was 1 : 2 and that of the inner slope 1 : 4. A small pilot channel was made in the upper part of the dike at the glass-wall to ensure breaching started near the glass-wall. This initial breach had a more or less rectangular cross-section with a width of 10 cm and a depth of 3.0 cm (see Figure 6.19).

Water was pumped into the inflow section of the basin (see Figure 6.17) through two pipes at a maximum capacity of $0.66 \text{ m}^3/\text{s}$. The water level against the dike in the upstream section was kept constant as good and long as possible by increasing the rate of inflow to the

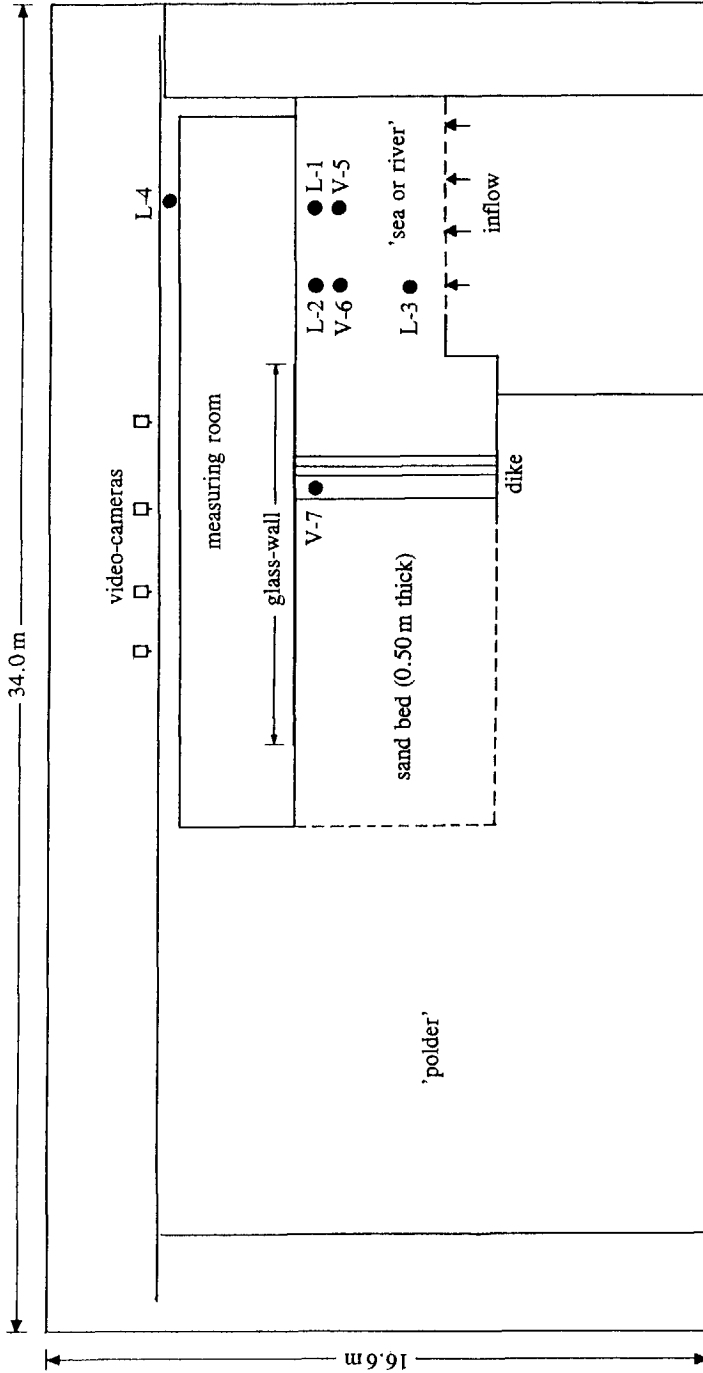


Figure 6.17 Top view of sand-dike in wave basin and position of water level and flow velocity probes.

Breach growth in sand-dikes

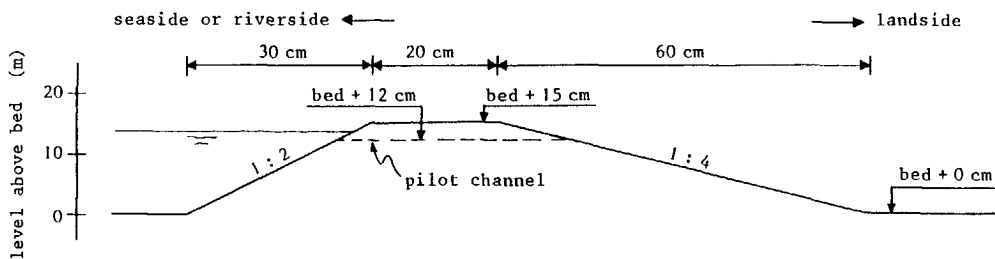


Figure 6.18 Cross-section of sand-dike in laboratory experiment.

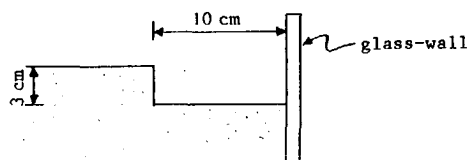


Figure 6.19 Section along sand-dike over pilot channel.

basin.

Figure 6.17 also shows the positions of the water level and flow velocity probes in the basin. Water level measurements were done with wave height probes in three positions in the 'sea or river' section (L-1, L-2 and L-3) and in one position in the 'polder' section (L-4). Flow velocity measurements were done using electromagnetic flow velocity meters in two positions upstream of the breach (V-5 and V-6) and one in the breach (V-7). The flow velocity probe in V-7 was placed in the breach as soon as the breach erosion process made that possible. The data of these instruments were recorded on a personal computer placed in the measuring room (see Figure 6.17) and stored on its hard disk.

The development of the breach and the scour hole at the glass-wall was video-taped with four video-cameras placed just above the wave board of the wave generator at a horizontal distance of about 3.7 m from the glass-wall (see Figure 6.17). Vertical and horizontal lines drawn on the glass-wall at mutual distances of 5 cm allowed the reading of the vertical position of the breach bottom and the scour hole from the video-pictures. The increase of the breach width was photographed every 20 s from above with a photo-camera at a height of about 5.5 m above the dike.

In the first of the preparatory tests, it was also tried to observe the position of the breach bottom in five points near and away from the glass-wall with electronic profile followers. These instruments, however, were not able to follow the very dynamic breach erosion process, and were not applied furthermore.

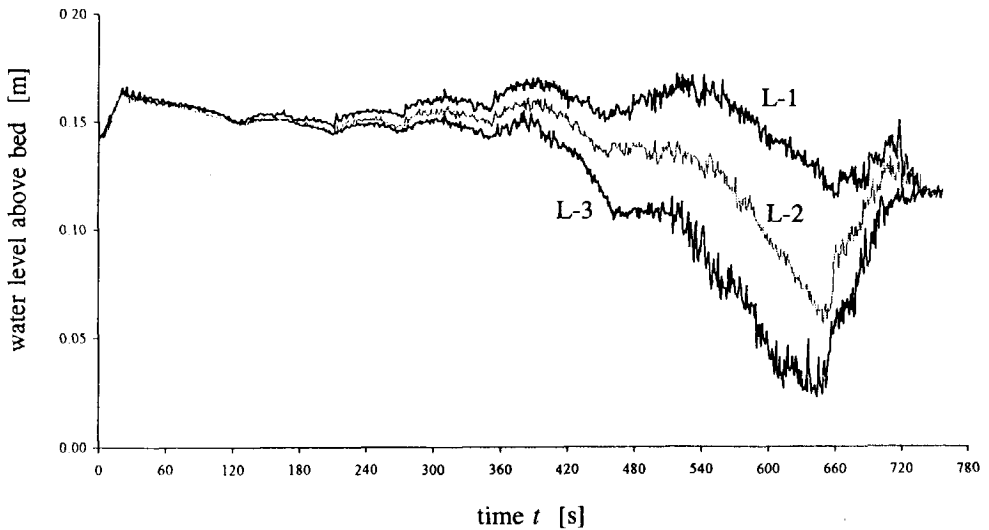


Figure 6.20 Results of water level measurements in L-1, L-2 and L-3.

6.3.3 Experimental results

The test started by pumping water into the inflow section to a level of 14.5 cm above the sand-bed. Then the small dam in the pilot channel was scrapped away at $t = t_0 = 0$ which started the flow of water through the pilot channel. In the initial phase of the test, the water level in L-1, L-2 and L-3 increased further (from 14.5 cm above the bed at $t = 0$) to about 16 cm above the bed at $t \approx 20$ s (see Figure 6.20). Figure 6.20 shows that between $t \approx 20$ s and $t \approx 580$ s the water level above the bed in L-1 varied between about 15 cm and 16 cm.

At $t = t_1 \approx 45$ s Stage I of the breach growth process was completed, at $t = t_2 \approx 80$ s the width of the crest of the dike became zero, and at $t \approx t_3 \approx 135$ s Stage III was finished. The transition from critical flow into subcritical flow was at $t = t_4 \approx 610$ s. At $t = t_5 \approx 756$ s the flow velocities in the breach became so small that the process of sediment entrainment stopped.

Figures 6.21 and 6.22 show the results of the flow velocity measurements in V-5 (equipment failure for $t < 360$ s) and V-7, respectively. Figure 6.23 show the results of the observations (from slides) of the growth of breach width B_t in time (observed at the crest of the dike): B_t increased from $B_t \approx 0.20$ m at $t = t_0 = 0$ up to $B_t \approx 4.4$ m at $t = t_5 \approx 750$ s (two times the distance from the glass-wall to the top of the dike).

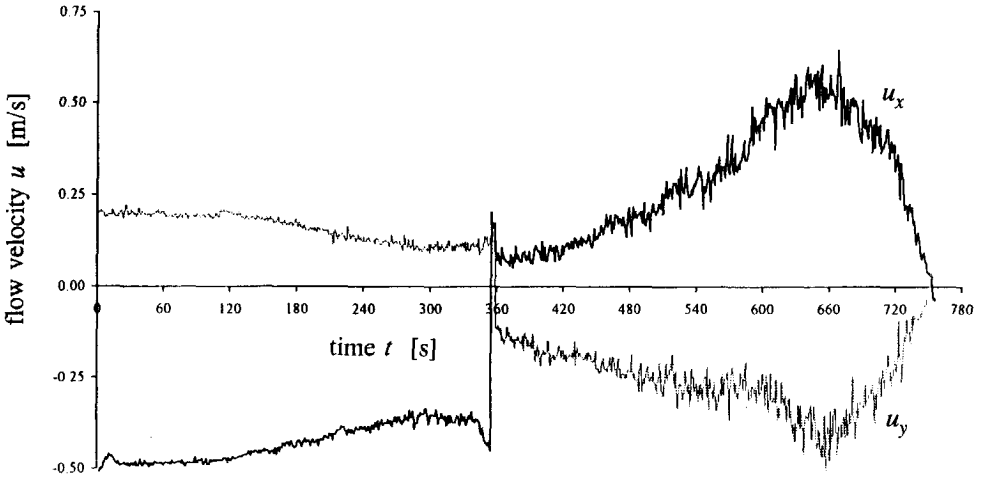


Figure 6.21 Results of flow velocity measurements in V-5.

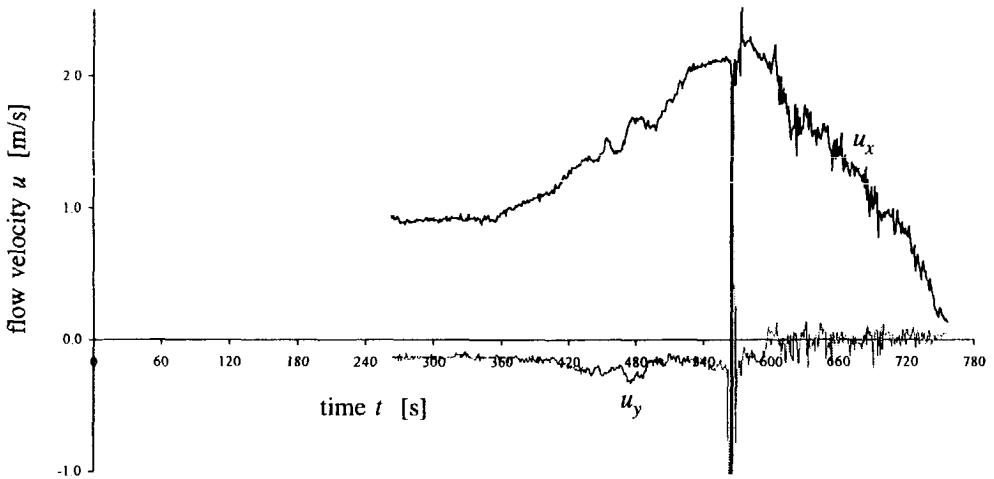


Figure 6.22 Results of flow velocity measurements in V-7 (in breach).

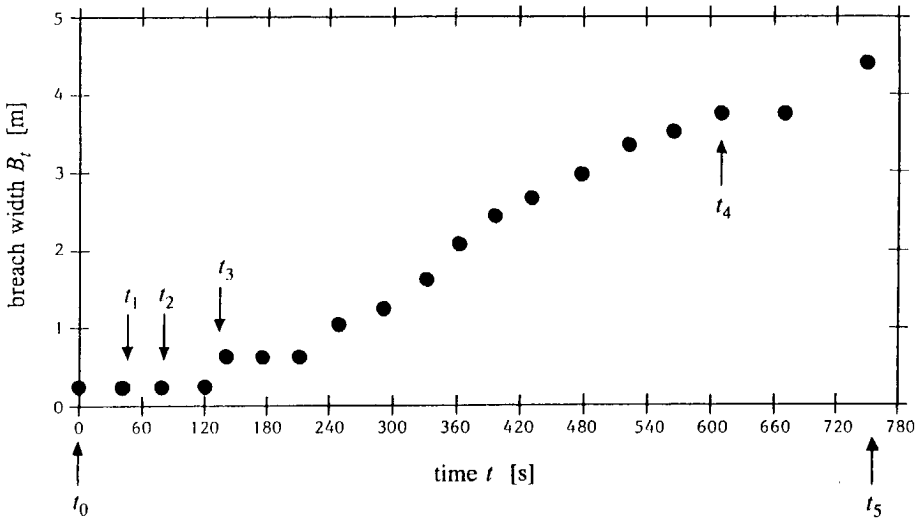


Figure 6.23 Increase of breach width B_t (twice the observed distance from the glass-wall to the crest of the dike).

Figures 6.24 through 6.26 show some examples of the results of the observations from the video-images, i.e. the development of the scour hole at the glass-wall for $21 \text{ s} \leq t \leq 756 \text{ s}$. The scour hole became very deep: at $t \approx 470 \text{ s}$ in Stage IV the scour hole touched the concrete basin bottom at 0.5 m below the bed downstream of the dike, that is more than 3 times the water depth above the bed upstream of the dike in the inflow section.

After the completion of the experiment, the scour hole was levelled. It was found that the shape of the upstream spillway was not circular but more or less elliptical (see Caan, 1996).

6.3.4 Discussion

The breach in the laboratory experiment is clearly of Type B. The experiment also confirms the five-step breach erosion mechanism as outlined in Chapters 3 and 4. The scour hole became in this experiment relatively much deeper than in the Zwin'94 experiment.

Breach growth in sand-dikes

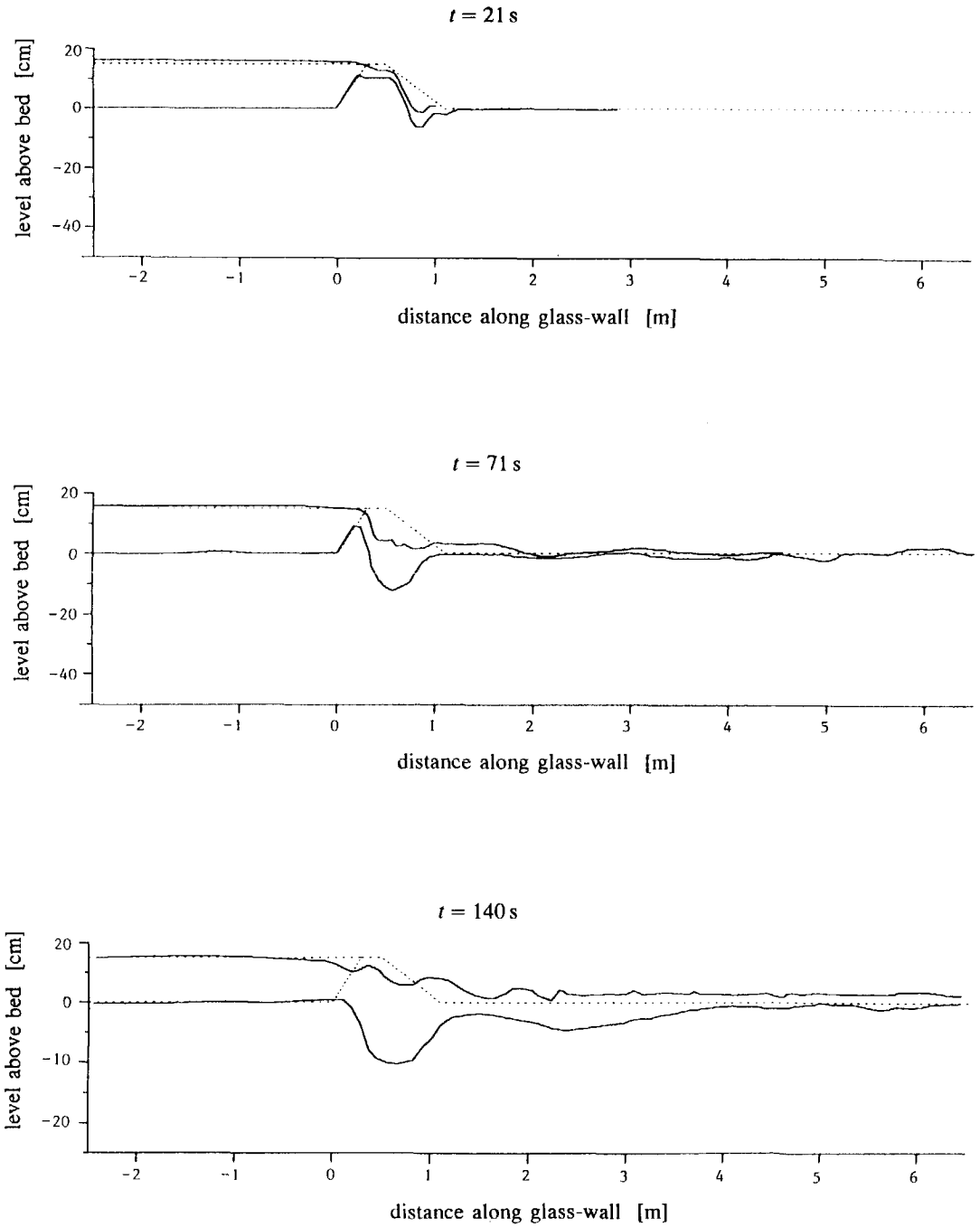


Figure 6.24 Development water level and scour hole at glass-wall for $21 \text{ s} \leq t \leq 140 \text{ s}$.

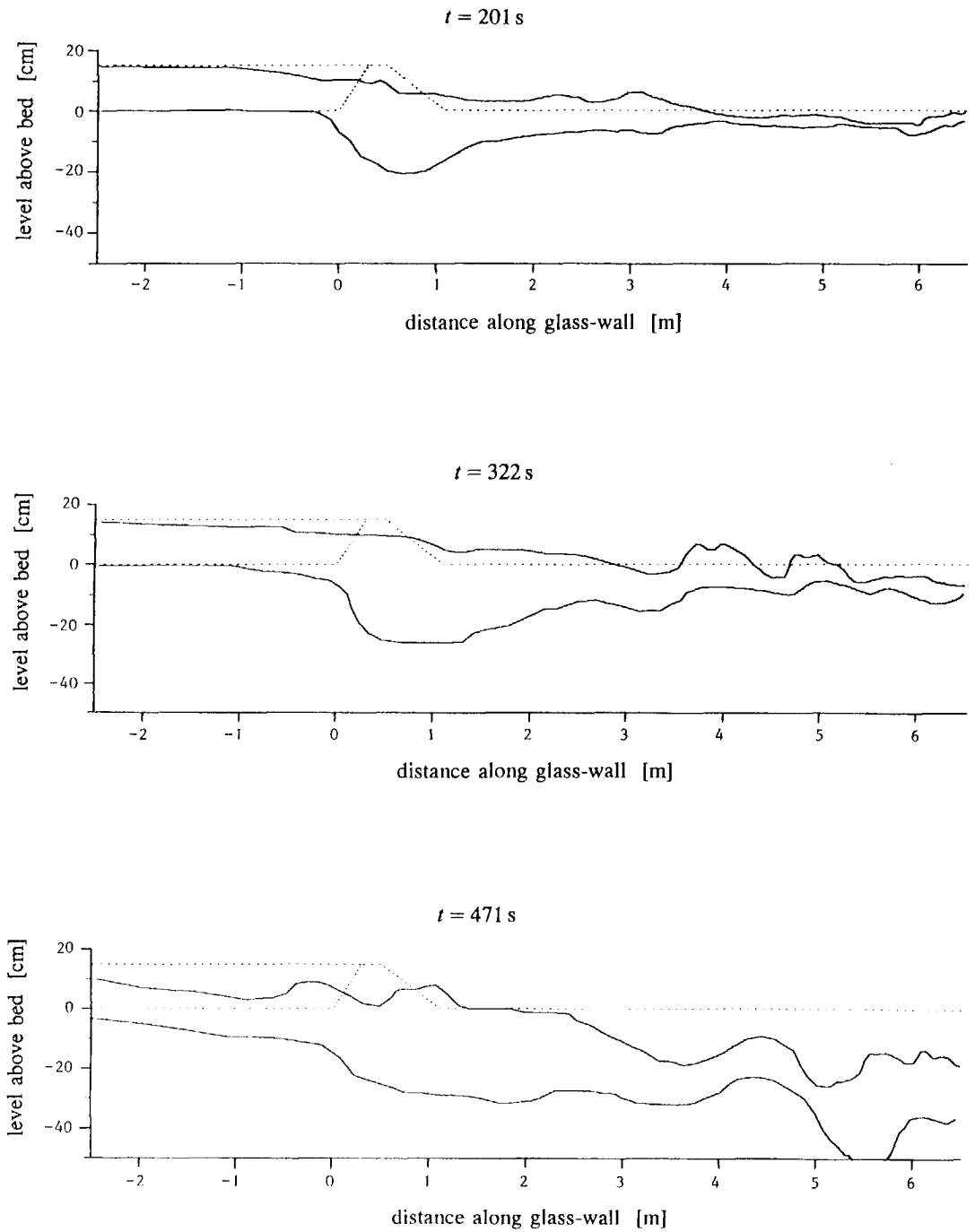


Figure 6.25 Development water level and scour hole at glass-wall for $201 \text{ s} \leq t \leq 471 \text{ s}$.

Breach growth in sand-dikes

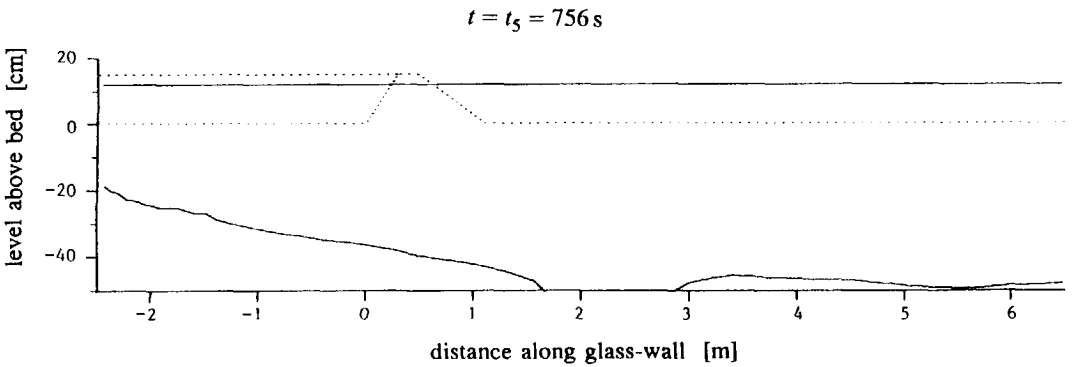
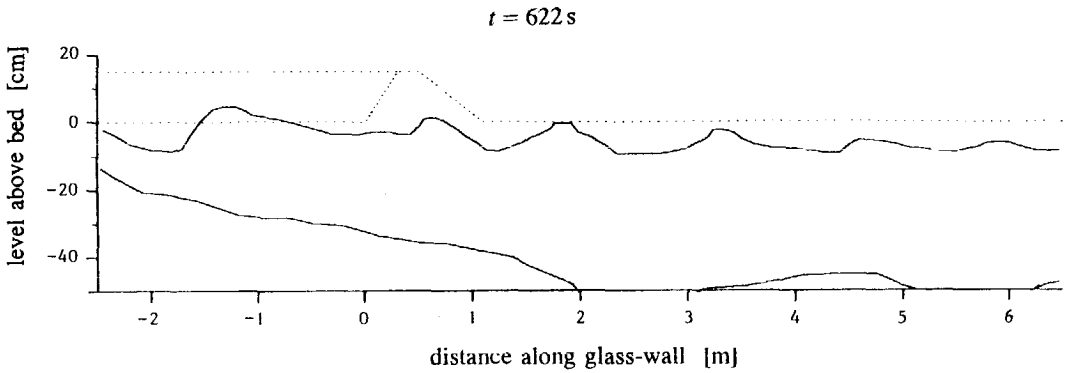
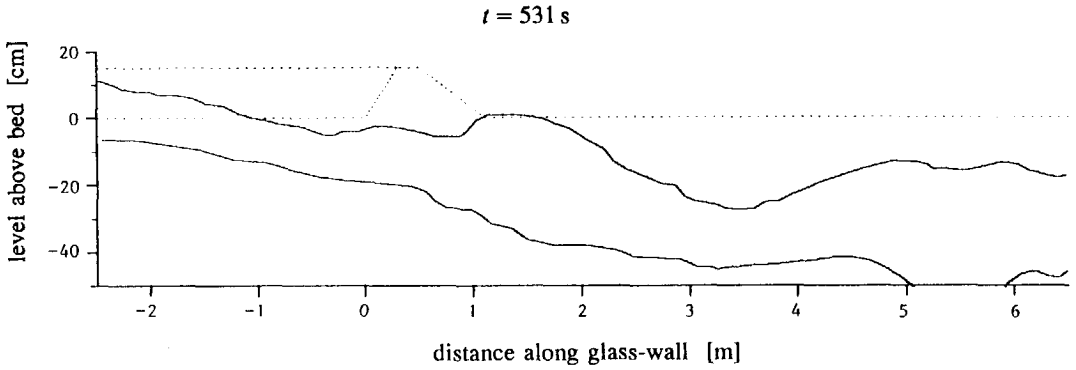


Figure 6.26 Development water level and scour hole at glass-wall for $531 \text{ s} \leq t \leq 756 \text{ s}$.

Chapter 7

Calibration and validation of the model

7.1 Introduction

This chapter contains first a description of the calibration of the breach growth model using the data of the Zwin'94 field experiment (in Paragraph 7.2). Then the calibrated model is tested with the data of the laboratory experiment (in Paragraph 7.3). Both experiments have yielded relatively reliable and detailed data for calibration and subsequent test (see Chapter 6).

As stated in Chapter 1, data of prototype dike failures are scarce, in spite of the large number of these occurrences in the past in The Netherlands. The poor data shown in Figure 1.2 are based on eye-witness reports, so not very reliable, and since not much is known about the hydraulic conditions in the river and the geotechnical parameters of these dikes, these data are not very usable.

In fact the 1953 flood in the south-western provinces of The Netherlands has provided the best prototype data for the comparison with the present model. These data consist mainly of widths and depths of final breaches and outside water levels during the process of dike breaching, see Rijkswaterstaat (1961). One of the best documented dike failures of this flood is that of the Noord Dike in Papendrecht. This dike had a large core of sand along a length of about 100 m, consequently the model can be validated against this prototype dike-burst. This validation is described in Paragraph 7.4.

In all computations the constant of Von Karman κ and the angle of repose of sand ϕ have been kept at their default values $\kappa = 0.4$ and $\phi = 32^\circ$, respectively. The Galappatti (1983) coefficient ξ of equation (4.37) has been kept at $\xi = 1$ in Stages I, II and III, and $\xi = 0.4$ in Stages IV and V.

7.2 Calibration with data of Zwin'94 field experiment

The procedure and results of the Zwin'94 field experiment have been described in Paragraph 6.2. The input data for the BRES model can be summarized as:

- outside water level $H_w(t)$ above the reference level NAP ($Z = 0$) for $t \geq 0$ as observed in

Breach growth in sand-dikes

MS-1 (see Figure 6.13);

- bottom level of water course $Z_w = \text{NAP} + 0.7 \text{ m}$;
- water temperature $T = 17^\circ \text{C}$, water density $\rho = 1025 \text{ kg/m}^3$;
- dike height $H_d = \text{NAP} + 3.3 \text{ m}$, width of the crest of the dike $W_d = 8.0 \text{ m}$;
- outer dike slope 1 : 1.6 ($\alpha = 32^\circ$) and inner dike slope 1 : 3 ($\beta_0 = 18^\circ$);
- sand: $D_{50} = 0.22 \text{ mm}$ (with $w_s = 0.028 \text{ m/s}$), $D_{90} = 0.35 \text{ mm}$ (those values are between the values of the 'original' Zwin sand and the suppletion sand, See Table 6.1), porosity $p = 0.40$, critical angle of slope in flow direction $\beta_1 = \phi = 32^\circ$ and $\beta_1 = 40^\circ$;
- level of breach bottom $Z_{br} = \text{NAP} + 2.5 \text{ m}$ at $t = 0$, breach side-slope angle γ is critical side-slope angle $\gamma_1 = \phi = 32^\circ$, width of breach bottom $b = 1.0 \text{ m}$ at $t = 0$ (consequently $B_t = 3.6 \text{ m}$ at $t = 0$), see Figure 6.4);
- polder bottom level $Z_p = \text{NAP} + 0.70 \text{ m}$, water level in polder $H_p = 1.30 \text{ m}$ at $t = 0$;
- polder area A_p as function of H_p :
 $A_p = (170000 \text{ m}) H_p - 100000 \text{ m}^2$ for $0.60 \text{ m} \leq H_p \leq \text{NAP} + 2.3 \text{ m}$,
 $A_p = (2100000 \text{ m}) H_p - 4540000 \text{ m}^2$ for $H_p > \text{NAP} + 2.3 \text{ m}$,
- discharge coefficient $m = 1.3$ in Stages IV and V (Type B breach; $m = 1.3$ gives depth-averaged flow velocities $U \approx 4.3 \text{ m/s}$ in the breach in Stage IV in agreement with the observed flow velocities at the water line u_w as given in Table 6.2, see Table 7.1).

t (min)	1.9	3.1	13.3	13.5	14.0	18.2	25.2
U (m/s)	1.1	1.1	4.3	4.3	4.3	4.4	4.4
u_w (m/s)	1.4	1.3	4.2	4.3	4.2	4.4	3.8

Table 7.1 Comparison of computed depth-averaged breach flow velocities U and measured flow velocities u_w in breach at the water line (U and u_w at $t = 1.9 \text{ min}$ and $t = 3.1 \text{ min}$ are the critical flow velocities at the top of the dike in the breach).

As described in Section 6.2.4, unfortunately the signals of the vibration probes in the measuring stations near the breach inflow (MS-7 and MS-8, see Figure 6.5) could not be recorded. This means that less is known about the development of the breach bottom near the breach inflow (Z_{br}), consequently also about the development of the upstream spillway.

Table 7.2 presents the comparison of the model predictions (applying the sediment transport formulae of Bagnold-Visser, Engelund-Hansen, Van Rijn and Wilson) for the durations of the Stages I, II and III ($t_1 - t_0$, $t_2 - t_1$ and $t_3 - t_2$, respectively) with those

	$t_1 - t_0$ [min]	$t_2 - t_1$ [min]	$t_3 - t_2$ [min]
Zwin'94 experiment	1.5	5.0	2.0
BRES (Bagnold-Visser, 1989)	2.2	11.2	502
BRES (Engelund-Hansen, 1967)	0.1	0.9	83
BRES (Van Rijn, 1984a,b)	4.0	24.1	70
BRES (Wilson, 1987)	1.4	8.0	590

Table 7.2 Comparison of predicted (BRES) and observed (Zwin'94 experiment) durations $t_1 - t_0$, $t_2 - t_1$ and $t_3 - t_2$ applying sediment transport formulae of Bagnold-Visser (1989), Engelund-Hansen (1967), Van Rijn (1984a,b) and Wilson (1987) when for U the flow velocity $U(L)$ at the toe of the slope is substituted into (4.39).

	$t_1 - t_0$ [min]	$t_2 - t_1$ [min]	$t_3 - t_2$ [min]	$t_4 - t_3$ [min]	$t_5 - t_4$ [min]	$B_f(t_5)$ [m]
Zwin'94 experiment	1.5	5.0	2.0	15	37	41
BRES (Bagnold-Visser, 1989)	2.2 (2.2)	8.0 (5.8)	1.9 (1.4)	54	29	16
BRES (Engelund-Hansen, 1967)	0.1 (0.1)	0.5 (0.4)	0.1 (0.1)	22	19	44
BRES (Van Rijn, 1984a,b)	4.4 (5.0)	20.0 (14.0)	6.1 (6.0)	22	18	39
BRES (Wilson, 1987)	1.3 (1.3)	4.7 (3.7)	2.9 (3.0)	67	64	13

Table 7.3 Comparison of predicted (BRES, with $\beta_1 = 32^\circ$ and between parentheses $\beta_1 = 40^\circ$) and observed (Zwin'94 experiment) durations $t_1 - t_0$, $t_2 - t_1$, $t_3 - t_2$, $t_4 - t_3$ and $t_5 - t_4$ and final breach width $B_f(t_5)$, applying sediment transport formulae of Bagnold-Visser (1989), Engelund-Hansen (1967), Van Rijn (1984a,b) and Wilson (1987) when for U the normal flow velocity U_n is substituted into (4.39).

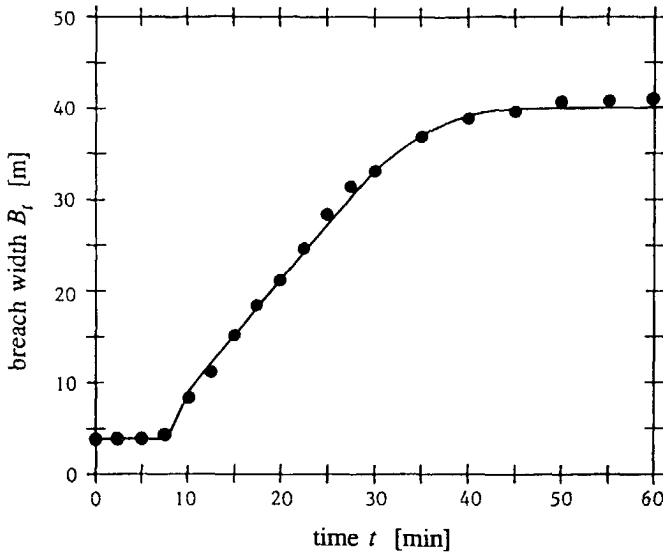


Figure 7.1 Comparison of computed (BRES, solid line) and observed (Zwin'94 experiment, dots) breach width $B_i(t)$ at the dike crest. BRES with the Bagnold-Visser formula in Stages I, II and III (with $\beta_1 = 40^\circ$), and Van Rijn's formulation in Stages IV and V.

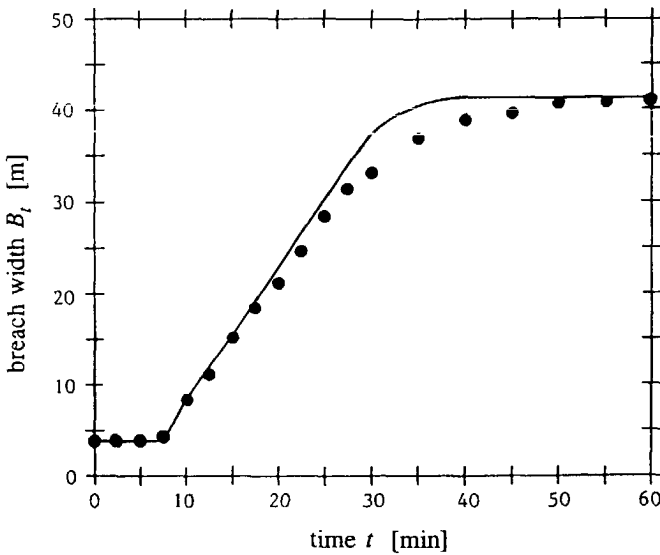


Figure 7.2 Comparison of computed (BRES, solid line) and observed (Zwin'94 experiment, dots) breach width $B_i(t)$ at the dike crest. BRES with the Bagnold-Visser formula in Stages I, II and III (with $\beta_1 = 40^\circ$), and Engelund-Hansen in Stages IV and V.

observed in the Zwin'94 experiment when in BRES the flow velocity $U(L)$ at the toe of the inner slope is substituted into (4.39) (i.e. the function FlowSlope is active in Stages I through III, called approach 1 in Chapters 4 and 5). Table 7.3 shows similar results after substitution of the normal flow velocity U_n into equation (4.39) of BRES (i.e. function FlowSlope is not working, called approach 2 in Chapters 4 and 5). It can be concluded that approach 1 results in unrealistic long durations $t_3 - t_2$ of Stage III; this approach is not applied further.

Table 7.3 indicates that in approach 2 the application of Engelund and Hansen's (1967) formula gives unrealistic small durations for Stages I, II and III. Table 7.3 also shows that the application of the formulae of Bagnold-Visser (1989) and Wilson (1987) in BRES yields fair agreement between predicted and observed durations of Stages I through III. Table 7.3 also indicates that with $\beta_1 = 40^\circ$ the performance of the Bagnold-Visser formula improves, as it will also improve the performance of the formulae in the tests of Chapter 5, see Table 5.3. Based on both the tests of Chapter 5 and the test of Table 7.3, it is concluded that the Bagnold-Visser formula gives the less inaccurate prediction for the sediment transport capacity in Stages I, II and III. For Stages IV and V the formulae of Van Rijn (1984a,b) and Engelund-Hansen (1967) give final breach widths B_f in agreement with the observed value.

Figure 7.1 shows the model prediction for the increase of the breach width B_f in the Zwin'94 experiment applying Bagnold-Visser (1989) in Stages I, II and III and Van Rijn (1984a,b) in Stages IV and V. Figure 7.2 shows the model prediction for B_f in the Zwin'94 experiment applying Bagnold-Visser (1989) in Stages I, II and III and Engelund-Hansen (1967) in Stages IV and V. It can be concluded that the agreement between computed and observed development of B_f is good, in Figure 7.1 somewhat better than in Figure 7.2.

7.3 Validation against data of laboratory experiment

For a description of the procedure and results of the laboratory experiment reference is made to Paragraph 6.3. The input data for the BRES model can be summarized as:

- outside water level $H_w(t)$ for $t \geq 0$ given by $H_{w1}(t) + [U_5(t)]^2/2g$, where $H_{w1}(t)$ is measured water level in L-1 and $U_5(t)$ is the measured flow velocity in V-5, see Figures 6.17, 6.20 and 6.21), water levels above reference level RL ($Z = 0$);
- bottom level of water course $Z_w = \text{RL} + 0.0 \text{ m}$;
- water temperature $T = 19^\circ\text{C}$, water density $\rho = 1000 \text{ kg/m}^3$;
- dike height $H_d = \text{RL} + 0.15 \text{ m}$, width of the dike top $W_d = 0.20 \text{ m}$;
- outer dike slope 1 : 2 ($\alpha = 27^\circ$) and inner dike slope 1 : 4 ($\beta_0 = 14^\circ$);
- sand: $D_{50} = 0.088 \text{ mm}$ (with $w_s = 0.0068 \text{ m/s}$), $D_{90} = 0.12 \text{ mm}$, porosity $p = 0.35$ (see Caan, 1996), critical slope angle $\beta_1 = 40^\circ$;

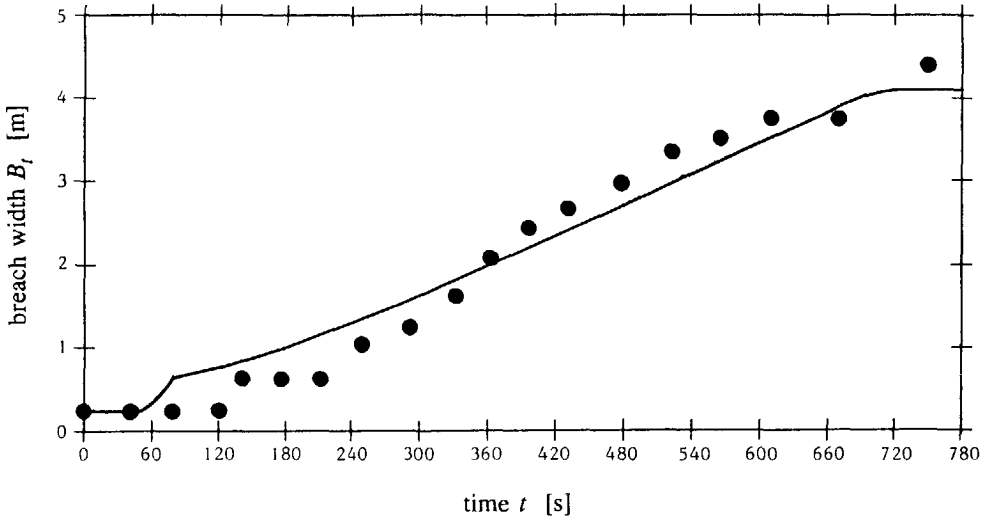


Figure 7.3 Comparison of computed (BRES, solid line) and observed (laboratory experiment, dots) breach width $B_t(t)$. BRES with the Bagnold-Visser formula in Stages I, II and III, and Van Rijn's formulation in Stages IV and V.

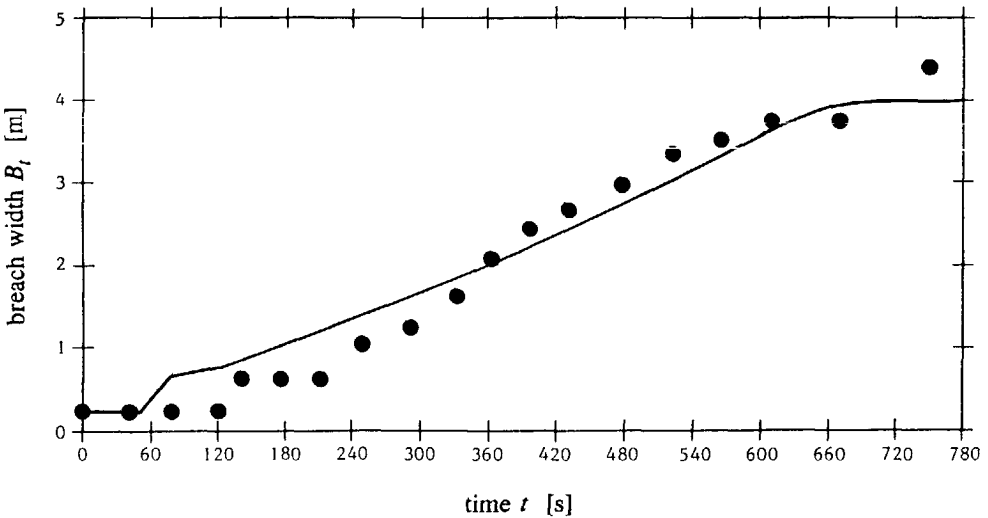


Figure 7.4 Comparison of computed (BRES, solid line) and observed (laboratory experiment, dots) breach width $B_w(t)$. BRES with the Bagnold-Visser formula in Stages I, II and III, and Engelund-Hansen in Stages IV and V.

- level of breach bottom $Z_{br} = \text{RL} + 0.12 \text{ m}$ at $t = 0$, width breach bottom $b = 0.20 \text{ m}$ at $t = 0$, side-slope angle of breach γ is critical side-slope angle $\gamma_1 = \phi = 32^\circ$;
- bottom level of polder near dike $Z_p = \text{RL} + 0.0 \text{ m}$, mean water level in polder $H_p = \text{RL} - 0.50 \text{ m}$ at $t = 0$ (see Figure 6.17), polder area $A_p = 360 \text{ m}^2$;
- discharge coefficient $m = 1.8$ in Stages IV and V (Type B breach, length of spillway was about $1.8b$; $m = 1.8$ gives depth-averaged flow velocities $U \approx 1.8 \text{ m/s}$ in the breach in Stage IV in agreement with the observed flow velocities, see Figure 6.22).

Figure 7.3 shows the model prediction for the growth of the breach width B_t in the laboratory experiment applying Bagnold-Visser in Stages I, II and III and Van Rijn in Stages IV and V. Figure 7.4 shows the model prediction for the increase of the breach width B_t in the Zwin'94 experiment applying Bagnold-Visser in Stages I, II and III and Engelund-Hansen in Stages IV and V. Again the agreement between both model predictions and observation is good.

7.4 Confrontation with 1953 failure of Noord Dike

As described in Chapter 3 the Noord Dike⁹⁾ in Papendrecht failed on 1 February 1953 just at the site of an auxiliary spillway (in Dutch 'hulpgat'), where the dike had a solid clay-foundation, a large core of sand (along a length of about 100 m) and solid heads at both sides of the spillway. The solid clay-base and the solid toe construction strongly slowed down the vertical erosion in Stages IV and V, see Figure 3.17, so it is a good example of a Type A.1 breach. The fact that the dike was locally constructed with sand means that the present model for sand-dike breach erosion may be applied to this prototype dike-burst.

The dimensions of the Noord Dike were: dike height $H_d = \text{NAP} + 3.8 \text{ m}$, crown width $W_d = 7.0 \text{ m}$, angle inner slope $\beta_0 = 29^\circ$ (1 : 1.8) and angle outer slope $\alpha = 29^\circ$ (1 : 1.8). The averaged level of the bottom of the inundated polder was $Z_p \approx \text{NAP} - 1.5 \text{ m}$.

The Noord Dike is located between the measuring stations Dordrecht (at a distance of about 1.5 km) and Alblasserdam (at a distance of about 3.5 km). Figure 7.5 shows the observed river water levels around 1 February 1953 in these measuring stations. The dike started to fail at 05.30 hr am, about 1.0 hr before the water level in the river reached a maximum value of $H_w \approx \text{NAP} + 3.7 \text{ m}$. It is assumed that at 05.30 hr am ($t = t_0 = 0$) water

⁹⁾ At the time of this dike-burst the author (then 3.8 years old) lived with his parents in a house built on the outer dike-slope at about 500 m from the location where the dike failed. The event has left behind some clear pictures in author's memory (about 1 m water in the living room, a nightly evacuation, fortunately no panic broke out in the family).

started to flow through the initial breach. At some time between 08.00 hr and 9.00 hr am (so $2.5 \text{ hr} < t < 3.5 \text{ hr}$) the breach in the dike was already relatively large, according to an eye-witness report (H.A. Visser, Papendrecht, personal communication). Figure 7.6 shows the flow through the breach at a time between 11:00 hr and 12:00 hr am ($5.5 \text{ hr} < t < 6.5 \text{ hr}$) on 1 February 1953 (personal communication with the photographer L. Scheermeijer, Slie-drecht). At the time of the photo of Figure 7.6 the water level in the river measured about NAP + 2.15 m (see Figure 7.5), that is about 2.6 m above the breach bottom (see Figure 3.17). The photo indicates that the flow through the breach was virtually critical, which means that the water depth in the breach at the time of the photo was about 1.8 m and that the water level in the breach was at about NAP + 1.30 m (while the elevation of the crest of the dike was at NAP + 3.80 m).

The breach depth near the breach inflow became $Z_{br} \approx \text{NAP} - 0.50 \text{ m}$; the final breach width was $b = 85 \text{ m}$ near the breach bottom and $B_t = 110 \text{ m}$ near the dike top, that is about the length of the auxiliary spillway. If the observation of eye-witness reporter H.A. Visser is correct, most of this final breach width was formed in about 2.5 hr. A total area of about $94.4 * 10^6 \text{ m}^2$ in the polder Alblasserwaard was inundated with an estimated $100 * 10^6 \text{ m}^3$ water, i.e. the averaged inundation depth was about 1.1 m. The auxiliary spillway has restricted the depth and width of the breach, so also the breach inflow, and due to the relatively large polder area also the inundation speed and the flow velocities in the polder, leaving behind only two people drowned (both near the breach, both after warnings that a dike-failure was imminent). An early closure of the breach (on 5 February 1953) has limited the maximum depth of the scour hole downstream of the breach to about NAP - 7.2 m.

The input data for the BRES model can be summarized as:

- outside water level $H_w(t)$ above the reference level NAP ($Z = 0$) for $t \geq 0$ as shown in Figure 7.5 ($t = 0$ at 05.30 hr on 1 February 1953, see Rijkswaterstaat, 1961); for $t > 34.5 \text{ hr}$ (that is after 16.00 hr on 2 February 1953 the astronomical tidal curve also given in Figure 7.5 has been adopted);
- bottom level water course $Z_w = \text{NAP} - 0.50 \text{ m}$ (in fact bottom level of final breach);
- water temperature $T = 4^\circ \text{C}$, water density $\rho = 1000 \text{ kg/m}^3$;
- dike height $H_d = \text{NAP} + 3.80 \text{ m}$, width of the dike $W_d = 7.0 \text{ m}$;
- outer dike slope 1 : 1.8 ($\alpha = 29^\circ$) and inner dike slope 1 : 1.8 ($\beta_0 = 29^\circ$);
- sand (river sand from river Beneden Merwede): $D_{50} = 0.30 \text{ mm}$ (with $w_s = 0.035 \text{ m/s}$ at $T = 4^\circ \text{C}$), $D_{90} = 0.40 \text{ mm}$, porosity $p = 0.40$, critical slope angle $\beta_1 = 40^\circ$;
- level of breach $Z_{br} = \text{NAP} + 3.60 \text{ m}$ at $t = 0$, width breach bottom $b = 2.0 \text{ m}$ at $t = 0$, side-slope angle of breach γ is critical side-slope angle $\gamma_1 = 32^\circ$;
- polder level $Z_p = \text{NAP} - 1.50 \text{ m} =$ water level in polder H_p at $t = 0$;

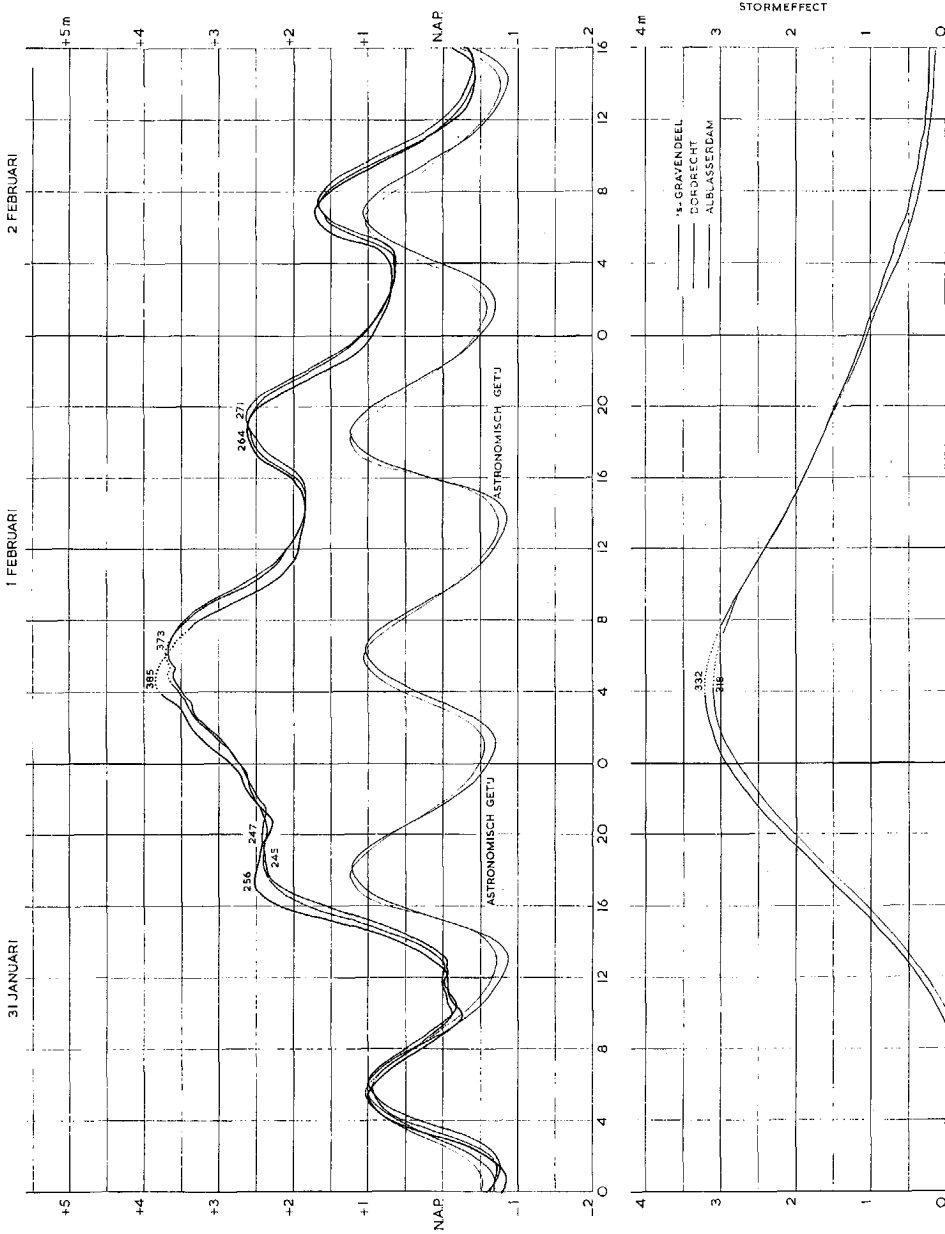


Figure 7.5 Water levels in the river Beneden Merwede near Dordrecht and the river Noord near Alblasdendam (The Netherlands) on 31 January, 1 and 2 February 1953.

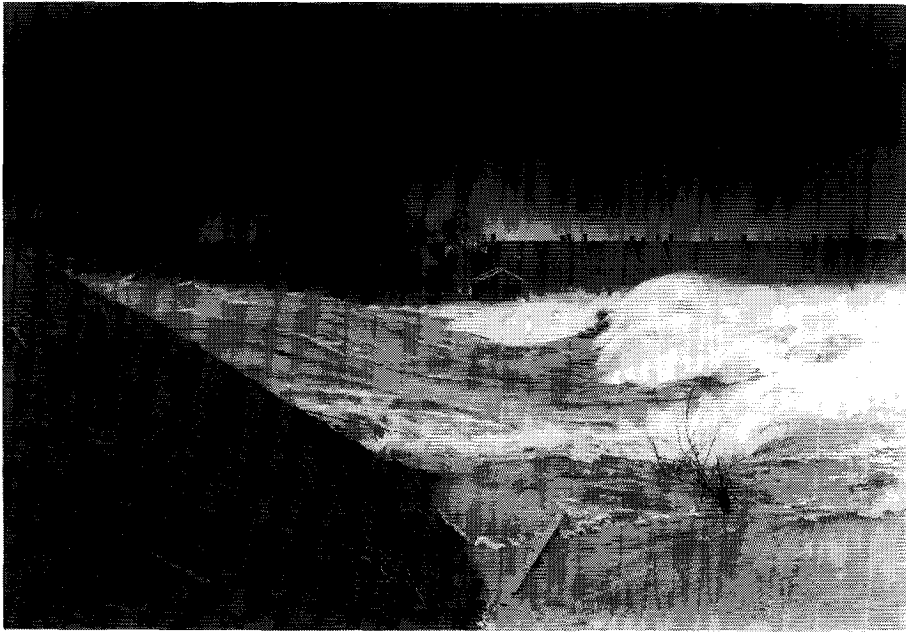


Figure 7.6 Flow through breach in Noord Dike in Papendrecht (The Netherlands, 1 February 1953, about 11:30 hr am) in stage IV of breach erosion process.

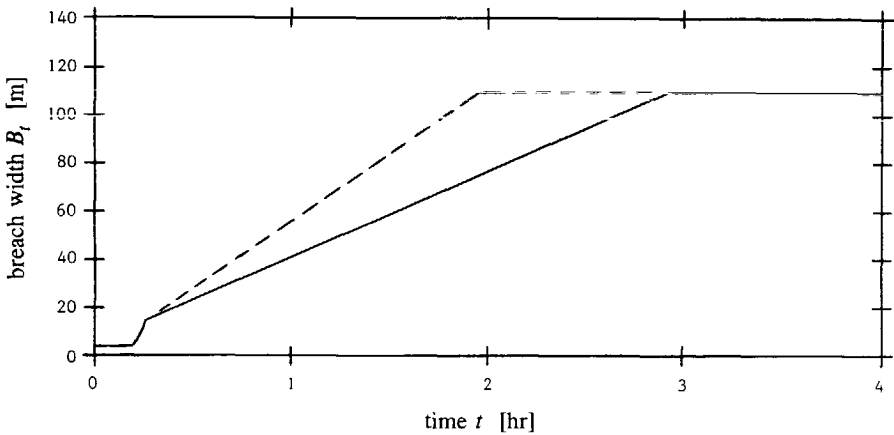


Figure 7.7 Predicted (BRES) breach width $B_w(t)$ for failure of Noord Dike in Papendrecht in 1953. BRES with the Bagnold-Visser formula in Stages I, II and III, and both the formulations of Van Rijn (dashed line) and Engelund-Hansen (solid line) in Stages IV and V.

- polder area A_p : $A_p = 94 * 10^6 \text{ m}^2$ (see Rijkswaterstaat, 1961),
- discharge coefficient $m = 1.0$ in Stages IV and V (Type A breach).

Further the increase of the breach width B_t has been limited to $B_t = 110 \text{ m}$. Figure 7.7 shows the model prediction for the increase of the width B_t of the breach in the Noord Dike applying the formula of Bagnold-Visser in Stages I, II and III (giving $t_3 - t_0 = 15 \text{ min}$) and the formulae of both Van Rijn and Engelund-Hansen in Stages IV and V. The BRES model reaches the final width $B_t = 110 \text{ m}$ in Stage IV at $t = 2.0 \text{ hr}$ (with Van Rijn) and $t = 2.9 \text{ hr}$ (with Engelund-Hansen). So the model prediction of a breach width $B_t = 110 \text{ m}$ achieved in about 2.0 hr to 3.0 hr is more or less in agreement with above described eye-witness report. With both formulae BRES completes its calculation at $t \approx 94 \text{ hr}$ when the polder water level $H_p \approx \text{NAP} - 0.50 \text{ m}$ (i.e. mean inundation depth of about 1.0 m) has become equal to the outside water level H_w .

For the case that the Noord Dike would have been constructed with sand along a much longer length, the model (applying Bagnold-Visser in Stages I, II and III and Van Rijn in Stages IV and V) computes a final breach width $B_t = 820 \text{ m}$, an inundation depth in the polder of 2.9 m and a total inundation duration of about 27 hr (with Engelund-Hansen these values are: $B_t = 890 \text{ m}$, inundation depth of 2.4 m, inundation duration of 28 hr). When also the breach is allowed to grow vertically down to $\text{NAP} - 1.50 \text{ m}$ (i.e. polder level), then the breach erosion stops at $t = 16.0 \text{ hr}$ when $B_t = 860 \text{ m}$ and the inundation depth is 2.7 m (with Engelund-Hansen: 17.5 hr, 667 m, 2.9 m). Indeed, the auxiliary spillway has limited the breach growth and the breach inflow significantly, so also the inundation speed and the flow velocities in the polder, so most likely also the number of victims.

7.5 Discussion

After suitable calibrations, the agreement of the model predictions with the data of both the Zwin'94 experiment and the laboratory experiment is good. These results have been obtained applying the Bagnold-Visser (1989) formula in Stages I, II and III and with both the Van Rijn (1984a,b) formulation and the Engelund-Hansen (1967) formula in Stages IV and V. The confrontation of the model with the failure of the Noord Dike in Papendrecht in 1953 indicates that the final breach width $B_t \approx 110 \text{ m}$ was present after about 2.5 hr, which is more or less in agreement with a rough eye-witness report.

For Type B breaches, the BRES model is (as yet) not able to compute the erosion of the relatively high foreland, so cannot predict the discharge coefficient m . A computation with $m = 1.5$ (with the Bagnold-Visser formula in Stages I, II and III, and the Van Rijn formula in Stages IV and V) yields for the Zwin'94 experiment a final breach width $B_t = 45 \text{ m}$ at

$t = t_5 = 45$ min, values which differ only slightly from the results obtained with $m = 1.3$ in Paragraph 7.3. So the model is not very sensitive for a proper choice of the discharge coefficient m .

From a hydraulic point of view, the process of breach growth in (sand)-dikes is exceptional: (1) the Froude number Fr varies from values of order 4 in the first three stages, to about 1 in Stage IV and practically 0 at the end of Stage V; (2) the Shields' parameter θ varies from values smaller than 1 at the top of the inner slope to values of 10 to above 100 near the toe of the slope inner slope (see Table 5.1) in Stages I, II and III, to order 1 in Stage IV and practically 0 at the end of Stage V. Hence, the application of two formulae (instead of one) in the present model, one for Stages I through III, one for Stages IV and V, is quite obvious.

The BRES model predicts for a sand-dike similar to the Noord Dike, but with a core of sand along a much longer length than about 100 m and without a solid foundation of clay, a final breach width $B_f \approx 800$ m developed in about 17 hr. Most likely the much shorter inundation period (17 hr instead of about 94 hr) and the larger inundation depth (2.8 m instead of 1.0 m) would have left behind more people drowned. Even worse scenario's would have taken place in smaller polders than the polder West-Alblasserwaard:

- for $A_p = 9.4 * 10^6$ m²: final breach width $B_f \approx 280$ m developed in about 4.5 hr, final inundation depth of about 4.1 m (with Engelund-Hansen: 220 m, 5.6 hr, 4.1 m),
- for $A_p = 0.94 * 10^6$ m²: final breach width $B_f \approx 100$ m developed in about 1.6 hr, total inundation depth of about 5.1 m (with Engelund-Hansen: 80 m, 2.0 hr, 4.9 m).

In small polders in tidal areas the inundation depth (and speed) can become very large since the polder fills when the outside water level is still relatively high. Figure 1.1 indicates that the percentage of casualties increases exponentially when the inundation depth becomes larger than about 3 m. This is also what happened in the 1953 flood disaster in The Netherlands: most of the 1835 victims drowned in polders with relatively small areas.

In the past most of the dikes in The Netherlands were built with clay, which is cohesive and consequently, compared to sand, less easy to erode by flowing water. So, the present version of BRES may not be applied to most of the past dike-failures in The Netherlands. Erosion of cohesive sediment is a very complicated process, and the mathematical description of it is in a very embryonic phase. Possibly, however, the model can relatively simple be adapted for applications of clay-dikes. Such an adaptation requires detailed and reliable data of clay-dike breaching. To the author's knowledge, these data are as yet not available.

Chapter 8

Conclusions and recommendations

8.1 Introduction

In this thesis a mathematical model for sand-dike breach erosion has been developed. The model simulates the growth of a relatively small initial breach in the top of a sand-dike and the progress of the flow rate through the breach. The initial damage to the dike is assumed to be so large that it has uncovered the sand-core of the dike. It is assumed that the remaining clay-layers and revetments on the dike slopes will not slow down the breach erosion process. The effect of side-slope instability is not incorporated in the model. Possible tail-water effects are taken into account by assuming a horizontal water level in the inundating polder at all times.

An essential part of a breach erosion model is the description of the entrainment of sand and its transport through the breach. In the mathematical model a simplified version of Galappatti's (1983) description for sediment entrainment is applied. For the equilibrium value of the sediment transport, four formulae have been implemented in the model for the test with experimental results and prototype data.

The numerical version of the mathematical model (BRES) has been calibrated with the data of the Zwin'94 field experiment and next tested with the data of Caan's (1996) laboratory experiment. Finally, the BRES model has been validated against the relatively poor data of the failure of the Noord Dike in Papendrecht in 1953.

8.2 Conclusions

The following conclusions are drawn from this study:

- In the process of sand-dike breach erosion, generally five stages can be distinguished. Hereby it is assumed that the flow of water through a relatively small initial breach in the top of the dike starts the breach erosion process. In the first two stages, the breach eats its way into the dike due to erosion of the inner slope, with hardly any increase of the breach inflow rate. In the third stage the breach growth accelerates, consequently also the

discharge through the breach. In this stage the breach width grows in proportion to the breach depth. After the wash-out of the dike in the breach at the end of the third stage, the flow through the breach is virtually critical throughout the breach in the fourth stage, and the breach grows further mainly laterally (at a constant outside water level the width of the breach grows linearly with time). In the fifth stage, back-water in the polder decelerates the subcritical flow through the breach, and so also the increase of the breach width. Rising tail-water ultimately stops the flow of water through the breach.

- In the important last two stages, the breach growth depends on the erodibility of the base of the dike and, in situations where the base of the dike has not much resistance against erosion, on the stability of the toe construction of the outer dike slope, or on the height and the resistance against erosion of the foreland. Three breach types can be distinguished (Types A, B and C). The numerical version of the model (BRES) computes the breach growth and the discharge through the breach as function of these conditions.

In a Type A breach the sand-dike has a solid (i.e. with a high strength against erosion) base, or a solid toe construction on the outer slope, or a relatively high foreland with a large resistance against erosion. Then the base of the dike, the toe construction or the high foreland act as spillways (broad-crested or narrow-crested, which has only a secondary influence on the discharge coefficient of the spillway) controlling both the breach inflow rate and the breach erosion. The possible scour hole downstream of the spillway has only a minor effect on both breach growth and breach discharge.

In Types B and Type C breaches the dike does not have a base or a foreland with a relatively large resistance against erosion, nor a solid toe construction on the outer slope. In these breaches a spillway is formed upstream of the breach which controls the breach inflow. The alignment of this spillway depends on the height of the foreland of the dike. This alignment will be curved (elliptic or circular) in a Type B breach in a dike with a relatively high foreland. Due to this curvature the inflow rate is larger than in a Type A breach, consequently also the rate of erosion in the breach.

In a Type C breach the outer slope abuts on the water and the spillway is straight and relatively deep in the middle and curved near the side-slopes. The larger water depth above the spillway causes the inflow rate to be larger than in Types A and B breaches. In a Type C breach, the scour hole downstream of the spillway has only a secondary effect on both breach growth and breach discharge.

- The process of breach erosion in (sand-)dikes is exceptional from a hydraulic point of view:
 - (1) the Froude number Fr varies from values of order 4 at the toe of the inner slope in

- the first three stages to 1 in Stage IV and practically 0 at the end of Stage V;
- (2) the Shields' mobility parameter θ varies from values of 10 to above 100 at the toe of the inner slope (yielding depth-averaged sand concentration values up to $c \approx 0.25$) in Stages I, II and III to order 1 in Stage IV and practically 0 at the end of Stage V; in Stages I, II and III θ varies from values smaller than 1 at the top of the inner slope to values of 10 to above 100 near the toe of the slope (see Table 5.1);
- (3) in Stages I, II and III the roughness factor k in the equations (4.9) and (4.10) increases theoretically from $3D_{90}$ at the top of the slope to values having the order of magnitude of the water depth near the toe of the slope;
- (4) both the angle of inclination β of the inner slope and the side-slope angle γ attain values of $\phi \approx 32^\circ$ and larger.

None of the present sediment transport formulae have been set-up for and tested to such a wide range of conditions. In Stages I, II and III the validity ranges of the formulae (if known) are well exceeded, especially those of the mobility parameter θ , the slope angle β and (to a lesser extent for some formulae) the depth-averaged concentration c .

- With suitable calibrations the model is able to simulate the breach growth in both the Zwin'94 experiment and Caan's (1996) laboratory experiment fairly well when the sand transport formula of Bagnold-Visser (1989) is applied in Stages I, II and III and the formulations of Engelund-Hansen (1967) or Van Rijn (1984a,b) in Stages IV and V. The confrontation of the model with the relatively poor data of the failure of the Noord Dike in Papendrecht in 1953 indicates roughly fair agreement with an eye-witness report.

8.3 Recommendations

The following recommendations result from the present study:

- In the present version of BRES the approximation (4.35) with (4.36) of Galappatti's (1983) description for sediment entrainment has been applied. This approximation is valid for values of u_* / w_s much larger than the unity, i.e. for dikes and dams erected with sand having not too large grain sizes. In order to extend the applicability of the model it is recommended to refine the approximation (4.34) of Galappatti's (1983) model for the pick up of sediment.
- It is recommended to design and construct dikes in such a way that the growth of the breach after a possible failure of the dike will be limited, both vertically and horizontally.

A solid toe construction of the outer dike slope (see Figures 3.13 and 3.15) may prevent further vertical erosion of the breach, plugs in the cross-section of the dike (for instance vertical sheet-piling or clay-cores, say every 100 m) can stop further grow of the breach horizontally. The simulations of the failure of the Noord Dike in Papendrecht in 1953 described in this thesis clearly show that the inundation speed will be limited significantly by these measures, and consequently also the number of casualties.

- It is recommended to perform large-scale experiments of breaching in prototype sand-dikes in order to investigate the failure mechanism of dikes and to measure the effect of clay-layers, revetments and toe constructions on the breach erosion process.
- The review of the literature performed in this study (see Chapters 1, 2, 3, 4 and 7) has shown that data of breaching of real prototype dikes are scarce and far from complete. These data are, however, urgently needed for the calibration and validation of breach erosion models.

In order to increase the chance that possible future dike failures will leave behind reliable and detailed data sets of the breaching process, it is recommended to form 'observation teams' and to support these teams with sufficient financial means. The main task of these teams should be to set up scenarios for data collection of floodings and to perform this data collection at the proper time.

- The present model has been developed for the breach erosion in sand-dikes, i.e. dikes constructed with cohesionless sediment. Application to dikes constructed with cohesive sediment (clay or a mixture of sand, silt and clay) will yield overestimations of the breach growth. Erosion of cohesive sediment is, however, a very complicated process, and the mathematical description of it is in a very embryonic phase. It is therefore recommended to investigate the feasibility of simple adaptations of the present model for applications of clay-dikes. Such a calibration requires, however, detailed and reliable data of clay-dike breaching. Therefore, it is also recommended to perform large-scale experiments of breaching of prototype clay-dikes.

Appendix A

Tested sediment transport formulae

A.1 Introduction

The purpose of this appendix is to summarize the sediment transport formulations that have been included in this study. Most of these formulations consist of one or two formula(e), for example the well-known formula of Engelund and Hansen (1967). Some formulations have a series of equations, for example that of Van Rijn (1984a,b).

The application range of the formulae in terms of Shields' mobility parameter (θ) and the Froude number (Fr) and experimental conditions as sediment diameter, bottom slope, flow velocity and sediment concentration are listed with the formulation if these are known. The absence of experimental verification (to the author's knowledge) is indicated by dashes.

The formulae give the equilibrium values for the rates of sediment transport expressed in amounts of volumes of sediment transport per unit of time per unit of (breach)width (SI-unit: $(\text{m}^3/\text{s})/\text{m}$), that is without voids.

The equilibrium value for the sediment transport is given as bed-load transport (s_b), total sediment transport (s_t) or total sediment transport with a bed-load and a suspended load component ($s_t = s_b + s_s$). The conception of Mastbergen and Winterwerp (1987) differs from the other formulae in the sense that it is an erosion/deposition formulation and not a formula for the sediment transport capacity.

A.2 Formulae for sand-water mixture flows

A.2.1 Wilson (1966, 1987)

Bed-load transport:	$s_b = 12.1 (\Delta g D^3)^{0.5} [\mu \theta - 0.047]^{1.5}$	(A.1)
Ranges of θ and Fr :	$1 < \mu \theta < 10$	
Sediment:	sand with a diameter between 0.4 mm and 1.3 mm ($D_{50} \approx 0.8$ mm), nylon particles with an equivalent sphere diameter of 3.9 mm, 13 mm gravel (Wilson, 1987)	
Slope angles:	horizontal, pressurized conduit	
Flow velocities:	-	
Concentrations:	high	

The parameter μ in equation (A.1) is the ripple factor ($\mu = 1$ for a plane bed). The solid particles in Wilson's (1966) experiments were generally transported in a 'dense layer immediately above the bed', 'supported by intergranular collision rather than by fluid turbulence'. Wilson (1966, and personal communication in 1992) has termed this bed-load transport, but since the thickness of the 'dense layer' in his experiments was much larger than a few particle diameters (see Figure A.1), the term total sediment transport seems more proper.

For the empirical determination of (A.1), Wilson (1966) used only the data of his tests with a plane bed and not his (small number of) experiments with ripples and dunes. This means for the ripple factor in (A.1) that $\mu = 1$.

Equation (A.1) is similar to the formula of Meyer-Peter and Müller (1948):

$$s_b = 8 (\Delta g D^3)^{0.5} [\mu \theta - 0.047]^{1.5} \quad \text{for } 0.03 < \mu \theta < 0.2 \quad (\text{A.2})$$

Meyer-Peter and Müller (1948) derived (A.2) using data from experiments in flumes with bed slopes: $0.0004 < \tan \beta < 0.02$, sand with a mean particle diameter D : $0.4 \text{ mm} < D < 29 \text{ mm}$, and a water depth d : $0.01 \text{ m} < d < 1.20 \text{ m}$.

Wilson (1966) argued that (A.1) agrees for $\mu\theta < 1$ almost as well with the data of Meyer-Peter and Müller (1948) as (A.2). In a sequel publication Wilson (1987) has presented an equation similar to (A.1):

$$s_b = 11.8 (\Delta g D^3)^{0.5} \theta^{1.5} = 11.8 \frac{(u_*')^3}{\Delta g} \quad (\text{A.3})$$

Also (A.3) has an empirical basis. Equation (A.3) gives similar results as (A.1), except for small values of θ , see Visser (1995b).

Figure A.1 shows 'data points (concentration $c(z)$ at various heights z) for 13 mm gravel at a volumetric in situ solids concentration of 0.09 in a pipe of internal diameter 0.26 m. These data are typical of moderate concentrations of particles with large fall velocities, i.e., the upper portion of the flow is virtually particle-free, while the maximum concentration of particles, near the bottom of the pipe, approaches the bed concentration c_{be} . In between, the concentration decreases with height in an essentially linear fashion' (after Wilson, 1987).

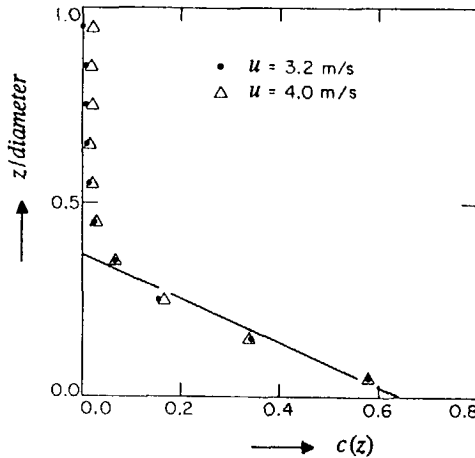


Figure A.1 Concentration profile measurements for coarse particle slurry in a pipe of internal diameter of 0.26 m (after Shook et al., 1982).

A.2.2 Mastbergen and Winterwerp (1987)

$$\text{Sediment transport: } s(x_1) = s(x_0) + (x_1 - x_0)(E - S_e) \quad (\text{A.4})$$

$$\text{where: } E = 0.012 \frac{(\Delta g D)^{0.5} D^{0.3} (\Delta g / \nu^2)^{0.1} (\theta^{0.5} - 1.3)}{1 - \frac{\tan \beta}{\tan \phi}} \quad (\text{A.5})$$

$$S_e = w_s c (1 - c)^4 \quad (\text{A.6})$$

$$\theta = \frac{C_f U^2}{\Delta g D} = 0.0125 \frac{U^2}{\Delta g D} \quad (\text{A.7})$$

Ranges of θ and Fr : $3 < \theta < 24$

Sediment: sand with $0.12 \text{ mm} < D_{50} < 0.23 \text{ mm}$

Slope angles: $0.003 < \tan \beta < 0.4$

Flow velocities: -

Concentrations: $0 < c < 0.40$

E in (A.4) and (A.5) is the erosion rate and S_e in (A.4) and (A.6) is the sedimentation rate (E and S_e have the dimension of volume per unit of time and per unit of area [SI-unit: (m³/s)/m²]); ν is the kinematic viscosity and ϕ the angle of repose.

The formulation of Mastbergen and Winterwerp (1987) has resulted from a study for the construction of the Philipsdam and the Oesterdam (part of Deltaworks in the Netherlands) with the sand-closure method, see also Winterwerp et al. (1990) and Winterwerp, et al. (1992).

Winterwerp et al. (1990) have described field experiments (during the construction of a sand dam closing the Slaak estuary) and laboratory experiments in a small sloping flume (length 1.5 m) and a larger sloping flume (length 9.0 m). The flow in the experiments was supercritical and the bed was plane.

Winterwerp et al. (1990) has presented a formula for the equilibrium bed slope above the water line at which sedimentation and erosion are in balance. 'For laminar flow conditions this slope is only dependent on the average sand concentration, whereas for turbulent

conditions the flow rate per unit width (q) is the main parameter. The sand concentration near the bed (c_b) measured about 35% by volume for most test conditions. The vertical gradient in sand concentration ($\partial c(z)/\partial z$) decreased with increasing mean sand concentration (c), indicating a decrease in the damping of turbulence. The velocity distribution ($u(z)$) behaved fairly logarithmically, showing a variation in slope with varying concentration c . A minimum value of the effective Von Karman constant ($\kappa \approx 0.2$) was found at concentrations of about 0.20. At high concentrations the viscous sublayer is thicker, resulting in a larger bed shear stress' (after Winterwerp et al., 1990).

In a sequel Winterwerp et al. (1992) have described situations with slopes slightly smaller than the equilibrium slope (yielding a sedimentation rate larger than the erosion rate). At these slopes, starting from a plane bed, sand bars will form. The supercritical flow over the upstream part of these bars decelerates and the sediment transport capacity decreases. The deceleration can be so large that a hydraulic jump is formed upstream from the bar. 'The flow is now subcritical up to the crest of the bar. Beyond the crest on the lee side of the bar, the flow accelerates, becoming supercritical again.' A bar consists of a nearly horizontal terrace with subcritical flow, a steep lee side with supercritical flow and a hydraulic jump in between. On the subcritical part of the bar, net sedimentation will occur; at the lee side net erosion. Because of this a bar moves upstream. Thus, a cascade of sandbars can be formed, propagating upstream, resembling 'the behaviour of antidunes and chute-pool systems. According to the classical regime theory, these bed forms can develop at high Froude numbers and low Shields' numbers¹⁰⁾, see Kennedy (1969), Engelund (1970) and Allen (1982)', after Winterwerp et al. (1992).

The erosion rate at the lee side of the bar was generally limited due to the large concentrations and, according to Winterwerp et al. (1992), more moderate than predicted by the pick-up functions used in classical sediment transport theory (see Van Rijn, 1984c). The high concentrations did also restrict the sedimentation, described in (A.6) by the factor $(1-c)^4$, termed 'hindered settling'.

The value 0.0125 for the friction coefficient C_f , see equation (A.7), approaches the value measured in the field experiments in the Slaak estuary (construction of Philipsdam), see also Section A.4.1.

Mastbergen and Winterwerp (1987) and Winterwerp et al. (1992) schematized the cascade of antidunes as a series of triangles and introduced the erosion/deposition function (A.4) with (A.5), (A.6) and (A.7) to describe the physics of such a chute-pool system. Winterwerp et al. (1992) claimed that the agreement with the experimental data is reasonable.

¹⁰⁾ Shields' number is very large in Stages I, III and III of the breach erosion process.

A.3 Formulae for sediment transport on steep slopes

A.3.1 Smart and Jaeggi (1983)

Bed-load transport:

$$s_b = 4 C_f^{-0.5} (\Delta g D^3)^{0.5} \left[\frac{D_{90}}{D_{30}} \right]^{0.2} (\tan \beta)^{0.6} \theta^{0.5} [\theta - \theta_{cr}(\beta)] \quad (\text{A.8})$$

$$\text{where: } \theta_{cr}(\beta) = \theta_{cr} \cos \beta \left[1 - \frac{\tan \beta}{\tan \phi} \right] \quad (\text{A.9})$$

Ranges of θ and Fr : $0.1 < \theta < 3.3$ $1.1 < Fr < 3.3$

Sediment: sand with $0.4 \text{ mm} < D < 29 \text{ mm}$ and $D_{90}/D_{30} < 8.5$

Slope angles: $0.03 < \tan \beta < 0.2$

Flow velocities: $0.8 \text{ m/s} < U < 2.0 \text{ m/s}$

Concentrations: $0.006 < c < 0.19$

θ_{cr} in (A.8) is the critical value of θ , at which incipient motion takes place, see Figure A.2. Equation (A.8) has resulted from Smart en Jaeggi's (1983) experimental investigation in the laboratory into the sediment transport capacity of flows on relatively steep slopes, see also Smart (1984) and Rickenmann (1991). Smart and Jaeggi calibrated (A.8) also to the old data of Meyer-Peter and Müller (1948), for which $0.0004 < \tan \beta < 0.02$. The parameter D_{90}/D_{30} in (A.8) represents the effect of non-uniform sand.

A test of the original formula of Meyer-Peter and Müller (1948) with Smart and Jaeggi's new data has shown that the MPM formula underestimates the transport capacity for slopes with $\tan \beta > 0.03$.

A.3.2 Bathurst, Graf and Cao (1987)

Bed-load transport: $s_b = 2.5 \frac{\rho}{\rho_s} (\tan\beta)^{3/2} (q - q_{cr})$ (A.10)

where: $q_{cr} = 0.21 g^{0.5} (D_{16})^{1.5} (\tan\beta)^{-1.12}$ (A.11)

Ranges of θ and Fr : $0.1 < \theta < 0.4$ $0.3 < Fr < 2.2$

Sediment: gravel with $12 \text{ mm} < D_{50} < 44 \text{ mm}$

Slope angles: $0.005 < \tan\beta < 0.09$

Flow velocities: -

Concentrations: $0 < c < 0.03$

Equation (A.10) is a modified Schoklitsch (1930) formula. The confrontation of (A.10) with experimental data has indicated that (A.10) underestimates the sediment transport capacity for $\theta > 0.4$ and for $\tan\beta < 0.01$ and $\tan\beta > 0.1$, see Bathurst et al. (1987).

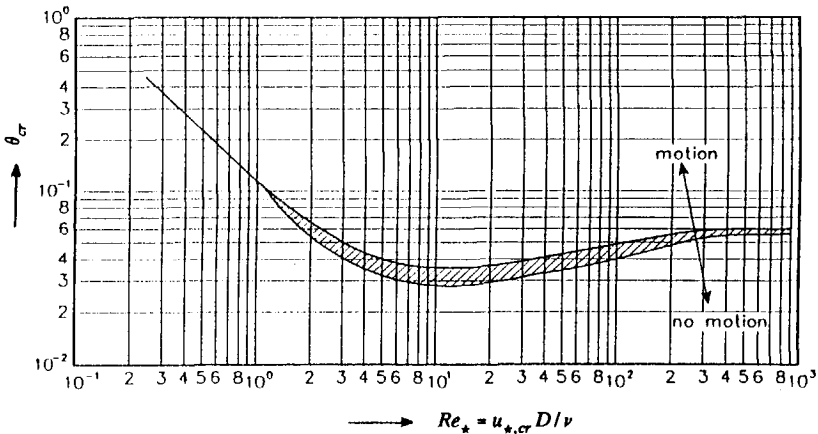


Figure A.2 Initiation of motion for a current over a plane, weakly sloping bed according to Shields (1936), $\theta_{cr} = f(Re_*)$; after Van Rijn (1993).

A.3.3 Rickenmann (1991)

Bed-load transport in water and in clay suspensions:

$$s_b = 12.6 \Delta^{-1.6} \left[\frac{D_{90}}{D_{30}} \right]^{0.2} (\tan \beta)^2 (q - q_{cr}) \quad (\text{A.12})$$

where: $q_{cr} = 0.065 \Delta^{1.67} g^{0.5} (D_{50})^{1.5} (\tan \beta)^{-1.12}$ (A.13)

Ranges of θ and Fr : $0.1 < \theta < 3.3$ $1.5 < Fr < 2.8$

Sediment: sand with $0.4 \text{ mm} < D < 29 \text{ mm}$ and $D_{90}/D_{30} < 8.5$ (sand in clear water),
gravel with $D = 1.0 \text{ cm}$ and $D_{90} = 1.2 \text{ cm}$ (debris flow: gravel in clay suspension)

Slopes: $0.03 < \tan \beta < 0.20$

Flow velocities: $0.8 \text{ m/s} < U < 2.0 \text{ m/s}$

Concentrations: $0.006 < c < 0.19$

Density clay-suspension: $998 \text{ kg/m}^3 < \rho_s < 1246 \text{ kg/m}^3$

Equation (A.12) has resulted from an analysis of data of experiments on bed-load transport on relatively steep slopes, i.e. Smart and Jaeggi's (1983) experiments, and Rickenmann's (1991) experiments with clay suspensions (only those experiments with negligible viscous effects).

Rickenmann (1991) has presented also an empirical transport formula, valid for both mild and steep slopes (i.e. $0.001 < \tan \beta < 0.20$):

$$s_b = 3.1 \frac{(\Delta g D^3)^{0.5}}{\Delta^{0.5}} \left[\frac{D_{90}}{D_{30}} \right]^{0.2} \theta^{0.5} [\theta - \theta_{cr}(\beta)] Fr^{1.1} \quad (\text{A.14})$$

A.4 Formulae for total sand transport in river regimes

A.4.1 Engelund and Hansen (1967)

Total load transport:	$s_t = 0.05 C_f^{-1} (\Delta g D_{50}^3)^{0.5} \theta^{2.5}$	(A.15)
Ranges of θ and Fr :	$0.07 < \theta < 6$ $0.1 < Fr < 0.8$	(Voogt et al., 1991)
Sediment:	sand with $0.19 \text{ mm} < D < 0.93 \text{ mm}$	
Slope angles:	$\tan \beta < 0.005$	(Voogt et al., 1991, estimated)
Flow velocities:	$U < 2.8 \text{ m/s}$	(Voogt et al., 1991)
Concentrations:	$c < 0.0004$	(Voogt et al., 1991)

Engelund and Hansen (1967) have tested their formula with the experimental data of Guy et al. (1966) for $0.07 < \theta < 6$. The effect of the sloping bed has not explicitly been taken into account in the derivation and test of this formula.

Voogt et al. (1991) have tested Engelund and Hansen's formula for relatively large flow velocities with the data of Peterson and Howells (1973), the data of the measurements of Van Rijn (1985) in a laboratory flume and to the data of field measurements (on a sandy sill during the construction of the Philipsdam, see also Section A.2.2). The main features of these experiments are: subcritical flow, sand with a diameter between 0.1 mm and 0.4 mm, depth-averaged flow velocities (U) and values for the mobility parameter (θ) and the Froude number (Fr) as indicated above.

A.4.2 Van Rijn (1984a,b)

Total load transport:	$s_t = s_b + s_s$ (see next page)	(A.16)
-----------------------	-----------------------------------	--------

Ranges of θ and Fr :	$\theta < 6$ $0.1 < Fr < 0.8$	(Voogt et al., 1991)
-------------------------------	-------------------------------	----------------------

Sediment:	sand with diameter between 0.09 mm and 2.0 mm
-----------	---

Slope angles:	$\tan\beta < 0.005$	(Voogt et al., 1991, estimated)
---------------	---------------------	---------------------------------

Flow velocities:	$U < 2.8$ m/s	(Voogt et al., 1991)
------------------	---------------	----------------------

Concentrations:	$c < 0.0004$	(Voogt et al., 1991)
-----------------	--------------	----------------------

Van Rijn (1984a,b) has tested his formulae for bed-load and suspended load transport with a large number of experimental data from the field and the laboratory. The slope effect has not explicitly been taken into account in these formulae.

Van Rijn's formulation for the total transport capacity holds a large number of formulae, which are reproduced on the next page. The following symbols still need to be defined: T is the transport stage parameter, D_* is a dimensionless particle parameter, u_*' is the bed-shear velocity related to grains and a is a reference level above the bed, where the sediment concentration is c_a . The factor ζ_1 in (A.25) is of order 10.

Voogt et al. (1991) has tested Van Rijn's formulation for relatively large flow velocities with the data mentioned in Section A.4.1. The flow in these experiments was subcritical, the sand had a diameter between 0.1 mm and 0.4 mm and depth-averaged flow velocities (U) and values for the mobility parameter (θ) and Froude number (Fr) as given above. Voogt et al. (1991) have concluded that Van Rijn's formulation gives reasonable good agreements with the experimental data (somewhat better than Engelund and Hansen's formula).

A.4.2 Van Rijn (1984a,b), continuation

$$\text{Bed-load transport: } s_b = 0.053 (\Delta g D_{50}^3)^{0.5} \frac{T^{2.1}}{(D_\star)^{0.3}} \quad \text{for } T < 3 \quad (\text{A.17})$$

$$s_b = 0.1 (\Delta g D_{50}^3)^{0.5} \frac{T^{1.5}}{(D_\star)^{0.3}} \quad \text{for } T \geq 3 \quad (\text{A.18})$$

$$\text{where: } T = \frac{(u_\star')^2 - (u_{\star,cr})^2}{(u_{\star,cr})^2} \quad (\text{A.19})$$

$$u_\star' = \frac{\kappa U}{\ln(12d/3D_{90})} \leq u_\star \quad (\text{A.20})$$

$$u_{\star,cr} = \text{critical } u_\star \quad (\text{given by } \theta_{cr}, \text{ see Figure A.3})$$

$$D_\star = D_{50} (\Delta g / \nu^2)^{1/3} \quad (\text{A.21})$$

$$\text{Suspended load transport: } s_s = F c_a U d \quad (\text{A.22})$$

$$\text{where: } F = \frac{(a/d)^{Z'} - (a/d)^{1.2}}{(1 - a/d)^{Z'} (1.2 - Z')} \quad (\text{A.23})$$

$$Z' = \frac{w_s}{[1 + 2 (w_s/u_\star)^2] \kappa u_\star} + 2.5 \left[\frac{w_s}{u_\star} \right]^{0.8} \left[\frac{c_a}{c_{be}} \right]^{0.4}$$

$$\text{for } 0.01 < w_s/u_\star < 1, \quad c_a/c_{be} \leq 1 \quad (\text{A.24})$$

$$a = k \quad \text{with } 0.01 d \leq a < 0.3 d \quad (a < \zeta_1 D_{90}) \quad (\text{A.25})$$

$$c_a = 0.015 \frac{D_{50}}{a} \frac{T^{1.5}}{(D_\star)^{0.3}} \quad (\text{A.26})$$

$$c_{be} = 1 - p = \text{sediment concentration in bed}$$

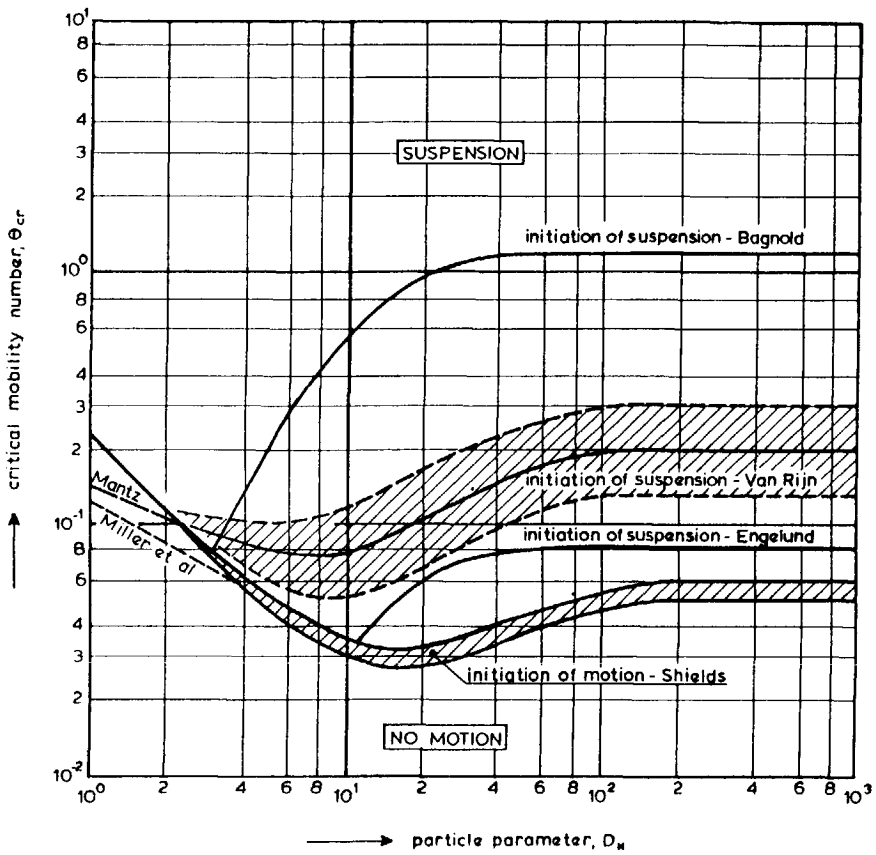


Figure A.3 Initiation of motion and suspension for a current over a plane, weakly sloping bed, $\theta_{cr} = f(D_*)$; after Van Rijn (1993).

The Shields curve of Figure A.3 can be represented as (Van Rijn, 1993):

$$\theta_{cr} = 0.24 D_*^{-1} \quad \text{for} \quad 1 < D_* \leq 4 \quad (\text{A.27})$$

$$\theta_{cr} = 0.14 D_*^{-0.64} \quad \text{for} \quad 4 < D_* \leq 10 \quad (\text{A.28})$$

$$\theta_{cr} = 0.04 D_*^{-0.1} \quad \text{for} \quad 10 < D_* \leq 20 \quad (\text{A.29})$$

$$\theta_{cr} = 0.013 D_*^{0.29} \quad \text{for} \quad 20 < D_* \leq 150 \quad (\text{A.30})$$

$$\theta_{cr} = 0.055 \quad \text{for} \quad D_* > 150 \quad (\text{A.31})$$

A.5 Energetics-based formulae

A.5.1 Bagnold-Bailard (1981)

$$\text{Total load transport: } s_t = s_b + s_s \quad (\text{A.16})$$

$$\text{where: } s_b = \frac{e_b}{\tan \phi - \tan \beta} \frac{C_f U^3}{\Delta g} \quad (\beta < \phi) \quad (\text{A.32})$$

$$s_s = \frac{e_s}{w_s/U - e_s \tan \beta} \frac{C_f U^3}{\Delta g} \quad (e_s \tan \beta < w_s/U) \quad (\text{A.33})$$

Ranges of θ and Fr : -

Sediment: -

Slope angles: -

Flow velocities: -

Concentrations: -

The Bailard-Bagnold (1981) formulation is based on Bagnold's (1963, 1966) energetics-based sediment transport model. Bagnold has distinguished two distinct modes for the sediment transport, each differing by way of the support of the sediment grains. Particles transported as bed-load are supported by the bed via the grain-grain interactions. Grains transported as suspended load are supported by the stream via turbulent diffusion. In both modes, energy is expended by the stream in transporting the sediment load.

Bagnold has defined the sediment transport efficiency as the ratio of the rate of energy expenditure in transporting either the bed-load or the suspended load, divided by the total rate of energy production of the stream. If ω is the rate of energy production by the stream ($\omega = \tau_b U$), then $e_b \omega$ is used for bed-load transport and $e_{sl}(1 - e_b) \omega = e_s \omega$ for suspended load transport (e_b is the bed-load efficiency, e_{sl} and e_s are suspended load efficiencies, $e_b \approx 0.13$ and $e_s \approx 0.01$ according to Bagnold, 1966). Bagnold has determined these values for e_b and e_s in a semi-empirical way.

Bailard's (1981) formula (A.32) for the bed-load capacity is exactly equal to the original formula of Bagnold (1963, 1966). Equation (A.33) differs from Bagnold's original formula

Breach growth in sand-dikes

$$s_s = \frac{e_s}{w_s/U - \tan\beta} \frac{C_f U^3}{\Delta g} \quad (\tan\beta < w_s/U) \quad (\text{A.34})$$

by the inclusion of the factor $e_s \approx 0.01$ in the denominator. This difference arises because Bailard assumed that the stream power contribution from the suspended sediment load (owing to a gravity slope $\tan\beta$) contributes not directly to the suspended sediment transport rate but through the efficiency e_s .

A.5.2 Bagnold-Visser (1989)

$$\text{Total load transport: } s_t = s_b + s_s \quad (\text{A.16})$$

$$\text{where: } s_b = \frac{e_b}{(\tan \phi - \tan \beta) \cos \beta} \frac{C_f U^3}{\Delta g} \leq \zeta_2 (1 - p) D_{50} U \quad (\beta \leq \phi) \quad (\text{A.35})$$

$$s_s = \frac{e_s}{(w_s/U) (\cos \beta)^2} \frac{C_f U^3}{\Delta g} = \frac{e_s C_f U^4}{\Delta g w_s (\cos \beta)^2} \quad (\text{A.36})$$

$$\text{Ranges of } \theta \text{ and } Fr: \quad 11 < \theta < 106 \quad 2.8 < Fr < 4.1 \quad (\text{Visser, 1995b})$$

$$\text{Sediment:} \quad \text{sand with } D_{50} = 0.10 \text{ mm and } D_{50} = 0.22 \text{ mm}$$

$$\text{Slope angles:} \quad 0.36 < \tan \beta < 0.62 \quad (\text{Visser, 1995b})$$

$$\text{Flow velocities:} \quad 1.2 \text{ m/s} < U < 3.5 \text{ m/s} \quad (\text{Visser, 1995b})$$

$$\text{Concentrations:} \quad 0.007 < c < 0.28 \quad (\text{Visser, 1995b})$$

The first difference between (A.35) and (A.32) is the term $\cos \beta$ in the denominator of (A.35). This difference originates from the definition by Bagnold (1963) of the 'dynamic transport rate' (immersed weight of sediment in water column multiplied with transport velocity multiplied with $\cos \beta$). In practice this difference is not relevant: also for somewhat larger slopes is $\cos \beta \approx 1$, and as $\beta \rightarrow \phi$, then both (A.32) and (A.35) predict very large amounts of bed-load transport which cannot actually occur. The second difference is the adoption in (A.35) of an upper limit for the bed-load transport:

$$s_b \leq \zeta_2 (1 - p) D_{50} U \quad (\text{A.37})$$

where ζ_2 is a coefficient of order 2. Such a limit is relevant in cases where $\beta \rightarrow \phi$ as in the first stages of the sand-dike breaching process.

The difference between (A.36) and (A.34) can be significant for sediment transport on relatively steep slopes. Visser (1989) has argued that the existence of a power gradient in the flow direction (owing to a gravity slope $\tan \beta$) does not reduce the work done by the fluid in a situation where erosion predominates and neglected this term. For $\beta \rightarrow 0$ both (A.33) and (A.36) reduce to Bagnold's (1963, 1966) original (A.34).

Appendix B

Computer program

B.1 Introduction

This appendix provides a description of the computational procedures applied in the present version of the BRES model.

B.2 Computation of sediment fall velocity

For relatively fine sand, the sediment fall velocity w_s depends on the kinematic viscosity ν of the water. In BRES the viscosity ν is calculated as

$$\nu = \frac{\rho + 1505}{2500\rho} 10^{\frac{13}{10 - 0.081(20 - T)}}^{-4.3} \quad \text{for } 0^\circ\text{C} \leq T \leq 20^\circ\text{C} \quad (\text{B.1})$$

$$\nu = \frac{\rho + 1505}{2500\rho} 10^{\frac{1.33(20 - T)}{T + 104} - 3.0} \quad \text{for } 20^\circ\text{C} \leq T \leq 40^\circ\text{C} \quad (\text{B.2})$$

The relationships between viscosity ν and temperature T given in (B.1) and (B.2) follow from similar relationships between dynamic viscosity η and temperature T for water given by the National Bureau of Standards (1975).

The sediment fall velocity w_s is calculated as (see Van Rijn, 1993)

$$w_s = \frac{\Delta g (D_{50})^2}{18\nu} \quad \text{for } 0.001 \text{ mm} \leq D_{50} \leq 0.1 \text{ mm} \quad (\text{B.3})$$

$$w_s = \frac{10\nu}{D_{50}} [(1 + 0.01\Delta g (D_{50})^3 \nu^{-2})^{0.5} - 1] \quad \text{for } 0.1 \text{ mm} < D_{50} < 1 \text{ mm} \quad (\text{B.4})$$

$$w_s = 1.1 (\Delta g D_{50})^{0.5} \quad \text{for } D_{50} \geq 1 \text{ mm} \quad (\text{B.5})$$

B.3 Definition of functions

In BRES the following subprograms or functions are defined: 1) Discharge, 2) NormalFlow, 3) FlowSlope, 4) FrictionCoeff and 5) SedTransCap.

Function Discharge

This function computes in Stages I, II, III and IV:

- the critical water depth d_c in the breach (i.e. in Stages I, II and III the water depth in the channel at the top of dike);
- the breach widths B , B_w and B_t at the breach inflow;
- the critical flow velocity U_c in the breach;
- the discharge Q_{br} through the breach.

The function Discharge reads as follows:

$$d_c = 0.7 (H_w - Z_{br}), \quad d_{cc} = 0.9 d_c \quad (\text{B.6, B.7})$$

$$\text{while } |(d_c - d_{cc})/d_c| > 0.01 \quad (\text{B.8})$$

$$\{ d_{cc} = d_c \quad (\text{B.9})$$

$$B = b + \frac{d_c}{\tan \gamma}, \quad B_w = b + \frac{2d_c}{\tan \gamma} \quad (\text{4.1, 4.2})$$

$$d_c = \frac{2}{2 + B/B_w} (H_w - Z_{br}) \quad (\text{4.71})$$

$$U_c = (g d_c B/B_w)^{1/2} \quad (\text{4.74})$$

$$B_t = b + \frac{2(H_d - Z_{br})}{\tan \gamma} \quad (\text{4.5})$$

$$Q_{br} = m B U_c d_c \quad (\text{4.72})$$

The equations (4.71) and (4.74) derived in Paragraph 4.4 for Stage IV apply also to the flow along the crown of the dike in the breach in Stages I, II and III. Equations (B.6) and (B.9) provide a predictor d_{cc} for d_c . In Bres $m = 1$ in Stages I, II and III and m is adjustable in Stages IV and V ($m \approx 1$ in Types A and C breaches and $m \approx 1.5$ in a Type B breach).

Function NormalFlow

This function computes in Stages I, II and III:

- the normal values of water depth d , flow velocity U , breach widths B and B_w , hydraulic radius R , roughness height k and bed friction coefficient C_f , i.e. $d_n, U_n, B_n, B_{wn}, R_n, k_n$ and C_{fn} ;
- the magnitudes of the adaptation lengths l_n and l_a ;

and makes:

- the attributions $d = d_n, U = U_n$ and $C_f = C_{fn}$ for the computation of the normal sediment transport capacity.

The function NormalFlow reads as follows:

$$d_n = 0.4 (H_w - Z_{br}) , \quad B_n = b + \frac{d_n}{\tan \gamma} \quad (\text{B.10, 4.1})$$

$$d_n = \frac{[C_f(Q_{br}/B_n)^2]^{1/3}}{[g \sin \beta]^{1/3}} , \quad d_{nn} = 0.9 d_n , \quad C_{fn} = C_f \quad (\text{B.11, B.12, B.13})$$

$$\text{while } |(d_n - d_{nn})/d_n| > 0.01 \quad (\text{B.14})$$

$$\{ \quad d_{nn} = d_n \quad (\text{B.15})$$

$$B_n = b + \frac{d_n}{\tan \gamma} , \quad R_n = \frac{B_n d_n}{b + 2 d_n / \sin \gamma} \quad (\text{4.1, 4.3})$$

$$U_n = (g R_n \sin \beta / C_{fn})^{1/2} , \quad d_n = \frac{Q_{br}}{U_n B_n} , \quad \theta_n = \frac{C_{fn} (U_n)^2}{g \Delta D_{50}} \quad (\text{4.15, 4.16, 4.11})$$

$$\text{if } \theta_n < 1: k_n = 3 D_{90} , \quad \text{else: } k_n = 3 D_{90} \theta_n \quad (\text{B.16})$$

$$C_{fn} = \frac{\kappa^2}{[\ln(12 R_n / k_n)]^2} \quad \} \quad (\text{4.8})$$

$$B_{wn} = b + \frac{2 d_n}{\tan \gamma} , \quad Fr_n = \frac{U_n}{[g d_n (B_n / B_{wn}) \cos \beta]^{1/2}} \quad (\text{4.2, 4.20})$$

$$l_n = \frac{2.5 (Fr_n^2 - 1) d_n}{\tan \beta} , \quad l_a = \xi \frac{B_w}{B_t} \frac{Q_{br}}{B_n w_s \cos \beta} \quad (\text{4.26, 4.37})$$

$$\text{if } l_a < l_n: l_a = l_n \quad (\text{B.17})$$

$$d = d_n, \quad U = U_n, \quad C_f = C_{fn} \quad (\text{B.18, B.19, B.20})$$

Equation (B.10) is a first predictor for d_n , while equations (B.11) and (B.15) yield a second predictor d_{nn} for d_n .

Function FlowSlope

This function computes in Stages I, II and III:

- the distance x_E from the top of the inner slope where the erosion rate on this slope reaches a maximum;
- the water depth d_E , flow velocity U_E , breach width B_E , hydraulic radius R_E , bed roughness height k_E and bed friction coefficient C_{fE} at $x = x_E$; and makes:
- the attributions $d = d_E$, $U = U_E$ and $C_f = C_{fE}$ for the computation of t_1 and the sediment transport capacity.

The function FlowSlope reads as follows:

$$L = (Z_{br} - Z_p) / \sin \beta \quad (\text{B.21})$$

$$\text{if } l_n > L: x_E = L, \quad \text{else: } x_E = l_n \quad (\text{B.22})$$

$$d_E = d_n + (d_c - d_n) e^{-5x_E/l_n}, \quad B_E = b + \frac{d_E}{\tan \gamma} \quad (\text{4.27, 4.1})$$

$$U_E = \frac{Q_{br}}{B_E d_E}, \quad R_E = \frac{B_E d_E}{b + 2d_E / \sin \gamma} \quad (\text{B.23, 4.3})$$

$$C_{fE} = C_f, \quad C_{ff} = 0.9 C_{fE} \quad (\text{B.24, B.25})$$

$$\text{while } |(C_{fE} - C_{ff}) / C_{fE}| > 0.01 \quad (\text{B.26})$$

$$\left\{ \begin{array}{l} C_{ff} = C_{fE}, \quad \theta_E = \frac{C_{fE} (U_E)^2}{g \Delta D_{50}} \end{array} \right. \quad (\text{B.27, 4.11})$$

$$\text{if } \theta_E < 1: k_E = 3 D_{90}, \quad \text{else: } k_E = 3 D_{90} \theta_E \quad (\text{B.28})$$

$$C_{fE} = \frac{\kappa^2}{[\ln(12R_E/k_E)]^2} \quad \} \quad (\text{4.8})$$

$$d = d_E, \quad U = U_E, \quad C_f = C_{fE} \quad (\text{B.29, B.30, B.31})$$

C_{ff} is an auxiliary symbol for C_{fE} .

Function FrictionCoeff

This function computes the bed friction coefficient C_f for the computation of the sediment transport capacity of the flow through the breach in Stages IV and V. It reads as follows:

$$C_{ff} = 0.9 C_f \quad (B.32)$$

$$\text{while } |(C_f - C_{ff})/C_f| > 0.01 \quad (B.33)$$

$$\left\{ C_{ff} = C_f, R = \frac{Bd}{b + 2d/\sin\gamma}, \theta = \frac{C_f U^2}{g \Delta D_{50}} \right. \quad (B.34, 4.3, 4.11)$$

$$\text{if } \theta < 1: k = 3 D_{90}, \text{ else: } k = 3 D_{90} \theta \quad (B.35)$$

$$C_f = \frac{\kappa^2}{[\ln(12R/k)]^2} \quad (4.8)$$

C_{ff} is an auxiliary symbol for C_f .

Function SedTransCap

This function holds the sediment transport formulations of Bagnold-Visser (1989), Engelund-Hansen (1967), Van Rijn (1984a,b) and Wilson (1987) for the equilibrium value of the sand transport (in BRES s_t , see Paragraphs B.4 through B.8). These formulae are described in Appendix A. By adopting s_t for s_s in the present model (see Chapter 4), it is implicitly assumed that also bed-load transport has an adaptation length l_a (see Paragraph 5.5). For each stage one of these sediment transport formulae can be selected. The default formulae are Bagnold-Visser (1989) for Stages I through III and Van Rijn (1984a,b) for Stages IV and V.

B.4 Module Stage I

This module reads as follows:

$$H_w = H_w(t_0), \beta_0^+ = (\beta_1 + \beta_0)/2, \beta = \beta_0^+ \quad (B.36, 4.52, B.37)$$

$$\text{Discharge, NormalFlow, FlowSlope, SedTransCap} \quad (B.38)$$

$$t_1 = t_0 + \frac{B_t}{B_w} \frac{(1-p)l_a(\beta_1 - \beta_0)x_E}{s_t [1 + 5n(x_E/l_n)(U_n/U - 1)]} \quad (\text{B.39})$$

$$H_p(t_1) = H_p(t_0) + Q_{br} t_1 / A_p \quad (\text{4.89})$$

Equation (B.39) follows from the substitution of (4.28), (4.33) and (4.45) into (4.53).

B.5 Module Stage II

This module reads as follows:

$$H_w = H_w(t_1) , \quad \beta = \beta_1 \quad (\text{B.40, B.41})$$

$$\text{Discharge} , \text{ NormalFlow} , \text{ FlowSlope} , \text{ SedTranspCap} \quad (\text{B.38})$$

$$W_1 = W_d + (H_d - Z_{br}) \left(\frac{1}{\tan \alpha} + \frac{1}{\tan \beta_0} \right) \quad (\text{4.59})$$

$$t_2 = t_1 + \frac{B_t}{B_w} \frac{W_1 (1-p)l_a \sin \beta}{s_t} \quad (\text{4.60})$$

$$H_p(t_2) = H_p(t_1) + Q_{br}(t_2 - t_1)/A_p \quad (\text{4.89})$$

B.6 Module Stage III

This module reads as follows:

$$H_w = H_w(t_2) , \quad \beta = \beta_1 , \quad \text{select } \Delta t \quad (\text{B.42, B.41, B.43})$$

$$\text{while } Z_{br} - Z_w > 0 \quad (\text{B.44})$$

$$\{ \text{Discharge} , \text{ NormalFlow} , \text{ FlowSlope} , \text{ SedTranspCap} \quad (\text{B.38})$$

$$Z_{br}(t + \Delta t) = Z_{br} - \frac{B_w}{B_t} \frac{\sin \alpha}{\sin(\alpha + \beta)} \frac{s_t}{(1-p)l_a} \Delta t \quad (\text{4.65})$$

$$H_p(t + \Delta t) = H_p(t) + (Q_{br} \Delta t) / A_p \quad (\text{4.89})$$

$$t = t + \Delta t \quad \} \quad (B.45)$$

$$t_3 = t - \Delta t \quad (B.46)$$

B.7 Module Stage IV

This module reads as follows:

$$\text{select } \Delta t \quad (B.43)$$

$$\text{while } H_p - Z_{br} < d_c \quad (B.47)$$

$$\{ H_w = H_w(t), \text{ Discharge}, d = d_c, U = \frac{Q_{br}}{Bd}, \text{ SedTranspCap} \quad (B.48)$$

$$l_a = \xi \frac{d}{H_d - Z_{br}} \frac{Ud}{w_s} \quad (4.78)$$

$$b(t + \Delta t) = b(t) + 2 \frac{d}{H_d - Z_{br}} \frac{s_t \Delta t}{(1 - p)l_a \tan \gamma} \quad (4.83)$$

$$H_p(t + \Delta t) = H_p(t) + (Q_{br} \Delta t) / A_p \quad (4.89)$$

$$t = t + \Delta t \quad \} \quad (B.45)$$

$$t_4 = t - \Delta t \quad (B.49)$$

B.8 Module Stage V

This module reads as follows:

$$\text{select } \Delta t \quad (B.43)$$

$$D_* = D_{50} (g \Delta / \nu^2)^{1/3} \quad (A.21)$$

$$\theta_{cr} = 0.24 D_*^{-1} \quad \text{for} \quad 1 < D_* \leq 4 \quad (A.27)$$

$$\theta_{cr} = 0.14 D_*^{-0.64} \quad \text{for} \quad 4 < D_* \leq 10 \quad (A.28)$$

Breach growth in sand-dikes

$$\theta_{cr} = 0.04 D_{\star}^{-0.1} \quad \text{for} \quad 10 < D_{\star} \leq 20 \quad (\text{A.29})$$

$$\theta_{cr} = 0.013 D_{\star}^{0.29} \quad \text{for} \quad 20 < D_{\star} \leq 150 \quad (\text{A.30})$$

$$\theta_{cr} = 0.055 \quad \text{for} \quad D_{\star} > 150 \quad (\text{A.31})$$

$$\text{while } H_w > H_p \quad (\text{B.50})$$

$$\{ H_w = H_w(t) \quad (\text{B.51})$$

$$U = [2g(H_w - H_p)]^{1/2} \quad (\text{4.91})$$

$$d = H_p - Z_{br} \quad (\text{4.90})$$

$$B = b + \frac{d}{\tan \gamma}, \quad B_w = b + \frac{2d}{\tan \gamma} \quad (\text{4.1, 4.2})$$

$$B_t = b + \frac{2(H_d - Z_{br})}{\tan \gamma} \quad (\text{4.5})$$

$$Q_{br} = mBUd \quad (\text{4.92})$$

$$\text{if } \theta > \theta_{cr} \quad (\text{B.52})$$

$$\{ U = \frac{Q_{br}}{Bd}, \text{ FrictionCoeff}, \text{ SedTransCap} \quad (\text{B.53})$$

$$l_a = \xi \frac{d}{H_d - Z_{br}} \frac{Ud}{w_s} \quad (\text{4.78})$$

$$b(t + \Delta t) = b(t) + 2 \frac{d}{H_d - Z_{br}} \frac{s_t \Delta t}{(1-p)l_a \tan \gamma} \quad (\text{4.83})$$

$$t_5 = t \quad \} \quad (\text{B.54})$$

$$H_p(t + \Delta t) = H_p(t) + (Q_{br} \Delta t) / A_p \quad (\text{4.89})$$

$$t = t + \Delta t \quad \} \quad (\text{B.46})$$

$$t_6 = t - \Delta t \quad (\text{B.55})$$

Acknowledgements

This thesis was financially supported by the Dienst Weg- en Waterbouwkunde of Rijkswaterstaat (Ministry of Transport, Public Works and Water Management) in the Netherlands.

The author wishes to thank his promotor J.A. Battjes for his stimulating support during the investigation and his critical review of this thesis (especially his suggestions how to mend an earlier draught version of it). The author is greatly indebted to A.M. den Toom for writing the software of the BRES program and to M.Z. Voorendt for his support in managing the operating system of author's PC. The many discussions with P. Huisman in 1997 and 1998 about inundations, construction of dikes in the past and nowadays, etc. are highly appreciated.

The author thanks the many people who have joined him in various breach erosion studies: J.S. Ribberink, J.P.Th. Kalkwijk, J.M.L. Dieteren, P.H. Pottinga, J.K. Vrijling, H.J. Verhagen, H.J. Steetzel, A.W. Kraak, W.T. Bakker, J. van de Graaff, M.J. Smit, D.W. Snip, C. Somers, A.P. de Looff, C.P. Caan, Ye Shiqiang, D. Broere and T.D.S. Feenstra, they all contributed to a better understanding of the fascinating dike breaching process. The contributions of the Meetdienst Zeeland of Rijkswaterstaat to the successful Zwin'94 field experiment and of the colleagues of the Laboratory of Fluid Mechanics of the Department of Civil Engineering to the Zwin'94 experiment and various laboratory studies are gratefully acknowledged.

The following sources are acknowledged: Foto Scheermeijer, Sliedrecht (Front cover and Figure 7.6), CUR/TAW, Gouda (Figures 1.1 and 3.5), US Army Corps of Engineers, Nashville, Tennessee (Figures 2.2 and 2.3), Kluwer Academic Publishers, Dordrecht (Figures 2.4 and 2.5), American Society of Civil Engineers, New York (Figures 2.6 and A.1), Topografische Dienst, Emmen (Figure 3.22), Rijkswaterstaat, Meetkundige Dienst, Afdeling Grafische Technieken, Delft (Figure 6.1), Staatsdrukkerij, Den Haag (Figure 7.5), Aqua Publications, Amsterdam (Figures A.2 and A.3).

Finally, the author is grateful to his parents for their stimulation and support during this study and, already many years ago, throughout his years at school and university.

List of main symbols

Roman letters

Symbol	Description	SI-unit
a	reference level above bed in formulation of Van Rijn (1984b)	[m]
A	cross-sectional breach flow area	[m ²]
A_p	polder area	[m ²]
b	width of breach at breach bottom	[m]
B	depth-averaged (over water depth d) breach width	[m]
B_a	depth-averaged (over breach depth h) breach width	[m]
B_t	width breach at top of dike	[m]
B_w	width breach at water line	[m]
c	depth-averaged sand concentration (by volume)	[-]
c_a	sand concentration at height a above bottom	[-]
c_{be}	bed concentration	[-]
C	Chézy coefficient	[m ^{1/2} /s]
C_f	friction coefficient	[-]
d	water depth (above breach bottom)	[m]
d_a	width-averaged water depth	[m]
d_c	critical flow depth	[m]
d_n	normal flow depth (equilibrium value of water depth d)	[m]
D	mean particle diameter	[m]
D_*	dimensionless particle parameter, see equation (A.21)	[-]
D_i	particle diameter such that $i\%$ of sediment volume has a diameter smaller than D_i	[m]
D_{50}	median particle diameter	[m]
E	rate of erosion	[m/s]
Fr	Froude number	[-]
g	acceleration of gravity	[m/s ²]
h	depth of breach at breach bottom = $H_d - Z_{br}$	[m]
H_d	height of dike above $Z = 0$	[m]
H_p	water level in polder above $Z = 0$ (inside water level)	[m]
H_w	water level against dike above $Z = 0$ (outside water level)	[m]
k	roughness height	[m]

Breach growth in sand-dikes

Symbol	Description	SI-unit
l_a	adaptation length of suspended load	[m]
l_n	length along inner slope over which the flow velocity approaches the normal flow velocity (adaptation length of flow)	[m]
L	length inner slope	[m]
m	discharge coefficient	[-]
n	dimensionless exponent in $s_s = MU^n$ (where M is a dimensional coefficient)	[-]
p	bed porosity	[-]
q_{br}	specific flow discharge through breach	[(m ³ /s)/m]
Q_{br}	breach inflow rate	[m ³ /s]
r	ϵ if $\epsilon \geq 1$ and $1/\epsilon$ if $\epsilon < 1$	[-]
\bar{r}	mean value of r over eight cases under consideration	[-]
R	hydraulic radius of breach	[m]
Re_*	Reynolds number for flow around a sand particle = $u_* D / \nu$	[-]
s_b, s_s, s_t	capacity of bed-load, suspended load and total load, respectively (subscript of s indicates a transport capacity)	[(m ³ /s)/m]
$s(x)$	total transport at location x along the inner slope per unit breach width (s without subscript means the actual sediment transport, not necessarily the transport capacity)	[(m ³ /s)/m]
$S(x)$	$B_w s(x)$	[m ³ /s]
t	time	[s]
T	water temperature	[°C]
u_*	bed shear velocity	[m/s]
u_w	flow velocity at water line	[m/s]
U	depth-averaged flow velocity	[m/s]
U_c	critical value of U	[m/s]
U_n	normal flow velocity (equilibrium U value of flow velocity U)	[m/s]
w_s	sediment fall velocity	[m/s]
W_d	width of crest of dike	[m]
W_i	length of (initial) breach in crest of dike at $t = t_1$	[m]
x	coordinate along inner slope (in Stages I, II and III, $x = 0$ at the top of the inner slope)	[m]
x_E	distance from top of inner slope where the erosion rate on this slope reaches a maximum	[m]
z	coordinate normal to the inner slope (in Stages I, II and III, $z = 0$ at inner slope)	[m]

Symbol	Description	SI-unit
z_b	position of bed in z-direction at inner slope (in Stages I, II and III)	[m]
Z	vertical coordinate, $Z = 0$ is reference level	[m]
Z_b	vertical position of bed above $Z = 0$ in Stages IV and V	[m]
Z_{br}	height of breach bottom above reference level $Z = 0$	[m]
Z_p	polder level above reference level $Z = 0$	[m]
Z_w	level of bottom of water course above reference level $Z = 0$	[m]

Greek letters

Symbol	Description	SI-unit
α	inclination angle of outer slope of dike	[°]
β	inclination angle of inner slope of dike	[°]
β_0	inclination angle of inner slope at t_0	[°]
β_1	critical value of β	[°]
γ	inclination angle of side-slopes	[°]
γ_1	critical value of γ	[°]
Δ	specific density = $(\rho_s - \rho)/\rho$	[-]
ϵ	ratio (computed transport)/(measured transport)	[-]
θ	mobility parameter (Shields number)	[-]
θ_{cr}	critical value of θ for incipient motion	[-]
κ	constant of Von Karman	[-]
μ	ripple factor (ratio of grain shear stress and total bed shear stress)	[-]
ν	kinematic viscosity	[m ² /s]
ξ	constant of Galappatti in equation of l_a	[-]
ρ	water density	[kg/m ³]
ρ_s	sediment density	[kg/m ³]
τ_b	bed shear stress	[N/m ²]
ϕ	angle of repose of bed material	[°]

Subscripts

Symbol	Description
0	start of flow of water through initial breach
1	end of Stage I
2	end of Stage II
3	end of Stage III
4	end of Stage IV
5	end of Stage V
6	breach inflow stops
<i>b</i>	capacity of bed-load transport
<i>br</i>	breach
<i>c</i>	critical, where water depth is critical
<i>E</i>	position on inner dike slope where the erosion rate reaches a maximum
<i>n</i>	normal, where water depth has reached its normal (equilibrium) value
<i>s</i>	capacity of suspended load transport
<i>t</i>	capacity of total load transport

List of Dutch words

Dutch word	English translation
astronomisch getij	astronomical tide
blokken	blocks
bodem	bottom
drainage	drainage
dwarsprofiel	cross-section
dijkvoet	toe of outer slope of dike
geul	breach
in stand gebleven	original
klei	clay
oud	old
rijsbeslag met vlijstysteem	fascine layer with stones
schaal	length scale
stortsteen	rip-rap
zinkstuk	mattress

References

- Allen, J.R.L., 1982.** *Developments in sedimentology: sediment structures, their character and physical basis*, vol. 1. Elsevier Scientific Publication Co., Amsterdam, The Netherlands.
- Allersma, H.G.B., Ligtenberg, I.A.G. and Koehorst, B.A.N., 1994.** Simulation of failure of dikes by water infiltration by waves. In: *Centrifuge 94*, Leung, Lee and Tan (eds.), Balkema, Rotterdam, The Netherlands, pp. 289–294.
- Anonymous, 1977.** Teton Dam failure. *Civil Eng.*, ASCE, vol. 47, August, pp. 56–61.
- Ashida, K., Takahashi, T. and Mizuyama, T., 1978.** Study of bed load equations for mountain streams. *Shin-sabo*, vol. 30, no. 4, pp. 9–17 (in Japanese).
- Bagnold, R.A., 1963.** Mechanics of marine sedimentation. In *The Sea: Ideas and Observations*, vol. 3. Interscience, New York, USA, pp. 507–528.
- Bagnold, R.A., 1966.** An approach to the sediment transport problem from general physics. Geological Survey Professional Paper 422-I, U.S. Government Printing Office, Washington, D.C., USA.
- Bailard, J.A., 1981.** An energetics total load sediment transport model for a plane sloping beach. *J. Geophysical Res.*, vol. 86, no. C11, pp. 10938–10954.
- Bathurst, J.C., Graf, W.H. and Cao, H.H., 1987.** Bed load discharge equations for steep mountain rivers. In: *Sediment Transport in Gravel-Bed Rivers*, Thorne, Bathurst and Hey (eds.), John Wiley & Sons, Chichester, Great Britain, pp. 453–477.
- Bechteler, W. and Broich, K., 1991.** Effects in dam-break modeling. *Proc. 24th Congress IAHR*, Madrid, Spain, pp. A189–A200.
- Brown, C.B., 1950.** Sediment transportation. In: *Engineering Hydraulics*, Rouse (ed.), John Wiley & Sons, Wiley, New York, USA.
- Brown, R.J. and Rogers, D.C., 1981.** BRDAM Users Manual. Water and Power Resources Services, U.S. Department of the Interior, Denver, CO, USA.
- Caan, C.P., 1996.** Bresgroei; een experimental onderzoek naar de ontwikkeling van de ontgrondingskuil (Breach growth; an experimental investigation of the development of the scour hole). Master's thesis, Hydraulic and Geotechnical Eng. Div., Dept. Civ. Eng., Delft Univ. Techn., Delft, The Netherlands.
- Chee, S.P., 1978.** Mobile controls for water resources projects. *Water Resources Bulletin*, American Water Resources Association, vol. 14, no. 1.
- Cristofano, E.A., 1965.** Method of computing erosion rate for failure of earth-fill dams. Bureau of Reclamation, Denver, CO, USA.
- De Loeff, A.P., 1990.** Bresgroei in een zanddijk; feitenverslag van een proef (Breach growth

in a sand-dike; report of a field experiment. Rep. WBA-R-90.041, Dienst Weg- en Waterbouwkunde, Rijkswaterstaat, Ministry of Transport, Public Works and Water Management, Delft, The Netherlands.

Du Boys, P., 1879. Etudes du régime du Rhône et l'action exercée par les laux sur un lit à fond de graviers indéfiniment affouillable. *Ann. Ponts et Chaussées*, vol. 18, pp. 141–195.

Edelman, T., 1960. Het bezwijken van dijken in 1953; stabiliteit van belopen onder invloed van een daarover stromende laag water (Failure of dikes in February 1953; stability of slopes under the influence of overflowing water). *De Ingenieur*, vol. 72, no. 11, pp. B35–B40.

Einstein, H.A., 1942. Formulas for transportation of bed-load. *Trans. Am. Soc. Civil. Eng.*, vol. 107, pp. 561–573 (see Brown, 1950, for Einstein-Brown formula).

Engelund, F., 1970. Instability of erodible beds. *J. Fluid Mech.*, vol. 42, pp. 225–244.

Engelund, F. and Hansen, E., 1967. A monograph on sediment transport. Technisk Forlag, Copenhagen, Denmark.

Fread, D.L., 1984a. DAMBRK: The NWS dam break flood forecasting model. National Weather Service (NWS) Report, NOAA, Silver Spring, MA, USA.

Fread, D.L., 1984b. A breach erosion model for earthen dams. National Weather Service (NWS) Report, NOAA, Silver Spring, MA, USA.

Fletcher, B.P. and Gilbert, P.A., 1992. Center Hill Fuseplug Spillway, Caney Fork River, Tennessee; Hydraulic Model Investigation. Techn. Rep. HL-92-15, Waterways Experiment Station, Corps of Engineers, U.S. Department of the Army, Vicksburg, MS, USA.

Fujita, Y. and Tamura, T., 1987. Enlargement of breaches in flood levees on alluvial plains. *Natural Disaster Science*, vol. 9, no.1, pp. 37–60.

Fujita, Y., Tamura, T. and Muramoto, Y., 1984. Experiments on enlarging process of river bank breaches, *Annuals, Disaster Prevention Research Institute*, no. 27B-2, Kyoto Univ., pp. 369–392 (in Japanese; translated in Dutch by TNO, see Rep. no. 87-bg-7(31)).

Galappatti, R., 1983. A depth-integrated model for suspended transport. Communications on Hydraulics, Rep. 83-7, Dept. Civil Eng., Delft Univ. Techn, Delft, The Netherlands.

Galappatti, R. and Vreugdenhil, C.B., 1985. A depth-integrated model for suspended sediment transport. *J. Hydraulic Res.*, IAHR, vol. 23, no. 4, pp. 359–377.

Gordon, A.D., 1991. Coastal lagoon entrance dynamics. *Proc. 22nd Int. Conf. Coastal Eng.*, Delft, The Netherlands, 1990, pp. 2880–2893.

Guy, H.P., Simons, D.B. and Richardson, E.V., 1966. Summary of alluvial channel data from flume experiments, 1956–1961. U.S. Geological Survey Professional Paper 462-1, Washington, D.C., USA.

Havnø, K., Van Kalken, T. and Olesen, K., 1989. A modeling package for dam break solution. *Proc Int. Symp. on Analytical Evaluation of Dam Related Safety Problems*, Copenhagen, Denmark, vol. 1, pp. 475–491.

- Kennedy, J.F., 1969.** The formation of sediment ripples, dunes and anti-dunes. *Ann. Rev. Fluid Mech.*, vol. 1, pp. 147–168.
- Kraak, A.W., Bakker, W.T, Van de Graaff, J., Steetzel, H.J. and Visser, P.J., 1995.** Breach-growth research programme and its place in damage assessment for a polder. *Proc. 24th Int. Conf. Coastal Eng.*, Kobe, Japan, 1994, pp. 2197–2206.
- Louws, D. and Van der Weijde, P., 1995.** Meetverslag Bresgroei Zwingeul (Measuring report Zwin'94 experiment). Rep. ZLMD-94.N.039, Meetdienst Zeeland, Directie Zeeland, Rijkswaterstaat, Vlissingen, The Netherlands.
- MacDonald, T.C. and Langridge-Monopolis, J., 1984.** Breaching characteristics of dam failures. *J. Hydr. Eng.*, ASCE, vol. 110, no. 5, pp. 567–586.
- Mastbergen, D.R. and Winterwerp, J.C., 1987.** Het gedrag van zand-watermengselstromingen boven water; verslag experimentele vervolgstudie (The behaviour of sand-water mixture flows above the water level). Delft Hydraulics, Rep. Z46-02, Delft, The Netherlands.
- Meyer-Peter, E. and Müller, R., 1948.** Formulas for bed-load transport. *Proc. 2nd Congress IAHR*, Stockholm, Sweden, Appendix 2, pp. 39–64.
- Mizuyama, T., 1977.** Bed load transport in steep channels. Ph.D thesis, Kyoto Univ., Kyoto, Japan (in Japanese).
- Mojib, R.M, 1990.** Development of a computer program for gradual failure of earthen dams due to over topping. Ph. D. Tesis, Univ. of Tennessee, Knoxville, TN, USA.
- National Bureau of Standards, 1975.** The viscosity of water 0°C to 100°C. In: *Handbook of chemistry and physics* (56th edition of 1975), Weast (ed.). CRC Press, Cleveland, Ohio, USA, p. F-49.
- Odd, N.V.M, Roberts, W. and Maddocks, J., 1995.** Simulation of lagoon breakout. *Proc. 26th Congress IAHR*, London, UK, Volume 3, pp. 92–97.
- Peterson, A.W. and Howells, R.F., 1973.** A compendium of solids transport data for mobile boundary channels. Rep. HY-1973-ST3, Dept. Civil Eng., Univ. of Alberta, Canada.
- Ponce, V.M. and Tsivoglou, A.J., 1981.** Modeling gradual dam breaches. *J. Hydr. Div.*, ASCE, vol. 107, no. HY7, pp. 829–838.
- Pugh, C.A., 1985.** Hydraulic model studies of fuse plug embankments. Rep. REC-ERC-85-7, Bureau of Reclamation, U.S. Department of the Interior, Denver, CO, USA.
- Rickenmann, D., 1991.** Hyperconcentrated flow and sediment transport at steep slopes. *J. Hydr. Eng.*, ASCE, vol. 117, no. 11, pp. 1419–1439.
- Rijkswaterstaat, 1961.** *Verslag over de stormvloed (Report on the 1953 flood)*. Staatsdrukkerij, Den Haag, The Netherlands.
- Schoklitsch, A., 1930.** *Handbuch des Wasserbaues* (3rd edition of 1962), Springer-Verlag, Vienna, Austria.

- Scheermeijer, L., 1997.** Personal communication, Slidrecht.
- Shields, A., 1936.** Anwendung der Aehnlichkeitsmechanik und der Turbulenzforschung auf die Geschiebebewegung. *Mitt. der Preuss. Versuchsanstalt für Wasserbau und Schiffbau*, Heft 26, Berlin, Germany.
- Shook, C.A., Gillies, R., Haas, D.B., Husband, W.H.W. and Small, M. 1982.** Flow of coarse and fine sand slurries in pipelines. *J. Pipelines*, Elsevier, vol. 3, pp. 13–21.
- Sieben, A., 1993.** Hydraulics and morphology of mountain rivers: a literature survey. Communications on hydraulic and geotechnical engineering, Rep. 93-4, Fac. Civil Eng., Delft Univ. Techn., Delft, The Netherlands.
- Singh, V.P. and Scarlatos, P.D., 1987.** Modeling of gradual earthfill dam erosion. In: *Environmental Geotechnics and Problematic Soils and Rocks*, Balasubramaniam, Chandra, Bergado and Nutulaya (eds.), pp. 129–138, Balkema, Rotterdam, The Netherlands.
- Singh, V.P., 1996.** *Dam Breach Modeling Technology*, Kluwer, Dordrecht, The Netherlands.
- Smart, G.M. and Jaeggi, M., 1983.** Sediment transport on steep slopes. *Mitteilungen der Versuchsanstalt für Wasserbau, Hydrologie und Glaziologie*, No. 64, Eidgenössischen Technischen Hochschule, Zurich, Switzerland.
- Smart, G.M., 1984.** Sediment transport formula for steep channels. *J. Hydr. Eng.*, ASCE, vol. 110, no. 3, pp. 267–276.
- Smit, M.J. and Snip, D.W., 1995.** Voorbereiding van een bresgroeiproef in het Zwin 1994; Deel I: theoretisch vooronderzoek (Preparation of Zwin'94 experiment; Part I: theoretical investigation). M.Sc.-thesis Hydraulic and Geotechnical Eng. Div., Fac. Civil Eng., Delft Univ. Techn., Delft, The Netherlands.
- Steezel, H.J. and Visser, P.J., 1992.** Bresgroeï, Deel II: 2DV-ontwikkeling initiële bres; Band A: Verslag modelonderzoek Scheldegoet (Breach growth, Part II: 2DV-development initial breach; Report experiments in Schelde Flume). Rep. H1242-IIA, Delft Hydraulics and Delft Univ. Techn., Delft, The Netherlands.
- Steezel, H.J. and Visser, P.J., 1993.** Profile development of dunes due to overflow. *Proc. 23rd Int. Conf. Coastal Eng.*, Venice, Italy, 1992, pp. 2669–2679.
- Steezel, H.J., 1996a.** Bresgroeï, Deel III: 2DH/3D-ontwikkeling initiële bres; Band A: Verslag onderzoek Scheldebak (Breach growth, Part III: 2DH/3D-development initial breach; Report experiments in Schelde Basin). Rep. H1242-IIIA, Delft Hydraulics, Delft, The Netherlands.
- Steezel, H.J., 1996b.** Bresgroeï, Deel I: Mathematisch model; Band A: Opzet en eerste resultaten (Breach growth, Part I: Mathematical model; Format and first results). *Rep. H1242-IA*, Delft Hydraulics, Delft, The Netherlands.
- Takahashi, T., 1978.** Mechanical characteristics of debris flow. *J. Hydr. Div.*, ASCE, vol. 104, no. HY8, pp. 1153–1169.

- Takahashi, T., 1980.** Debris flow on prismatic open channel. *J. Hydr. Div.*, ASCE, vol. 106, no. HY3, pp. 381-396.
- Takahashi, T., 1987.** High velocity flow in steep erodible channels. *Proc. 22nd Congress IAHR*, Lausanne, Switzerland, pp. A42-A53.
- Takahashi, T., 1991.** *Debris flow*. IAHR monograph, Balkema, Rotterdam, The Netherlands, 165 pp.
- TAW/CUR, 1990.** Probabilistic design of flood defences. Rep. 141, Technical Advisory Committee on Water Defences, Centre for Civil Engineering Research and Codes, Gouda, The Netherlands.
- TAW/CUR, 1991.** Guide for the design of river dikes. Rep. 142, Technical Advisory Committee on Water Defences, Centre for Civil Engineering Research and Codes, Gouda, The Netherlands.
- TAW/TNO, 1984.** Stroomgaten in dijken (Breaches in dikes). Technical Advisory Committee on Water Defences, Report PM 84-13, Rijswijk, The Netherlands.
- Tinney, E.R. and Hsu, H.Y., 1961.** Mechanics of washout of an erodible fuse plug. *J. Hydr. Div.*, ASCE, vol. 87, no. HY3, pp. 1-29.
- Van Rijn, L.C., 1984a.** Sediment transport, Part I: bed load transport. *J. Hydr. Eng.*, ASCE, vol. 110, no. 110, pp. 1431-1456.
- Van Rijn, L.C., 1984b.** Sediment transport, Part II: suspended load transport. *J. Hydr. Eng.*, ASCE, vol. 110, pp. 1613-1641.
- Van Rijn, L.C., 1984c.** Sediment pick-up functions. *J. Hydr. Eng.*, ASCE, vol. 110, pp. 1494-1502.
- Van Rijn, L.C., 1985.** Sand transport at high velocities; report on experimental research. Delft Hydraulics, Rep. M2127 parts A and B, Delft, The Netherlands.
- Van Rijn, L.C., 1993.** *Principles of sediment transport in rivers, estuaries and coastal seas*. Aqua Publications, Amsterdam, The Netherlands.
- Visser, H.A., 1998.** Personal communication, Papendrecht.
- Visser, P.J., 1989.** A model for breach growth in a dike-burst. *Proc. 21st Int. Conf. Coastal Eng.*, Malaga, Spain, 1988, pp. 1897-1910.
- Visser, P.J., 1995a.** A model for breach growth in sand-dikes. *Proc. 24th Int. Conf. Coastal Eng.*, Kobe, Japan, 1994, pp. 2755-2769.
- Visser, P.J., 1995b.** Application of sediment transport formulae to sand-dike breach erosion. Communications on hydraulic and geotechnical engineering, Rep. 94-7, Fac. Civil Eng., Delft Univ. Techn., Delft, The Netherlands.
- Visser, P.J., Ribberink, J.S. and Kalkwijk, J.P.Th., 1986.** Ontwikkeling stroomgat en debiet bij dijkdoorbraak; deelstudie voor een pompaccumulatiecentrale (Development of the breach and flow discharge in a dike-burst. Rep. 8-86, Hydraulic and Geotechnical Eng. Div.,

Dept. Civ. Eng., Delft Univ. Techn., Delft, The Netherlands.

Visser, P.J., Vrijling, J.K. and Verhagen, H.J., 1991. A field experiment on breach growth in sand-dikes. *Proc. 22nd Int. Conf. Coastal Eng.*, Delft, The Netherlands, 1990, pp. 2087-2100.

Visser, P.J., Kraak, A.W., Bakker, W.T., Smit, M.J., Snip, D.W., Steetzel, H.J. and Van de Graaff, J., 1996a. A large-scale experiment on breaching in sand-dikes. *Proc. Coastal Dynamics '95*, Gdansk, Poland, 1995, pp. 583-594.

Visser, P.J., Smit, M.J. and Snip, D.W., 1996b. Zwin'94 experiment; meetopstelling en overzicht van alle meetresultaten (Zwin'94 experiment; measuring procedure and experimental results). Rep. 4-96, Hydraulic and Geotechnical Eng. Div., Fac. Civil Eng., Delft Univ. Techn., Delft, The Netherlands.

Voogt, L., 1985. Doorbraak ringdijk (Burst of enclosing dike). Rijkswaterstaat, Internal Rep., Den Haag, The Netherlands (see also **PAC-projectgroep, 1985.** Pomp Accumulatie Centrale IJsselmeer, Deelrapportage fase 1, "Veiligheid". Utrecht, The Netherlands).

Voogt, L., Van Rijn, L.C. and Van den Berg, J.H., 1991. Sediment transport of fine sands at high velocities. *J. Hydr. Eng.*, ASCE, vol. 117, no. 7, pp. 869-890.

Wilson, K.C., 1966. Bed-load transport at high shear stress. *J. Hydr. Div.*, ASCE, vol. 92, no. HY6, pp. 49-59.

Wilson, K.C., 1987. Analysis of bed-load motion at high shear stress. *J. Hydr. Eng.*, ASCE, vol. 113, no. 1, pp. 97-103.

Wilson, K.C., 1989. Mobile-bed friction at high shear stress. *J. Hydr. Eng.*, ASCE, vol. 115, no. 6, pp. 825-830.

Wilson, K.C. and Nnadi, F.N., 1993. Motion of mobile beds at high shear stress. *Proc. 23rd Int. Conf. Coastal Eng.*, Venice, Italy, pp. 2917-2925.

Winterwerp, J.C., De Groot, M.B., Mastbergen, D.R. and Verwoert, H., 1990. Hyper-concentrated sand-water mixture flows over flat bed. *J. Hydr. Eng.*, ASCE, vol. 116, no. 1, pp. 36-54.

Winterwerp, J.C., Bakker, W.T., Mastbergen, D.R. and Van Rossum, H., 1992. Hyper-concentrated sand-water mixture flows over erodible bed. *J. Hydr. Eng.*, ASCE, vol. 118, no. 11, pp. 1508-1525.

Wurbs, R.A., 1987. Dam-breach flood wave models. *J. Hydr. Eng.*, ASCE, vol. 113, no. 1, pp. 29-46.

Yang, C.T., 1979. Unit stream power equations for total load. *J. Hydrology*, vol. 40, pp. 123-138.

Curriculum Vitae

- 23/04/1949: Pleun Joris Visser, geboren te Sliedrecht
- 1956–1962: lagere school te Papendrecht
- 1962–1967: Christelijk Lyceum te Dordrecht
- 1967: diploma HBS B
- 1967–1975: studie civiele techniek, Afdeling der Weg- en Waterbouwkunde, Technische Hogeschool Delft
- 1975: diploma civiel ingenieur
- 1975–1986: wetenschappelijk medewerker Vakgroep Kustwaterbouwkunde, Afdeling der Civiele Techniek, Technische Hogeschool Delft
- 1986–1997: universitair docent Vakgroep Waterbouwkunde (sectie Vloeistofmechanica), Faculteit der Civiele Techniek, Technische Universiteit Delft
- 1988–1989: visiting scientist Department of Coastal and Oceanographic Engineering, University of Florida, Gainesville, Florida, USA
- 1989–1993: secretaris Vakgroep Waterbouwkunde
- 1994–1995: lid bestuur Faculteit der Civiele Techniek
- 1998– universitair docent Sectie Waterbouwkunde (vakgebied Rivierwaterbouwkunde), Faculteit Civiele Techniek en Geowetenschappen, Technische Universiteit Delft